2005-03-18

Analytical Modeling of Wood-Frame Shear Walls and Diaphragms

Johnn Paul Judd
Brigham Young University - Provo

ANALYTICAL MODELING OF

WOOD-FRAME SHEAR WALLS AND DIAPHRAGMS

by

Johnn P. Judd

A thesis submitted to the faculty of

Brigham Young University

in partial fulfillment of the requirements for the degree of

Master of Science

Department of Civil and Environmental Engineering

Brigham Young University

April 2005

BRIGHAM YOUNG UNIVERSITY

GRADUATE COMMITTEE APPROVAL

of a thesis submitted by

Johnn P. Judd

This thesis has been read by each member of the following graduate committee and by majority vote has been found to be satisfactory.

_____	_____
Date	Fernando S. Fonseca, Chair
_____	_____
Date	Richard J. Balling
_____	_____
Date	Steven E. Benzley
_____	_____
Date	Warren K. Lucas

BRIGHAM YOUNG UNIVERSITY

As chair of the candidate's graduate committee, I have read the thesis of Johnn P. Judd in its final form and have found that (1) its format, citations, and bibliographical style are consistent and acceptable and fulfill university and department style requirements; (2) its illustrative materials including figures, tables, and charts are in place; and (3) the final manuscript is satisfactory to the graduate committee and is ready for submission to the university library.

_____
Date

_____
Fernando S. Fonseca
Chair, Graduate Committee

Accepted for the Department

_____
E. James Nelson
Graduate Coordinator

Accepted for the College

_____
Douglas M. Chabries
Dean, Ira A. Fulton College of Engineering and Technology

ABSTRACT

ANALYTICAL MODELING OF WOOD-FRAME SHEAR WALLS AND DIAPHRAGMS

Johnn P. Judd

Department of Civil and Environmental Engineering

Master of Science

Analytical models of wood-frame shear walls and diaphragms for use in monotonic, quasi-static (cyclic), and dynamic analyses are developed in this thesis. A new analytical model is developed to accurately represent connections between sheathing panels and wood framing members (sheathing-to-framing connections) in structural analysis computer programs. This new model represents sheathing–to–framing connections using an oriented pair of nonlinear springs. Unlike previous models, the new analytical model for sheathing–to–framing connections is suitable for both monotonic, cyclic, or dynamic analyses. Moreover, the new model does not need to be scaled or adjusted.

The new analytical model may be implemented in a general purpose finite element program, such as *ABAQUS*, or in a specialized structural analysis program, such as *CASHEW*. The analytical responses of several shear walls and diaphragms employing this new model are validated against measured data from experimental testing.

A less complex analytical model of shear walls and diaphragms, *QUICK*, is developed for routine use and for dynamic analysis. *QUICK* utilizes an equivalent single degree of freedom system that has been determined using either calibrated parameters from experimental or analytical data, or estimated sheathing–to–framing connection data.

Application of the new analytical models is illustrated in two applications. In the first application, the advantages of diaphragms using glass fiber reinforced polymer (GFRP) panels in conjunction with plywood panels as sheathing (hybrid diaphragms) are presented. In the second application, the response of shear walls with improperly driven (overdriven) nails is determined along with a method to estimate strength reduction due to both the depth and the percentage of total nails overdriven.

ACKNOWLEDGMENTS

Many people have contributed to the successful completion of this research. Foremost among them is my advisor, Dr. Fernando Fonseca, who provided the genesis for this research and gave ideas, guidance, and confidence along the way. I am also indebted to him for the many opportunities he afforded me to present and publish our research.

The assistance of Professor Helmut Prion and Professor Frank Lam, and Mr. Jianzhong Gu (Department of Wood Science, and Department of Civil Engineering, University of British Columbia) in furnishing data from testing of oriented strand board shear walls is gratefully acknowledged.

I appreciate the support of my graduate committee members, Dr. Steven Benzley, Dr. Warren Lucas, and Dr. Richard Balling. I especially appreciate the help Dr. Balling has provided over the past few years. His suggestions were crucial to the development of the new sheathing-to-framing connection model.

The Department of Civil and Environmental Engineering has been very helpful. Dr. Woodruff Miller (Department Chair), Dr. James Nelson (Graduate Coordinator), and the entire office staff have been supportive of my research efforts. I appreciate the help of David Anderson (Department Technician) during coupon testing, and the help of Lynda Richmond (College Secretary), Selby Herrin (ETD Coordinator), and Drew Johnson (University Press Building Copy Center Assistant) during publication of this thesis.

The support family and friends has been invaluable. I thank both my parents, Jerry and Linda Judd for teaching the value of education and work. I thank my brother Allyn for the many hours he spent editing and proof-reading manuscripts. I thank my brother Glenn for solving numerous computer programming problems with surgical precision. I especially appreciate Sharon Meilstrup for her help editing the final manuscript, and Eric Nielsen for his help organizing and printing the thesis.

Funding for this thesis was provided in part by the Department of Civil and Environmental Engineering. The glass fiber reinforced polymer panels (GFRP) panels used during coupon testing were graciously donated by Strongwell, Inc.

This thesis is dedicated to my mother.

TABLES OF CONTENTS

LIST OF TABLES

LIST OF FIGURES

NOTATION

The following symbols are used in this thesis:

A	=	input value for yield Modes II–IV, general dowel equation parameter;
	=	or, sheathing-to-framing connection load-displacement curve parameter;
a_1, a_2	=	sheathing-to-framing connection load-displacement curve parameter;
B	=	input value for yield Modes II–IV, general dowel equation parameter;
	=	or, sheathing-to-framing connection load-displacement curve parameter;
b	=	diaphragm width;
c	=	system damping
C	=	input value for yield Modes II–IV, general dowel equation parameter;
	=	or, sheathing-to-framing connection load-displacement curve parameter;
C_1, C_2	=	sheathing-to-framing connection load-displacement curve parameter;
D_s	=	dowel shank diameter at maximum stress in side member, general dowel equation parameter;
D_m	=	dowel shank diameter at maximum stress in main member, general dowel equation parameter;
e_{shear}	=	sheathing panel elongation due to shear;
e_{frame}	=	frame elongation;
E_a	=	energy absorption of a sheathing–to–framing connection;
F	=	shear wall or diaphragm load;
$\boldsymbol{F}$	=	force vector;
F_{ave}	=	measured diaphragm load (per ram) when pushing, pulling;
f_b	=	dowel-bending stress, general dowel equation parameter;
$f_{b,pl}$	=	proportional limit dowel-bending stress, general dowel equation parameter;
$f_{b,5\%}$	=	5% offset dowel-bending stress, general dowel equation parameter;
$f_{b,ult}$	=	ultimate dowel-bending stress, general dowel equation parameter;
f_{es}	=	dowel-bearing stress for side member, general dowel equation parameter;
f_{em}	=	dowel-bearing stress for main member, general dowel equation parameter;

$f_{e,pl}$ = proportional limit dowel-bearing stress, general dowel equation parameter;

$f_{e,5\%}$ = 5% offset dowel-bearing stress, general dowel equation parameter;

$f_{e,ult}$ = ultimate dowel-bearing stress, general dowel equation parameter;

$F_{\max}^{+}$ = maximum diaphragm load per ram when pushing the diaphragm during cyclic loading;

$F_{\max}^{-}$ = maximum diaphragm load per ram when pulling the diaphragm during cyclic loading;

F_{ubc} = design lateral load strength determined from the *Uniform Building Code* (ICBO 1997)

G_d = unblocked diaphragm shear stiffness, diaphragm deflection equation parameter;

g = gap between side and main member, general dowel equation parameter;

$\boldsymbol{K}$ = stiffness matrix;

K_E = effective initial diaphragm stiffness;

K_{ij} = stiffness component of a sheathing–to–framing connection at the i^{th} node in the j^{th} direction;

K_r = stiffness component of a sheathing–to–framing connection in the r direction;

K_x = stiffness component of a sheathing–to–framing connection in the x direction;

K_y = stiffness component of a sheathing–to–framing connection in the y direction;

K_u = stiffness component of a sheathing–to–framing connection in the u direction;

K_v = stiffness component of a sheathing–to–framing connection in the v direction;

K_1 = initial stiffness of a sheathing–to–framing connection;

K_2 = secondary stiffness of a sheathing–to–framing connection;

K_3 = softening stiffness of a sheathing–to–framing connection;

K_4 = unloading stiffness of a sheathing–to–framing connection;

K_5 = slipping stiffness of a sheathing–to–framing connection;

K_6 = reloading stiffness of a sheathing–to–framing connection;

$K^{tangent}$ = tangent stiffness of a sheathing–to–framing connection;

K^{secant} = secant stiffness of a sheathing–to–framing connection;

$K^{initial}$ = initial stiffness of a sheathing–to–framing connection;

l_s = dowel bearing length for side member, general dowel equation parameter;

l_m = dowel bearing length for main member, general dowel equation parameter;

LF_{ubc} = design load factor with respect to the *Uniform Building Code* (ICBO 1997)

ℓ_{panel} = length of sheathing panel diagonal;

P_I = residual (pinching) load of a sheathing–to–framing connection, hysteresis model parameter;

P_{LD} = loading load of a sheathing–to–framing connection, hysteresis model parameter;

P_r = load component of a sheathing–to–framing connection in the r direction;

P_x = load component of a sheathing–to–framing connection in the x direction;

P_y = load component of a sheathing–to–framing connection in the y direction;

P_u = load component of a sheathing–to–framing connection in the u direction;

P_v = load component of a sheathing–to–framing connection in the v direction;

P_y' = apparent yield load of a sheathing–to–framing connection;

P_R = reversal load of a sheathing–to–framing connection, hysteresis model parameter;

P_{ult} = ultimate load of a sheathing–to–framing connection;

P_{UN} = unloading load of a sheathing–to–framing connection, hysteresis model parameter;

$P(\delta)$ = connection load as a function of connection displacement, load–displacement curve;

R = transition curvature between the initial and secondary stiffnesses, load–displacement curve parameter;

$\boldsymbol{U}$ = displacement vector;

v = diaphragm unit shear;

x = displacement;

$\dot{x}$ = velocity;

$\ddot{x}$ = acceleration;

X = distance from chord splice connection to nearest support; deflection equation parameter;

α = sheathing-to-framing connection degredation hysteresis model parameter;

β = normalized secondary stiffness, load–displacement curve parameter;

= also, sheathing-to-framing connection degredation hysteresis model parameter;

δ = displacement of a sheathing–to–framing connection;

δ_E = envelope excursion displacement of a sheathing–to–framing connection, hysteresis model parameter;

δ_{fail} = softening displacement corresponding to the failure load of a sheathing–to–framing connection;

δ_{LD} = loading displacement of a sheathing–to–framing connection, hysteresis model parameter;

δ_R = reversal displacement of a sheathing–to–framing connection, hysteresis model parameter;

δ_S = stiffening displacement of a sheathing–to–framing connection, hysteresis model parameter;

δ_{yield} = apparent yield displacement of a sheathing–to–framing connection

δ_R = reversal displacement of a sheathing–to–framing connection, hysteresis model parameter;

δ_{ult} = displacement corresponding to the ultimate load of a sheathing–to–framing connection;

δ_{UN} = unloading displacement of a sheathing–to–framing connection, hysteresis model parameter;

δ_0 = crossing–0 displacement of a sheathing–to–framing connection, hysteresis model parameter;

δ_1 = crossing–1 displacement of a sheathing–to–framing connection, hysteresis model parameter;

δ_{UN} = unloading displacement of a sheathing–to–framing connection, hysteresis model parameter;

Δ = displacement at top of shear wall, or displacement at midspan of diaphragm;

Δ_{max}^{+} = maximum mid–span displacement when pushing the diaphragm during cyclic loading;

Δ_{max}^{-} = maximum mid–span displacement when pulling the diaphragm during cyclic loading;

Δ_{total} = total deflection of a shear wall or a horizontal diaphragm;

$\Delta_{bending}$ = flexure contribution to the deflection of a shear wall or a horizontal diaphragm;

Δ_{shear} = shear contribution to the deflection of a shear wall or a horizontal diaphragm;

Δ_{nail} = sheathing-to-framing deformation contribution to the deflection of a shear wall or a horizontal diaphragm;

$\Delta_{anchorage}$ = anchorage connection deformation contribution to the deflection of a shear wall or a horizontal diaphragm; and

Δ_{chord} = chord splice connection deformation contribution to the deflection of a shear wall or a horizontal diaphragm;

θ = displacement angle for a sheathing-to-framing connection with respect to the x axis and y axis;

ϕ = displacement angle for a sheathing-to-framing connection with respect to the initial displacement;

μ = displacement ductility for a sheathing-to-framing connection.

Chapter 1

INTRODUCTION

1.1 Overview

In wood housing, lateral forces induced by earthquakes or strong winds are usually resisted by a system of wood-frame shear walls and diaphragms (roofs or floors). Lateral forces are transferred from the roof and floors, as depicted in Fig. 1.1, through diaphragm action, to supporting shear walls and eventually into the foundation. In Fig. 1.2 the primary structural components of wood shear walls and diaphragms are shown. Wood framing and sheathing panels are connected using fasteners (nails or staples). Additionally, shear walls may employ anchorage devices, and large diaphragms may require chord splice connections. Conventionally, sheathing panels consist of a wood material, such as plywood or oriented strand board (OSB).

Wood shear walls and diaphragms have generally performed well during earthquakes, in terms of preserving life (Zacher 1994). In spite of this performance, the costs of building damage to wood structures—for example, in the Northridge 1994 earthquake and 1992 Hurricane Andrew—has prompted an interest in shifting design emphasis from life-safety to damage control (Rosowsky and Ellingwood 2002). Although the design philosophy of the current codes in North America has not changed from life-safety, limiting structur-

al damage may become a primary objective of next-generation performance-based design procedures (FEMA 2000). For wood structures, performance-based design may more precisely be termed displacement-based design, because the primary objective is to limit inter-story drift.

Displacement-based design is considered to have a number of advantages compared to conventional force-based design (Filiatrault and Folz 2002). In the conventional forced-based design, the force required so that wood structures remain elastic is determined. The

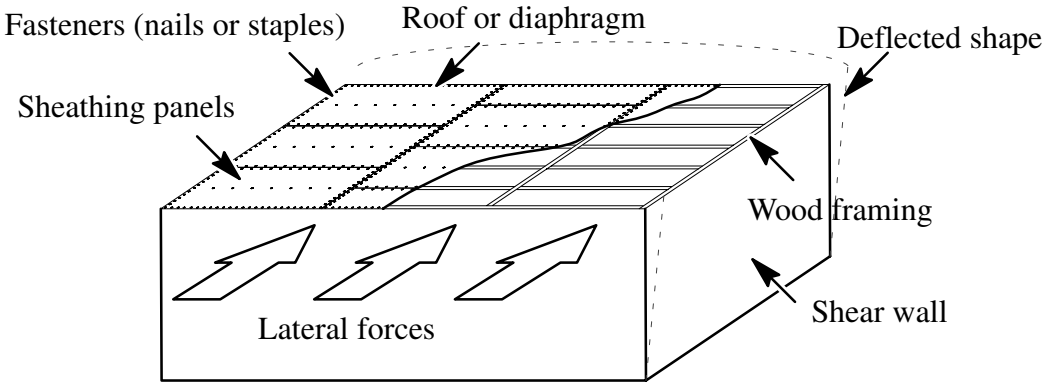

Fig. 1.1. Lateral force resisting system in wood-frame structures

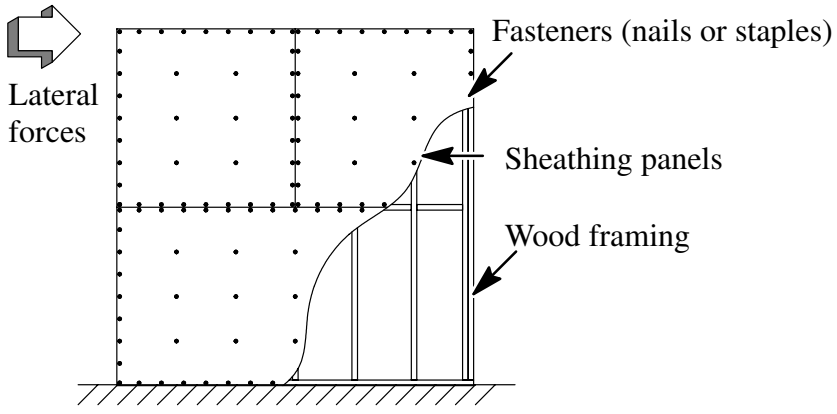

Fig. 1.2. Primary structural components of wood-frame shear walls and diaphragms

design force is then obtained by dividing the elastic force by a reduction factor R, which is used to account for structural ductility. The R factor is difficult to determine, however, because wood structures are inelastic, even at lower load levels. In a displacement-based design, the structure must meet a target displacement (such as inter-story drift) instead of a force requirement. Thus, neither an elastic estimate of the structure, nor a reduction factor is necessary.

Displacement-based design requires an understanding of the pushover (monotonic) response and energy dissipation characteristics of the wood shear wall or diaphragm (Filiatrault and Folz 2002). This knowledge can be acquired through experimental testing and structural analysis. Although experimental testing cannot be completely replaced, executing a structural analysis computer program is typically less expensive and less time-consuming than testing.

For wood shear walls, a variety of structural analysis tools are available. The most simple consist of a single degree of freedom (SDOF) system (Medearis 1970; Stewart 1987; Foliente 1995; van de Lindt and Walz 2003). In a SDOF system, the relationship between the applied force and lateral displacement at the top of a shear wall is calibrated to data from experimental testing. An advantage of using a SDOF system is that it may easily be employed in a subsequent dynamic analysis. Nevertheless, SDOF systems are limited to the specific materials and configurations used to calibrate the model and are seldom used for wood diaphragm analysis.

A number of specialized structural analysis programs for wood shear walls have been developed based on the understanding that the overall lateral behavior is dominated by the individual behavior of sheathing-to-framing connections (Tuomi and McCutcheon 1978; Gupta and Kuo 1985: Gupta and Kuo 1987; Filiatrault 1990; Dinehart and Shenton 2000;

Folz and Filiatrault 2000; Richard et al. 2002). In these structural analysis programs, sheathing-to-framing connections are represented using a single nonlinear spring or using a pair of orthogonal nonlinear springs. In general, wood framing is assumed to be rigid and pin-connected, and all sheathing panels are assumed to undergo the same rotation and translation. It is important to note that this latter assumption is not valid for wood diaphragms, however, since sheathing panels near the midspan may rotate less relative to panels near the supports.

The finite element method has been successfully used to develop structural analysis programs for both wood shear walls and diaphragms (Easley et al. 1982; Itani and Cheung 1984; Dolan and Foschi 1991; White and Dolan 1995; Fonseca 1997; He et al. 2001; Symans et al. 2001; Hite and Shenton 2002). Wood framing is represented using standard linear beam elements. Sheathing panels, insulation, exterior (stucco) and interior (gypsum wall board) finish materials, if included, may be represented using linear plane-stress elements. Sheathing-to-framing connections are represented using nonlinear spring elements, and chord splices are represented using linear spring elements. An advantage of a finite element analysis is increased understanding of force distribution between structural components. A disadvantage is that the amount of information and detailed computer modeling required are cumbersome for routine design. Besides, for wood shear walls, the more sophisticated finite element analysis programs yield approximately the same accuracy as the simpler specialized structural analysis programs (Folz and Filiatrault 2001).

An overarching concern with currently available structural analysis programs is the lack of a rigorous analytical model for sheathing-to-framing connections. Structural analysis programs that represent sheathing-to-framing connections using one nonlinear spring (single spring model) are incapable of reversed cyclic loading (Folz and Filiatrault 2001). This limitation is significant because reversed cyclic loading is required to determine energy

dissipation characteristics. Furthermore, structural analysis programs using a single spring model may be unstable, especially near ultimate loading.

Structural analysis programs that represent sheathing-to-framing connections using two orthogonal nonlinear springs (non-oriented spring pair model) overestimate connection strength and stiffness. For wood shear walls, Folz and Filiatrault (2001) proposed a method to compensate for the overestimation of strength and stiffness using the structural analysis program *CASHEW* (Folz and Filiatrault 2000). In *CASHEW*, the sheathing-to-framing connection spacing is scaled, or adjusted, internally within the computer program until the energy absorbed by the wall using a non-oriented spring pair model agrees with the energy absorbed by the wall using a single spring model. Although this method successfully compensates for the overestimation for wood shear walls, it is not a feasible method for many structural analysis programs, such as a general purpose finite element program.

1.2 Objectives and Scope

The primary objective of this paper is to develop analytical models of wood-frame shear walls and diaphragms for monotonic, quasi-static (cyclic), and dynamic analyses, and to quantify the effects of sheathing-to-framing connection parameters, hysteresis model parameters, and analytical complexity.

The effects of various aspects of wood-frame shear walls and diaphragms are beyond the scope of this thesis. Namely, anchorage devices, non-structural finishes, and various support conditions are not considered. Therefore, the findings of this thesis need to be viewed in proper perspective because the actual (in-situ) response shear walls and diaphragms are influenced by these additional aspects. Notwithstanding, the analytical models developed

in this thesis may be used to clarify the contribution of non-structural elements or anchorage devices to the overall structural response.

1.3 Thesis Organization

In Chapter 2 the measured response of sheathing–to–framing connections (or coupons) and shear walls and diaphragms is discussed. Since the response of sheathing–to–framing connections is important to the overall analysis of shear walls and diaphragms, the methods used in coupon testing, coupon assembly, coupon configuration, and data reduction are discussed in detail. Also, the strength and behavior of individual connections between glass fiber reinforced polymer panels (GFRP) sheathing panels and wood framing are determined (Judd and Fonseca 1998; 2002).

In Chapter 3 analytical modeling of sheathing-to-framing connections is discussed. The theoretical connection capacity is predicted using a general form of the European Yield Model (EYM). The discussion of the monotonic and cyclic force-displacement relationship for sheathing–to–framing connections includes previously developed hysteresis models, such as the Bilinear, Clough, Q-Hyst, and modified Stewart models, as well as a newly developed model, the Q-Pinch model.

A new analytical model for representing sheathing–to–framing connections in structural analysis is also proposed in Chapter 3. The new model is likely the most consequential contribution of this thesis. The new analytical model represents sheathing–to–framing connections using an oriented pair of nonlinear springs. In contrast with the single spring model and the nonoriented spring pair model, the new model is suitable for monotonic, quasi-static (cyclic), and dynamic analyses. The new analytical model is implemented in a general pur-

pose finite element program in Chapter 4 and in a specialized structural analysis program in Chapter 5.

In Chapter 4, finite element analysis of shear walls and diaphragm is discussed. Two commercial finite element programs, *ANSYS* (2003) and *ABAQUS* (2000) are demonstrated. The new analytical model is implemented into *ABAQUS* and validated against measured experimental data for monotonic, cyclic, and dynamic analysis (Judd and Fonseca 2002a; 2003a; 2004a). Parametric studies are also conducted to determine the sensitivity of the finite element models to changes in material and section properties, hysteresis model, and model complexity.

In Chapter 5 the new analytical model is implemented in a specialized structural analysis program, *CASHEW* (Folz and Filiatrault 2000) for cyclic analysis of shear walls and validated against measured data (Fonseca and Judd 2004a).

In Chapter 6 another analytical model for shear walls and diaphragms that is less complex in comparison to the models discussed in previous chapters is discussed. The model is intended for either routine use or for dynamic analysis where the complexity of the finite element models or limitations of the *CASHEW* models preclude their effective use. The new analytical model, *QUICK*, consists of a equivalent single degree of freedom system where the parameters may be determined using either of two methods. In the first method an equivalent response is calibrated using experimental or analytical data. In the second method an equivalent response is estimated based on the relative contribution of structural elements and using sheathing-to-framing connection data. The model is validated against measured experimental data and used in a parametric study to quantify the effects of hysteresis model parameters, including loading, unloading, pinching, and strength and stiffness degradation parameters, on dynamic response (Judd and Fonseca 2004d).

In Chapter 7 two applications of the analytical models are illustrated. In the first application, the advantages of hybrid shear walls or diaphragms, with glass fiber reinforced polymer (GFRP) panels in conjunction with plywood panels, are studied. The potential use of hybrid shear walls and diaphragms is considered for rehabilitation or new construction (Judd and Fonseca 2000a,b; 2001; 2002c; 2003b). In the second application, the response of shear walls with improperly driven (or overdriven) nails is determined (Rabe et al. 1999; Judd and Fonseca 2004c; Fonseca and Judd 2004b). A method to estimate the reduction in capacity caused by both the depth and the percentage of total nails overdriven is proposed.

In Chapter 9 a summary of the research findings are given and the conclusions are drawn. Recommendations for future research and indications as to the potential impact of the research findings in this thesis are then suggested.

Chapter 2

MEASURED RESPONSE

In this chapter, the measured response of individual connections between sheathing panels and wood framing and the measured response of shear walls and diaphragms are discussed. The methods used in testing, assembly, configuration, and data reduction are discussed in detail. The strength and behavior of individual connections between glass fiber reinforced polymer (GFRP) sheathing panels and wood framing are tested as part of this thesis. Other measured responses reported are compiled or extracted from the sources cited.

2.1 Overview

A wide variety of shear wall, diaphragm, and sheathing-to-framing (coupon) experimental data exists (van de Lindt 2004). Specific configurations and materials used in this thesis are not intended to be exhaustive. Instead, the results are indicative of common materials used in current construction. Shear walls or diaphragms using different sheathing materials, fastener types, and wood framing could be expected to have similar trends in strength and behavior. General dowel equations discussed in Chapter 3 provide a basis for extrapolating sheathing-to-framing connection response to connections with different components.

In addition to discussing the measured response of shear walls and diaphragms, the measured response of individual connections between sheathing and wood framing deter-

mined through coupon testing is also discussed. The coupon testing results are valid for several reasons. Research experience has demonstrated that the overall response of a shear wall or diaphragm is governed by the behavior of the individual sheathing–to–framing connections (Foliente 1995). Testing coupon specimens also allows a spectrum of connection configurations, materials, and loading protocols to be considered efficiently. Moreover, coupon tests are less expensive and faster to complete, compared to testing of full-scale shear walls or diaphragms.

Although the measured response of in-situ wood-frame shear walls and diaphragms is beyond the scope of this thesis, recent findings are briefly discussed. Filiatrault et al. (2002) tested in-situ diaphragms under quasi-static loading to investigate diaphragm flexibility. The results indicated that, among other factors, supporting walls acting as chord members significantly increased the diaphragm stiffness. Paevere et al. (2003) tested a one-story L-shaped wood-frame house under static and cyclic loading. The results indicated that significant redistribution of lateral load between shear walls and diaphragms is possible.

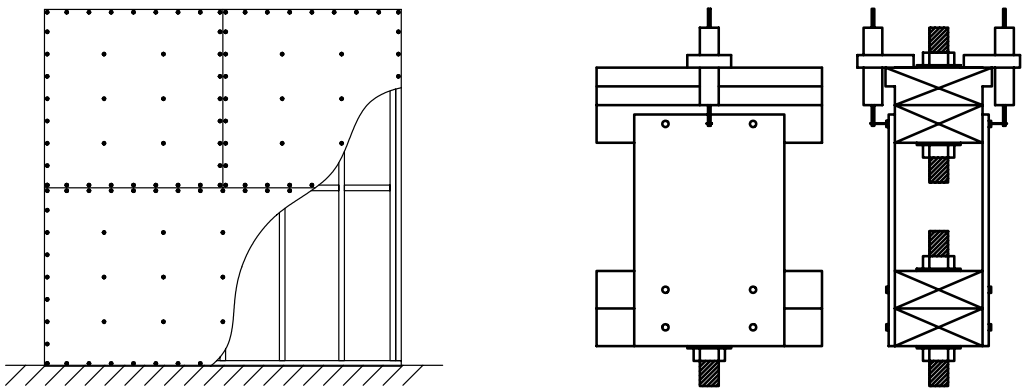

(a) Full-scale specimen (b) Coupon specimen

Fig. 2.1. Primary structural components of wood-frame shear walls and diaphragms

2.2 Sheathing-to-Framing Connections

A survey summary of sheathing–to–framing connection testing is shown in Table 2.1. Although sheathing–to–framing connections were first tested over fifty years ago by Countryman (1952), the bulk of the data was developed in the last twenty years. Perhaps one reason the amount of testing has ballooned in recent years may be that increased computational capacity has rendered analytical modeling of shear walls and diaphragms more feasible. Analytical modeling, in turn, is dependant upon the response of sheathing–to–framing connections. The Table also shows that recent research has emphasized the importance of ascertaining the cyclic and dynamic response.

Table 2.1. Survey Summary of Sheathing-to-Framing Connection Testing

Reference	Monotonic	Cyclic	Dynamic	Primary components
Cruz (1993)	✓	✓		plywood, nails
Kent, Gupta, Miller (1996)	✓	✓	✓	plywood, nails
Ni, Chui (1994)	✓	✓	✓	plywood, nails
Gutshall (1994)	✓	✓	✓	plywood, nails, bolts
Dolan, Gutshall, McLain (1994)	✓	✓	✓	plywood, nails, bolts
Winistorfer, Soltis (1993)		✓		floor-wall-foundation
Dolan, Madsen (1992)	✓	✓		plywood, nails
Gavrilovic, Gramatikov (1991)	✓	✓		metal plate
Dolan (1989)	✓	✓		plywood, nails
Dean (1988)		✓		plywood, nails
Girhammar, Anderson (1988)	✓			plywood, nails, bolts
Chui, Ni, Jiang (1998)		✓		plywood, nails
Polensek, Schimel (1988)			✓	floor-wall-foundation
Polensek, Bastendorff (1987)		✓		various
Soltis, Mtenga (1985)			✓	floor-wall-foundation
Jacobsen (1960)		✓		plywood, nails, bolts
Kaneta (1958)		✓		plywood, nails
Countryman (1952)	✓			plywood, nails

Table 2.2. identifies a number of parameters that influence the response of sheathing-to-framing connections. The dominating parameters are the fastener type and diameter, the wood thickness (for both the side and main members, if applicable), and the applied loading. The connection strength and stiffness is affected by the specific gravity of the wood (Fonseca et al. 2002; McLain 1975; Wilkinson 1972; Mack 1960). The strength of the connection is altered if the wood seasons in service.

Table 2.2. Parameters Influencing Sheathing-to-Framing Connection Response

Connection Component	Parameter	Reference
Wood member	Wood specie	Fonseca et al. (2002), Hunt and Bryant (1990), Ehlbeck (1979)
	Moisture content	Fonseca et al. (2002), Hunt and Bryant (1990), Leach (1964)
	Thickness	Fonseca et al. (2002), Leach (1964), Mack (1960)
	Edge distance	Fonseca et al. (2002)
Fastener	Type, Diameter	Albert and Johnson (1967)
	Material	Fonseca et al. (2002), Hunt and Bryant (1990)
	Surface texture	Hunt and Bryant (1990)
	Wood penetration	Fonseca et al. (2002), Hunt and Bryant (1990)
	Head depth	Fonseca et al. (2002)
Configuration	Type	Fonseca et al. (2002), Hunt and Bryant (1990)
	Fastener pattern	Hunt and Bryant (1990)
	Grain direction	Hunt and Bryant (1990)
	Friction	Hunt and Bryant (1990)
Loading	Direction	Dolan et al. (1994), Hunt and Bryant (1990)
	Duration	Hunt and Bryant (1990)

If the moisture content is below the wood fiber saturation point, however, then this alteration is negligible (Leach 1964). Although the strength of the connection correlates in relation to the thickness of the wood members, the initial stiffness does not change significantly (Leach 1964; Mack 1960). All other parameters held the same, increased fastener diameter generally results in an increased connection capacity (Albert and Johnson 1967). A more complete review of these parameters is given by Fonseca et al. (2002), Hunt and Bryant (1990), and Ehlbeck (1979).

The sheathing-to-framing connection types considered in this study are described in Table 2.3. The inclusion of a connection type was based on two criteria: first, relevance of the connection type, and second, availability of both coupon test data and full-size wall or diaphragm test data. GFRP sheathing-to-framing connections tested in this research have not been considered previously. Other connection types considered in this investigation have been previously tested and, as a consequence, primarily only the results of those studies are included here. For the GFRP connections, the testing specimens, configuration, and loading protocols used will be explained in detail. Information for the connection types not tested as a part of this study are available in the references shown in Table 2.3.

2.2.1 GFRP Sheathing-to-Framing Connection Testing

Testing Schedule. The coupon testing schedule is shown in Table 2.4. Three types of connections using 3.33-mm-diameter × 63.5-mm-long (8d common) nails, 3.76-mm-diameter × 76.2-mm-long (10d common) nails, and 4.12-mm-diameter × 88.9-mm-long (16d common) nails were tested. The coupon tests using the nail sizes chosen give an indication of the effect of nail diameter on connection strength and behavior.

Table 2.3. Sheathing-to-Framing Connections Considered

Sheathing		Nail			
Thickness (mm)	Material	Diameter × length (mm)	Overdriven depth (mm)	Loading protocol	Source
9.53	OSB	2.67 × 50.0	—	Monotonic, Cyclic	(Durham 1998)
6.35	GFRP	3.33 × 63.5	—	Monotonic, Modified ISO Cyclic	Appendix A
		3.76 × 76.2	—	Monotonic, Modified ISO Cyclic	
		4.12 × 88.9	—	Monotonic, Modified ISO Cyclic	
9.53	Plywood	3.33 × 63.5	—	Monotonic, Modified ISO Cyclic	Appendix A (Dugan 1995)
			—	Monotonic, Cyclic	(Dolan and Madsen 1992)
9.53	Waferboard	3.33 × 63.5	—		(Dolan and Madsen 1992)
11.1	OSB	3.33 × 63.5	—	SPD Cyclic	(Rabe 2000)
		2.87 × 60.3	—		
			1.59		
			3.18		
			4.76		
11.9	Plywood	3.33 × 63.5	—	SPD Cyclic	(Burns 2001)
		2.87 × 60.3	—		
			1.59		
			3.18		
			4.76		
12.7		3.76 × 76.2	—	Monotonic	(Countryman 1952)

Table 2.4. GFRP Coupon Testing Schedule

Nail diameter × length (mm)	GFRP sheathing thickness (mm)	Loading protocol	Replicates
3.33 × 63.5	6.35	Monotonic	9
		Modified ISO Cyclic	10
3.76 × 76.2		Monotonic	12
		Modified ISO Cyclic	13
4.12 × 88.9		Monotonic	9
		Modified ISO Cyclic	12

Since 9.53-mm (3/8 in.)-thick GFRP panels (which would match the thickness of commonly used plywood panels) were not available, the next closest panel thickness, 6.35 mm (1/4 in.), was selected.

As a preliminary study, connections using 3.76-mm-diameter × 82.6-mm-long (12d common) nails were tested to investigate the effect of nail length—the only difference between a 10d and a 12d nail is the length; whereas 10d nails are 76.2-mm (3 in.)-long, 12d nails are 82.6-mm (3.25 in.)-long. After three tests, no significant differences between connections using 10d and 12d nails were evident. Subsequently, specimens using 12d common nails were not considered further.

Plywood sheathing–to–framing tests were not performed. This type of connection was tested previously using similar coupon specimen configuration and loading protocols as part of an analysis of plywood horizontal diaphragms (Fonseca 1997). For Fonseca's study, Dugan (Dugan 1995) tested connections using 8d common nails and 9.53 mm (3/8 in.) thick structural grade plywood sheathing (C–D Exterior). Monotonic loading was applied to 10 specimens and cyclic loading was applied to 12 specimens. For purposes of comparison, the response of these plywood connections are presented along side the GFRP connection results. The loading protocol (either monotonic or cyclic) is listed and the replicates,

or number of specimens tested for each connection type are shown. The number of specimens tested varied because some were damaged prior to testing or because additional specimens were constructed. A total of 65 coupon specimens were tested.

Assembly Procedure. The assembly procedure for construction of the GFRP sheathing-to-framing connection coupon specimens is given in this section. The specimens were constructed of 2×4 in. (nominal) Douglas Fir–Larch No.2 wood framing members, sawn into 9 in. long segments. Each specimen required two wood segments in the bottom and one segment in the top (to be replaced later by another segment, after completion of the cyclic test). Four wood segments were stacked (on the wide side), held together with tape, and then a 3/4 in. hole was drilled directly through the middle of the wide side. This procedure yields consistently aligned holes for the framing members in each specimen.

The GFRP panels were provided in standard 4 ft. $\times$ 8 ft. sheets from the lumber yard. The sheets were cut by a water–jet saw into 9 in. $\times$ 6 in. panels. The sheets were cut so that the fibers in the GFRP panel would be aligned perpendicular to the force applied. The cut panels were handled similar to that of the wood framing members (in that similar panels, from the same batch ideally, were taped together in stacks, ready for predrilling). Two panels were used to construct each specimen. Pilot holes were drilled into the panels to allow the nails to pass through the holes. The recommended pilot hole sizes are given in Table 2.5.

Table 2.5. GFRP Sheathing Panel Pilot Hole Drill–Bit Diameter (mm)

Fastener Type	Drill–Bit Diameter (in.)
8d Common Nail	3.10 (0.122)
10d Common Nail	3.66 (0.144)
16d Common Nail	4.01 (0.158)

The appropriate size of the pilot hole was determined by trial and error using a sample panel and wood framing member. This trial and error process was the basis for the first 10 (or so) specimens. However, during the construction of some of the specimens, it was difficult to drive the nails because the holes were too tight. If the pilot holes are too small for the nail, cracks will develop radially from the hole. Pilot holes were drilled, as shown in Fig. 2.2, with the line of holes offset from the opposite side, to prevent nails from being driven into the nails of the opposite side.

The specimens were constructed by placing one of the rods (used to apply the load in the testing machine) through all four wood framing members, as shown in Fig. 2.3. The wood members were secured with washers and nuts. Then one GFRP panel was fastened to the wood framing, as shown in Fig. 2.4. This procedure insured that the loading rod holes in the top of the specimen remained aligned with the bottom loading rod holes while the nails were driven through the GFRP panel pilot holes and into the wood framing. The coupon test specimen was rotated and this process was repeated to fasten the remaining GFRP panel to the opposite side. A typical coupon specimen is shown in Fig. 2.5.

Coupon Specimen Configuration. Each specimen consisted of 6.35-mm (0.25 in.)-thick GFRP panels nailed to 38.1×88.9 mm (2×4 in.-nominal) Douglas Fir–Larch No.2 wood members using 8d, 10d, or 16d common nails. The GFRP panels are oriented so that the fibers are parallel to the wood framing (or orthogonal to the applied loads). The grain of the wood framing was oriented orthogonal to the applied load as well.

Dry wood was used (14–15% moisture content) to simulate the "in-situ" environment of wood–frame construction. The wood specie and commercial grade chosen are typical of materials used in current construction.

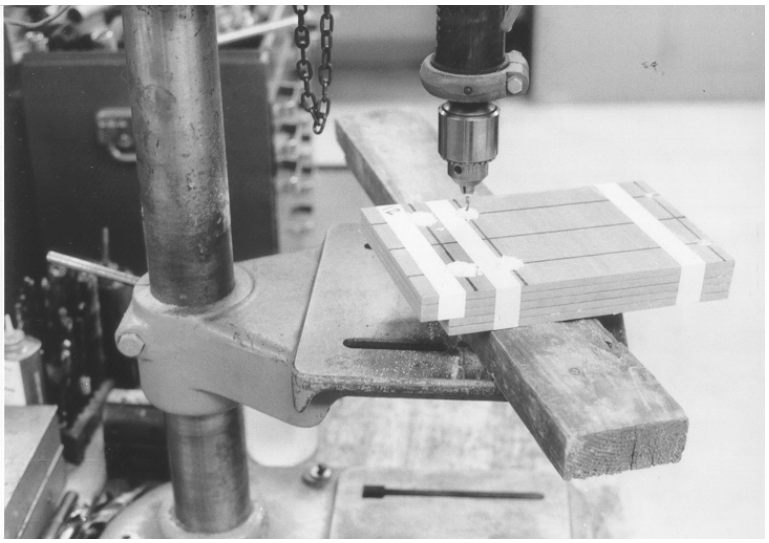

Fig. 2.2. Pre-drilling pilot holes in GFRP sheathing panels

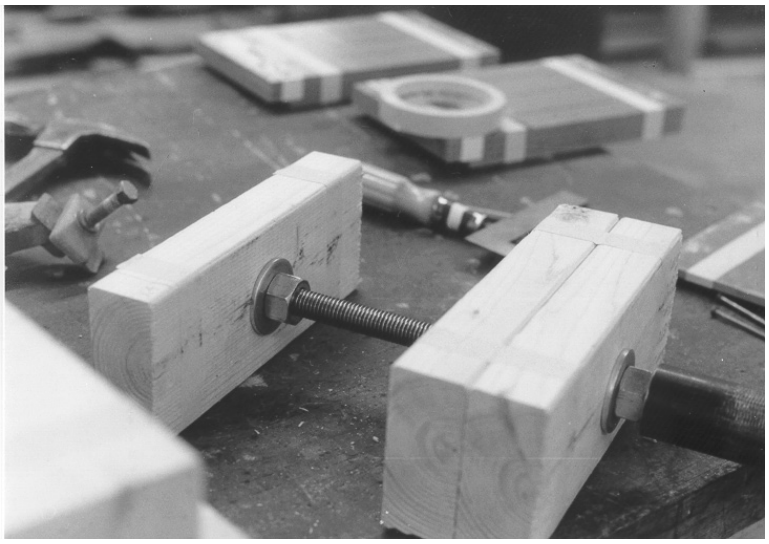

Fig. 2.3. Aligning loading holes in wood framing

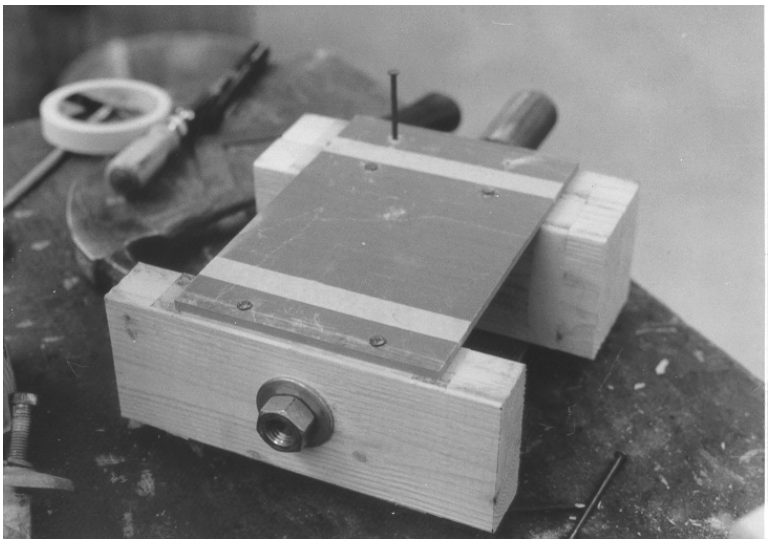

Fig. 2.4. Fastening GFRP sheathing panels to wood framing

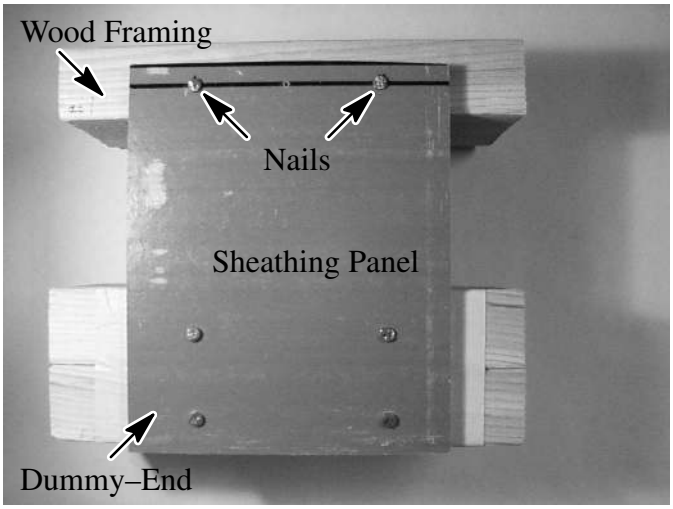

Fig. 2.5. GFRP coupon testing specimen

The nails were driven through pre–drilled holes. The hole diameters, 3.10 mm, 3.66 mm, and 4.01 mm were slightly smaller than the diameter of 8d, 10d, and 16d common nails, respectively. In construction practice, it is likely impractical to first drill pilot holes through the GFRP sheathing panels and then apply nails. An alteration of the panel, or holes pre–drilled in the "shop," may be necessary. Adhesives may also be considered as a means to attach the panels to the framing. These considerations are beyond the scope of the current study, however, and require further research.

All specimens used GFRP panels purchased retail or "off the shelf." The GFRP panels are a unidirectional combination of glass fiber reinforcement and isophthalic resin (*EXTREN™ Series 500*) fabricated using a pultrusion process. A bidirectional panel was not used because cracking parallel to the applied load was not anticipated. The mechanical properties of the GFRP panels are published by the manufacturer (Strongwell, Inc. 1998). The modulus of elasticity is 17,940 MPa, the shear modulus is 2,932 MPa, and poisson's ratio is 0.33 for the GFRP panels used in this study.

Previous Testing Apparatuses. *ASTM D 1761–88 (2000)* Standard Test Methods for Mechanical Fasteners in Wood, describes the standard fixture and procedure for lateral testing of wood connections. The ASTM standard is intended to be used for a single fastener in simple shear. Because of eccentricity, however, the applied load also causes a moment within the connection. The test fixture partially accounts for this accidental moment by providing a roller to counter the moment. The ASTM test fixture gives rise to several concerns: (1) eccentricities are applied through the connection; (2) friction exists between the sheathing and framing members; and (3) the apparatus is not viable for cyclic loading schemes.

Previous research has suggested several alternative fixtures (Antonides et al. 1979; DeBonis and Bodig 1975; Jenkins et al. 1979; McClain 1975; Stone et al. 1980: Lau and

George 1987). Pellicane and Bodig (1982) compared many fixtures and indicated there was no significant difference between the results after 0.1 in (0.25 cm) of slip. Smaller levels of slip, unfortunately, were highly dependent on the testing fixture. Pellicane (1991; 1993) has developed a modified ASTM test fixture which moves the line of the applied force to the interface of the two members being tested to eliminate loading eccentricity, and allows for the control of the gap between the two members being tested.

Liu and Soltis (1984) developed a new testing apparatus and noted that no consensus had been reached on the preferred method of testing. Their fixture clamps the framing member and uses rollers to control the movement of the panel and the gap distance. The line of force was also moved to act through the interface of the members to minimize load eccentricity. Their fixture allows testing of connections with framing members of different dimensions.

One problem with many of the modified designs is that a significant amount of preparation time is required for each sheathing-to-framing connection specimen. The apparatus developed by Liu and Soltis, for example, requires the adjustment of twelve bolts for each sample. As previously discussed, the primary motivation for coupon testing is the ability to consider a wide variety of specimens quickly. Therefore, the time required for use of Liu and Soltis's apparats is not optimum.

Rabe (2000) designed a simplified apparatus to minimize the preparation time required and to minimize the clamping forces on the specimen. In Rabe's apparatus, the sheathing panel is restrained to in–plane movement, a predetermined gap distance is maintained, monotonic and cyclic loading protocols may be used, and the apparatus is adjustable.

Proposed Testing Apparatus. The problems inherent with a testing apparatus were avoided in this research by using the coupon specimen configuration and apparats shown in

Fig. 2.6. The configuration used has a number of unique features. Two load–displacement relationships are provided (one per face) for each specimen. The inelastic response of the connection was limited to one of the ends by using only 4 nails (2 nails on each face) at the top end of the specimen, while using 8 nails (4 nails on each face) at the bottom, or dummy–end, of the specimen. A Linear Variable Differential Transducer (LVDT) attached to each face measured the relative displacement between the wood framing and the GFRP sheathing panels. The LVDTs were mounted on a wood block at the top end of the specimen. Additionally, the specimen configuration allows out–of–plane movement of the sheathing. Since out–of–plane movement is unrestrained in full–scale diaphragms, the coupon specimen replicates actual conditions.

Lateral Loading Procedure. A modified form of the proposed ISO 1997 lateral loading procedure (ISO 1997) was used to test the coupon specimens. This procedure consists of two loading protocols: The first loading protocol (monotonic loading) is similar to the *ISO Standard 6891–1983* (ISO 1983) where a ramp load is applied, 2.54 mm (0.1 in.)

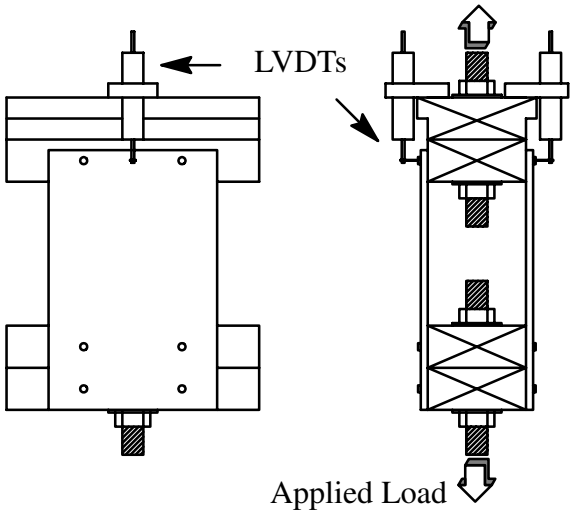

Fig. 2.6. GFRP coupon testing specimen and configuration

per minute, until failure. The second loading protocol (cyclic loading) consists of a quasi–static fully–reversed cyclic scheme. This multi–step loading protocol uses three fully–reversed cycles of constant displacement amplitude followed by three cycles of increased displacement amplitude. This pattern continues until failure.

The cyclic loading protocol is shown in Table 2.6. The loading step number, number of fully–reversed cycles, amplitude, and completion time for each step are listed. In this loading protocol, the loading frequency for the initial step is 0.033 hz. The loading frequency decreases to 0.017 hz for the next five steps and to 0.011 hz for the remaining steps.

The lateral loading procedure used is appropriate. Monotonic loading provides an indication of the connection load–displacement envelope, energy absorption, and stiffness. The cyclic protocol allows a load–displacement relationship to be established and connection degradation properties to be estimated. Also, the load steps during cyclic loading are much smaller than the expected displacement at failure. Perhaps more importantly, the specimen response under cyclic loading protocols is indicative of the stiffness, ultimate strength, strength degradation, and failure mechanism of connections in diaphragms during actual lateral loading. This is evident even though cyclic loading protocols are not descriptive of seismic or wind loading per se (Dolan and Madsen 1992).

Observed Failure Mechanisms. During testing of the coupon specimens, four primary failure mechanisms were observed: nail withdrawal, nail fatigue, sheathing failure, and wood splitting. Each failure mechanism is also shown in Fig. 2.7. Summaries of observed responses for monotonic and cyclic loading are shown in Table 2.7 and in Table 2.8, respectively. For each connection type, the failure mechanism as a percentage of the total specimens observed is given.

Table 2.6. Modified ISO Cyclic Loading Protocol

Step No.	Number of Fully–Reversed Cycles	Amplitude (mm)	Step Completion Time (min.)
1	3	1.02	1.5
2	3	1.52	1.5
3	3	2.03	3.0
4	3	2.54	3.0
5	3	3.05	3.0
6	3	4.06	3.0
7	3	5.08	4.5
8	3	6.35	4.5
9	3	7.62	4.5
10	3	8.89	4.5
11	3	10.2	4.5

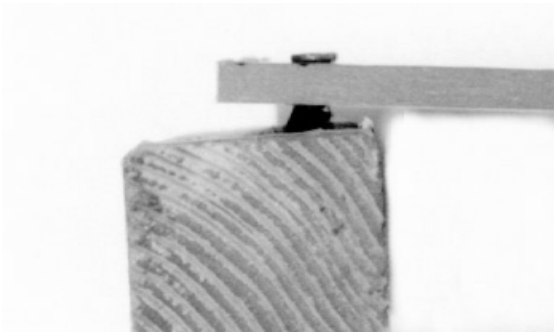

(a) Nail withdrawal

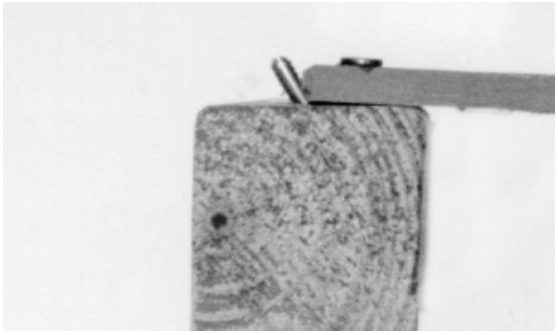

(b) Nail fatigue

(c) Sheathing cracking

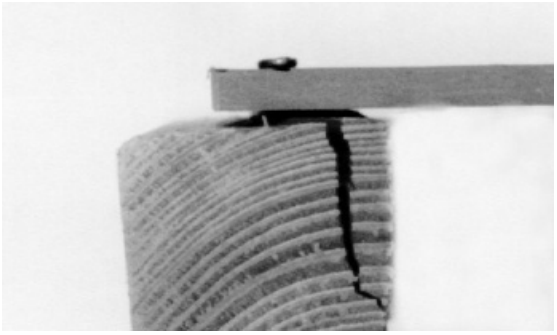

(d) Wood splitting

Fig. 2.7. GFRP coupon testing: primary failure mechanisms

Table 2.7. GFRP Coupon Testing: Observed Monotonic Response

	Primary failure mechanism (% of total specimens)			
Sheathing-to-framing connection	Nail withdrawal	Nail fatigue	Sheathing failure	Wood splitting
9.53-PLY–3.33-COMMON–FLUSH	—	—	100	—
6.35-GFRP–3.33-COMMON–FLUSH	56	—	—	44
6.35-GFRP–3.76-COMMON–FLUSH	17	—	—	83
6.35-GFRP–4.12-COMMON–FLUSH	11	—	—	89

Table 2.8. GFRP Coupon Testing: Observed Cyclic Response

	Primary failure mechanism (% of total specimens)			
Sheathing-to-framing connection	Nail withdrawal	Nail fatigue	Sheathing failure	Wood splitting
9.53-PLY–3.33-COMMON–FLUSH	—	50	50	—
6.35-GFRP–3.33-COMMON–FLUSH	—	100	—	—
6.35-GFRP–3.76-COMMON–FLUSH	8	62	—	30
6.35-GFRP–4.12-COMMON–FLUSH	25	—	17	58

In the Nail Withdrawal Mechanism, the connection fails due to the nail(s) being pulled out, or withdrawn, from the wood framing. See Fig. 2.7*a*. This occurs when, as the nails are deformed, the clamping force between the framing and the panels is reduced. During this failure mode, the test may be terminated prematurely to insure that instrumentation equipment is not impaired or damaged. In the Nail Fatigue Mechanism, after fatigue induced by the cyclic loading, the connection fails as the nail(s) fracture. See Fig. 2.7*b*. In the Sheathing Failure Mechanism, the connection failure occurs as nails tear through sheathing edges or sheathing panels crack, breaking off an edge section of the panel. See Fig. 2.7*c*. Tearing through was observed with plywood connections; cracking and breaking was observed with GFRP connections. In the Wood Splitting Mechanism, the connection failure occurs as the nails split the wood framing. See Fig. 2.7*d*.

All plywood specimens exhibited sheathing failure during monotonic loading. During cyclic loading, half of the plywood specimens exhibited sheathing failure, while the remaining specimens failed due to nail fatigue. Such specimens, however, failed due to fatigue only after significant plywood tearing and repeated load reversals (Dugan 1995). Despite the nail fatigue observed, therefore, the primary failure mechanism of PLY–8dc connections appears to be sheathing failure.

The primary failure mechanisms of GFRP–8dc specimens during monotonic loading was withdrawal of the nails from the framing and splitting of the wood. As the larger nail GFRP specimens were tested, the failure mechanism changed to splitting of the wood and there was less nail withdrawal. During cyclic loading, a similar response was observed. As the nail diameter increased, the failure mechanism changed from nail fatigue and withdrawal to wood splitting. Only two GFRP–16d specimens exhibited failure (cracking) of the GFRP sheathing panels. This may indicate that the panel failures are spurious and not representative of typical connection behavior. In any case, the sheathing cracking could presumably be prevented by using bidirectional GFRP panels instead of unidirectional panels.

2.2.2 Idealization of Sheathing-to-Framing Connection Load-Displacement Response

The process for idealization of sheathing-to-framing connection measured response is two tiered: first, idealize the envelope curve, and second, idealize all other response (hysteresis). A typical monotonic response of a sheathing-to-framing connection to a load applied along one line of action is shown in Fig. 2.8. The force-displacement curve may be described using four regions. In Region I, the response is initially linear—an incremental load increase is proportional to the corresponding incremental increase in displacement (ini-

tial stiffness). Here the wood fibers, sheathing, material, and fasteners are essentially elastic. In Region II, a non–linear response characterizes the curve. The non–linearity arises as wood and sheathing fibers crush and/or fasteners begin to yield. In Region III, a nearly plastic plateau is reached and a nearly linear load-displacement relationship is again established (secondary stiffness). Here, depending on the yield mechanism controlling, which may be predicated using the European Yield Model (EYM), either the sheathing, framing, fastener and a combination thereof are yielding (see explanation of modes in the EYM). In Region IV, just prior to failure, the load capacity of the specimen decreases with increasing displacement. This region may be approximated using a negative linear relationship (tertiary stiffness).

Previously, a number of mathematical expressions have been successfully used to idealize envelope (monotonic) load-displacement curves of sheathing-to-framing connections. The discussion here is limited to the most common curves, described as one of four types: power curves, logarithmic curves, exponential curves, and asymptotic curves.

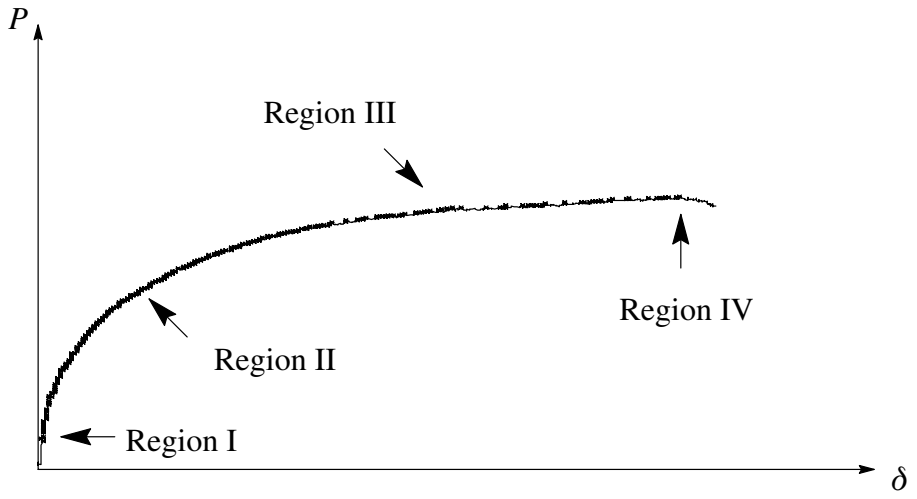

Fig. 2.8. Sheathing-to-framing connection loading (monotonic one-direction) curve

Power Curve. Perhaps one of the first mathematical expressions used was a power curve. A distinct advantage of using a power curve over other expressions is that a power curve may be inverted (i.e. connection force as a function of connection displacement, or displacement as a function of force). Invertability is particularly appealing for design applications. With this in mind, Mack (1977) derived Eq. 2.1 intended for design purposes.

$$P = C_1 d^{\alpha_1} D\delta^{\alpha_2} \tag{2.1}$$

where P is the connection force, δ is the connection displacement, d is the fastener diameter, D is the wood oven-dry density, and C_1, α_1, and α_2 are empirical parameters.

The American Plywood Association (APA) used the power curve given in Eq. 2.2 to idealize tests performed by Countryman (1952).

$$P = C\delta^{1/\alpha} \tag{2.2}$$

where C and α are constants determined from coupon testing. In Eq. 2.2 a limiting load or displacement value is usually stipulated, and the curve past some limiting value is not idealized. The APA power curve was later cast into SI units during the development of a LRFD standard for wood engineering (AF&PA/ASCE 1996) and is readily available in a number of publications, including the Design/construction Guide for Diaphragms and Shear Walls (APA 2004).

Logarithmic Curve. One commonly used mathematical expression is a logarithmic curve developed by McLain (1975), given in Eq. 2.3.

$$P = A \log (1 + B\delta) \tag{2.3}$$

where A and B are constants derived from coupon testing or from using mechanical properties (such as the specific gravity of the members). Pellicane et al. (1991) expanded the applicability of Eq. 2.3 by using mechanical properties (based on coupon tests) to predicting the constants A and B for a range of sheathing-to-framing connection configurations.

Exponential Curve. Another mathematical expression used is an exponential curve, such as those given in Eq. 2.4, Eq. 2.5, and Eq. 2.6. Mack (1966) showed that the load-displacement curve can be idealized up to displacements of 2.54 mm (0.1 in.) using Eq. 2.4.

$$P = C_1(B + A\,\delta)\left[1 - e^{C_2\delta}\right]^{\alpha} \tag{2.4}$$

In Eq. 2.4 A, B, C_1, C_2 and α are empirical parameters accounting for wood specie and moisture content, as well as nail diameter.

Easley et al. (1982) used the curve given in Eq. 2.5 for idealizing the curve up to a certain point, F_{S0} after which the curve was then instead idealized using a linear hardening branch, or secondary stiffness.

$$P = C_1\left(1 - e^{-C_2\delta}\right) \tag{2.5}$$

In Eq. 2.5, C_1 and are empirical constants determined by coupon testing.

A more common exponential curve is given in Eq. 2.6. This curve was first proposed by Foschi (1974; 1977) to idealize sheathing-to-framing connection response without considering a limiting value.

$$P = (P_0 + K_2\,\delta)\left[1 - e^{\frac{-K_1\delta}{P_0}}\right] \tag{2.6}$$

where K_1 is the initial stiffness, K_2 is the secondary stiffness, and P_0 is the secondary stiffness y–axis intercept (not shown is a softening branch past the limiting point, where K_3 is the tertiary stiffness). Note that K_1, K_2, and K_3 are physically identifiable parameters. By defining it as a "physically identifiable parameter" it is intended to signify a parameter inherent (fundamental) to behavior (such as stiffness) that is not specific to any particular equation, in contrast to a parameter that is only a modifier of the equation, and thus indirectly related to behavior.

Dolan (1989) expanded Eq. 2.6 to idealize the curve past the ultimate point by including a softening branch (or negative tertiary stiffness) until failure (when the force is zero). Folz and Filiatrault (2001) made an additional modification to this exponential curve by stipulating a failure displacement, δ_{fail} that terminates the softening branch, as described in Eq. 2.7.

$$P = \begin{cases} (P_0 + r_1 K_0 \delta)\left[1 - e^{\frac{-K_0 \delta}{P_0}}\right], \text{ if } \delta \leq \delta_{ult} \\ P_{ult} + r_2 K_0 (\delta - \delta_{ult}), \text{ if } \delta_{ult} < \delta \leq \delta_{fail} \\ 0, \text{ if } \delta > \delta_{fail} \end{cases} \tag{2.7}$$

Asymptotic curve. Asymptotic curves are also used for idealizing load-displacement response. Originally, the impetus for using an asymptotic curve was that the power and logarithmic curves are continually increasing (unless, of course, a softening branch is used). This behavioral model is clearly incorrect for all loading possibilities. McCutcheon (1985) consequently proposed the curve given in Eq. 2.8.

$$P = \frac{A \delta}{B + \delta} \tag{2.8}$$

where, in Eq. 2.8, A and B are empirical constants determined using coupon testing.

Menegotto and Pinto (1973) developed a more refined asymptotic curve. The curve was originally intended to idealize the response of steel rebars embedded in reinforced concrete beams and used by Stanton and McNiven (1979) for analytical models of the same. Fonseca (1997) and Dugan (1995) subsequently coined the application of Eq. 2.9 for sheathing-to-framing connections in wood-frame diaphragms.

$$P = \frac{P_{yield}\,\delta}{\delta_{yield}}\left[\frac{K_2}{K_1} + \frac{(1 - K_2/K_1)}{\left(1 + \left(\delta/\delta_{yield}\right)^R\right)^{1/R}}\right] \tag{2.9}$$

In Eq. 2.9, K_1 and K_2 are the initial and secondary stiffnesses, respectively, δ_{yield} is the yield displacement, and R is a constant that defines the transition curvature joining the initial and secondary stiffnesses. The curve is terminated at the ultimate displacement δ_{ult} or ultimate load P_{ult}), after which a linear softening branch continues until a failure displacement. Note that Eq. 2.9 degrades into Eq. 2.8 when $K_2/K_1 = 0$ and $R = 1$. In Eq. 2.9, the initial and secondary stiffnesses intersect at the point (δ_{yield} , P_{yield}), or "apparent" yield point.

In summary, although most any load-displacement curve equation is suitable for use, the following criteria are useful in selecting the most amenable curve equation: (1) the curve should use physically identifiable parameters so that the values may be exported easily to other curve equations; (2) the curve should not exhibit problems with fitting data in one region versus another region; and (3) most importantly the curve should be free from possible numerical problems due to an infinite initial stiffness (e.g. the APA power curve) or due to sharp discontinuities.

2.2.3 Idealization of the Response Hysteresis

A typical cyclic response is shown in Fig. 2.9. The load–displacement response of sheathing–to–framing connections under cyclic loading is complex, exhibiting pronounced hysteresis loops. This response is indicative of the highly non–linear, non–conservative, and history–dependant nature of the connections. A comprehensive analysis of the cyclic load–displacement relationship for connections is not considered here. However, the hysteresis

response will be considered in Chapter 3. Instead, envelope curves were identified for each positive and each negative half–cycle to simplify analysis. The envelope curve for each half–cycle is constructed by selecting all the maximum load points for each excursion until the maximum load is attained.

2.2.4 Data Reduction Procedure

Each load–displacement curve was idealized up to the ultimate displacement. See Fig. 2.10. The load–displacement response was not idealized beyond the maximum load. Discontinuous average load–displacement curves were calculated using these idealized curves. In calculating average curves, the measured cyclic response of three GFRP–10dc and two GFRP–16dc specimens were ignored. This was done because either the machine load was incorrectly calibrated or the data acquisition system failed. For similar reasons, one

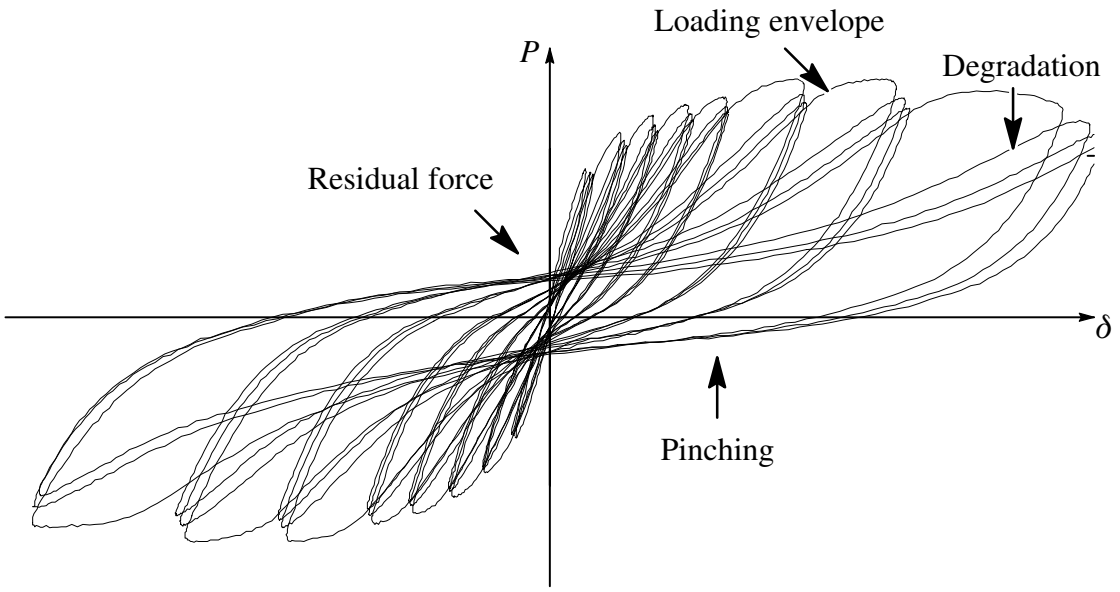

Fig. 2.9. Sheathing-to-framing connection load-displacement hysteresis

measured monotonic response of a GFRP–16dc specimen was not included in the average monotonic curve. Discontinuous average curves were then idealized and terminated where the probability of failure exceeded 50%.

During cyclic loading, the negative half–cycles typically exhibited slightly greater maximum loads and maximum displacements compared to the positive half–cycles. This difference can be attributed to the specimen configuration, which allows bearing between wood framing and fractured nails. Because this bearing is not characteristic of sheathing–to–framing connections in diaphragms, only the positive half–cycle data were used in calculating average curves.

Using the first data points up to a limit, n_1 (about 10 points) the initial stiffness, m_1 was calculated using a linear "least squares" best–fit (for the bivariate case) fit defined by Eq. 2.10.

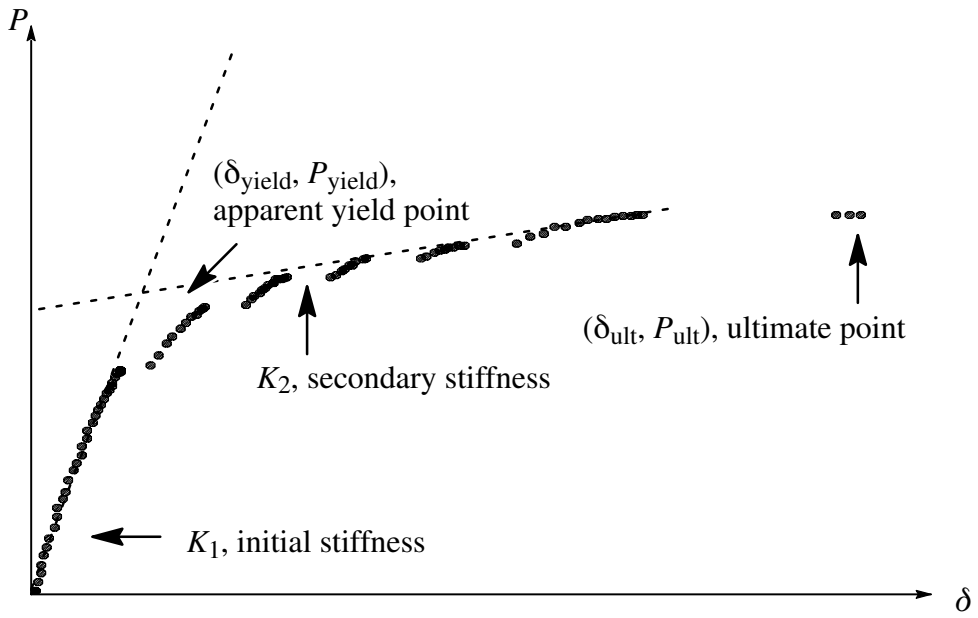

Fig. 2.10. Sheathing-to-framing connection load-displacement idealization

$$m_1 = \frac{\left(\sum_{i=0}^{n_1} {x_i}^2\right)\left(\sum_{i=0}^{n_1} y_i\right) - \left(\sum_{i=0}^{n_1} x_i\right)\left(\sum_{i=0}^{n_1} x_i y_i\right)}{n_1\left(\sum_{i=0}^{n_1} {x_i}^2\right) - \left(\sum_{i=0}^{n_1} x_i\right)^2} \tag{2.10}$$

The line defining the initial stiffness is therefore Eq. 2.11, where the "y-axis intercept" for this line is Eq. 2.11.

$$y_1 = m_1 x - I_1 \tag{2.11}$$

$$I_1 = \frac{\left(\sum_{i=0}^{n_1} x_i y_i\right) - \left(\sum_{i=0}^{n_1} x_i\right)\left(\sum_{i=0}^{n_1} y_i\right)}{n_1\left(\sum_{i=0}^{n_1} {x_i}^2\right) - \left(\sum_{i=0}^{n_1} x_i\right)^2} \tag{2.12}$$

The secondary stiffness, m_2 was defined using the same "least squares" fit, only a different number of data points (starting from the end of the measured set) were used. Correlation coefficients, r_1 for the initial and secondary stiffnesses, was calculated using

$$r_1 = \frac{n_1\left(\sum_{i=0}^{n_1} x_i y_i\right) - \left(\sum_{i=0}^{n_1} x_i\right)\left(\sum_{i=0}^{n_1} y_i\right)}{\sqrt{n_1\left(\sum_{i=0}^{n_1} x_i^2\right) - \left(\sum_{i=0}^{n_1} x_i\right)^2}\sqrt{n_1\left(\sum_{i=0}^{n_1} y_i^2\right) - \left(\sum_{i=0}^{n_1} y_i\right)^2}} \tag{2.13}$$

The initial and secondary stiffnesses meet at an "apparent yield" point location, (x' , y'):

$$x' = \frac{I_2 - I_1}{m_1 - m_2} \tag{2.14}$$

$$y' = m_1 x_0 - I_1 \tag{2.15}$$

If the load and displacement values are normalized with respect to the apparent yield point, then these follow

$$x_{NOR} = \frac{x}{x_0} \tag{2.16}$$

$$y_{NOR} = \frac{y}{y_0} \tag{2.17}$$

$$x_{NOR} = I_{NOR} \tag{2.18}$$

For analysis of stiffness degradation through cycles, each load–displacement curve was shifted along the horizontal axis until the initial load offset was zero (so that each curve starts at the origin, in other words). The value of the horizontal shifting, x_{SHIFT}, was determined as follows in Eq. 2.19. Note that the load values were not altered; there was no shifting along the vertical axis.

$$x_{SHIFT} = \frac{I_1}{m_1} \tag{2.19}$$

A discontinuous average load–displacement curve was determined as the mean load for a given fastener displacement, based upon the total data range used for each fastener and panel combination. The mean load–displacement curve was idealized and terminated where the probability of failure exceeded 25% and 50%. Similarly, discontinuous average load–displacement curves, for plus or minus one standard deviation, were determined and idealized. A study of the distribution of failure displacements and forces was determined using the following definitions for mean, $\bar{x}$ deviation, σ and distribution, $f(x)$.

$$\bar{x} = \frac{\sum_{i=0}^{n} x_i}{n} \tag{2.20}$$

$$\sigma = \sqrt{\frac{\sum_{i=0}^{n} (x_i - \bar{x})}{n - 1}} \tag{2.21}$$

$$f(x) = \left[\frac{1}{\sigma\sqrt{2\pi}}\right] \exp\left[-\frac{1}{2}\left(\frac{x - \bar{x}}{\sigma}\right)^2\right] \tag{2.22}$$

2.2.5 Summary of GFRP Sheathing-to-Framing Connection Response

A summary of the measured response is shown in Table 2.9. For each connection type, the initial stiffness, secondary stiffness, apparent yield displacement, transition curvature, ultimate displacement, and ultimate load are listed. In the case of cyclic loading, only the first and second positive half–cycle results are shown. The second and third half–cycle results are used to determine strength and stiffness degradation. The results indicate that GFRP–8dc connections are approximately twice as stiff under monotonic loading compared to PLY–8dc connections. Under cyclic loading, GFRP connections retained from 75 to 80% of the initial stiffness, whereas plywood connections retained approximately 60% of the initial stiffness.

Table 2.9. Coupon Testing: Envelope Load-Displacement Curve Parameters

Sheathing-to-framing connection	K_1 (kN/mm)	K_2 (kN/mm)	δ_{yield} (mm)	R	δ_{ult} (mm)	P_{ult} (kN)
(a) Monotonic loading						
9.53-PLY–3.33-COMMON–FLUSH	1.643	0.094	0.514	2.000	3.736	1.139
6.35-GFRP–3.33-COMMON–FLUSH	3.922	0.020	0.413	1.500	4.466	1.673
6.35-GFRP–3.76-COMMON–FLUSH	4.663	0.040	0.454	1.350	2.488	2.056
6.35-GFRP–4.12-COMMON–FLUSH	4.738	0.050	0.597	1.00	3.420	2.555
(b) Cyclic loading: positive 1						
9.53-PLY–3.33-COMMON–FLUSH	2.152	0.091	0.356	2.000	3.048	1.004
6.35-GFRP–3.33-COMMON–FLUSH	2.316	0.020	0.653	2.000	3.169	1.534
6.35-GFRP–3.76-COMMON–FLUSH	3.615	0.070	0.564	1.600	3.338	2.164
6.35-GFRP–4.12-COMMON–FLUSH	3.116	0.040	0.650	2.000	3.934	2.131
(c) Cyclic loading: positive 2						
9.53-PLY–3.33-COMMON–FLUSH	0.832	0.084	0.914	6.150	2.794	0.919
6.35-GFRP–3.33-COMMON–FLUSH	1.527	0.020	0.916	3.300	3.083	1.434
6.35-GFRP–3.76-COMMON–FLUSH	2.187	0.080	0.854	2.800	3.502	2.068
6.35-GFRP–4.12-COMMON–FLUSH	2.136	0.030	0.878	3.000	3.706	1.953

A comparison between monotonic load–displacement curves is shown in Fig. 2.11. The monotonic strength of GFRP–8dc connections exhibited a 47% increase in capacity over plywood connections. Respective increases of 81% and 125% were produced with GFRP connections using 10d and 16d common nails. The GFRP–10dc connection average maximum load occurred earlier than expected. This irregularity may be explained by changes in the primary failure mechanism (*e.g.* from nail fatigue to wood splitting) or by an insufficiency in the number of tests required to precisely determine maximum displacements.

The cyclic strength of GFRP connections demonstrated similar improvements. GFRP–8dc connections were 53% stronger than the PLY–8dc connections. GFRP connections using 10d and 16d common nails were 115% stronger than conventional plywood connections. Also, GFRP connections retained 94% and 90% of the initial strength in the second and third cycles, respectively, whereas plywood connections retained 91% and 86% of the

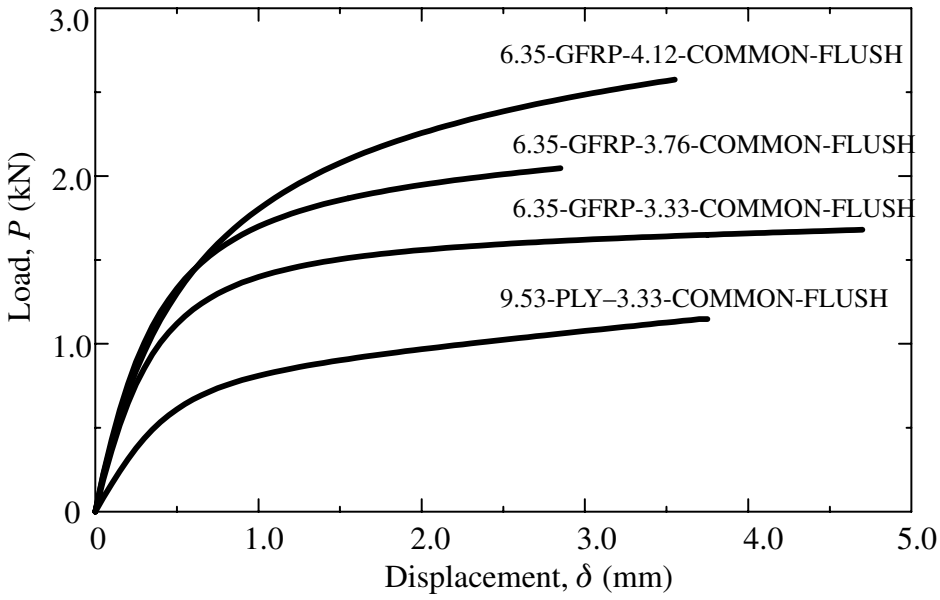

Fig. 2.11. Monotonic load-displacement curves for sheathing-to-framing connections

initial strength in the second and third cycles. Accordingly, degradation in GFRP connection strength is less than that of plywood connections.

Energy absorption E_a of each connection type listed in Table 2.10 was calculated using Eq. 2.23.

$$E_a = \int_0^{\delta_{ult}} P(\delta)\, d\delta \tag{2.23}$$

where, the area underneath the load–displacement curve up to the ultimate displacement was calculated (Atherton et al. 1980). Based on these calculations, conventional plywood connections absorb a range of 50 to 100% less energy than GFRP connections.

Table 2.10. Coupon Testing: Ductility and Energy Absorption

Connection type	δ_{fail} (mm)	μ	E_a (kN · mm)
(a) Monotonic loading			
9.53-PLY–3.33-COMMON–FLUSH	(3.74)	(7.27)	3.25
6.35-GFRP–3.33-COMMON–FLUSH	5.82	14.1	6.49
6.35-GFRP–3.76-COMMON–FLUSH	3.50	7.70	4.07
6.35-GFRP–4.12-COMMON–FLUSH	3.60	6.04	6.69
(a) Cyclic loading: positive 1			
9.53-PLY–3.33-COMMON–FLUSH	NA	NA	2.41
6.35-GFRP–3.33-COMMON–FLUSH	NA	NA	3.98
6.35-GFRP–3.76-COMMON–FLUSH	NA	NA	5.77
6.35-GFRP–4.12-COMMON–FLUSH	NA	NA	6.99

2.2.6 Response of Sheathing-to-Framing Connections with Overdriven Nails

Nailed sheathing-to-framing connections were tested by Rabe (2000) using four nail-head depths: flush driven, 1.59 mm, 3.18 mm, and 4.76 mm overdriven. In that study, individual connection (or coupon) specimens were constructed using 11.1 mm oriented strand board sheathing, 38.1×88.9 mm Douglas Fir-Larch wood members, and 8d cooler (2.87×60.3 mm) nails. Ten coupon specimens (for each nail-head depth) were tested using a pseudo-dynamic procedure.

In that study, Rabe (2000) measured load-displacement curves corresponding to maximum connector force for increasing connector displacement. For this study, however, the measured load-displacement curves during the second positive cycles are idealized consistent with data from GFRP testing. In Table 2.11 the force-displacement response is idealized using Eq. 2.9.

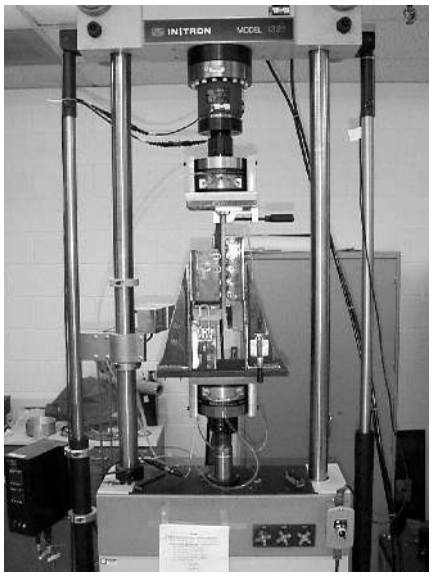

(a) Testing apparatus

(b) Coupon specimen

Fig. 2.12. Testing apparatus and specimen for overdriven nail study (Rabe 2000).

Table 2.11. Force-Displacement Curve Parameters for Overdriven Connections

Nail-head depth	K_1 (kN/mm)	K_2 (kN/mm)	δ_{yield} (mm)	R	δ_{ult} (mm)	P_u (kN)
Flush (properly driven)	2.28	0.035	0.431	2.1	3.73	1.10
Overdriven 1.59 mm	2.03	0.026	0.487	2.2	2.64	1.05
Overdriven 3.18 mm	1.80	0.044	0.480	3.5	2.34	0.97
Overdriven 4.76 mm	2.10	0.000	0.414	2.7	1.91	0.87

2.3 Shear Walls

A brief description of the shear walls considered in this study is given in Table 2.12. Eleven tests of 2.44×2.44 m (8×8 ft) shear walls are considered: three plywood walls and four waferborad walls tested by Dolan (1989), two oriented strand board (OSB) walls tested by Jones and Fonseca (2002), and two plywood walls tested by Burns (2001).

Table 2.12. Description of Shear Walls

Size (m)	Sheathing-to-framing connection	Spacing (mm)		Loading protocol	Source
		Perimeter	Framing		
2.44×2.44	9.53-OSB-2.67-SPIRAL-FLUSH	152	406	Monotonic	Durham (1998)
2.44×2.44	9.53-PLY-3.33-COMMON-FLUSH	102	610	Monotonic	Dolan (1989)
2.44×2.44	9.53-WAF-3.33-COMMON-FLUSH	102	610	Monotonic	Dolan (1989)
2.44×2.44	11.1-OSB-2.87-COOLER-FLUSH	76.2	406	SPD Cyclic	Jones (2000)
2.44×2.44	11.1-OSB-2.87-COOLER-1.59-OD	76.2	406	SPD Cyclic	Jones (2000)
2.44×2.44	11.1-OSB-2.87-COOLER-3.18-OD	76.2	406	SPD Cyclic	Jones (2000)
2.44×2.44	11.1-OSB-2.87-COOLER-4.76-OD	76.2	406	SPD Cyclic	Jones (2000)
2.44×2.44	11.9-PLY-2.87-COOLER-FLUSH	76.2	406	SPD Cyclic	Burns (2001)
2.44×2.44	11.9-PLY-2.87-COOLER-1.59-OD	76.2	406	SPD Cyclic	Burns (2001)
2.44×2.44	11.9-PLY-2.87-COOLER-3.18-OD	76.2	406	SPD Cyclic	Burns (2001)
2.44×2.44	11.9-PLY-2.87-COOLER-4.76-OD	76.2	406	SPD Cyclic	Burns (2001)
2.44×2.44	11.9-PLY-3.33-COMMON-FLUSH	102	406	Half-Cycles	Dinehart et al. (1998)

2.3.1 Shear Wall using 2.67 mm Spiral Nails

The configuration of a 2.44×2.44 m (8×8 ft) wood shear wall tested by Durham (1998) is depicted in Fig. 2.13. The wall used 9.53-mm (3/8 in.)-thick oriented strand board (OSB) sheathing panels. Sheathing was attached to framing using 2.67-mm-diameter $\times$ 50.0-mm-long threaded-hardened (spiral) nails spaced at 152 mm (6 in.) on center along panel edges and 305 mm (12 in.) on center in panel fields. Framing consisted of top and side double plates using two 38.1×88.9 mm (2×4-in.-nominal) members, a bottom single plate using one 38.1×88.9 mm (2×4-in.-nominal) member, and 38.1×88.9 mm (2×4-in.-nominal) studs spaced 406 mm (16 in.) on center. The wall was loaded monotonically and cyclically along the top side and restrained along the bottom side. A discussion on the effect of different cyclic loading protocols is given in this thesis since this is provided by Gatto and Uang (2003).

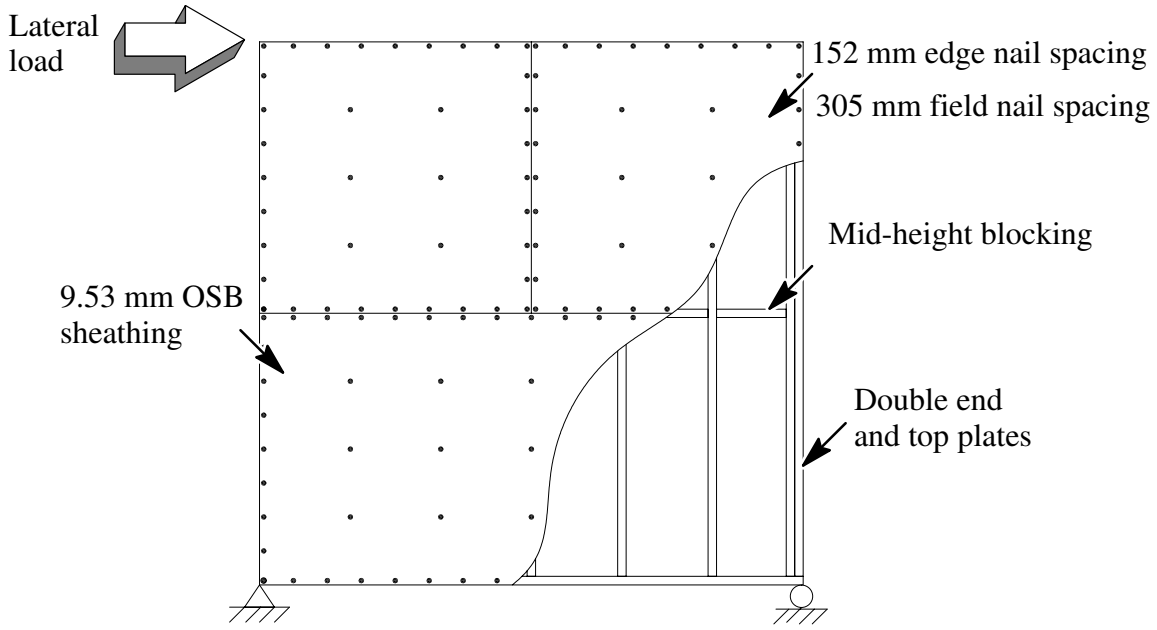

Fig. 2.13. Configuration of 2.44×2.44 m shear wall using 2.67×50.0 mm spiral nails

2.3.2 Shear Walls using 3.33 mm Common Nails

The configuration of seven 2.44 × 2.44 m (8 × 8 ft) wood shear walls tested by Dolan (1989) is depicted in Fig. 2.14. Four of the walls used 9.53-mm (3/8 in.)-thick softwood plywood panels. The remaining three walls used 9.53-mm (3/8 in.)-thick waferboard panels. Sheathing was attached to framing using 3.33-mm-diameter × 63.5-mm-long (8d common) nails spaced at 102 mm (4 in.) on center along panel edges and 152 mm (6 in.) on center in panel fields. Framing consisted of double plates using two 38.1 × 88.9 mm (2 × 4-in.-nominal) members, and 38.1 × 88.9 mm (2 × 4-in.-nominal) studs spaced 0.61 m (24 in.) on center. The wall was loaded monotonically along the top side and restrained along the bottom side.

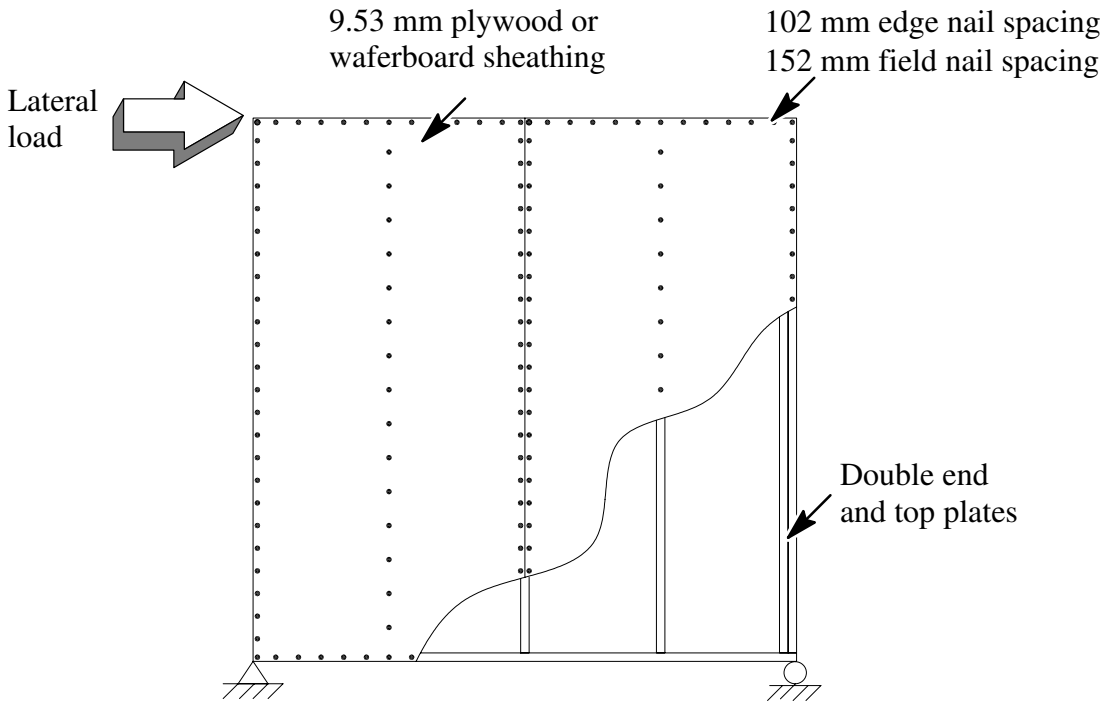

Fig. 2.14. Configuration of 2.44 × 2.44 m shear wall using 3.33 × 63.5 mm common nails

2.3.3 Shear Walls using 2.87 mm Cooler Nails

The configuration of four 2.44 × 2.44 m (8 × 8 ft) wood shear walls tested by Jones (2000) and Burns (2001) is depicted in Fig. 2.15. The two walls tested by Jones used 11.4-mm (7/16 in.)-thick OSB panels. The two walls tested by Burns used 11.9-mm (15/32 in.)-thick plywood panels. All four walls used sheathing attached to framing using 2.87-mm-diameter × 60.3-mm-long (8d cooler) nails spaced at 76.2 mm (3 in.) on center along panel edges and 304 mm (12 in.) on center in panel fields. Framing consisted of double plates using two 38.1 × 88.9 mm (2 × 4-in.-nominal) members, and 38.1 × 88.9 mm (2 × 4-in.-nominal) studs spaced 0.41 m (16 in.) on center. The walls were loaded monotonically and cyclically along the top side and restrained along the bottom side.

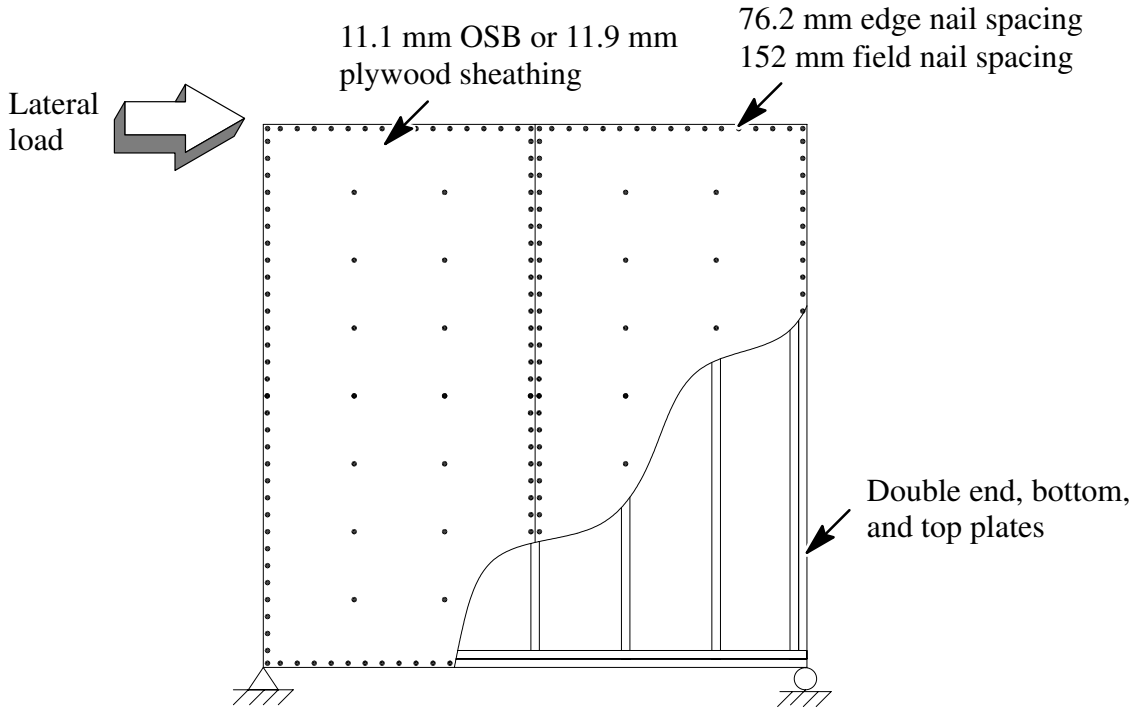

Fig. 2.15. Configuration of 2.44 × 2.44 m shear wall using 2.87 × 60.3 mm cooler nails

2.4 Diaphragms

A brief description of the diaphragms considered in this study is given in Table 2.13. Three tests of diaphragms are considered: one 4.88×14.6 m (16×48 ft) plywood diaphragm tested by Tissell and Elliott (1997), and two 3.66×7.32 m (12×24 ft) diaphragms tested by Olpin (1998).

2.4.1 Diaphragm using 3.76 × 76.2 mm Common Nails

A 4.88×14.6 m (16×48 ft) horizontal diaphragm tested by Tissell and Elliott (1997) is depicted in Fig. 2.16. The diaphragm used 12.7-mm (1/2 in.)-thick Structural I C-D plywood sheathing panels. The sheathing was attached to the framing using 3.76-mm-diameter × 76.2-mm-long (10d common) nails spaced 102 mm (4 in.) on center along exterior panel edges, 152 mm (6 in.) on center along interior panel edges, and 305 mm (12 in.) on center in the panel fields. The framing consisted of 88.9×241 mm (4×10-in.-nominal) chords, 130×305 mm (5 1/8 × 12-in.-nominal) glulams, 88.9×241 mm (4×10-in.-nominal) purlins, and 38.1×88.9 mm (2×4-in.-nominal) sub-purlins spaced 0.61 m (24 in.) on center. The diaphragm was cyclically loaded and restrained at the corners.

Table 2.13. Description of Diaphragms

Size (m)	Sheathing-to-framing connection	Spacing (mm)		Loading protocol	Source
		Perimeter	Framing		
4.88×14.6	12.7-PLY-3.76-COMMON-FLUSH	102	(various)	Cyclic	Tissell and Elliott (1997)
3.66×7.32	9.53-PLY-3.33-COMMON-FLUSH	102	(various)	Cyclic	Olpin (1998)
3.66×7.32	6.35-GFRP-3.33-COMMON-FLUSH 9.53-PLY-3.33-COMMON-FLUSH	102 102	(various)	Cyclic	Olpin (1998)

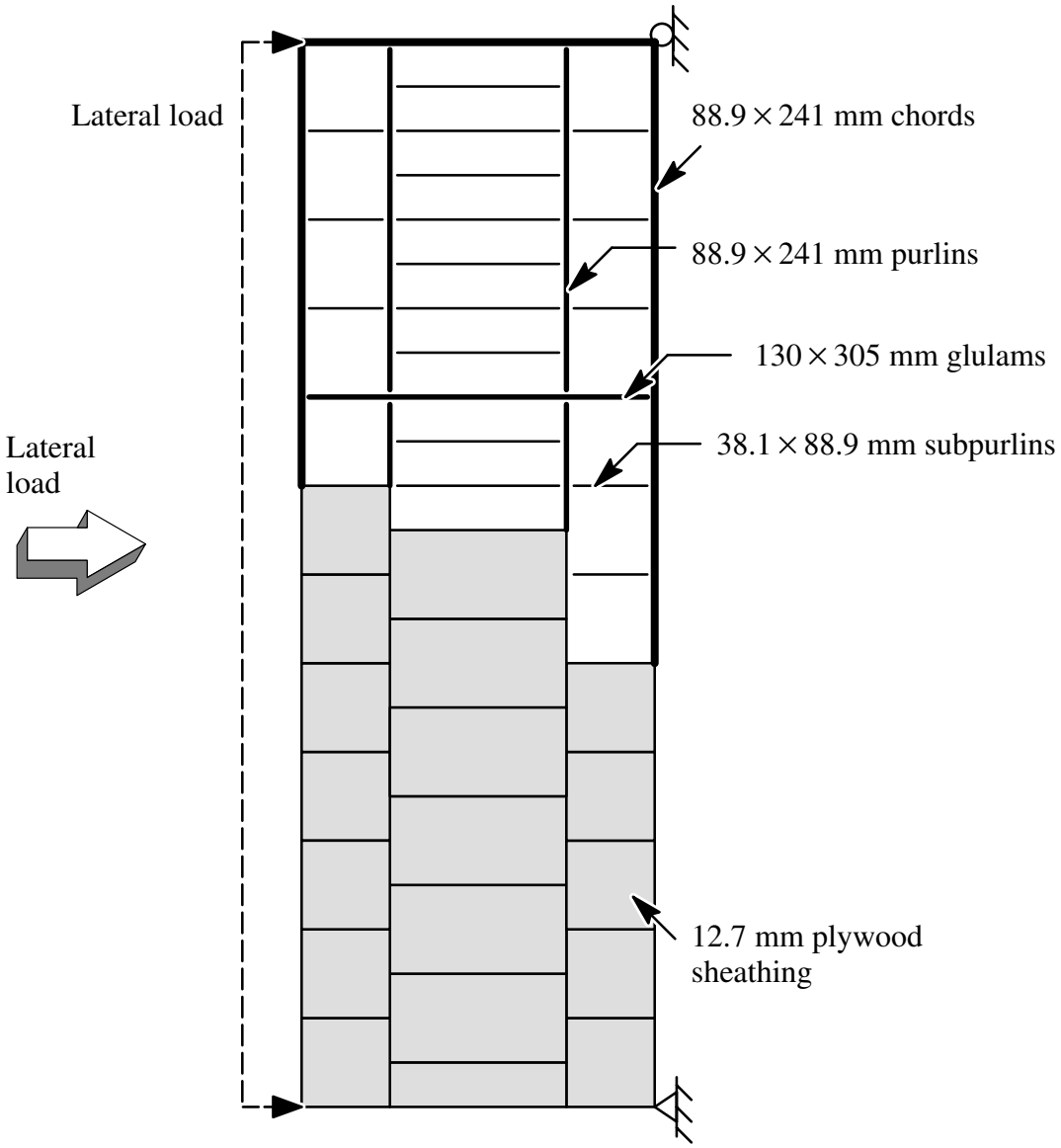

Fig. 2.16. Configuration of 4.88 × 14.6 m plywood diaphragm using 3.76 × 76.2 mm common nails

2.4.2 Diaphragms using Plywood and GFRP Sheathing

Two types of diaphragms were tested in this pilot study. First, a conventional diaphragm was tested. The diaphragm configuration is shown in Fig. 2.17. The 3.66×7.32 m (12×24 ft) diaphragm used wood framing, 9.53-mm (0.375 in.)-thick structural grade (A–C Exterior) plywood sheathing, 3.33-mm-diameter $\times$ 63.5-mm-long (8d common) nails, and 50.8×102 mm (2×4 in.-nominal) subpurlins spaced 610 mm (24 in.) on center. A typical nailing schedule was used: 102 mm (4 in.) on center along the diaphragm perimeter and continuous panel edges, 152 mm (6 in.) on center along non-continuous panel edges, and 305 mm (12 in.) on center in the field. Though smaller in size, the diaphragm specimen is representative of those constructed in practice. The smaller size of the diaphragm simply facilitates testing within laboratory housing (Fonseca 1997).

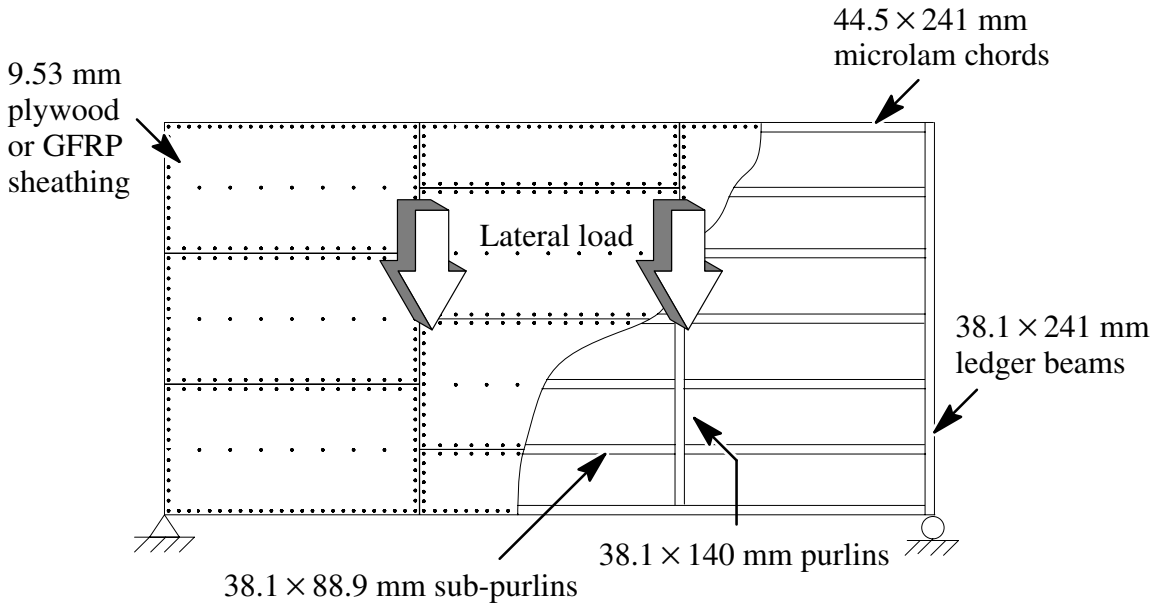

Fig. 2.17. Configuration of 3.66×7.32 m diaphragm using 3.33×63.5 mm common nails

The conventional diaphragm set–up is shown in Fig. 2.18. The diaphragm was tested using two equal concentrated loads symmetrically placed along the length of the diaphragm (at the third–points). The load was applied using two hydraulic actuators (rams) using horizontal links that attached to the diaphragm sheathing. The diaphragm, similar to the coupon specimens, was tested using displacement controlled cyclic loading. A complete description of the testing configuration, procedure, instrumentation, and results are available (Olpin 1998).

After testing the conventional diaphragm, the hybrid diaphragm was assembled and tested. See Fig. 2.19. The assembly of the hybrid diaphragm consisted of replacing the damaged corner plywood panels in the conventional diaphragm with new 6.35-mm (1/4 in.)-thick GFRP sheathing panels. The GFRP panels were attached using 8d common nails

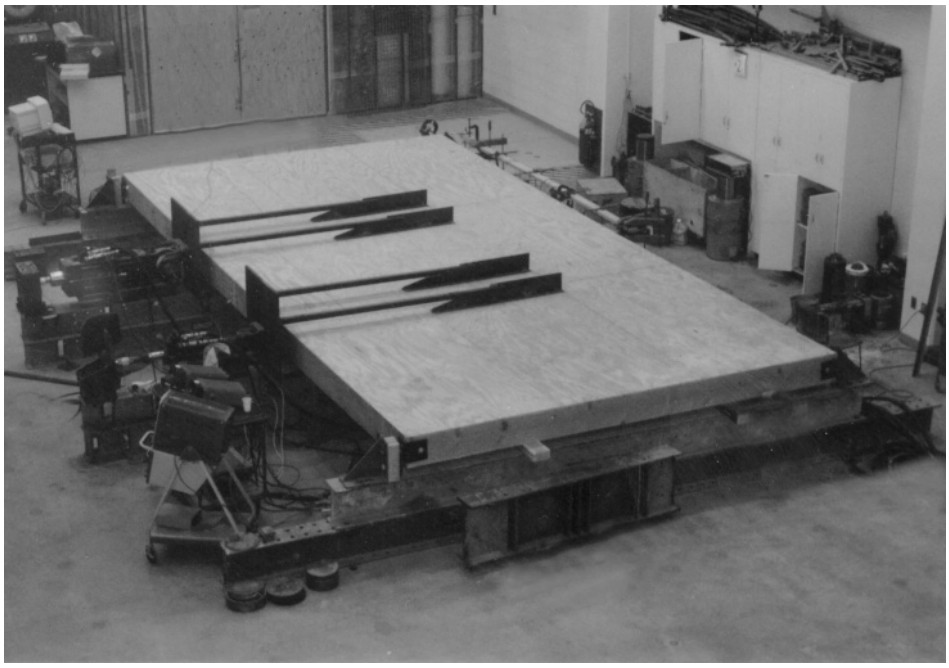

Fig. 2.18. Testing set-up for 3.66×7.32 m plywood diaphragm

driven through 3.10-mm-diameter pre-drilled holes. Nails in GFRP panels were offset from nails in adjacent plywood panels. Although additional nails were driven into an interior edge of one plywood panel because the nails had torn through the sheathing, no other modifications were made. The remaining, slightly damaged plywood sheathing panels were used again in the hybrid diaphragm without any strengthening or retrofitting.

Most of the damage sustained by the conventional diaphragm was in the corner plywood sheathing panels. Sheathing failure was caused by the nails along the diaphragm perimeter tearing through the panel edges. Further investigation indicated that the nails remained essentially undeformed. This observation suggests that the nails had remained largely within the linear elastic range and were not loaded to capacity. Thus, plywood sheathing appears to limit diaphragm strength.

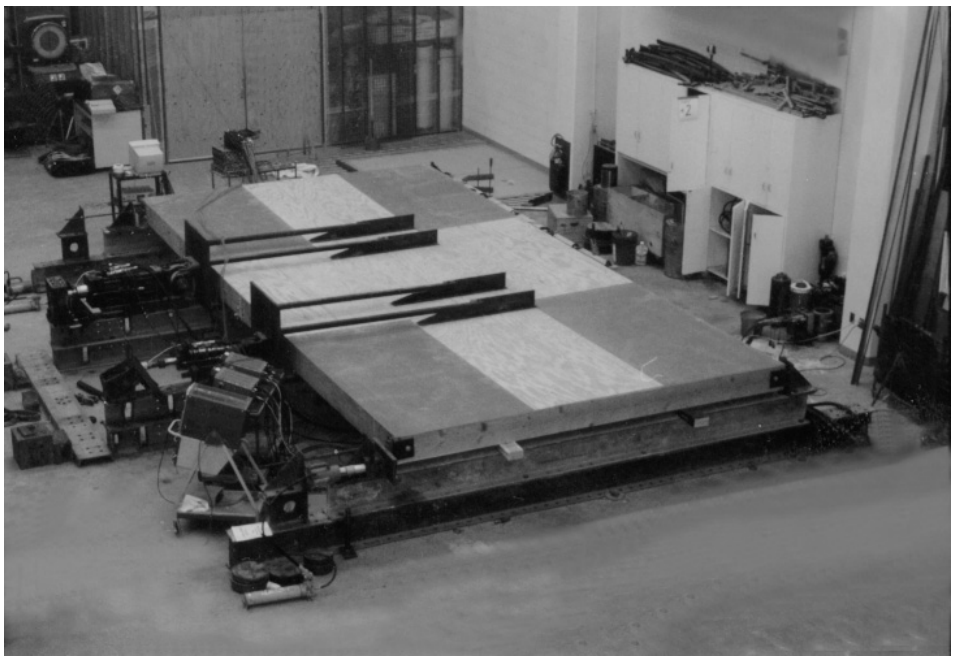

Fig. 2.19. Testing set-up for 3.66×7.32 m hybrid diaphragm

Most of the damage observed during testing of the hybrid diaphragm was sustained by the plywood sheathing panels. These panels failed as in the previous diaphragm test; the nails tore through the panel edges. The GFRP sheathing panels in the corners of the diaphragm, however, were undamaged. A few of the GFRP sheathing–to–framing connections failed as the nails fatigued and fractured.

The measured response of the diaphragms may be evaluated using the data shown in Table 2.14. For each diaphragm type (column 1), the maximum displacement of the mid–span (Δ_{max}^{+}) and corresponding force per ram (F_{max}^{+}) during pushing of the diaphragm (actuator extension) is tabulated in columns 2 and 3. The maximum displacement of the mid–span (Δ_{max}^{-}) and corresponding force per ram (F_{max}^{-}) during pulling of the diaphragm (actuator contraction) is listed in columns 4 and 5. The larger forces measured during pulling of the diaphragm were occasioned by movement of the diaphragm reaction frame (Olpin 1998).

The measured load–displacement response of full–scale diaphragms is similar in form, although different in magnitude, to that of individual sheathing–to–framing connections. Therefore, as in coupon testing, a simplified analysis of the data was used. Equivalent diaphragm stiffness and load–displacement envelope curves were established. In column 6 of Table 2.14, the effective initial stiffness, K_E for each diaphragm is given. The effective initial stiffness was calculated using Eq. 2.24.

$$K_E = \frac{F_{max}^{+} - F_{max}^{-}}{\Delta_{max}^{+} - \Delta_{max}^{-}} \tag{2.24}$$

Notably, the effective stiffness of the hybrid diaphragm is approximately 25% higher than the effective stiffness of the conventional diaphragm. This suggests that hybrid diaphragms may eliminate some of the problems caused by excessive diaphragm flexibility.

The approximate energy absorption, E_a of each diaphragm is listed in column 7. Energy absorption was estimated by summing the area underneath the envelope load–displacement curve. The hybrid diaphragm absorbed roughly 46% more energy than the conventional diaphragm.

The strength of the diaphragm is given in column 8. The measured diaphragm strength, F_{ave} is the average of the maximum forces per ram during pushing (column 3) and pulling (column 5) of the diaphragm. The hybrid diaphragm strength is 34% greater than the conventional diaphragm strength. Significantly, this value may represent a lower–bound on the capacity of a hybrid diaphragm—the plywood panels used were already damaged and were neither reinforced nor strengthened.

2.4.3 Summary of Measured Response

A summary of the measured response of the shear wall and diaphragm tests considered in this thesis is shown in Table 2.15.

2.4.4 Estimation of Shear Wall and Diaphragm Strength

The strength of shear walls and diaphragms may be based on the number of "resisting" sheathing-to-framing connections. For a shear wall loaded along the top edge, the "resisting" connections are the perimeter connections (on the top and bottom). Likewise, for a diaphragm loaded along the length of one chord, the "resisting" connections are primarily the transverse perimeter connections (on each side).

Table 2.14. Measured Response for 3.66×7.32 m Diaphragms

	Push		Pull				
Diaphragm	$\Delta_{max}{}^{+}$ (mm)	$F_{max}{}^{+}$ (kN)	$\Delta_{max}{}^{-}$ (mm)	$F_{max}{}^{-}$ (kN)	K_E (kN/mm)	E_a (kN·mm)	F_{ave} (kN/Ram)
(a)	20.3	27.6	–23.4	–37.4	1.49	46.1	32.5
(b)	21.6	37.4	–21.6	–49.8	1.86	67.2	43.6

Table 2.15. Measured Response of Shear Walls and Diaphragms

		Monotonic response			Cyclic response		
Size (m)	Sheathing-to-framing connection type	Δ_{ult} (mm)	F_{ult} (kN)	E_a (kN·m)	Δ_{ult} (mm)	F_{ult} (kN)	E_a (kN·m)
	(a) Shear Walls						
2.44×2.44	9.53-OSB-2.67-SPIRAL-FLUSH[a]	57.4	17.4	—	66.0	20.4	2.59
2.44×2.44	9.53-PLY-3.33-COMMON-FLUSH[b]	84.0	33.5	—	—	—	—
2.44×2.44	9.53-WAF-3.33-COMMON-FLUSH[b]	74.0	31.8	—	—	—	—
2.44×2.44	11.1-OSB-2.87-COOLER-FLUSH[c]	—	—	—	41.2	36.7	NA
2.44×2.44	11.1-OSB-2.87-COOLER-1.59-OD[c]	—	—	—	41.5	34.7	NA
2.44×2.44	11.1-OSB-2.87-COOLER-3.18-OD[c]	—	—	—	32.3	32.3	NA
2.44×2.44	11.1-OSB-2.87-COOLER-4.76-OD[c]	—	—	—	18.1	28.0	NA
2.44×2.44	11.9-PLY-2.87-COOLER-FLUSH[d]	—	—	—	NA	41.5	3.82
2.44×2.44	11.9-PLY-2.87-COOLER-1.59-OD[d]	—	—	—	NA	39.4	3.33
2.44×2.44	11.9-PLY-2.87-COOLER-3.18-OD[d]	—	—	—	NA	32.3	1.95
2.44×2.44	11.9-PLY-2.87-COOLER-4.76-OD[d]	—	—	—	NA	29.3	1.50
2.44×2.44	11.9-PLY-3.33-COMMON-FLUSH[e]	83.1	33.3	NA	54.6	32.0	NA
	(a) Diaphragms						
4.88×14.6	12.7-PLY-3.76-COMMON-FLUSH[f]	—	—	—	NA	127	NA
3.66×7.32	9.53-PLY-3.33-COMMON-FLUSH[g]	—	—	—	23.4	37.4	NA
3.66×7.32	6.35-GFRP-3.33-COMMON-FLUSH[g] 9.53-PLY-3.33-COMMON-FLUSH	—	—	—	21.6	49.8	NA

[a] Folz and Filiatrault (2001), Table 2.
[b] Dolan (1989), Table 8.2. See also Dolan and Madsen (1992), Table 2, and Dolan and Foschi (1991), Table 2.
[c] Jones and Fonseca (2002), Table 1.
[d] Average from Burns (2001), Table 10.
[e] From Dinehart and Shenton III (1998), Tables 1 and 2.
[f] Tissell and Elliott (1997), Table 3. Also, see footnote (4) that explains the test was terminated before failure of the diaphragm because some loading rams had fully extended.
[g] Table 2.14, ultimate force during pulling.

The strength contribution of each sheathing-to-framing connection is assumed to be the average maximum value of that particular connection configuration determined through coupon testing, by using general dowel equations, or by using published values. The accuracy of this approach is validated against measured data from shear wall and diaphragms tests.

A comparison between the calculated and measured unit shear for the shear walls and diaphragms is given in Table 2.16. For each wall or diaphragm, the number of resisting connections, the connection type, the connection strength, and the overall calculated and measured capacity is given. Error is defined as the over or under estimation of the measured capacity. On average, the calculated strength is within 12% of the measured strength.

The difference between the calculated and measured strengths may be due to a number of factors not considered in this thesis. For example, an overestimation of strength is likely due, at least in part, to the fact that sheathing-to-framing connections in coupon specimens are slightly "stiffer" than comparable connections in the actual shear wall or diaphragm. This extra stiffness is a result of "scale effects:" in full scale testing, local buckling of sheathing and nail withdrawal may be magnified. One possible solution to improve the accuracy of the predicted strength would be to include commonly accepted "design factors" used for shear walls (Tissell 1993). These factors are shown in Table 2.17.

Table 2.16. Predicted Lateral Load Strength Based on the Number of Resisting Connections

Size (m)	Sheathing-to-framing connection			Calculated capacity	
	Type	P_{ult} (kN)	Resisting connections	F_{ult} (kN)	Error (%)
	(a) Shear walls				
2.44 × 2.44	9.53-OSB-2.67-SPIRAL-FLUSH	1.18	17	22.4	(+10)
2.44 × 2.44	9.53-PLY-3.33-COMMON-FLUSH	(1.33)	26	34.6	+3
2.44 × 2.44	9.53-WAF-3.33-COMMON-FLUSH	(1.42)	26	36.9	+16
2.44 × 2.44	11.1-OSB-2.87-COOLER-FLUSH	1.23	34	41.8	+14
2.44 × 2.44	11.1-OSB-2.87-COOLER-1.59-OD	1.12	34	38.1	+10
2.44 × 2.44	11.1-OSB-2.87-COOLER-3.18-OD	1.07	34	36.4	+13
2.44 × 2.44	11.1-OSB-2.87-COOLER-4.76-OD	0.96	34	32.6	+16
2.44 × 2.44	11.9-PLY-2.87-COOLER-FLUSH	1.01	34	34.3	–17
2.44 × 2.44	11.9-PLY-2.87-COOLER-1.59-OD	1.02	34	34.7	–12
2.44 × 2.44	11.9-PLY-2.87-COOLER-3.18-OD	1.01	34	34.3	+6
2.44 × 2.44	11.9-PLY-2.87-COOLER-4.76-OD	0.90	34	30.6	+4
2.44 × 2.44	11.9-PLY-3.33-COMMON-FLUSH	NA	26	NA	NA
	(a) Diaphragms				
4.88 × 14.6	12.7-PLY-3.76-COMMON-FLUSH	2.11	51	108	–15
3.66 × 7.32	9.53-PLY-3.33-COMMON-FLUSH	1.00	39	39.0	+4
3.66 × 7.32	6.35-GFRP-3.33-COMMON-FLUSH	1.53	26	52.8	+6
	9.53-PLY-3.33-COMMON-FLUSH	1.00	13		

Table 2.17. Suggested Design Factors for Adjusting Calculated Capacity

Structural configuration	Factor
Nailed sheathing-to-framing connections used in diaphragm construction	1.10
2 in. nominal wood framing	0.89
Non-Structural I rated sheathing	0.90
Framing spaced at 24 in. o.c.	0.83

2.4.5 Design Lateral Load Strength and Load Factor

The design lateral load strength F_{ubc} for the shear walls and diaphragms is given in Table 2.18. The design strength is determined by multiplying the allowable unit shear from the *Uniform Building Code* (ICBO 1997) Table 23-II-I-1 (for shear walls) and Table 23-II-H (for diaphragms) by the respective width or span length. The design load factor LF_{ubc} is determined by dividing the measured lateral load strength by the design strength.

Table 2.18. Design Lateral Load Strength for Shear Walls and Diaphragms

Size (m)	Sheathing-to-framing connections: Type[a]	Perimeter spacing (mm)	Framing spacing (mm)	F_{ubc}	LF_{ubc}
	(a) Shear walls[b]				
2.44 × 2.44	9.53-OSB-2.67-SPIRAL-FLUSH	152	406	9.25	1.9
2.44 × 2.44	9.53-PLY-3.33-COMMON-FLUSH	102	610	12.8	2.6
2.44 × 2.44	9.53-WAF-3.33-COMMON-FLUSH	102	610	11.4	2.8
2.44 × 2.44	11.1-OSB-2.87-COOLER-FLUSH	76.2	406	17.4	2.1
2.44 × 2.44	11.1-OSB-2.87-COOLER-1.59-OD	76.2	406	17.4	1.9
2.44 × 2.44	11.1-OSB-2.87-COOLER-3.18-OD	76.2	406	17.4	1.8
2.44 × 2.44	11.1-OSB-2.87-COOLER-4.76-OD	76.2	406	17.4	1.6
2.44 × 2.44	11.9-PLY-2.87-COOLER-FLUSH	76.2	406	19.6	2.1
2.44 × 2.44	11.9-PLY-2.87-COOLER-1.59-OD	76.2	406	19.6	2.0
2.44 × 2.44	11.9-PLY-2.87-COOLER-3.18-OD	76.2	406	19.6	1.7
2.44 × 2.44	11.9-PLY-2.87-COOLER-4.76-OD	76.2	406	19.6	1.5
2.44 × 2.44	11.9-PLY-3.33-COMMON-FLUSH	102	406	15.3	2.1
	(b) Diaphragms[b]				
4.88 × 14.6	12.7-PLY-3.76-COMMON-FLUSH	102	(various)	30.3	4.2
3.66 × 7.32	9.53-PLY-3.33-COMMON-FLUSH	102	(various)	19.2	2.0
3.66 × 7.32	6.35-GFRP-3.33-COMMON-FLUSH 9.53-PLY-3.33-COMMON-FLUSH	102 102	(various)	—	—

[a] "Common nail" values are shown, although the *Uniform Building Code* does not apply, because cooler nails are often substituted wrongfully in field construction (Jones and Fonseca 2002).
[b] From the *Uniform Building Code 1997* (ICBO 1997).

Chapter 3

ANALYTICAL MODELING OF SHEATHING-TO-FRAMING CONNECTIONS

The theoretical response of sheathing-to-framing connections is calculated using general dowel equations based on the European Yield Model (EYM). In addition, a new analytical model for sheathing-to-framing connections in wood shear walls and diaphragms is discussed in this paper. The model represents sheathing-to-framing connections using an oriented pair of nonlinear springs. Unlike previous models, the new analytical model is suitable for both monotonic and cyclic analyses and does not need to be scaled or adjusted. As such, the analytical model may be implemented in a general purpose finite element program or in a specialized structural analysis program.

3.1 Theoretical Connection Capacity Using General Dowel Equations

Sheathing-to-framing connection lateral load strength may be calculated theoretically using general dowel equations based on the European Yield Model (EYM). In the EYM, connection strength is limited by either the dowel-bearing strength of the members, the bending strength of the dowel, or the combination thereof.

The more general form of the yield limit equations specified in the National Design Specification (NDS) for Wood Construction (AF&PA, 2001a) permit connection strength to be calculated at limit states (e.g. ultimate load) other than the yield point. The NDS for

Wood Construction considers the effects of member thickness, fastener size, and fastener strength. Steel side–members may also be considered. In addition to these conditions, the general dowel equations permit gaps, fastener moment resistance, and various connection limit states to be considered as well. This expansion of the NDS for Wood Construction yield limit equations is outlined in *Technical Report No. 12* by the American Wood Council (AWC) (1999).

3.1.1 Derivation of General Dowel Equations

Yield Mode I. Mode I_s occurs when the dowel bearing strength of the side member (sheathing) is exceeded. The nail does not bend or rotate; only the sheathing crushes. Therefore, the dowel equation to determine connection strength P for yield Mode I_s is

$$P = (f_{es} D) l_m \tag{3.1}$$

Yield Mode II. Mode II occurs when the nail rotates at the shear plane with crushing of both the sheathing and main member. Importantly, Mode II does not occur in sheathing-to-framing connections with minimum penetration, as discussed in Appendix I of the NDS for Wood Construction (AF&PA 2001a). Mode II is not derived for this reason.

Yield Modes III–IV. In Mode III_m , the strength of the main member (wood framing) is exceeded, and the nail bends and rotates within the wood framing, forming one plastic hinge near the shear plane. The same mechanism occurs in Mode III_s , except that the bearing strength of the sheathing is exceeded, instead of the bearing strength of the wood framing. Contrastingly, in Mode IV, the nail bends and two plastic hinges are formed, with limited crushing of the sheathing or wood framing. For yield Modes III_m, III_s, and IV, the strength is determined as

$$P = \frac{-B + \sqrt{B^2 - 4AC}}{2A} \tag{3.2}$$

where the constants A, B, and C are determined for each yield mode by the following equations:

Yield Mode III_m:

$$A = \frac{1}{2f_{es}D} + \frac{1}{4f_{em}D} \tag{3.3}$$

$$B = g + \frac{l_m}{2} \tag{3.4}$$

$$C = -f_b\left(D_s^3/6\right) - \frac{f_{em}Dl_m^2}{4} \tag{3.5}$$

Yield Mode III_s:

$$A = \frac{1}{4f_{es}D} + \frac{1}{2f_{em}D} \tag{3.6}$$

$$B = \frac{l_s}{2} + g \tag{3.7}$$

$$C = -f_b\left(D_m^3/6\right) - \frac{f_{es}Dl_s^2}{4} \tag{3.8}$$

Yield Mode IV:

$$A = \frac{1}{2f_{es}D} + \frac{1}{2f_{em}D} \tag{3.9}$$

$$B = g \tag{3.10}$$

$$C = -f_b\left(D_s^3/6\right) - f_b\left(D_m^3/6\right) \tag{3.11}$$

3.1.2 Dowel-Bearing Strength

The dowel-bearing strengths of various structural components of sheathing-to-framing connections is given in Table 3.1. For each material, the specific gravity SG and the proportional limit, $f_{e,pl}$ the 5% offset, $f_{e,5\%}$ and the ultimate dowel-bearing strength, $f_{e,ult}$ are listed.

Table 3.1. Dowel-Bearing Strength (MPa)

Material	SG[(a)]	$f_{e,pl}$	$f_{e,5\%}$	$f_{e,ult}$
Wood Framing[(b)]	0.50	22.3	32.0	44.5
Plywood	0.50	22.3	32.0	44.5
OSB	0.50	22.3	32.0	44.5
Waferboard[(c)]	0.42	18.2	23.2	36.4
GFRP[(d)]	—	—	—	221

The dowel-bearing strength of wood and wood-based products are determined using the test methods outlined in *ASTM D 5674–97a* (ASTM 2001a). Wilkinson (1991) derived a relationship between the specific gravity of the wood member and the corresponding 5% offset dowel-bearing strength, given in Eq. 3.13. Based on Wilkinson's data, similar relationships have been derived for the proportional limit and ultimate dowel-bearing strengths (AWC 1999), given in Eq. 3.12 and 3.14, respectively.

$$f_{e,pl} = 2542\, SG^{1.15}/D^{0.51} \tag{3.12}$$

$$f_{e,5\%} = 16600\, SG^{1.84} \tag{3.13}$$

$$f_{e,ult} = 5084\, SG^{1.15}/D^{0.51} \tag{3.14}$$

The dowel-bearing strength of sheathing panels, however, have not been conclusively determined. As a consequence, the NDS for Wood Construction suggests that panel products are treated like solid wood products (see NDS, Table 11.3.2B). In the case of the GFRP sheathing, the dowel-bearing strength was determined by the manufacture, Strongwell, Inc. (Bristol, Va.) using the tests methods outlined in *ASTM D 953–95* (ASTM 2001b). Only the minimum ultimate dowel-bearing strength was reported (Strongwell, Inc. 1998). The dowel-bearing strength of oriented strand board (OSB) is provided by the APA (1996).

3.1.3 Dowel-Bending Strength

The dowel-bending strengths of fasteners considered in this study are listed in Table 3.2. For each nail type, the shank diameter, proportional limit, 5% offset, and ultimate dowel-bending strengths are given. Dowel-bending strength is determined using the test method outlined in *ASTM F 1575-01* (ASTM 2001c). The *ASTM F 1575-01* test method essentially consists of applying a point load in the center of a nail that is simply supported near each end. Therefore, the dowel-bending stress f_b is

$$f_b = \frac{3 P_c S_{pb}}{2 D^3} \tag{3.15}$$

where f_b is the applied bending load at the center of the nail, S_{pb} is the bearing spacing, and D is the shank diameter of the nail.

Table 3.2. Literature Dowel-Bending Stress (MPa)

Nail type	D (mm)	$f_{b,pl}$	$f_{b,5\%}$	$f_{b,ult}$
2.67×50.0 mm spiral	2.67	NA	NA	NA
3.33×63.5 mm (8d) common	3.33	538	690	896
3.76×76.2 mm (10d) common	3.76	476	621	793
4.12×88.9 mm (16d) common	4.12	476	621	793

Design values for common nails are available in *Technical Report No. 12* (AWC 1999). Represenative values for common and cooler nails used in sheathing-to-framing connection coupon tests by Rabe (2000) and Burns (2001) and used in shear wall tests by Jones (2000) and Burns (2001) are given in Table 3.3. The values were determined from dowel-bending tests performed by Rabe (2000). Individual test results are given in Appendix B.

Table 3.3. Measured Dowel-Bending Stress (MPa)

Nail type	D (mm)	$f_{b,pl}$	$f_{b,5\%}$	$f_{b,ult}$
2.87×60.3 mm (8d) cooler	2.87	559	740	1040
3.33×63.5 mm (8d) common	3.33	640	789	937

Error in determining dowel-bearing strengths may be caused by the fact that (1) "nominal" values of specific gravity (in the case of wood framing) and estimated values of the specific gravity (in the case of wood-based sheathing) are used, and (2) minimum ultimate strength value (in the case of GFRP sheathing) is used. Similarly, with the exception of the measured strengths of some 8d common and 8d cooler nails, the dowel-bending strengths of the various fasteners are likely minimum values, and not average values.

To account for overdriven nails, the side-member thickness (or sheathing thickness) is reduced by the depth overdriven. One possible improvement in determining the overdriven connection strength could be made by increasing the bearing-strength of side member material due to compaction of material from the (overdriven) nail head. This would require future research, however, and is beyond the scope of this thesis.

3.1.4 Comparison Between Measured and Calculated Lateral Load Capacity

The theoretical and measured connection strengths of GFRP and plywood connections are shown in Table 3.4. For each connection type, the theoretical strengths at ultimate load, corresponding to possible connection yield modes, are listed in the next four columns. Mode I_s occurs when the dowel bearing strength of the side member (sheathing) is exceeded. The nail does not bend or rotate; only the sheathing crushes. In Mode III_m the strength of the main member (wood framing) is exceeded, and the nail bends and rotates within the wood

framing, forming one plastic hinge near the shear plane. The same mechanism occurs in Mode III_s except that the bearing strength of the sheathing is exceeded, instead of the bearing strength of the wood framing. Contrastingly, in Mode IV the nail bends and two plastic hinges are formed, with limited crushing of the sheathing or wood framing.

In Table 3.4 the controlling strength, or lowest theoretical value, for each connection type is underlined. The measured monotonic and cyclic strengths are shown in columns 6 and 7, respectively, for purposes of comparison. Note that the first positive cycle is used. Also, the results for 15/32 in. plywood and 7/16 in. OSB are extracted from Fonseca and Burns (2002), and Fonseca and Rabe (2002). Note that these values differ from those reported by Burns (2001).

In general, the theoretical and measured values agree. The theoretical strength is, on average, 82% of the measured strength for GFRP connections. Also, the theoretical controlling yield modes accord with observations. For example, crushing of the plywood with one plastic hinge in the nail (Mode III_s) was observed during testing (Dugan 1995). GFRP connections exhibited limited crushing of the wood framing or sheathing, and nails were bent (Modes III_s and IV).

Note that for the GFRP panels, even though Modes IIIs controls, the values for both Modes IIIs and IV are within approximately 10%. Since a minimum value for the GFRP bearing strength is used, then it could be that the average bearing strength is higher, which would (1) bump the yield mode to Mode IV, and (2) give a closer value to the measured value. The same line of reasoning may apply to the wood member. Of course, it is less significant compared to the GFRP.

A comparison between hybrid and conventional sheathing is shown in Table 3.5. The general agreement between calculated and measured values suggests that connection

strength can be reasonably predicted by using general dowel equations. Therefore these equations may be used to evaluate connections using different sheathing materials, thicknesses, mechanical fasteners, and wood framing.

A comparison between flush-driven and overdriven connections is shown in Table 3.6. Overdriven connection strength seems to be predicted with a similar amount of accuracy as that of the flush-driven connections. The rational method suggested (reducing the sheathing thickness) may be appropriate. Table 3.7. shows a comparison between nail types.

Table 3.4. Sheathing-to-Framing Connection Lateral Load Strength (kN)

	Calculated P_{ult}				Measured P_{ult}	
Connection type	Yield mode I_s	Yield mode III_m	Yield mode III_s	Yield mode IV	Monotonic	Cyclic[a]
9.53-OSB-2.67-SPIRAL-FLUSH	NA	NA	NA	NA	1.18	NA
6.35-GFRP-3.33-COMMON-FLUSH	4.66	3.44	1.49	1.65	1.67	1.53
6.35-GFRP-3.76-COMMON-FLUSH	5.27	4.45	1.70	1.93	2.06	2.16
6.35-GFRP-4.12-COMMON-FLUSH	5.77	5.50	1.92	2.26	2.56	2.13
9.53-PLY-3.33-COMMON-FLUSH	1.41	2.77	0.93	1.28	1.14	1.00
9.53-WAF-3.33-COMMON-FLUSH	1.16	2.67	0.87	1.21	1.42[b]	—
11.1-OSB-3.33-COMMON-FLUSH	1.65	2.70	0.98	1.31	—	0.93
11.1-OSB-2.87-COOLER-FLUSH	1.53	2.49	0.83	1.06	—	1.23
11.1-OSB-2.87-COOLER-1.59-OD	1.31	2.56	0.80	1.06	—	1.12
11.1-OSB-2.87-COOLER-3.18-OD	1.09	2.63	0.77	1.06	—	1.07
11.1-OSB-2.87-COOLER-4.76-OD	0.88	2.70	0.75	1.06	—	0.96
11.9-PLY-3.33-COMMON-FLUSH	1.76	2.66	1.00	1.31	—	1.08
11.9-PLY-2.87-COOLER-FLUSH	1.64	2.45	0.85	1.06	—	1.01
11.9-PLY-2.87-COOLER-1.59-OD	1.42	2.52	0.81	1.06	—	1.02
11.9-PLY-2.87-COOLER-3.18-OD	1.20	2.59	0.78	1.06	—	1.01
11.9-PLY-2.87-COOLER-4.76-OD	0.99	2.66	0.76	1.06	—	0.90
12.7-PLY-3.76-COMMON-FLUSH	2.00	3.44	1.14	1.49	2.11[c]	—

[a] Value corresponds to the first positive cycle if cyclic information is available,
[b] Calculated from Dolan and Foschi (1991), Table 1.
[c] Countryman (1952), page 17.

Table 3.5. Accuracy of GFRP Sheathing-to-Framing Connection Calculations

Connection type	Calculated P_{ult} (kN)	% of measured strength	
		Monotonic	Cyclic
9.53-PLY-3.33-COMMON-FLUSH	0.93	82	93
6.35-GFRP-3.33-COMMON-FLUSH	1.49	89	97
6.35-GFRP-3.76-COMMON-FLUSH	1.70	83	79
6.35-GFRP-4.12-COMMON-FLUSH	1.92	75	90

Table 3.6. Accuracy of Overdriven Sheathing-to-Framing Connection Calculations

Connection type	Calculated P_{ult} (kN)	% of measured strength	
		Monotonic	Cyclic
(a) Plywood sheathing			
11.9-PLY-2.87-COOLER-FLUSH	0.85	—	84
11.9-PLY-2.87-COOLER-1.59-OD	0.81	—	79
11.9-PLY-2.87-COOLER-3.18-OD	0.78	—	77
11.9-PLY-2.87-COOLER-4.76-OD	0.76	—	84
(b) OSB sheathing			
11.1-OSB-2.87-COOLER-FLUSH	0.83	—	68
11.1-OSB-2.87-COOLER-1.59-OD	0.80	—	71
11.1-OSB-2.87-COOLER-3.18-OD	0.77	—	72
11.1-OSB-2.87-COOLER-4.76-OD	0.75	—	78

Table 3.7. Accuracy of Nail-Type Sheathing-to-Framing Connection Calculations

Connection type (sheathing, nail, head-depth)	Calculated strength (kN)	% of measured strength	
		Monotonic	Cyclic
(a) Plywood sheathing			
11.9-PLY-3.33-COMMON-FLUSH	1.00	—	93
11.9-PLY-2.87-COOLER-FLUSH	0.85	—	84
(b) OSB sheathing			
11.1-OSB-3.33-COMMON-FLUSH	0.98	—	105
11.1-OSB-2.87-COOLER-FLUSH	0.83	—	68

3.2 Lateral Deformation of Connections in Shear Walls and Diaphragms

Lateral deformation of a basic panel section in a wood shear wall or diaphragm is depicted in Fig 3.1. In the undeformed configuration, the location of a specific fastener (nail) head in the sheathing panel, point A, is coincident with the location of the same nail shank embedded in the wood framing, point B. Thus, in Fig 3.1, points A and B are the same points. During lateral loading, the specific nail head displaces from point A to point A′. The nail shank embedded in the wood framing displaces from point B to point B′. Because the displacement of the sheathing is not necessarily equal to the displacement of the framing, due to the shear strength of the sheathing, point A′ and point B′ are not coincident.

In Fig 3.2 the lateral deformation of a specific sheathing-to-framing connection is depicted. The lateral force (connection force P) transferred from the sheathing through the nail displaces the nail head relative to the nail shank (connection displacement Δ).

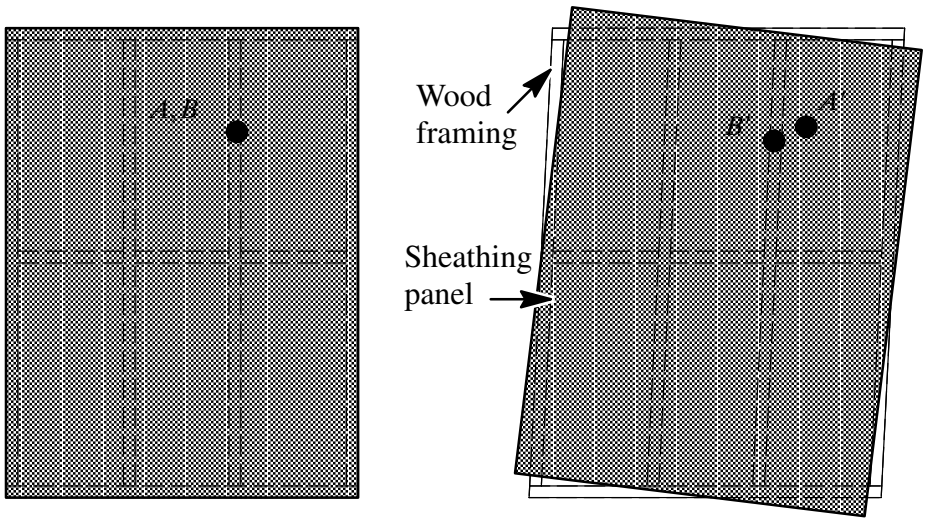

(a) Undeformed configuration (b) Deformed configuration

Fig. 3.1. Lateral deformation of a basic panel section in a wood shear wall or diaphragm

3.3 Idealized Force-Displacement Relationship

Initially, as the nail head displaces and the nail shank deforms, the force-displacement relationship is linear. The wood fibers, sheathing, and nail all remain elastic. As loading progresses, the displacement of the connection increases, the wood fibers crush, and the nail may yield. The angle of the applied lateral load with respect to the wood grain has a negligible effect on the connection behavior (Dolan and Madsen 1992). If the loading is reversed, the nail moves through the gap formed by the crushed wood fibers and the connection exhibits low stiffness and strength until the nail again comes into contact with the wood (see Chapter 2).

In Fig. 3.3 a typical force-displacement relationship for a sheathing-to-framing connection subjected to reversed-cyclic loading is shown. The primary characteristics of the relationship are pinched hysteresis loops (pinching behavior), inelastic behavior, and

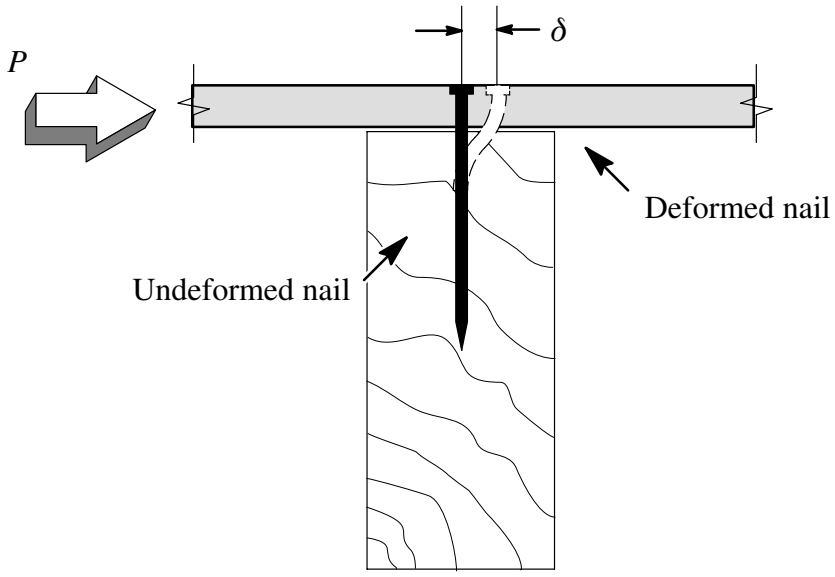

Fig. 3.2. Lateral deformation of a sheathing-to-framing connection

strength and stiffness degradation. If the loading continues after yielding of the nail, prior to failure the strength of the connection decreases with increasing displacement.

The force-displacement relationship for unidirectional loading may be idealized by modeling the connection as an elastoplastic pile (fastener) embedded into a nonlinear layered medium (wood framing and sheathing). In this approach, the mechanical properties of the sheathing, framing, and fastener are required (Foschi 2000).

Alternatively, the force-displacement relationship may be determined by experimental testing, or coupon testing, of individual sheathing-to-framing connection assemblies, as discussed in Chapter 2. In this approach, fastener withdrawal is considered implicitly. The force-displacement relationship during monotonic loading is idealized using a mathematical expression. During reversed-cyclic loading, the monotonic force-displacement relationship provides a response envelope (refer to Chapter 2), while hysteresis behavior is idealized using a predefined set of load-paths to describe unloading, load reversal, and reloading.

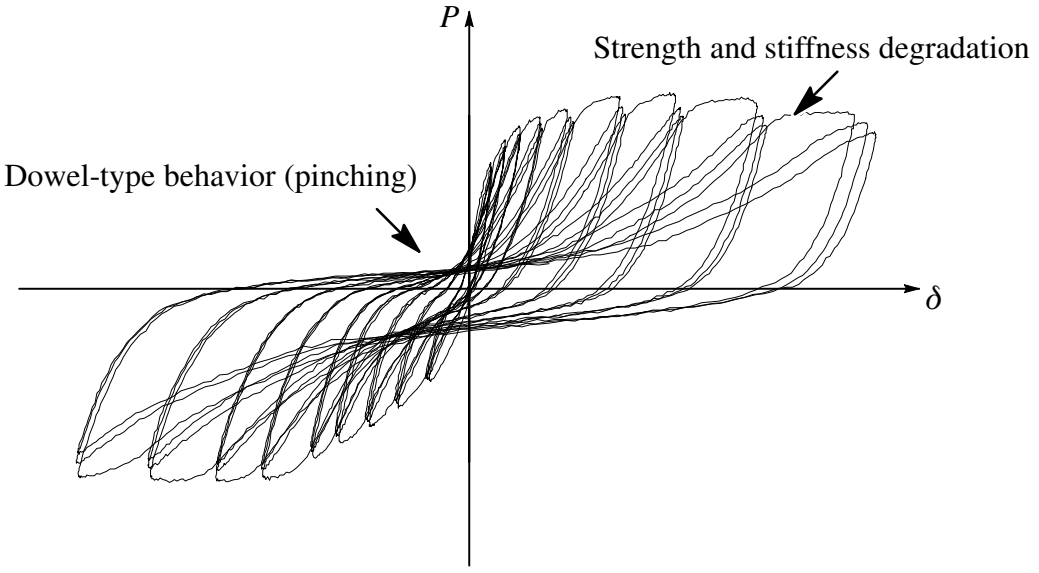

Fig. 3.3. Typical force-displacement relationship during reversed-cyclic loading

A comprehensive discussion of hysteresis models for sheathing-to-framing connections and other connections in wood-frame structures has been previously discussed by Foliente (1995; 1997). Hysteresis models for a variety of wood-frame structural systems exist, including models for bolted connections (Heine 2001; Heine and Dolan 2001), moment resisting connections (Kivell et al. 1981; Ceccotti and Vignoli 1990), entire shear walls (Kamiya 1988), and for composite beams (Lee 1987). The appropriate hysteresis models considered in this thesis consist of models that have general application, such as the Bilinear and Clough models, models that have instructive application, such as the Q-Hyst model, and models developed specifically for sheathing-to-framing connections.

As Foliente (1997) notes, many hysteresis models for sheathing-to-framing connections have adapted features from models originally developed to idealize the flexural behavior of reinforced concrete beams. The salient features of the hysteresis models are discussed in this thesis, with an emphasis on the hysteretic model features instead of the monotonic (envelope) model features. Many hysteresis models feature a piecewise linear (bilinear or trilinear) envelope curve. The hysteresis models are modified in this thesis, therefore, to incorporate many of the envelope curves presented in Chapter 2. This modification is justified because, with a few special exceptions, hysteretic features are essentially independent of the envelope curve.

3.3.1 Conservative Model

In the Conservative model loading and unloading follows the linear (or nonlinear) envelope curve. There is no inelastic deformation. The model is not a "true" hysteresis model, as a result, and requires no parameters. The model is primarily for code development.

3.3.2 Bilinear Hysteresis Model

The Bilinear model is shown in Fig. 3.4. In the model loading follows the initial stiffness K_1 (elastic slope) until yielding, and the secondary stiffness K_2 after yielding. Unloading follows the elastic slope. Elastoplastic behavior occurs when $K_2 = 0$. The Bilinear model is most helpful for code development and model validation, and less helpful for accurate prediction of structural response (see Chapter 6). The Bilinear model requires three parameters:

K_1 = initial stiffness (typically an envelope curve parameter)

K_2 = secondary stiffness (typically an envelope curve parameter)

δ_{yield} = yield displacement

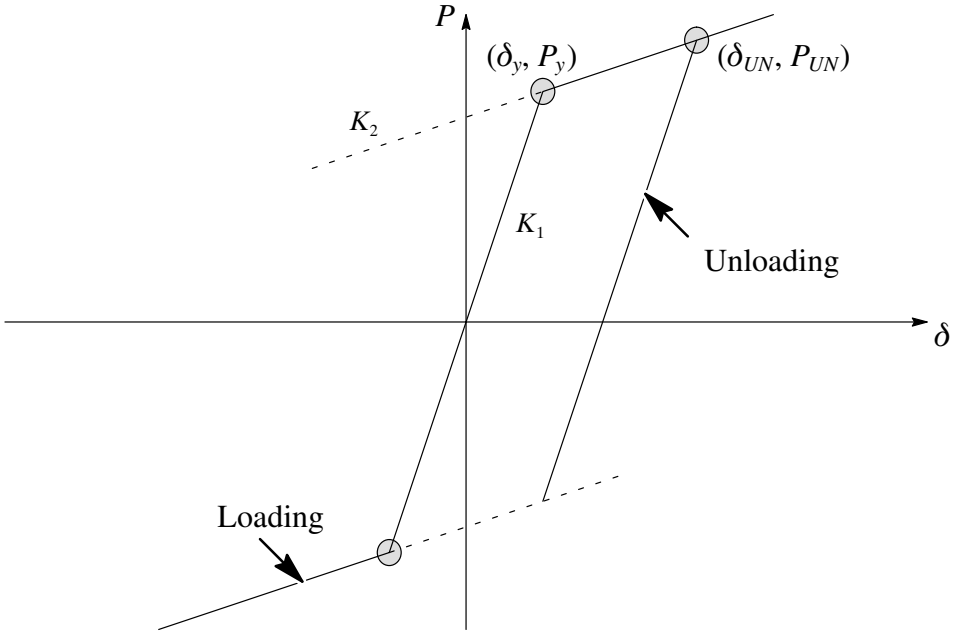

Fig. 3.4. Bilinear hysteresis model

3.3.3 Clough Hysteresis Model

The Clough model is shown in Fig. 3.5. The model developed by Clough (1966) provides a simple model: during loading (when the displacement is increasing in one direction) the response follows the envelope curve. If unloading occurs (when the displacement decreases in the loading direction), then behavior follows a linear unloading path defined by the unloading point (δ_{UN} , P_{UN}) and the unloading stiffness, K_4. If unloading continues, when the connection force is zero, a reloading path is followed and the displacement corresponding to zero force, or crossing displacement is defined. The reloading path is defined by the reloading stiffness, K_6 calculated using the crossing displacement and negative (the reflected positive) unloading point (δ'_{UN} , P'_{UN}). If reloading continues past the negative unloading point, then behavior follows the negative envelope curve. In the case that a reversal in the

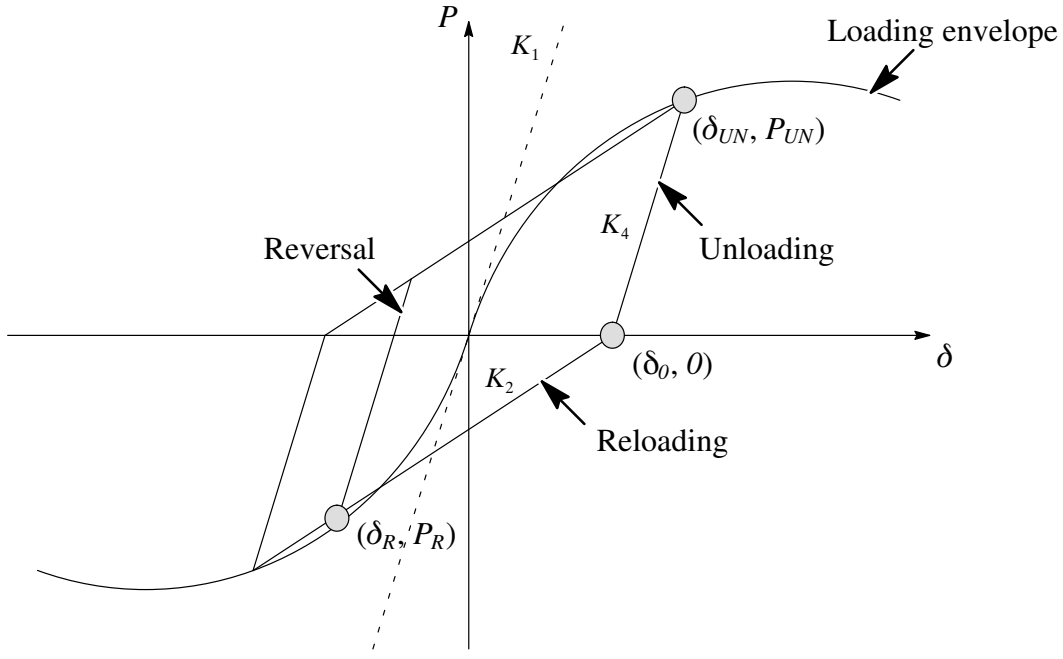

Fig. 3.5. Clough hysteresis model

loading direction occurs (during unloading or reloading), a reversal load path is followed that is defined by the reversal point, (δ_R, P_R). The reversal load path is parallel to the unloading path (with K_4), until the reflected reversal point, (δ_R', P_R') where the behavior then follows the reloading path. The Clough model requires one input parameter:

K_1 = initial stiffness (typically an envelope curve parameter)

3.3.4 Q-Hyst Hysteresis Model

The Q-Hyst model is shown in Fig. 3.6. The Q-Hyst model is a variant of the Clough model developed by Saiidi and Sozen (1979) where the unloading stiffness degrades (see also, Saiidi 1982). Stiffness degradation is accomplished using a method proposed by Takeda et al. (1970). When the displacement is past a yield displacement, δ_{yield}, in the Takeda model the unloading stiffness K_5 is a fraction of the original unloading stiffness K_1 defined in Eq. 3.16.

$$K_4 = K_1 \left(\frac{\delta_{yield}}{\delta_{UN}} \right)^{\alpha_{UN}} \tag{3.16}$$

where $K_4 \leq K_1$. Other than the degradation feature, the Q-Hyst model is identical to the Clough model and the load–paths are defined as before.

The Takeda model is not directly discussed in this thesis because the model incorporates complexities specific to the behavior of reinforced concrete members. Besides, the important features of the model are incorporated in other hysteresis models discussed in this thesis. An in-depth discussion of the Takeda model is available elsewhere (Otani 1974).

Additionally, quantitative analysis comparing the Clough, Q–Hyst, and Takeda models was performed by Saiidi (1982). A comparison of the energy absorbed by the Clough,

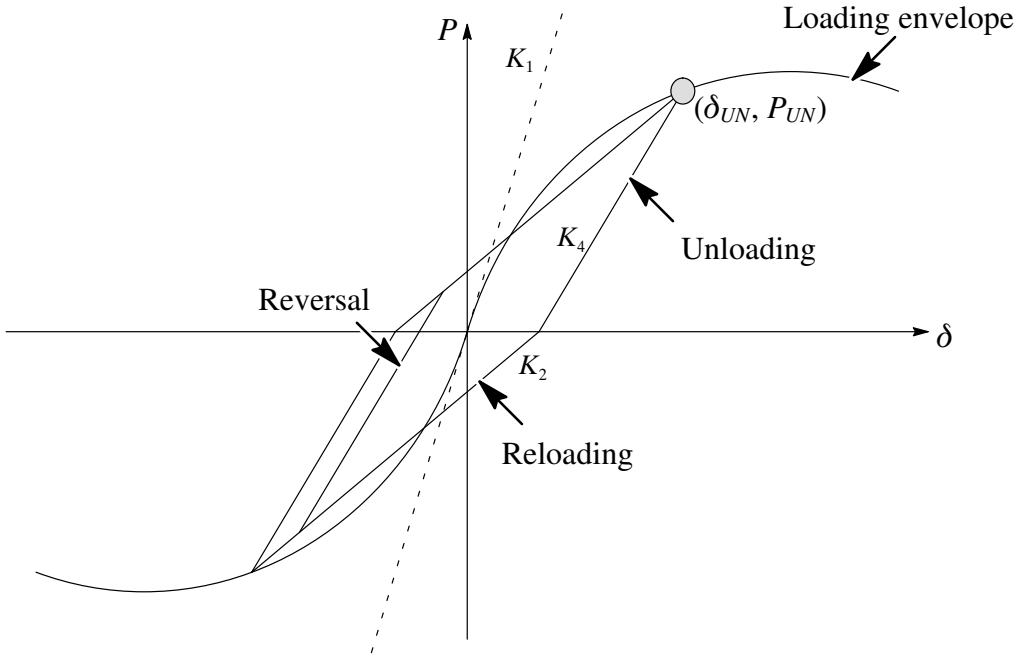

Fig. 3.6. Q-Hyst hysteresis model

Q-Hyst, and a few other hysteresis models (developed specifically for concrete) is available as well (Stojadinovic and Thewalt 1996). Other related models are not discussed in this thesis (Kamiya 1988). The Q-Hyst model requires three input parameters:

K_1 = initial stiffness (typically an envelope curve parameter)

δ_{yield} = yield displacement

α_{UN} = unloading degradation factor

3.3.5 Modified Stewart Hysteresis Model

The modified Stewart model is shown in Fig. 3.7. Folz and Filiatrault (2001) modified the exponential envelope curve used by Dolan (1989) to include hysteretic features of a model developed by Stewart (1987) to model wood-frame shear walls. The modified model is developed as part of the CUREe Wood-frame research project. In the model, unloading

exhibits a slipping or "pinching" stiffness K_5 where "pinching" force P_I corresponds to zero displacement, and the reversal load path follows the unloading stiffness. Reloading is defined in Eq. 3.17 and the stiffness and strength degradation are defined using Eq. 3.18.

$$K_6 = K_1 \left(\frac{\delta_{yield}}{\delta_{LD}} \right)^{\alpha} \tag{3.17}$$

$$\delta_{LD} = \beta \, \delta_{UN} \tag{3.18}$$

The model (coupled with the exponential envelope curve) requires ten input parameters:

K_1 = initial stiffness (envelope curve parameter)

r_1 = secondary stiffness factor $K_2 = r_1 K_1$ (envelope curve parameter)

r_2 = tertiary stiffness factor $K_3 = r_2 K_1$ (envelope curve parameter)

r_3 = unloading stiffness factor $K_4 = r_3 K_1$

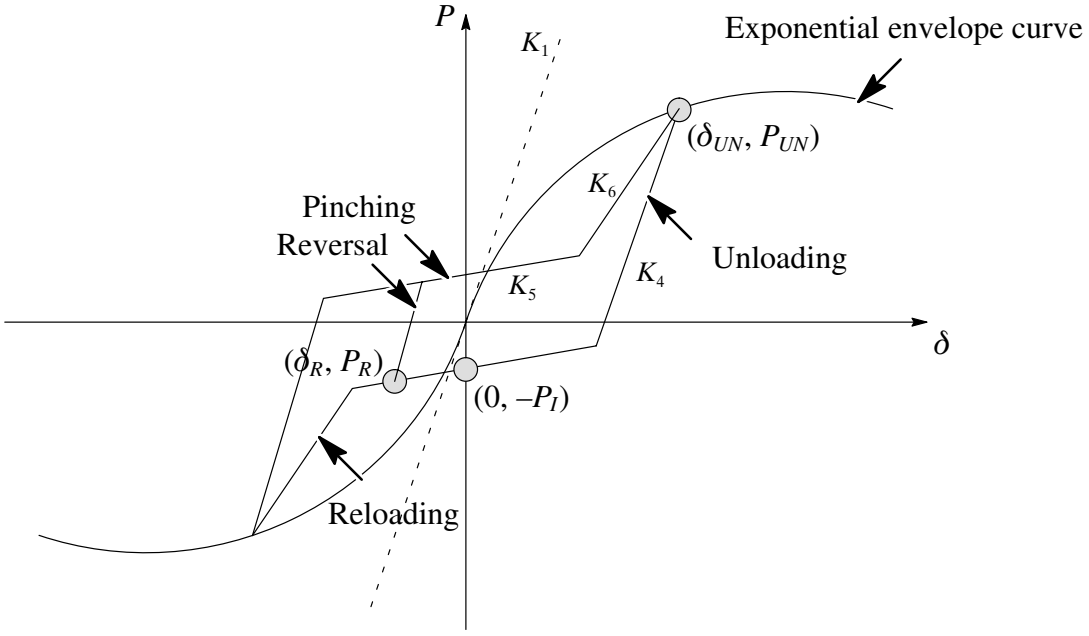

Fig. 3.7. Modified–Stewart hysteresis model

r_4 = loading stiffness factor $K_5 = r_4 K_1$

δ_{yield} = yield displacement

α_{LD} = reloading degradation factor

β = stiffness degradation factor

P_I = secondary stiffness force intercept (envelope curve parameter)

P_I = pinching force

3.3.6 Q-Pinch Hysteresis Model

The Q-Pinch hysteresis model is shown in Fig. 3.8. The Q-Pinch model is newly developed as part of this thesis. The model incorporates simple features of the previous models, while allowing for improved idealization. Loading first follows the envelope curve, unloading is defined as in the Q-Hyst model. Reloading consists of a slipping (pinching) branch and a reloading branch, like the modified Stewart model. The reloading stiffness K_6 is defined by the unloading points, where $K_1 \geq K_6 \geq F_{LD}/\delta_{LD}$. In the Q-Pinch model, however, the slipping branch is defined by the crossing point and the zero displacement load intercept. Also, unlike the modified Stewart model, the Q-Pinch model is not coupled with a specific envelope curve. Unloading stiffness degrades after displacement reaches δ_{yield} as follows:

$$K_4^{NEW} = K_4 \left(\frac{\delta_{yield}}{\delta_{LD}} \right)^{\alpha}; K_4 \geq P_{UN} \delta_{UN} \tag{3.19}$$

The reloading stiffness degradation is defined using Eq. 3.20.

$$K_6 = K_1 \left(\frac{\delta_{yield}}{\delta_{LD}} \right)^{\alpha_{LD}}; K_1 \geq K_6 \geq \frac{P_{LD}}{\delta_{LD}} \tag{3.20}$$

As a consequence, for small amplitude hysteresis the Q-Pinch model is identical to the Q-Hyst model. For large amplitude hysteresis, the model is an adapted form of the Stew-

art (1987) model, or modified Stewart model. The Q-Pinch model requires seven input parameters:

K_1 = initial stiffness (typically an envelope curve parameter)

K_4 = unloading stiffness

α_{UN} = unloading degradation factor

δ_{yield} = yield displacement

P_I = pinching force

β = stiffness degradation factor

α_{LD} = reloading degradation factor

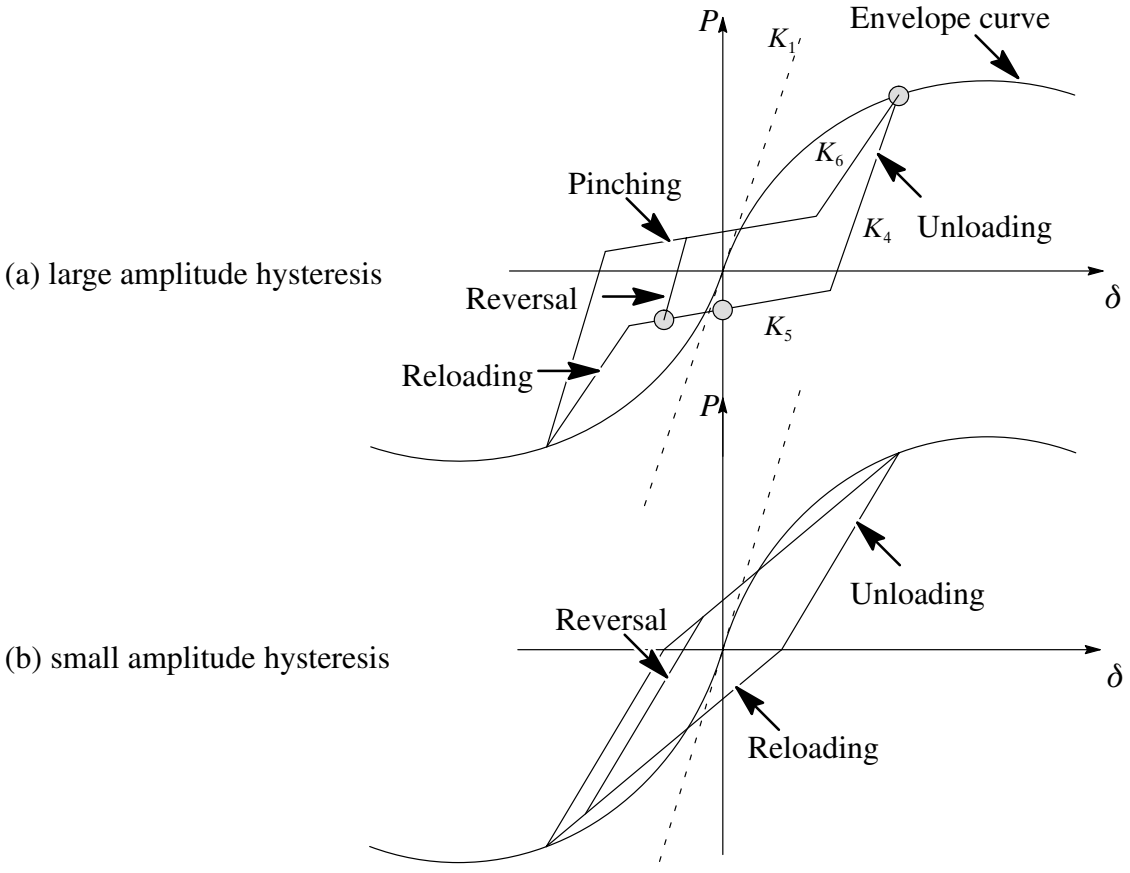

Fig. 3.8. Q-Pinch hysteresis model

3.4 Connection Representation for Structural Analysis

A sheathing-to-framing connection is commonly represented in a structural analysis program as a two-node element (Fig. 3.9). The first node (point A′) is the location of the nail head in the sheathing panel, and the second node (point B′) is the location of the nail shank in the wood framing. Each node has two degrees of freedom (DOF) corresponding to in-plane translations. The resultant connection displacement δ_r is calculated using the *x*–direction component δ_x and the *y*-direction component δ_y.

3.4.1 Single Spring Model

In the single spring model, a sheathing-to-framing connection is represented using one nonlinear spring (Fig. 3.10*a*). Since the displacement trajectory of a sheathing-to-framing connection is primarily unidirectional during monotonic loading (Tuomi and McCutcheon 1978), the total displacement of the connection may be estimated as the resultant displacement δ_r. Therefore the element stiffness matrix $\mathbf{K}$ is formulated as a "shear element," where the spring stiffness is equal in the *x*- and *y*-directions, and the nodal force vector $\mathbf{F}$ is

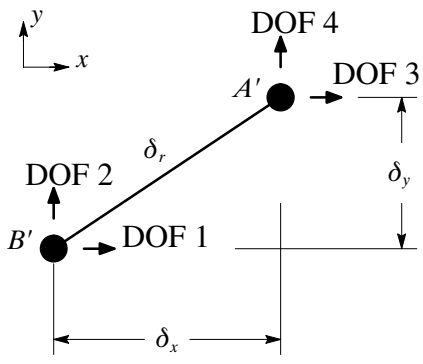

Fig. 3.9. Representation of a sheathing-to-framing connection

assumed to be proportional to the nodal displacements. The connection stiffness K_r and the connection force P_r are a function of the resultant displacement δ_r (Fig. 3.10*b*).

$$\mathbf{K} = \begin{bmatrix} K_r & 0 & -K_r & 0 \\ 0 & K_r & 0 & -K_r \\ -K_r & 0 & K_r & 0 \\ 0 & -K_r & 0 & K_r \end{bmatrix} \tag{3.21}$$

$$\mathbf{F} = \begin{Bmatrix} P_r\,(\delta_x/\delta_r) \\ P_r\,(\delta_y/\delta_r) \\ -P_r\,(\delta_x/\delta_r) \\ -P_r\,(\delta_y/\delta_r) \end{Bmatrix} \tag{3.22}$$

Two concerns arise when using the single spring model in a structural analysis program. The first concern is that the displacement trajectory can be bidirectional under re-

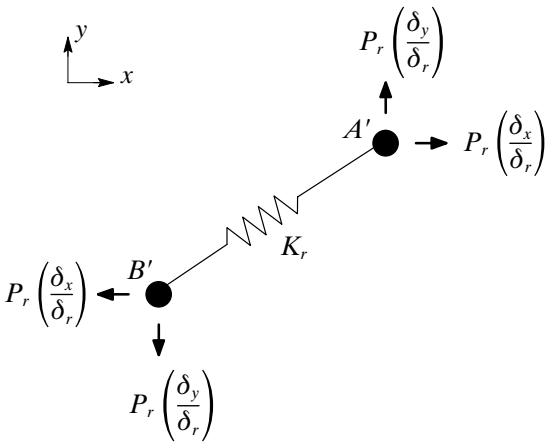

(a) Element representation

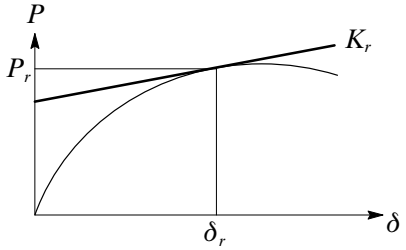

(b) Force-displacement behavior

Fig. 3.10. Single spring model

versed-cyclic loading or under highly nonlinear loading. As a consequence, the total connection displacement is path-dependent and not necessarily equivalent to the resultant displacement δ_r. In addition, it is not possible to define positive and negative displacement (required for hysteresis models) if a resultant displacement is used, notwithstanding the loading protocol.

The second concern when using the single spring model in a structural analysis program is that it may lead to numerical difficulties near the ultimate load. In fact, even at lower loads the single spring model may require alternate definitions of the element stiffness (using a secant stiffness definition, for instance) to facilitate a solution. Consequently, in order to provide numerical stability and allow bidirectional behavior, a non-oriented spring pair model has previously been used in structural analysis programs instead of the single spring model.

3.4.2 Non-Oriented Spring Pair

In the non-oriented spring pair model, a sheathing-to-framing connection is represented using two orthogonal nonlinear springs (Fig. 3.11*a*). The element stiffness matrix $\mathbf{K}$ and the nodal force vector $\mathbf{F}$ are uncoupled in the *x*- and *y*-directions. The connection stiffnesses, K_x and K_y , and connection forces, P_x and P_y , are a function of the respective *x*- and *y*-displacements (Fig. 3.11*b*). In the model, the stiffness represents the slope of the load-path at a specific point.

$$\mathbf{K} = \begin{bmatrix} K_x & 0 & -K_x & 0 \\ 0 & K_y & 0 & -K_y \\ -K_x & 0 & K_x & 0 \\ 0 & -K_y & 0 & K_y \end{bmatrix} \tag{3.23}$$

$$\mathbf{F} = \begin{Bmatrix} P_x \\ P_y \\ -P_x \\ -P_y \end{Bmatrix} \tag{3.24}$$

The primary concern with the non-oriented spring pair model is that it overestimates connection stiffness and force under nonlinear loading. With one spring in the x-direction and the other spring in the y-direction, the stiffness and force are arbitrary: the values of spring stiffness and force change relative to the displacement trajectory. For example, using the non-oriented spring pair model, sheathing-to-framing connections displaced along a tra-

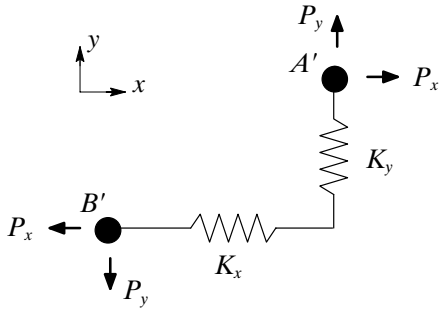

(a) Element representation

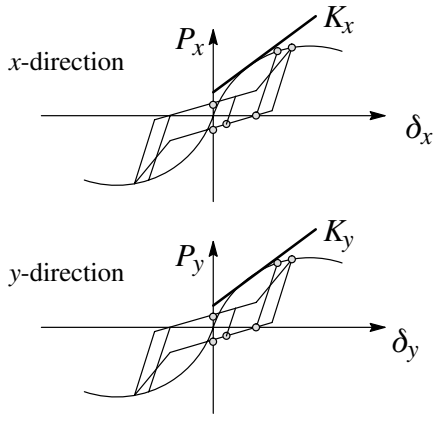

(b) Force-displacement hysteresis

Fig. 3.11. Non-Oriented Spring Pair Model

jectory of 45 degrees with respect to the *x*-direction, such as connections located near sheathing panel corners, have greater stiffness than identical connections equally displaced along a trajectory in the *x*-direction. Clearly, for a given displacement, this is incorrect. Actual connection stiffness is the same regardless of the displacement trajectory. Yet this overestimation is not confined to connections near panel corners because deformations of connections along panel edges vary approximately in proportion to the distance from the panel corner (Fonseca 1997; Schmidt and Moody 1989; McCutcheon 1985; Tuomi and McCutcheon 1978). As a result, structural analysis programs using the non-oriented spring pair model overestimate shear wall or diaphragm strength. The magnitude of overestimation is not accurately determined a priori, however, since the overestimation is a function of the wall (or diaphragm) aspect ratio, nail spacing, nail pattern, and shear modulus of the framing and sheathing.

To compensate for this overestimation, Folz and Filiatrault (2000) proposed a novel method for analysis of wood shear walls. In their method, the sheathing-to-framing connection spacing is adjusted until the energy absorbed by the wall using the non-oriented spring pair model agrees with the energy absorbed by the wall using a single spring model. Their model has subsequently been implemented into a structural analysis program (SAWS) for buildings composed of rigid horizontal diaphragms and wood shear walls (Folz and Filiatrault 2002). Although this adjustment is an ingenious solution for wood shear wall analysis, a rigorous solution is required for wood diaphragm analysis.

3.4.3 Oriented Spring Pair Model

In the oriented spring pair model, a sheathing-to-framing connection is represented using two orthogonal nonlinear springs that are oriented using the initial displacement trajectory (Fig. 3.12*a*). The initial displacement trajectory (u-direction) may be defined using the displacement at time zero, during a time-history analysis, or the linear displacement, during a linear analysis (Fig. 3.12*b*). The component of connection displacement along the initial displacement trajectory is δ_u , and the off-directional (v-direction) component is δ_v. The angle between the u- and x-directions is ϕ. In this way, the element stiffness matrix $\mathbf{K}$ and the nodal force vector $\mathbf{F}$ are coupled in the x- and y-directions. The connection stiffnesses, K_u and K_v, and connection forces, P_u and P_v , are a function of the respective u- and v-direction displacements (Fig. 3.12*c*).

$$\mathbf{K} = \begin{bmatrix} K_{11} & K_{12} & -K_{11} & -K_{12} \\ & K_{22} & -K_{12} & -K_{22} \\ & & K_{11} & K_{12} \\ sym. & & & K_{22} \end{bmatrix} \tag{3.25}$$

where

$$K_{11} = K_u \cos^2\phi + K_v \sin^2\phi \tag{3.26}$$

$$K_{12} = K_u \cos\phi \sin\phi - K_v \cos\phi \sin\phi \tag{3.27}$$

$$K_{22} = K_u \sin^2\phi + K_v \cos^2\phi \tag{3.28}$$

$$\mathbf{F} = \begin{Bmatrix} P_u \cos\phi - P_v \sin\phi \\ P_u \sin\phi + P_v \cos\phi \\ -P_u \cos\phi + P_v \sin\phi \\ -P_u \sin\phi - P_v \cos\phi \end{Bmatrix} \tag{3.29}$$

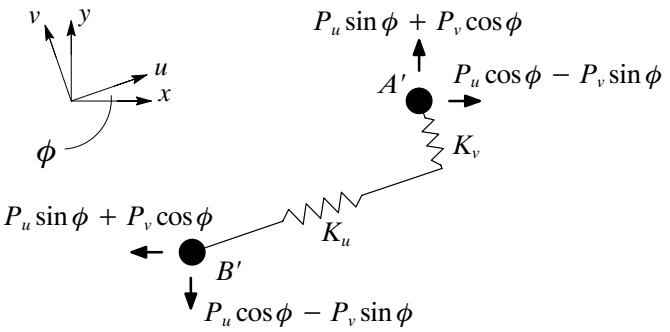

(a) Element representation

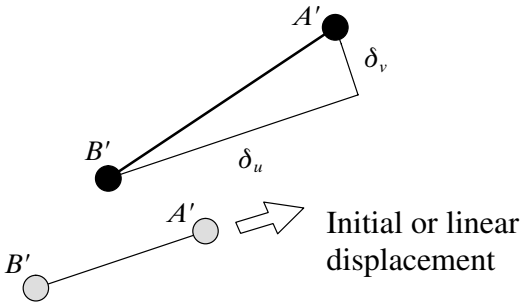

(b) Initial displacement trajectory

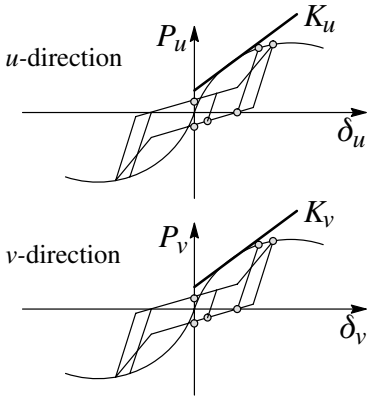

(c) Force-displacement hysteresis

Fig. 3.12. Oriented spring pair model

Nails pulling, or tearing, through sheathing panels is a dominate failure mode observed during reversed-cyclic loading of wood shear walls and diaphragms (Durham 1998; Olpin 1998; Jones and Fonseca 2002). Tearing of the sheathing prevents the connection displacement trajectory from subsequently following any established path, such as a circular path, and restricts the movement of the nail to a relatively narrow path. Consequently, even though the displacement trajectory can be bidirectional, the initial displacement trajectory is primarily unidirectional.

Accordingly, in the oriented orthogonal spring pair model, the orientation is representative of actual connection behavior: the off-directional, or orthogonal spring (v-direction), contribution to the element displacement is small since only the directional (u-direction) spring is principally deformed. Thus, by using the oriented spring pair model, the overestimation inherent in the non-oriented spring pair model is eliminated.

The oriented spring pair model may be refined to include off-directional stiffness degradation. The reduction in off-directional stiffness, or "true" off-directional stiffness, may be determined through coupon testing. In lieu of empirical data, off-directional stiffness may be incorporated based on the deformation of the directional spring using a continuous damage function, or a discrete set of damage levels. The relative importance of model refinement to include degradation is discussed in Chapter 4.

Chapter 4

FINITE ELEMENT ANALYSIS

In this chapter finite element analysis of shear walls and diaphragms is discussed. Two commercial finite element programs, *ANSYS* and *ABAQUS* are demonstrated. The new analytical model is implemented into *ABAQUS* and validated against measured experimental data for monotonic, cyclic, and dynamic analysis. Parametric studies are also conducted to determine the sensitivity of the finite element models to changes in material and section properties.

4.1 Finite Element Methods for Shear Wall and Diaphragm Analysis

A wide variety of wood shear wall analysis methods exist. Wood shear walls and diaphragms may be modeled as equivalent single-degree-of-freedom systems. Equivalent single degree of freedom systems are discussed in Chapter 6. More complex models have been developed by Gupta and Kuo (1985), Filiatrault (1990), and Dolan and Foschi (1991) to study static, cyclic (or quasi-static), and dynamic responses of wood shear walls. White and Dolan (1995) extended Dolan's previous method to include wall openings and to consider different wall aspect ratios. More recently, Folz and Filiatrault (2001) developed a five–degree-of-freedom model that predicts an overall cyclic response of shear walls and cali-

brates equivalent parameters for a single degree of freedom system. Folz and Filiatrault's model, *CASHEW*, is discussed in Chapter 5.

Analysis methods for both wood diaphragms and shear walls exist, though fewer in number. For instance, diaphragms have been modeled by employing elements that represent single lines of sheathing-to-framing connections by Foschi (1977), Itani and Cheung (1984), and Falk and Itani (1989). Later, Gutkowski and Castillo (1988) developed a non-commercial finite-element program in a more complex approach. In yet another approach, He et al. (2000) implemented a mechanics-based sheathing-to-framing connection element into a non-commercial program for both diaphragms and shear walls.

Finite element analysis using non–commercial, or in-house, software can be cumbersome. In-house software is usually intended for research and, as a result, is invariably awkward for ordinary usage. Although such in–house software may account for a number of complexities, some drawbacks are limited applicability, inflexible material nonlinearity, and a primitive interface.

An analysis method using commercial software avoids problems inherent in in–house software. For instance, commercial software is usually appropriate in general situations, and the interface is highly evolved and user–friendly. Traditionally, commercial software lacks behavioral models appropriate for sheathing–to–framing connections and is limited to uncoupled representation. As a consequence, the need to develop specialized elements in commercial software, instead of developing additional in–house software, has been recognized for some time (Foliente, 1995).

Analysis methods for shear walls and diaphragms using commercial software have been developed recently (Fonseca 1997; Judd and Fonseca 2002b). In these methods, sheathing–to–framing connections are represented using a pair of orthogonal uncoupled

spring elements using commercial software. Other researchers have represented sheathing–to–framing connections similarly (Symans et al. 2001). The difference between these methods is that the former method uses standard elements and uniquely defined connection behavior, whereas the latter method employs non–standard (user) elements with time–dependant connection behavior. Nonetheless, a reasonable overall response is obtained in both methods. Inherent in these uncoupled analysis methods, however, is an overestimation of shear wall and diaphragm stiffness that renders the models unreliable during ultimate loading.

Two standard commercial finite-element software programs, *ABAQUS* (2003) and *ANSYS* (2000) are used in this thesis. These programs were chosen because they are well-known and allow nonlinear material models to be used with spring elements. The method is widely applicable and flexible (Judd and Fonseca 2004b; Judd and Fonseca 2005). At the same time, the traditional limitations of commercial software are overcome by implementing a user element capable of coupled translational degrees–of–freedom and adaptable material nonlinearity. The analysis method is validated using experimental data.

4.2 Representation of Structural Components

The finite-element representation of structural components is shown in Table 4.1. Structural components are described, and the element type designation for *ANSYS* and *ABAQUS* is listed. Structural components are represented in a standard way. Wood framing is modeled using 2-node linear beam elements, sheathing panels are modeled using 8-node plane stress elements, and chord splices are modeled using 2-node linear spring elements with 1 translational degree-of-freedom. In a similar way to modeling the chord splices,

sheathing-to-framing connections are modeled using a pair of 2-node orthogonal nonlinear spring elements with 1 translational degree-of-freedom each.

The choice of element was based on the assumption that the nonlinear response of shear walls and diaphragms is primarily attributable to the sheathing-to-framing connections. Only linear elements were required to accurately represent the frame and sheathing. The 8-node plane stress element was chosen over a 4-node or a 9-node element to improve the model efficiency and reduce the computational effort required.

Table 4.1. Finite-Element Representation of Structural Components

		Element Designation	
Structural Component	Finite-Element Representation	*ANSYS*	*ABAQUS*
Framing	Beam element: 2-node	BEAM3	B21
Sheathing	Solid element: 8-node plain stress, reduced integration	PLANE82	CPS8R
Chord Splices	Spring element: 2-nodes, linear	COMBIN39	SPRING2
Sheathing-to-Framing Connections	User element pair: 2-node, nonlinear	COMBIN39	U1
Mass	Mass point elements: 1 node	—	MASS
Damping	Dashpot element: 2-node	—	DASHPOT

4.3 Mesh Size

An upper bound on the size of the finite element mesh is dictated by two factors: (1) the type of element used to represent the sheathing panels, and (2) the fastener spacing. Fonseca (1997) investigated the effect of using the upper bound "coarse" mesh (4 in. sq. ele-

ments) versus two "finer" meshes (2 in. sq. and 1 in. sq. elements) in the analysis of wood-frame diaphragms. The results demonstrated no appreciable difference in the model response. With this in mind, a "coarse" mesh was used the finite element models for this study, where the 8-node element size is dictated by the fastener spacing. Only square elements were used to avoid element distortions due to irregular midside nodes (Bathe 1996).

4.4 Solution Procedure

The solution of the nonlinear finite element equations is accomplished using the Newton-Raphson iteration algorithm. Typically automatic incrementation and solution control is used, where convergence is determined to occur when the magnitude of the out-of-balance force or moment is within 0.005% of the maximum magnitude of force or moment. Some analyses require direct control incrementation. Implicit direct-integration is used for dynamic analyses.

4.5 Monotonic Analysis

4.5.1 Response of 4.88 × 14.6 m Plywood Diaphragm

The response of a 4.88 × 14.6 m plywood diaphragm tested by the American Plywood Association (Tissell and Elliott 1997) is predicted using *ABAQUS*. These experimental results have previously been used to validate numerical models (Falk and Itani 1989; Fonseca 1997).

The plywood diaphragm uses 12.7-mm-thick Structural I C-D plywood sheathing panels. The sheathing is attached to the framing using 3.76-mm-diameter × 76.2-mm-long

nails spaced 102 mm on center along exterior panel edges, 152 mm on center along interior panel edges, and 305 mm on center in the panel fields. The framing consists of two 88.9×241 mm members along exterior edges perpendicular to applied load (chords), four 130×305 mm members spanning between chords (rafters), eight 88.9×241 mm members spanning between rafters (purlins), and 38.1×88.9 mm members spanning between rafters (sub-purlins) spaced at 0.61 m on center. During testing, the diaphragm was loaded in a non-reversed cyclic protocol (using load control) at 23 points along one chord (simulating a distributed load) and restrained at the corners of the opposite chord.

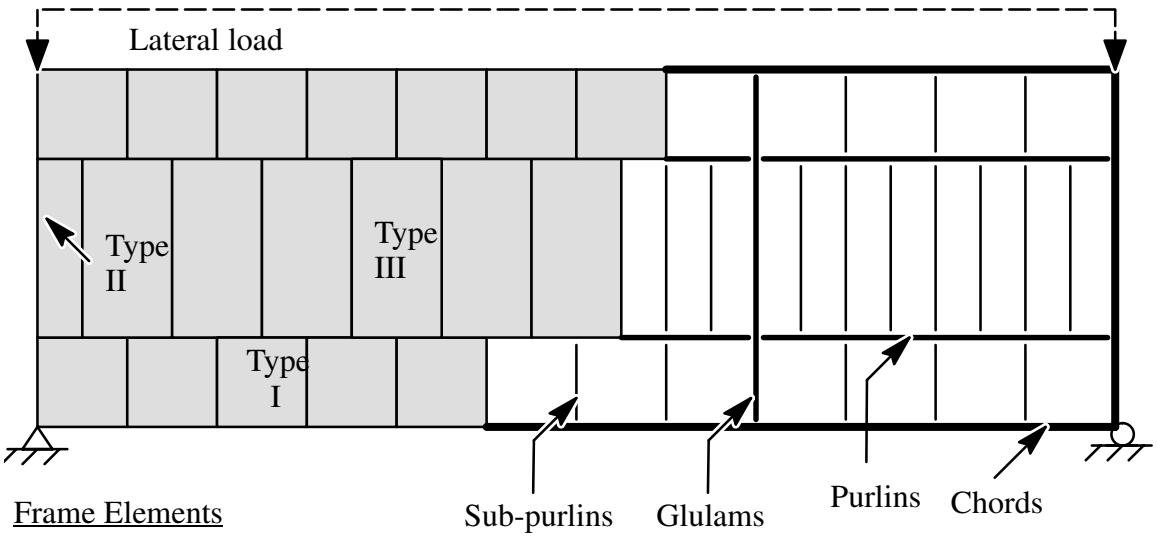

Frame Elements

Chord: 4 in. long 2-node linear beam elements

Glulam: 6–12 in. long 2-node linear beam elements

Purlins: 6 in. long 2-node linear beam elements

Sub-Purlins: 6 in. long 2-node linear beam elements

Panel Elements

Type I: 12×12 mesh of 8-node linear plain stress elements

Type II: 6×12 mesh of 8-node linear plain stress elements

Type III: 4×8 mesh of 8-node linear plain stress elements

Connection Elements

Splices: 2-node linear spring elements

Sheathing-to-framing connections: 2-node nonlinear user elements

Fig. 4.1. Diaphragm finite element model

For the finite element model, the modulus of elasticity of wood framing is approximated using the design values given in the National Design Specifications (NDS) for Wood Construction: Supplement (AF&PA 2001b). The modulus of elasticity, shear modulus, and effective shear thickness of sheathing are estimated using the design values given in the Plywood Design Specification (PDS) (APA 1997). The chord splice stiffness is extrapolated from chord displacements measured during testing.

The force-displacement behavior of the sheathing-to-framing connections is described using the mathematical expression suggested by APA—The Engineered Wood Association (APA 2004) for 12.7-mm-thick plywood and 3.76-mm-diameter × 76.2-mm-long nail connections (for units in inches and pounds):

$$P = 1.274\,\delta^{1/3.276} \tag{4.1}$$

The deformed shape of the finite element model is shown in Fig. 4.2. In Fig. 4.3 the measured response and the finite element model response of the plywood diaphragm are shown. The diaphragm configuration and loading are depicted in the figure inset. For pur-

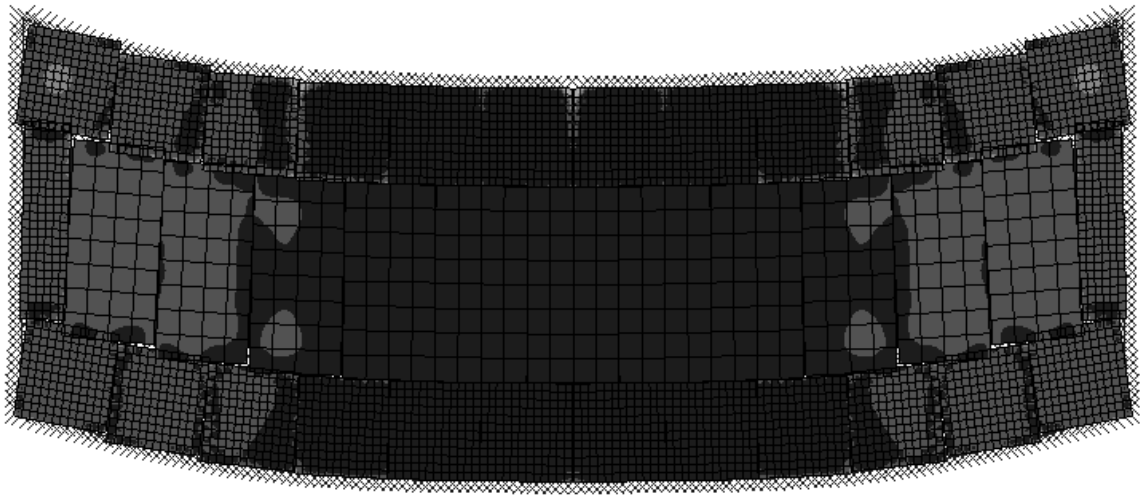

Fig. 4.2. Deformed shape of the 4.88×14.6 m plywood diaphragm model

poses of comparison, the finite element responses using both the non-oriented spring pair model and the oriented spring pair model are given.

The finite element model response generally agrees with the measured response. The stiffness of the finite element model is accurate during initial loading. As the applied force increases, the stiffness is slightly overestimated. This difference could be attributed to damage sustained during loading of the diaphragm. During testing, the applied load was halted at 127 kN (corresponding to a midspan displacement of 114 mm) when the hydraulic cylinders at the midspan reached maximum extension and observations suggested that failure was imminent. For this displacement, the finite element model using the oriented spring pair model overpredicts the force by 11% (the non-oriented spring pair model overpredicts by 18%). One possible cause of overestimation may be the use of linear chord splice stiffnesses.

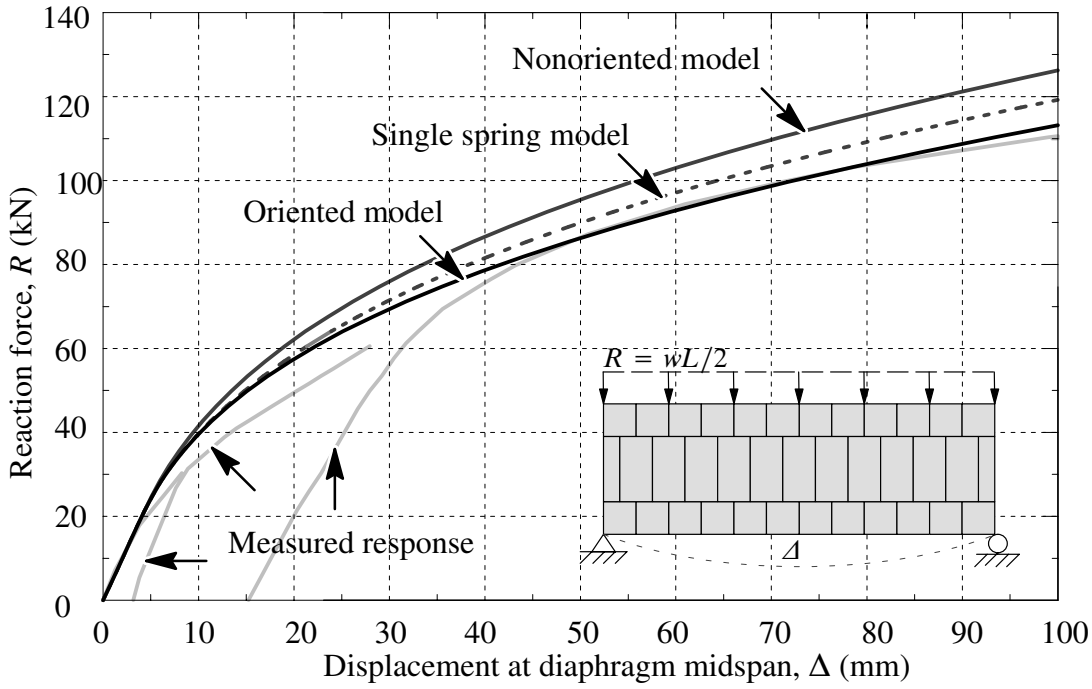

Fig. 4.3. Measured and finite element response of 4.88×14.6 m plywood diaphragm

Table 4.2. Finite Element Representation for a 4.88 × 14.6 m Diaphragm using 12.7 mm Plywood and 3.76 mm Common Nails

Structural Component	Finite Element Representation (*ABAQUS* element type)	Material and Section Properties
Chord	2-node linear beam element (B21)	E = 11.7 GPa (1,700,000 psi)[a]
Glulam		E = 11.0 GPa (1,600,000 psi)[a]
Purlin		E = 11.7 GPa (1,700,000 psi)[a]
Sub-Purlin		E = 10.3 GPa (1,500,000 psi)[a]
Plywood Sheathing	8-node linear reduced integration continuum element (CPS8R)	E = 12.4 GPa (1,800,000 psi)[b] G = 0.62 GPa (90,000 psi)[b] t = 13.8 mm (0.545 in.)[c]
Sheathing-to-Framing Connection	2-node nonlinear user element (U1)	12.7-PLY-3.76-COMMON-FLUSH Power Load-Displacement Curve Parameters[d] A = 769 B = 3.276
Tension Chord Splice Connection (quarter point)	2-node linear spring element (SPRING2)	K_1 = 31,500 N/mm (180,000 lb/in.)[e]
Tension Chord Splice Connection (center point)		K_1 = 24,500 N/mm (140,000 lb/in.)[e]
Compression Chord Splice Connection (quarter point)		K_1 = 315,000 N/mm (1,800,000 lb/in.)[e]
Compression Chord Splice Connection (center point)		K_1 = 420,000 N/mm (2,400,000 lb/in.)[e]

[a] NDS for Wood Construction: Supplement (AF&PA 2001b), Table 4A.
[b] PDS (APA 1997), Table 3.
[c] PDS, Table 2 (sanded).
[d] "Diaphragms and shear walls: design/construction guide," (APA 2004), Table A–2. For SI units multiply displacement by 2540 (see AF&PA/ASCE 1996, Table C9.5-1 M). Since the model was load-controlled the limiting load (1.16 kN) was not used.
[e] Approximate linear stiffness from "Cyclic loading response of reinforced concrete tilt–up structures with plywood diaphragms," (Fonseca 1997), Table 5.4., extrapolated from measured splice displacements given in Tissell and Elliott (1997).

4.5.2 Response of 2.44 × 2.44 m Plywood and Waferboard Shear Walls

The response of four 2.44 × 2.44 m plywood shear walls and three 2.44 × 2.44 m waferboard shear walls tested at the University of British Columbia (Dolan 1989) are predicted using *ABAQUS*. These experimental results have also previously been used to validate numerical models.

The configuration of the 2.44 × 2.44 m wood shear walls tested by Dolan (1989) is described in Chapter 2. Four walls used 3/8 in. softwood plywood panels and three walls used 3/8 in. waferboard panels. Sheathing was attached to framing using 8d common nails (0.131 in. diameter, 2.5 in. length) spaced at 4 in. on center along panel edges and 6 in. on center in panel fields. Framing consisted of double top, bottom and end plates (two 2 × 4 in. members nailed together) and 2 × 4 in. studs spaced at 2 ft on center. The wall was loaded monotonically along the top and restrained along the bottom. In the finite element model, one end of the shear wall base is pinned, and the other end is restrained in the vertical direc-

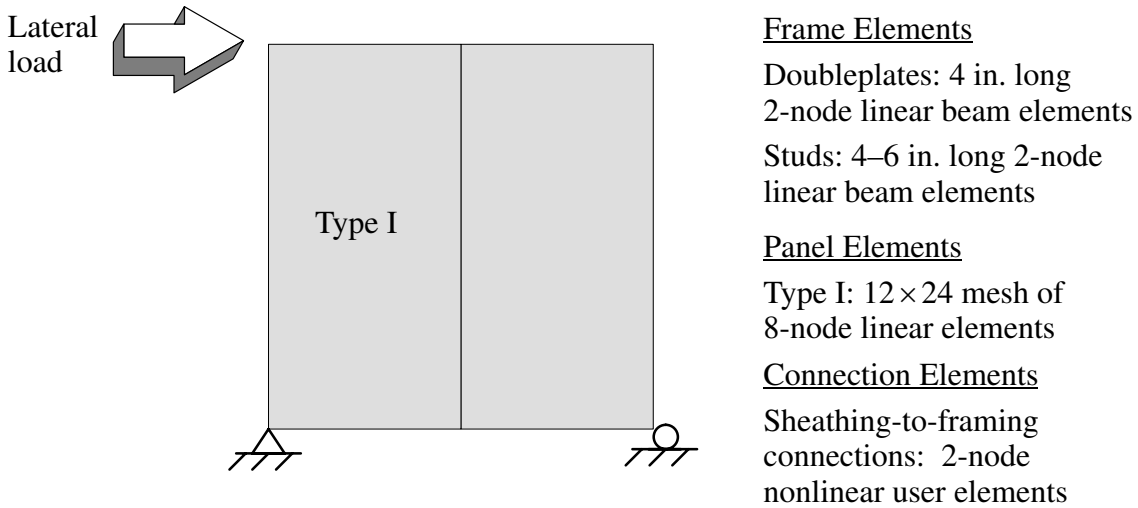

Fig. 4.4. Finite element model for 2.44 × 2.44 m plywood or waferboard shear wall

tion. Modeling of boundary conditions along the base of the shear wall are not usually significant because sheathing-to-framing connections govern the overall behavior (Easley et al. 1982).

Material and Section Properties. Material and section properties used in the finite element models are presented in Table 4.3 and Table 4.4 for the shear walls. For each structural component, a finite element description, *ABAQUS* element type designation, and member description is listed. Standard component material and section properties are listed in the last two columns since actual properties were not available. The sensitivity of the finite element model to using standard properties is presented later.

The analysis method presented is essentially independent of the load–displacement behavior. Therefore, although a number of mathematical curves effectively idealize the load–displacement behavior of sheathing–to–framing connections, in this section the exponential curve used by Dolan (1989) is applied in the shear wall models

$$P = (P_0 + K_2\,\delta)\left[1 - e^{\frac{-K_1\delta}{P_0}}\right] \tag{4.2}$$

where the initial stiffness K_1, the secondary stiffness K_2, and the load–intercept P_0, are physically identifiable parameters determined from experimental data. The values of the load–displacement curve are given in Table 4.3 for the plywood shear wall and in Table 4.4 for the waferboard shear wall.

Results. The deformed shape of a shear wall finite element model, shown in Fig. 4.5, is consistent with deformation observed during testing. The measured and calculated responses are shown in Fig. 4.6 for the plywood shear walls, and in Fig. 4.7 for the waferboard shear walls.

Table 4.3. Finite Element Representation for a 2.44 × 2.44 m Shear Wall using 9.53 mm Plywood and 3.33 mm Common Nails

Structural Component	Finite Element Representation (*ABAQUS* element type)	Material and Section Properties
Double Plate Stud	2-node linear beam element (B21)	E = 9.65 GPa (1,400,000 psi)[a]
Plywood Sheathing	8-node linear reduced integration continuum element (CPS8R)	E = 12.4 GPa (1,800,000 psi)[b] G = 0.62 GPa (90,000 psi)[b] t = 7.06 mm (0.278 in.)[c]
Sheathing-to-Framing Connection	2-node nonlinear user element (U1)	9.53-PLY-3.33-COMMON-FLUSH Exponential Load-Displacement Curve Parameters[d] K_1 = 853 N/mm (4870 lb/in.) K_2 = 42.0 N/mm (240 lb/in.) P_0 = 800 N (180 lb) δ_{ult} = 12.7 mm (0.5 in.) K_3 = 42.0 N/mm (240 lb/in.)[e] δ_{fail} = 27.9 mm (1.1 in.)[f]

[a] NDS for Wood Construction: Supplement (AF&PA 2001b), Table 4A.
[b] PDS (APA 1997), Table 3.
[c] PDS, Table 1.
[d] Dolan and Foschi (1991), Table 1, except K_3.
[e] Dolan and Madsen (1992), Table 3. Since there are discrepancies between Dolan and Foschi's, and Dolan and Madsen's parameters, the latter value for K_3 was used to facilitate solution convergence.
[f] This value is assumed.

Table 4.4. Finite Element Representation for a 2.44 × 2.44 m Shear Wall using 9.53 mm Waferboard and 3.33 mm Common Nails

Structural Component	Finite Element Representation (*ABAQUS* element type)	Material and Section Properties
Double Plate Stud	2-node linear beam element (B21)	E = 9.65 GPa (1,400,000 psi)[a]
Waferboard Sheathing	8-node linear reduced integration continuum element (CPS8R)	E = 4.14 GPa (600,000 psi)[b] G = 1.43 GPa (207,000 psi)[c] t = 9.53 mm (0.375 in.)[d]
Sheathing-to-Framing Connection	2-node nonlinear user element (U1)	9.53-WAF-3.33-COMMON-FLUSH Exponential Load-Displacement Curve Parameters[e] K_1 = 827 N/mm (4720 lb/in.) K_2 = 42.0 N/mm (240 lb/in.) P_0 = 890 N (200 lb) δ_{ult} = 12.7 mm (0.5 in.) K_3 = 42.0 N/mm (240 lb/in.)[f] δ_{fail} = 27.9 mm (1.1 in.)[g]

[a] NDS for Wood Construction: Supplement (AF&PA 2001b), Table 4A.
[b] 33% of the PDS, Table 3 value for plywood (Montrey 1983). For comparison, Itani and Cheung (1984) used E = 536,000 psi for their finite element model.
[c] 100% of the *Technical Bulletin No. 104* (PFS/RF 2003) Table A value for OSB. For comparison, Filiatrault (1990) used G = 217,557 psi for modeling Dolan's (1989) shear wall tests.
[d] Effective shear thickness = nominal thickness
[e] Dolan and Foschi (1991), Table 1, except K_3.
[f] Dolan and Madsen (1992), Table 3. Since there are discrepancies between Dolan and Foschi's, and Dolan and Madsen's parameters, the latter value for K_3 was used to facilitate solution convergence.
[f] This value is assumed.

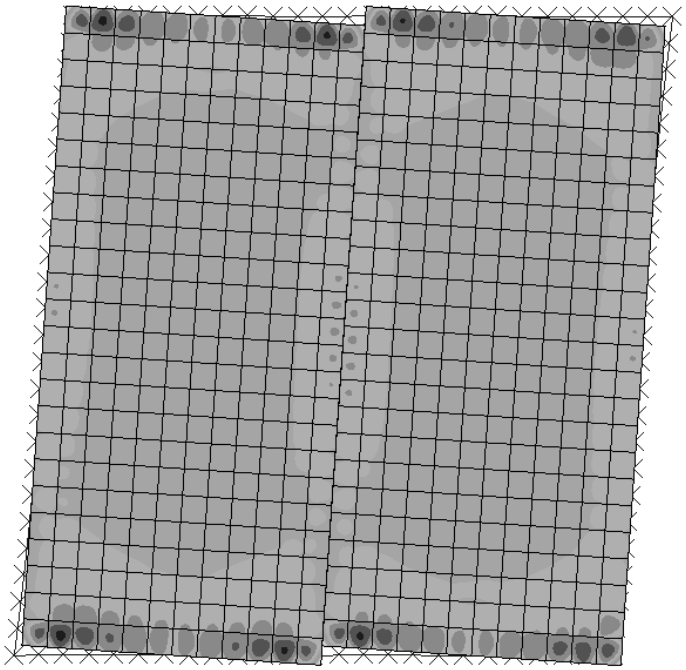

Fig. 4.5. Deformed shape of the 2.44 × 2.44 m plywood shear wall model

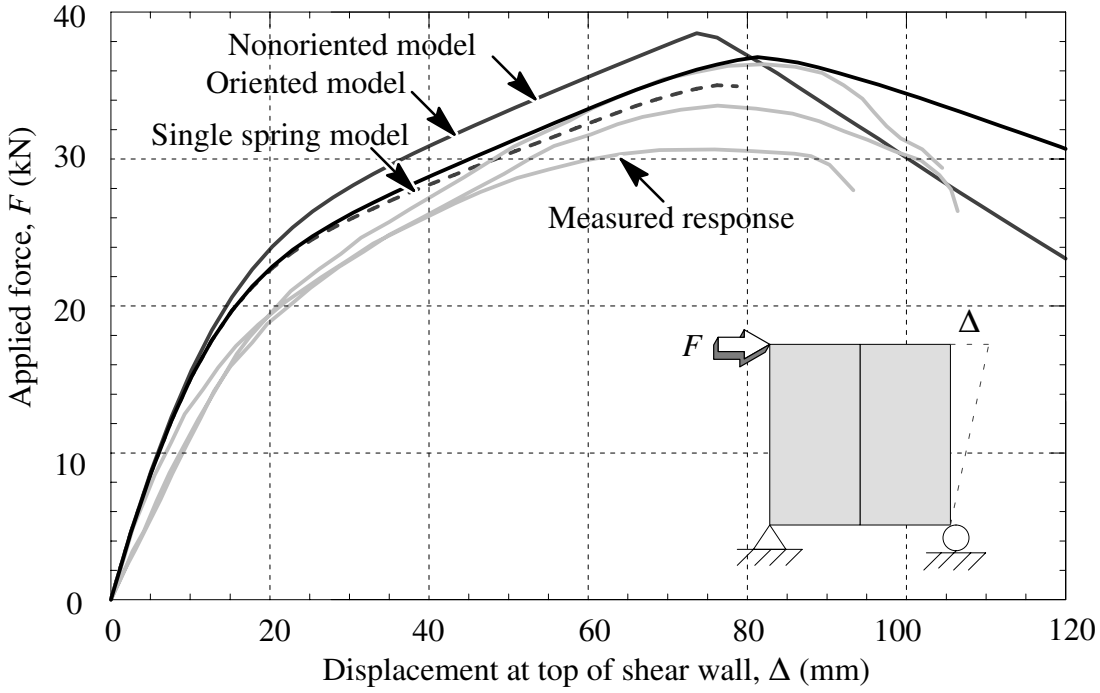

Fig. 4.6. Measured and finite element response of 2.44 × 2.44 m plywood shear wall

The response of all three plywood shear wall tests and all four waferboard shear wall tests are shown. A discussion of the individual (and nominally identical) tests would be irrelevant here since the tests are used for comparison. In the shear wall models, the initial stiffness of the finite element model is similar to the experimental initial stiffness for plywood walls, and slightly greater for waferboard walls. The difference in waferboard wall stiffness may be attributed to the lack of sheathing property information available. In general, though, the calculated response is reliable.

4.6 Quasi-Static (Cyclic) Analysis

4.6.1 Response of 2.44 × 2.44 m Oriented Strand Board Shear Walls

The response of two 2.44×2.44 m oriented strand board shear walls tested at the University of British Columbia (Durham 1998) are predicted using *ABAQUS*. These experimental results have also previously been used to validate numerical models (Folz and Filiatrault 2001; He et al. 2001). The two nominally identical shear walls use 9.53 mm thick OSB sheathing panels attached to framing using 2.67-mm diameter $\times$ 50.0 mm long spiral (threaded hardened-steel) nails. During testing, one wall was loaded monotonically and the other wall was loaded cyclicly. The load was applied along the top side, and the wall was restrained along the base. The finite element model is depicted in Fig 4.8. Table 4.5 gives the geometric and material properties of the finite element model.

The sheathing-to-framing connection force-displacement curve is described using a logarithmic expression with a linear softening branch:

Table 4.5. Finite Element Representation for a 2.44 × 2.44 m Shear Wall using 9.53 mm OSB and 2.67 mm Spiral Nails

Structural Component	Finite Element Representation (*ABAQUS* element type)	Material and Section Properties
Double Plate Stud	2-node linear beam element (B21)	E = 9.65 GPa (1,400,000 psi)[a]
OSB Sheathing	8-node linear reduced integration continuum element (CPS8R)	E = 4.93 GPa (714,000 psi)[b] G = 1.50 GPa (218,000 psi)[c] t = 9.53 mm (0.375 in.)
Sheathing-to-Framing Connection	2-node nonlinear user element (U1)	9.53-OSB-2.67-SPIRAL-FLUSH Exponential Load-Displacement Curve Parameters[d] K_1 = 561 N/mm (3200 lb/in.) K_2 = 34.2 N/mm (195 lb/in.) P_0 = 751 N (169 lb) δ_{ult} = 12.5 mm (0.49 in.) K_3 = 43.8 N/mm (250 lb/in.) δ_{fail} = 27.9 mm (1.1 in.)[e] CUREe Hysteresis Parameters[d] K_4 = 785 N/mm (4480 lb/in.) K_5 = 80.2 N/mm (458 lb/in.) P_I = 141 N (32.0 lb) δ_{yield} = 1.34 mm (0.053 in.)[f] α = 0.8 β = 1.1

[a] NDS for Wood Construction: Supplement (AF&PA 2001b), Table 4A.
[b] PDS (APA 1997), Table 3.
[c] Folz and Filiatrault (2001).
[d] Folz and Filiatrault (2001), Table 1.
[e] This value is assumed.
[f] determined by dividing P_0 by K_1.

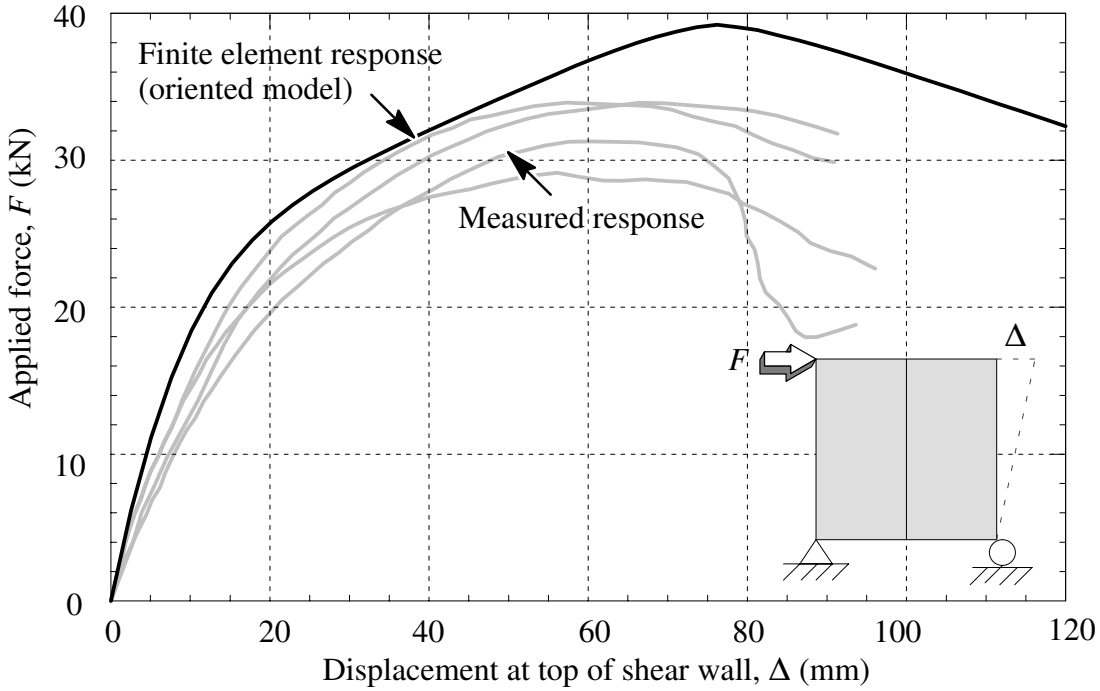

Fig. 4.7. Measured and finite element response of 2.44 × 2.44 m waferboard shear wall

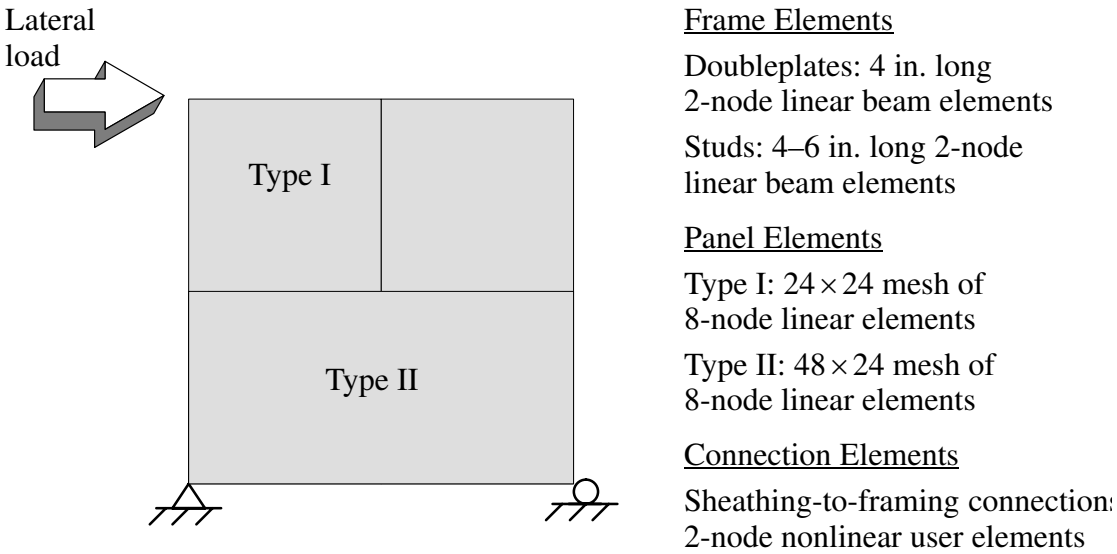

Fig. 4.8. Finite element model for 2.44 × 2.44 m oriented strand board shear wall

$$P = \begin{cases} (P_0 + r_1 K_0 \Delta)\left[1 - e^{\frac{-K_0 \Delta}{P_0}}\right], \text{ if } \Delta \le \Delta_{ult} \\ P_{ult} + r_2 K_0 (\Delta - \Delta_{ult}), \text{ if } \Delta_{ult} < \Delta \le \Delta_{fail} \\ 0, \text{ if } \Delta > \Delta_{fail} \end{cases} \quad (4.3)$$

For reversed-cyclic behavior, a modified form of the Stewart (1987) hysteresis model is used, which includes strength degradation, stiffness degradation, and pinching behavior. Table 4.5 gives the geometric and material properties of the finite element model. The parameters for Eq. 4.3 and the hysteresis model are given for 9.53-mm-thick oriented strand board and 2.67-mm-diameter × 50.0-mm-long spiral (threaded hardened-steel) nail connections. The parameter values are determined experimentally (Durham 1998), except the r_4 value is set to 0.05, in accordance with previous studies (Rosowsky 2002).

In Fig. 4.9 the deformed shape of the finite element model is shown. In Fig. 4.10 a comparison between the modified *CASHEW* response (using the oriented spring pair model) and the measured response is shown. The modified *CASHEW* response is fairly accurate during large amplitude loading, and less accurate during small amplitude loading. This response is reasonable because the hysteresis model does not consider loss of strength during small amplitude loading.

In Table 4.6 a summary of the cyclic response of the shear wall is given. The absolute difference between the measured value, as a percentage of the predicted value, is listed for the ultimate displacement Δ_{ult}, ultimate load F_{ult}, and energy dissipation E_a (energy dissipation is accumulated after each time step). The ultimate displacement and load values for the modified *CASHEW* response are about 3% closer to the measured values than the original *CASHEW* response.

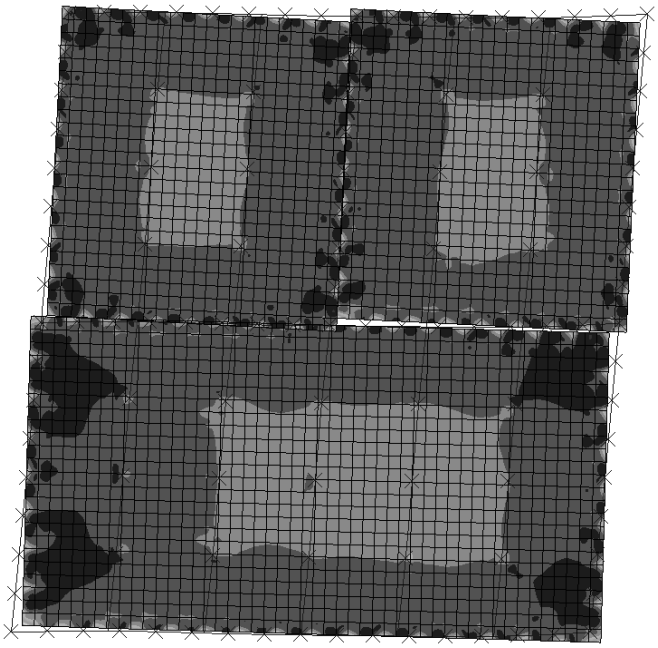

Fig. 4.9. Deformed shape of 2.44 × 2.44 m oriented strand board shear wall model

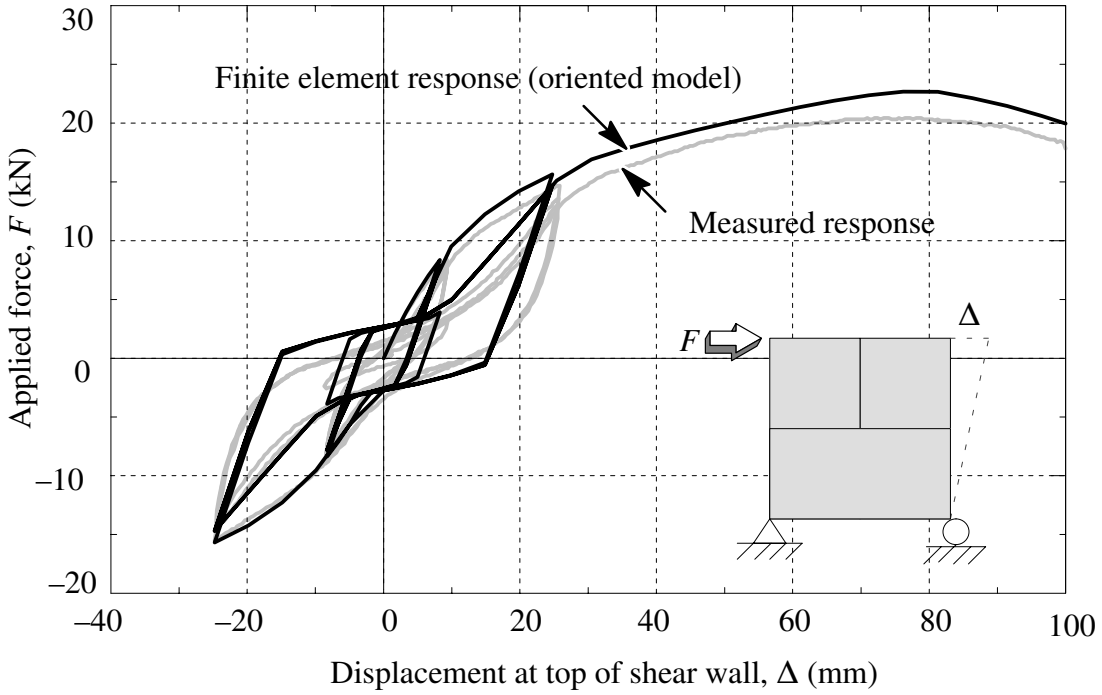

Fig. 4.10. Measured and finite element response of 2.44 × 2.44 m oriented strand board shear wall

Table 4.6. Cyclic Response of 2.44×2.44 m Oriented Strand Board Shear Wall

Sheathing-to-framing connection element representation	Δ_{ult}		F_{ult}		Energy Absorbed	
	(mm)	Difference (%)	(kN)	Difference (%)	(kN-mm)	Difference (%)
Measured response	66.0		20.4		2.59	
Non-oriented spring pair	60.0	9.1	24.0	17.7	2.92	12.7
Adjusted non-oriented spring pair	60.0	9.1	22.0	7.8	2.68	3.5
Oriented spring pair	70.0	6.1	21.4	4.9	2.64	1.9

* Difference = | measured / predicted |

Therefore, although either model may be considered as an acceptable design tool, the primary advantage of the oriented spring pair model is that no scaling or adjustment is required to compensate for overestimation of sheathing-to-framing strength and stiffness, as is done in previous non-oriented spring pair models. For comparison, the ultimate displacement and ultimate load values predicted by He et al. (2001) using a nonlinear finite element model *LIGHTFRAME3D* were 17 kN and 58 mm, respectively.

4.7 Dynamic Time-History Analysis

4.7.1 Response of 2.44 × 2.44 m Oriented Strand Board Shear Walls

The finite element model is used in a nonlinear dynamic time-history analysis of a 2.44×2.44 m oriented strand board shear wall tested at the University of British Columbia (Durham 1998). The shear wall configuration is identical to the previous 3-panel oriented strand board shear walls, except with the addition of 5,450 kg supported along the top.

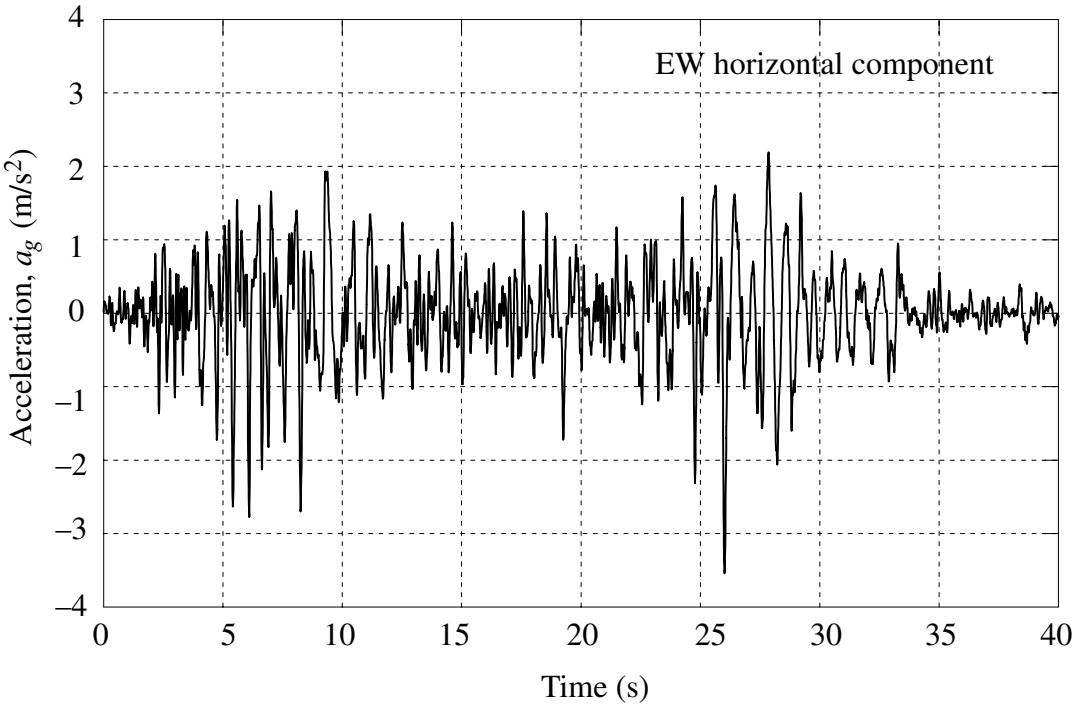

Fig. 4.11. Input ground motion: Landers 1992 Earthquake scaled to 0.35 g (Durham 1998)

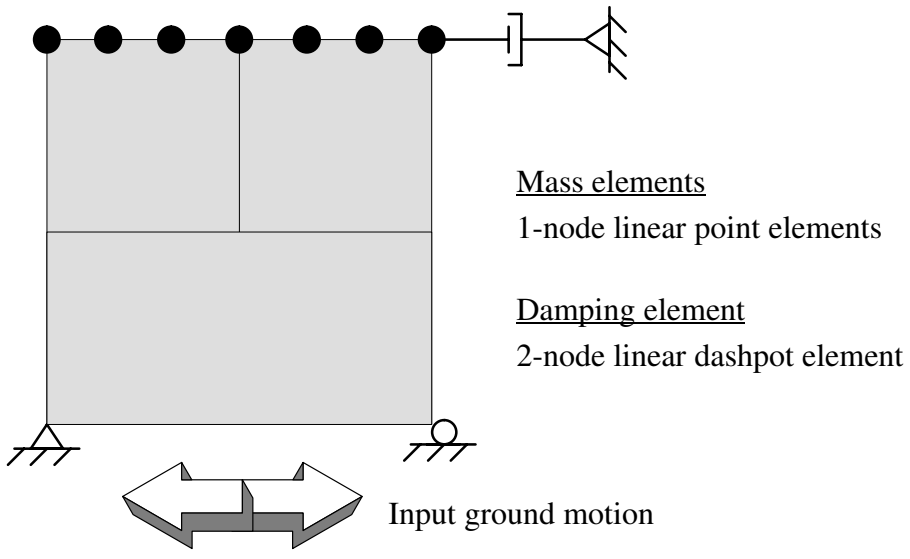

Fig. 4.12. Finite element model for a 2.44 × 2.44 m oriented strand board shear wall

The shear wall is subjected to a scaled input ground motion from the Landers 1992 Earthquake. The Landers ground motion record shown in Fig 4.11 is interesting because it includes two intervals of large accelerations over approximately 35 seconds, compared to other records with only one such interval.

The previous finite element model used in the cyclic analysis is modified to include mass elements, a damping element, and ground motion. Fig 4.12. shows the finite element model. The 5,450 kg supported load is represented in the finite element model using 7 point mass elements distributed along the wall top, consisting of 908 kg each interior element and 454 kg for exterior elements. A viscous damping ratio of 1% is implemented using a dashpot element.

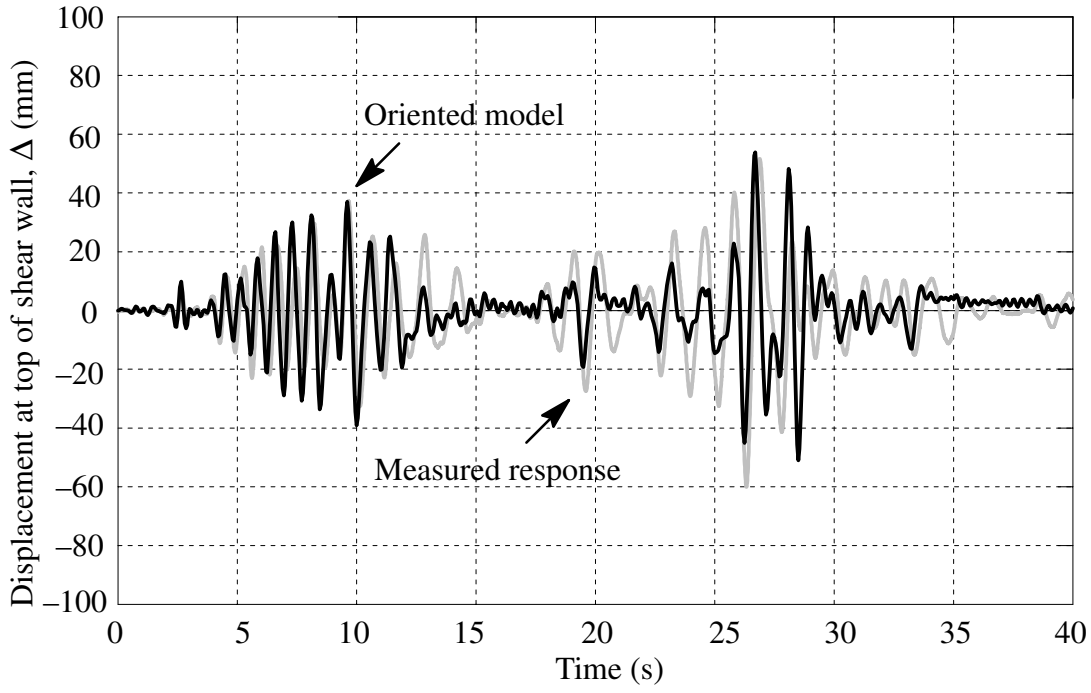

Fig. 4.13. Time-history response of 2.44 × 2.44 m oriented strand board shear wall

The dynamic equilibrium equations for the finite element model are solved using implicit direct-time integration with Newton-Raphson iterations. The finite element and measured time-history responses are shown in Fig 4.13. The finite element model overpredicts the displacement during large amplitudes, and underpredicts the displacement amplitude during the 10–25 second interval. In general, however, the finite element response is reasonably accurate.

4.8 Parametric Analysis

The sensitivity of the finite element model to parametric changes is determined through three short parametric analyses. In the first analysis the static sensitivity of the finite element model to changes in model and material parameters is determined using a nonoriented spring pair model. In the second analysis, the dynamic sensitivity of the finite element model to changes in the hysteresis model is determined using the oriented orthogonal spring pair model. In the third analysis, the static sensitivity of the finite element model to refinement of the oriented model is determined.

4.8.1 Static Sensitivity to Material and Geometric Parameters

The 2.44×2.44 m plywood shear wall model discussed earlier is considered for the static sensitivity study. The model sensitivity to various changes is summarized in Table 4.7. The model is most sensitive to the behavior of the sheathing-to-framing connections, as expected. Since only a 20% change in the connection response led to 40 to 60% change in the overall shear wall response, it is imperative that reliable load-displacement curve parameters are used.

The model is also very sensitive to the framing-to-framing connection idealization. However, this presents less of a problem because experience has demonstrated that the framing connections do not contribute to the shear wall rigidity. Thus, the idealization of "pinned" connections is justified. Similarly, the model is somewhat sensitive to the sheathing shear modulus. This is not an issue for OSB and plywood sheathing materials because the standard shear modulus is well established, but is more a consideration for uncommon sheathing materials, such as waferboard.

The model is only slightly sensitive to the finite-element software, framing modulus of elasticity, and sheathing thickness. Since changes in software caused a difference in the final stages of loading, the difference may be attributed to numerical tolerance of the out-of-balance loads and formation of the sheathing-to-framing connection stiffness. No appreciable changes to overall response are caused by changes of sheathing modulus of elasticity or boundary conditions, consistent with previous studies (Easley et al. 1982; Fonseca 1997).

Table 4.7. Finite Element Model Sensitivity to Material and Geometric Parameters

Parameter	Control	Deviation	Absolute difference (%)
Finite-element software	*ABAQUS*	*ANSYS*	4
Wall base boundary conditions	Ends restrained	length restrained	1
Framing-to-framing connections	Pinned	Fixed	45
Sheathing-to-framing connection L-D curve	Dolan and Foschi (1991)	+20%	37
		–20%	59
Framing modulus of elasticity	E_x = 9.65 GPa	$2E_x$ = 19.3 GPa	4
		$½E_x$ = 4.83 GPa	6
Sheathing modulus of elasticity	E_x = 12.4 GPa	$2E_x$ = 24.8 GPa	0
		$½E_x$ = 6.2 GPa	0
Sheathing shear modulus	G_{xy} = 0.62 GPa	$2G_{xy}$ = 1.24 GPa	7
		$½G_{xy}$ = 0.31 GPa	15
Sheathing thickness	t_{eff} = 7.06 mm	$t_{nominal}$ = 9.65 mm	4

4.8.2 Dynamic Sensitivity to Sheathing-to-Framing Connection Model Hysteresis

The 2.44×2.44 m oriented strand board shear wall model discussed earlier is considered for the dynamic sensitivity study. The finite element model is analyzed using *ABAQUS*. In Fig. 4.14 the finite element response using the Clough hysteresis model is contrasted with the response using the modified Stewart hystereis model. The results demonstrate the importance of a hysteresis model incorporating pinching and nonlinearity. A detailed finite element model, such the shear wall model considered here, is computationally demanding. Therefore, a more comprehensive study of the response sensitivity to hysteresis models is performed in Chapter 6 using an equivalent single degree of freedom system.

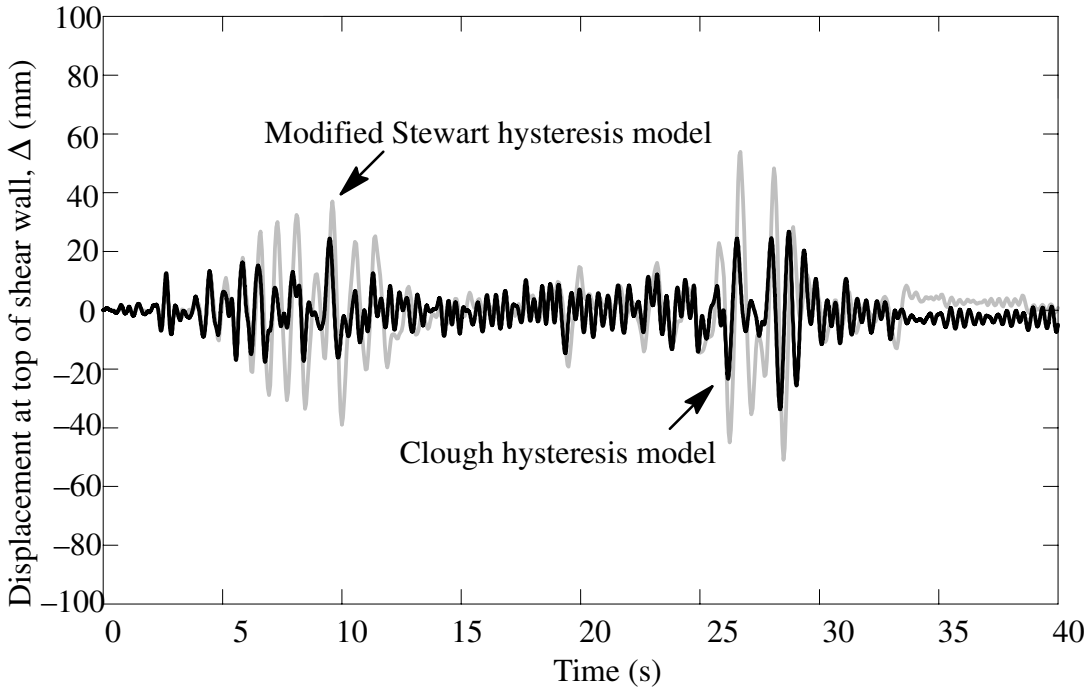

Fig. 4.14. Finite element model sensitivity to sheathing-to-framing connection model hysteresis

4.8.3 Dynamic Sensitivity to Sheathing-to-Framing Connection Model Refinement

The static sensitivity of the 2.44×2.44 m plywood shear wall model (considered earlier) to refinement of the oriented model is determined using *ABAQUS*. As discussed in Chapter 3, the oriented model may be refined to include off-directional stiffness degradation. The reduction in off-directional stiffness, or "true" off-directional stiffness, may be determined empirically, or incorporated based on the deformation of the directional spring using a continuous damage function, or a discrete set of damage levels. A continuous damage function described in Eq. 4.4–4.7, and shown in Fig. 4.15 is proposed.

$$P^* = D_f P \tag{4.4}$$

$$K^*_{TAN} = D_f K_{TAN} \tag{4.5}$$

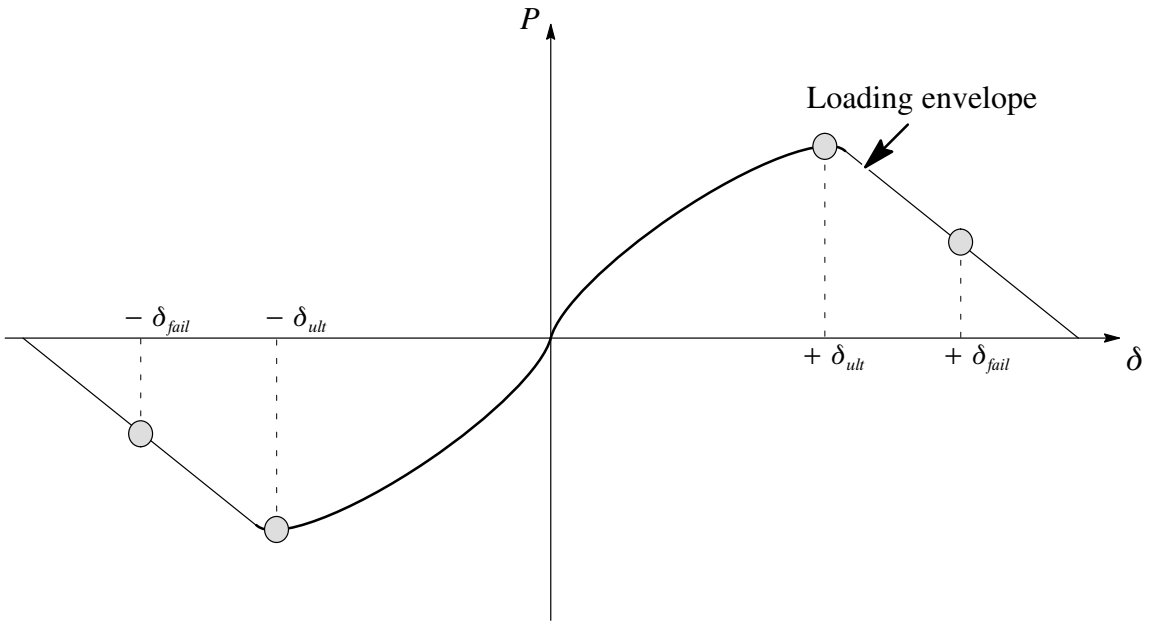

Fig. 4.15. Continuous damage function parameters

where the degraded force and stiffness, P^* and K^*_{TAN}, respectively, are proportional to the degradation factor, D_f given in Eq. 4.6–4.7. In this way, degradation is assumed to be proportional to the ratio between the cumulative displacement along the deformation trajectory, δ_{cum} and the failure displacement, δ_{fail}.

$$D_f = 0 \qquad \text{if } \delta_{cum} > \delta_{fail}\,, \tag{4.6}$$

$$D_f = 1 - \frac{\delta_{cum}}{\delta_{fail}} \qquad \text{otherwise.} \tag{4.7}$$

In Fig. 4.16 the finite element response using oriented model with no off-directional stiffness degradation is compared with the response using the refined model that includes off-directional stiffness degradation using the continuous damage function. The results suggest that the model refinement only improves response prediction after ultimate loading. Further research is needed to determine the robustness of this model refinement.

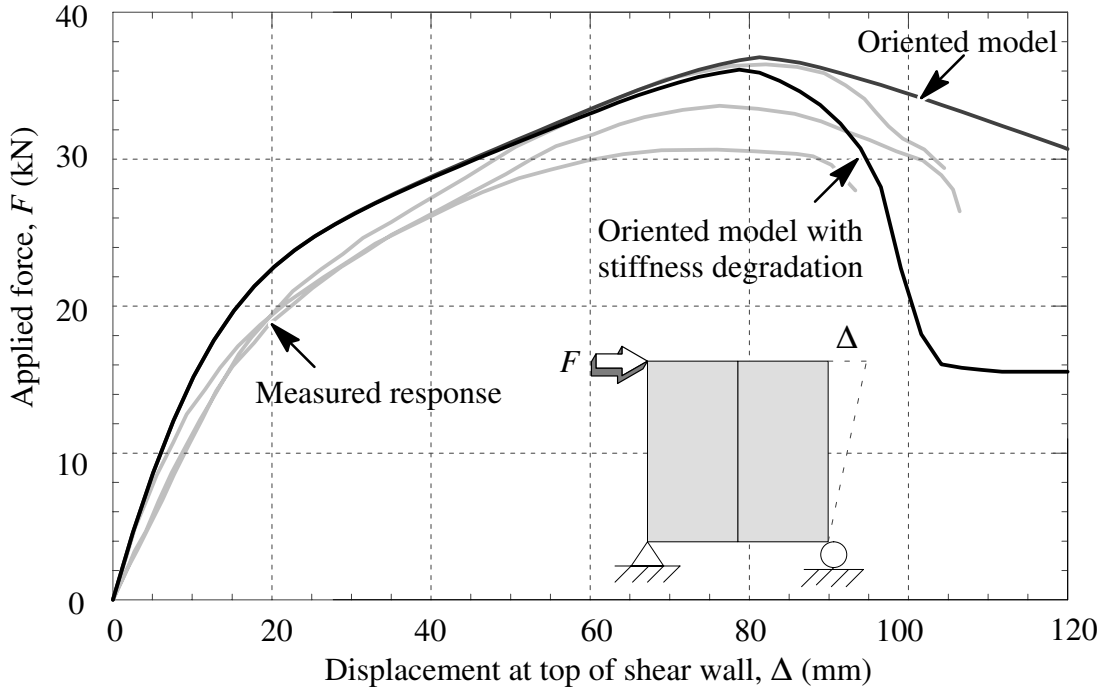

Fig. 4.16. Finite element model sensitivity to sheathing-to-framing model refinement

4.9 Summary

In these numerical examples, the results from laboratory testing of shear walls and diaphragms consisting of only framing, sheathing, and fasteners, need to be viewed in proper perspective. The response of actual wood structures under seismic loading is influenced by additional factors, such as the contribution of non-structural elements. In a recent study, interior and exterior finish materials, for example, significantly increased the lateral stiffness of a two-story, single-family wood frame house during shake table testing (Filiatrault et al. 2002). Interestingly, the study also concluded that the effect of finish materials on the response of larger wood structures remains unclear because the relative contribution of finish materials could not be quantified. The finite element model presented in this paper, therefore, may also be used to clarify the contribution of non-structural elements to the overall structural response.

Chapter 5

QUASI-STATIC ANALYSIS OF SHEAR WALLS

The oriented spring pair model is implemented into a specialized structural analysis program, *CASHEW* for quasi-static analysis of wood shear walls. A modified version of *CASHEW* that incorporates the oriented spring pair model is used. The original *CASHEW* computer program is modified by removing the connection spacing adjustment algorithm, replacing the non-oriented spring pair stiffness matrix with the oriented spring pair stiffness matrix, and adding an algorithm to extract the initial orientation of each sheathing-to-framing connection. The response of a 2.44×2.44 m oriented strand board shear wall is discussed.

5.1 The CASHEW program

A numerical model for cyclic analysis of shear walls (*CASHEW*) was developed as part of the CUREe-Caltech Woodframe project. The model is used to predict the load displacement and energy dissipation characteristics of wood shear walls. Additionally, the *CASHEW* program calibrates a single degree of freedom (SDOF) system to idealize the shear wall for dynamic analysis (Folz and Filiatrault 2000, 2001). Recently, *CASHEW* has also been used reliability studies (Filiatrault and Folz 2002; Rowsosky 2002; Rosowsky and Kim 2004; van de Lindt and Rosowsky 2005).

5.2 CASHEW Model Formulation

The formulation of the *CASHEW* model is an extension of an earlier model (Filiatrault 1990). The primary assertion is that the wood framing deforms rigidly as pin connected members, thus allowing a relationship between the sheathing-to-framing connection deformation and the overall shear wall deformation to be established. Additionally, it is asserted that uplift is nonexistent, that out-of-plane deformations are inconsequential, and that small displacement theory applies and, as a result, sheathing and wood framing deformations are linear. Thus, the relationships between the element (panel) degrees of freedom and the system (wall) degrees of freedom are

$$\begin{Bmatrix} u_p \\ v_p \\ u_f \\ v_f \end{Bmatrix} = \begin{bmatrix} 0 & 2y/H & 1 & 0 & -y \\ 0 & 0 & 0 & 1 & x \\ (y+\bar{y})/H & 0 & 0 & 0 & 0 \\ 0 & 0 & 0 & 0 & 0 \end{bmatrix} \begin{Bmatrix} U_F \\ U_S \\ \overline{U} \\ \overline{V} \\ \Theta \end{Bmatrix} \tag{5.1}$$

$$\underline{\boldsymbol{u}} = \underline{\underline{\boldsymbol{T}}}\,\underline{\boldsymbol{U}} \tag{5.2}$$

Therefore the total number of DOFs for a given wood shear wall equals *4 × (number of sheathing panels) + 1*. For convenience, let the connection displacements be defined in the global x and y directions:

$$\delta_x = u_p - u_f \tag{5.3}$$

$$\delta_y = v_p - v_f \tag{5.4}$$

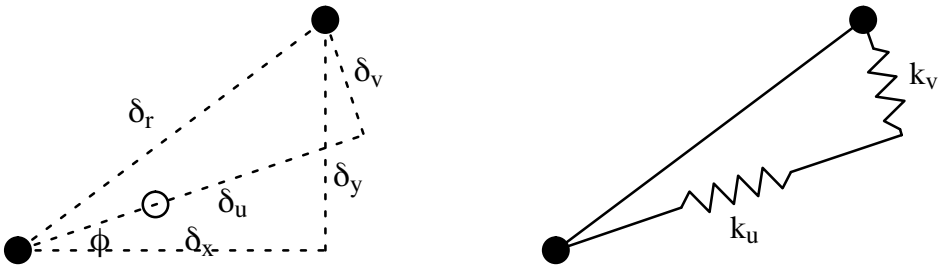

Fig. 5.1. Local and global connection displacements

5.2.1 Solution of the Governing Differential Equations

The governing differential equations are solved by a variational formulation from equating the internal work to the external work. This yields the Euler-Lagrange equation

$$\frac{\partial W_{INTERNAL}}{\partial \underline{\boldsymbol{D}}} = \frac{\partial W_{EXTERNAL}}{\partial \underline{\boldsymbol{D}}} \tag{5.5}$$

where

$$\frac{\partial W_{INTERNAL}}{\partial \underline{\boldsymbol{D}}} = \frac{\partial \left(W_{SHEATHING} + W_{CONNECTIONS}\right)}{\partial \underline{\boldsymbol{D}}} \tag{5.6}$$

Sheathing-to-Framing Connection Contribution. The internal work done by the several sheathing-to-framing connections is formulated in this section using Eq. 5.7.

$$W_C = \sum_{j=1}^{N_C} \int_0^{\delta_j} P_j \, d\xi \tag{5.7}$$

For convenience the summation sign is dispensed with, and instead, summation over the panels, connections, and local u and v directions is implied in all of the following equations. Thus Eq. 5.7 becomes

$$\begin{aligned} W_C &= \int_0^{\delta} P \, d\xi \\ &= \frac{1}{2} k \delta^2 \\ &= \frac{1}{2}\left(k_u \, \delta_u{}^2 + k_v \, \delta_v{}^2\right) \\ &= \frac{1}{2}\left[k_u \left(\delta_x \cos\phi + \delta_y \sin\phi\right)^2 + k_v \left(-\delta_x \sin\phi + \delta_y \cos\phi\right)^2\right] \\ &= \frac{1}{2} k_u \left(\delta_x{}^2 \cos^2\phi + 2\delta_x \delta_y \cos\phi \sin\phi + \delta_y{}^2 \sin^2\phi\right) \\ &\quad + \frac{1}{2} k_v \left(\delta_x^2 \sin^2\phi - 2\delta_x \delta_y \cos\phi \sin\phi + \delta_y^2 \cos^2\phi\right) \end{aligned}$$

$$= \frac{1}{2}\delta_x^2\left(k_u\cos^2\phi + k_v\sin^2\phi\right) + \delta_x\delta_y\left(k_u\cos\phi\sin\phi - k_v\cos\phi\sin\phi\right)$$

$$+ \frac{1}{2}\delta_y^2\left(k_u\sin^2\phi + k_v\cos^2\phi\right) \tag{5.8}$$

For convenience, let the member (panel) stiffness global components be written as

$$k_{xx} = k_u\cos^2\phi + k_v\sin^2\phi \tag{5.9}$$

$$k_{xy} = k_u\cos\phi\sin\phi - k_v\cos\phi\sin\phi \tag{5.10}$$

$$k_{yy} = k_u\sin^2\phi + k_v\cos^2\phi \tag{5.11}$$

Therefore

$$W_C = \frac{1}{2}k_{xx}\delta_x^2 + k_{xy}\delta_x\delta_y + \frac{1}{2}k_{yy}\delta_y^2 \tag{5.12}$$

From Eq. 5.1 the element (panel) deformations may be written in terms of the wall deformations, so that global horizontal displacement

$$\delta_x = \frac{-y+\bar{y}}{H}U_F + \frac{2y}{h}U_S + \overline{U} + 0 - y\,\Theta \tag{5.13}$$

and the global vertical displacement

$$\delta_y = 0 + 0 + 0 + \overline{V} + x\,\Theta \tag{5.14}$$

It follows that

$$\delta_x^2 = \frac{(y+\bar{y})^2}{H^2}U_F^2 - 4y\frac{(y+\bar{y})}{Hh}U_SU_F + \frac{4y^2}{h^2}U_S^2 + -2\frac{(y+\bar{y})}{H}\overline{U}U_F + \frac{4y}{h}\overline{U}U_S$$

$$+ \overline{U}^2 + 2y\frac{(y+\bar{y})}{H}\Theta U_F - 4\frac{y^2}{h}\Theta U_S - 2y\Theta\overline{U} + y^2\Theta^2 \tag{5.15}$$

$$\delta_y^2 = \overline{V}^2 + 2x\Theta\overline{V} + x^2\Theta^2 \tag{5.16}$$

$$\delta_x\delta_y = -\frac{(y+\bar{y})}{H}U_F\overline{V} + \frac{2y}{h}U_S\overline{V} - x(y+\bar{y})U_F\Theta + \frac{2yx}{h}\Theta U_S$$

$$+ \overline{U}\overline{V} + x\overline{U}\Theta - y\overline{V}\Theta - xy\Theta^2 \tag{5.17}$$

Therefore, the internal work done by the sheathing-to-framing connections

$$\frac{\partial W_C}{\partial \underline{\boldsymbol{D}}} = \frac{\partial\left(\frac{1}{2}k_{xx}\delta_x^2 + k_{xy}\delta_x\delta_y + \frac{1}{2}k_{yy}\delta_y^2\right)}{\partial \underline{\boldsymbol{D}}} \tag{5.18}$$

$$
\begin{aligned}
&= \frac{\partial\left(\frac{1}{2}k_{xx}\delta_x^2\right)}{\partial\underline{\boldsymbol{D}}} + \partial\frac{\left(k_{xy}\delta_x\delta_y\right)}{\partial\underline{\boldsymbol{D}}} + \partial\frac{\left(\frac{1}{2}k_{yy}\delta_y^2\right)}{\partial\underline{\boldsymbol{D}}} \\
&= k_{xx}\begin{bmatrix}
\frac{(y+\bar{y})}{H^2} & -2y\frac{(y+\bar{y})}{Hh} & -\frac{(y+\bar{y})}{H} & 0 & y\frac{(y+\bar{y})}{H} \\
 & 4\frac{y^2}{h^2} & \frac{2y}{h} & 0 & \frac{-2y^2}{h} \\
 & & 1 & 0 & -y \\
 & & & 0 & 0 \\
 & & & & y^2
\end{bmatrix}\begin{Bmatrix} U_F \\ U_S \\ \overline{U} \\ \overline{V} \\ \Theta \end{Bmatrix} \\
&\quad + k_{xy}\begin{bmatrix}
0 & 0 & 0 & -\frac{(y+\bar{y})}{H} & -x\frac{(y+\bar{y})}{H} \\
0 & 0 & 0 & \frac{2y}{H} & \frac{2xy}{h} \\
0 & 0 & 0 & 1 & x \\
-\frac{(y+\bar{y})}{H} & \frac{2y}{h} & 1 & 0 & -y \\
-x\frac{(y+\bar{y})}{H} & \frac{2xy}{h} & x & -y & -xy
\end{bmatrix}\begin{Bmatrix} U_F \\ U_S \\ \overline{U} \\ \overline{V} \\ \Theta \end{Bmatrix} \\
&\quad + k_{yy}\begin{bmatrix}
0 & 0 & 0 & 0 & 0 \\
 & 0 & 0 & 0 & 0 \\
 & & 0 & 0 & 0 \\
 & & & 1 & x \\
 & & & & x^2
\end{bmatrix}\begin{Bmatrix} U_F \\ U_S \\ \overline{U} \\ \overline{V} \\ \Theta \end{Bmatrix} \qquad (5.19) \\
&= \left(k_{xx}\,\underline{\underline{\boldsymbol{Q}}}_{xx} + k_{xy}\,\underline{\underline{\boldsymbol{Q}}}_{xy} + k_{yy}\,\underline{\underline{\boldsymbol{Q}}}_{yy}\right)\underline{\boldsymbol{D}} \qquad (5.20)
\end{aligned}
$$

Sheathing Panel Contribution. The internal work done by the sheathing panels

$$
\begin{aligned}
W_S &= \left(\frac{2Gbt_p}{h}\right)U_S^2 \qquad (5.21) \\
\frac{\partial W_S}{\partial\underline{\boldsymbol{D}}} &= \left(\frac{4Gbt_p}{h}\right)U_S \qquad (5.22) \\
&= \begin{bmatrix}
0 & 0 & 0 & 0 & 0 \\
 & \frac{4GBt_p}{h} & 0 & 0 & 0 \\
 & & 0 & 0 & 0 \\
 & & & 0 & 0 \\
 & & & & 0
\end{bmatrix}\begin{Bmatrix} U_F \\ U_S \\ \overline{U} \\ \overline{V} \\ \Theta \end{Bmatrix} \\
&= \underline{\underline{\boldsymbol{Q}}}_S\,\underline{\boldsymbol{D}} \qquad (5.23)
\end{aligned}
$$

External Force Contribution. The external work done by the applied force at the top of the shear wall

$$\frac{\partial W_{EXTERNAL}}{\partial \underline{\boldsymbol{D}}} = \underline{\boldsymbol{F}} \tag{5.24}$$

$$= \begin{Bmatrix} F_F \\ 0 \\ 0 \\ 0 \\ 0 \end{Bmatrix} \tag{5.25}$$

Final Equilibrium Equations. The final equilibrium equations to be solved are

$$\underline{\underline{\boldsymbol{K}}}\,\underline{\boldsymbol{D}} = \underline{\boldsymbol{F}} \tag{5.26}$$

where

$$\underline{\underline{\boldsymbol{K}}} = k_{xx}\,\underline{\underline{\boldsymbol{Q}_{xx}}} + k_{xy}\,\underline{\underline{\boldsymbol{Q}_{xy}}} + k_{yy}\,\underline{\underline{\boldsymbol{Q}_{yy}}} + \underline{\underline{\boldsymbol{Q}_S}} \tag{5.27}$$

The equations are solved using a displacement control solution strategy (Batoz 1979; Ramm 1981).

5.3 Modifications to CASHEW program

The following modifications were made to the *CASHEW* FORTRAN code to incorporate the formulation described, namely (1) elimination of the `TIMER` portions of the code in the `MAIN` routine; (2) addition of author/modification information into title blocks; (3) elimination of adjustment of connector spacing in subroutine `STATIC1`; (4) redefinition of the local displacements in subroutine `PSTIF2` and `UPDATE`, and redefinition of the element (panel) stiffness in subroutine `PSTIF2`; (5) addition of a loop to extract the initial orientation (displacements) from each sheathing-to-framing connection in subroutine `STATIC1`; and (6) expansion of the size of the `CSTOR1` and `CSTOR2` arrays in all routines. The modified subroutines are given in Appendix C.

5.4 Verification of Modified CASHEW program

The response of two 2.44 × 2.44 m oriented strand board shear walls tested at the University of British Columbia (Durham 1998) are predicted using *CASHEW*. The shear wall configuration is shown in Fig. 5.2. These experimental results have also previously been used to validate numerical models (Folz and Filiatrault 2001; He et al. 2001).

The two nominally identical shear walls use 9.53 mm thick OSB sheathing panels attached to framing using 2.67-mm-diameter × 50.0 mm long spiral (threaded hardened-steel) nails. During testing, one wall was loaded monotonically and the other wall was loaded cyclicly. The load was applied along the top side, and the wall was restrained along the base. The sheathing-to-framing connection force-displacement curve is described using a logarithmic expression with a linear softening branch:

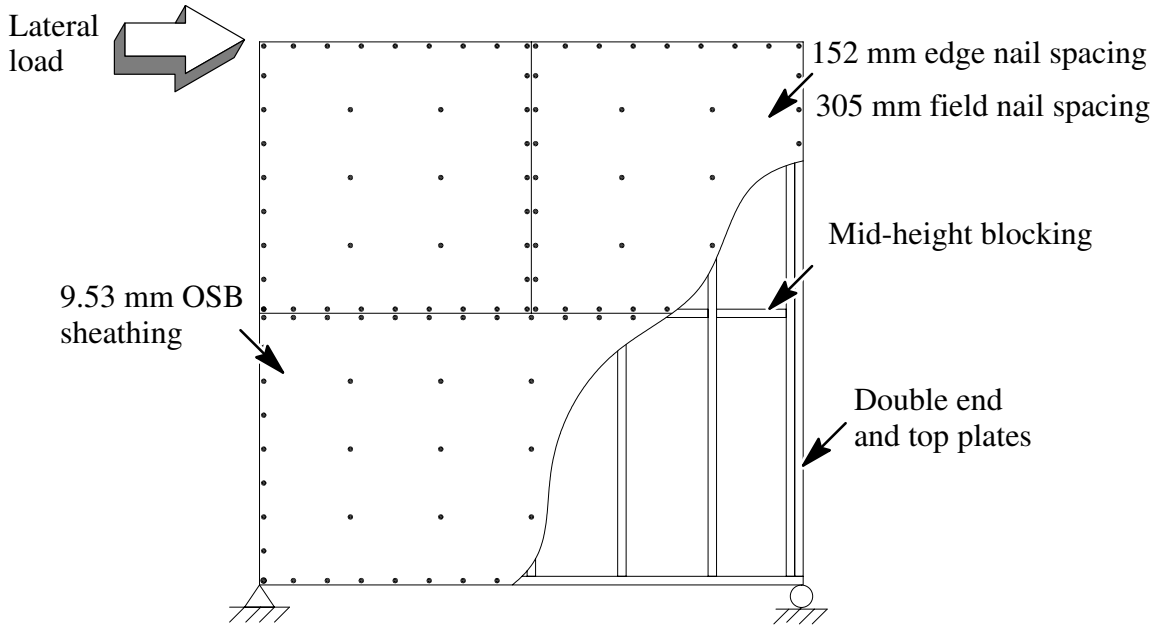

Fig. 5.2. Configuration of 2.44 × 2.44 m shear wall using 2.67 × 50.0 mm spiral nails

$$P = \begin{cases} (P_0 + r_1 K_0 \Delta)\left[1 - e^{\frac{-K_0 \Delta}{P_0}}\right], \text{ if } \Delta \leq \Delta_{ult} \\ P_{ult} + r_2 K_0 (\Delta - \Delta_{ult}), \text{ if } \Delta_{ult} < \Delta \leq \Delta_{fail} \\ 0, \text{ if } \Delta > \Delta_{fail} \end{cases} \tag{5.28}$$

For reversed-cyclic behavior, *CASHEW* uses a modified form of the Stewart (1987) hysteresis model, which includes strength degradation, stiffness degradation, and pinching behavior. In Table 5.1 the parameters for Eq. 5.28 and the hysteresis model are given for 9.53-mm-thick oriented strand board and 2.67-mm-diameter × 50.0-mm-long spiral (threaded hardened-steel) nail connections. The parameter values are determined experimentally (Durham 1998), except the r_4 value is set to 0.05, in accordance with previous studies (Rosowsky 2002).

Table 5.1. Force-Displacement Curve Parameters: 9.53 mm OSB / 2.67 mm Spiral Nail

K_0 (kN/mm)	r_1	r_2	r_3	r_4	P_0 (kN)	P_1 (kN)	Δ_{ult} (mm)	α	β
0.561	0.061	–0.078	1.40	0.143	0.751	0.141	12.5	0.8	1.1

In Fig. 5.3 and Fig. 5.4, a comparison between the modified *CASHEW* response (using the oriented spring pair model) and the measured response is shown. The modified *CASHEW* response is fairly accurate during large amplitude loading, and is less accurate during small amplitude loading. This response is reasonable because the hysteresis model does not consider loss of strength during small amplitude loading.

In Table 5.2 a summary of the cyclic response of the shear wall is given. The absolute difference between the measured value, as a percentage of the predicted value, is listed for the ultimate displacement Δ_{ult}, ultimate load F_{ult}, and energy dissipation E_a (energy dissipation is accumulated after each time step). A comparison between the energy absorbed by the wall models is shown in Fig. 5.5.

The ultimate displacement and load values for the modified *CASHEW* response are about 3% closer to the measured values than the original *CASHEW* response. Therefore, although either model may be considered an as acceptable design tool, the primary advantage of the oriented spring pair model is that no scaling or adjustment is required to compensate for overestimation of sheathing-to-framing strength and stiffness, as is done in previous non-oriented spring pair models. For comparison, the ultimate displacement and ultimate load values predicted by He et al. (2001) using a nonlinear finite element model (*LIGHT-FRAME3D*) were 17 kN and 58 mm, respectively.

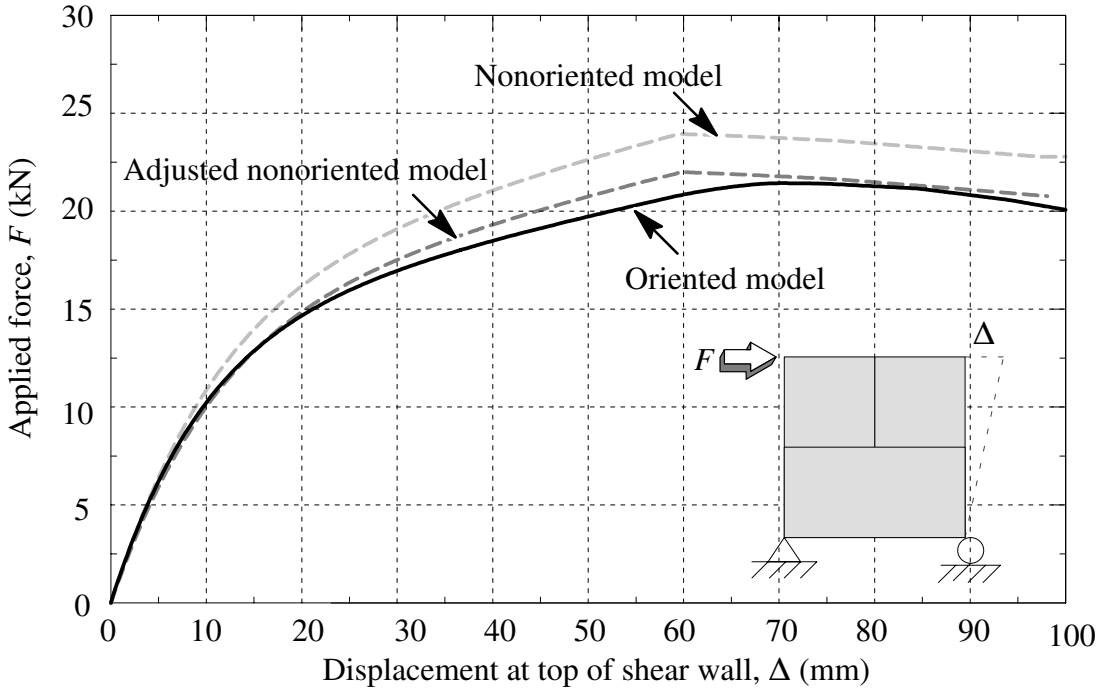

Fig. 5.3. Monotonic response of 2.44×2.44 m oriented strand board shear wall

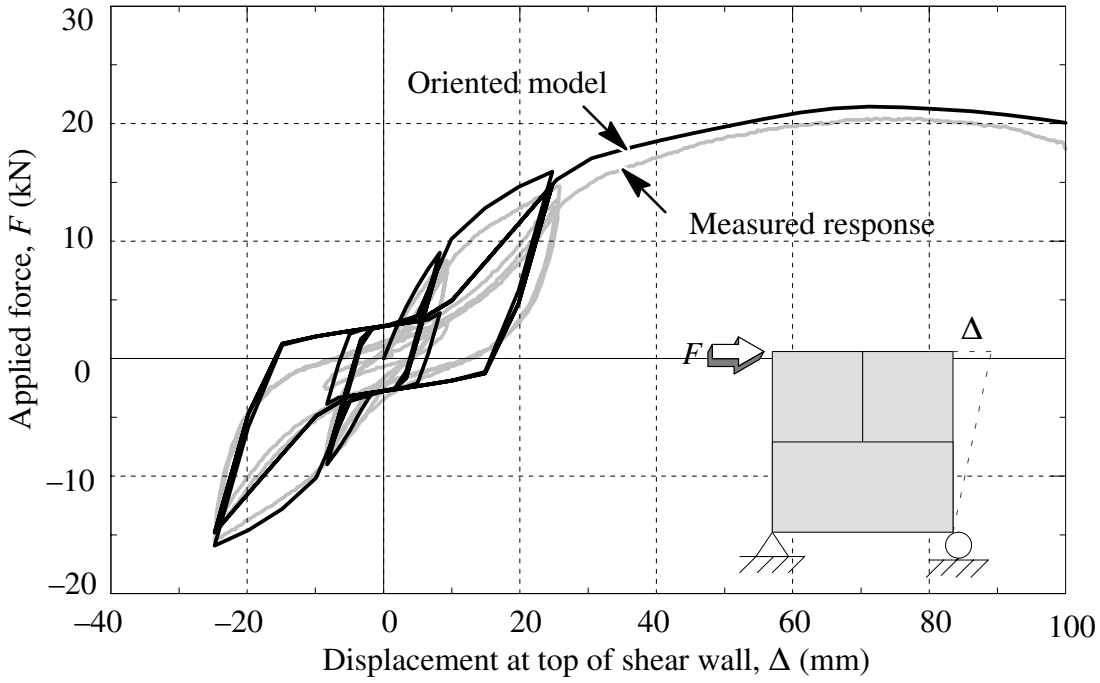

Fig. 5.4. Response of 2.44 × 2.44 m oriented strand board shear wall

Table 5.2. Cyclic Response of 2.44 × 2.44 m Oriented Strand Board Shear Wall

Sheathing-to-framing connection element representation	Δ_{ult}		F_{ult}		Energy Absorbed	
	(mm)	Difference (%)	(kN)	Difference (%)	(kN-mm)	Difference (%)
Measured response	66.0		20.4		2.59	
Non-oriented spring pair	60.0	9.1	24.0	17.7	2.92	12.7
Adjusted non-oriented spring pair	60.0	9.1	22.0	7.8	2.68	3.5
Oriented spring pair	70.0	6.1	21.4	4.9	2.64	1.9

* Difference = | measured / predicted |

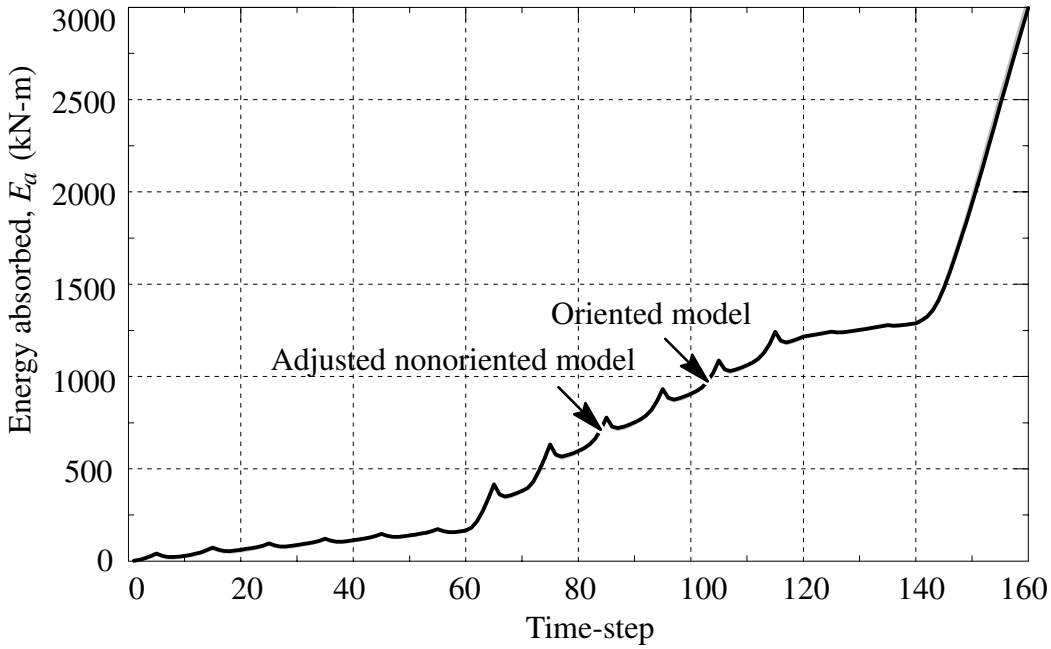

Fig. 5.5. Response of 2.44 × 2.44 m oriented strand board shear wall

5.4.1 Calibration of Equivalent Single Degree of Freedom Parameters

A system identification procedure is used in *CASHEW* to determine an equivalent model calibrated with analytical data instead of experimental data. This is discussed in Chapter 6. A comparison between the equivalent parameters determined using the adjusted nonoriented spring pair model (original *CASHEW* model) and parameters determined using the oriented spring pair model (modified *CASHEW* model) are given in Table 5.3.

Table 5.3. Calibrated Parameters for a 2.44 × 2.44 m Oriented Strand Board Shear Wall

Analytical model	K_0 (kN/mm)	r_1	r_2	r_3	r_4	P_0 (kN)	P_1 (kN)	Δ_{ult} (mm)	α	β
Adjusted non-oriented spring pair	1.44	0.081	–0.022	1.31	0.064	15.1	3.13	60.0	0.74	1.10
Oriented spring pair	1.53	0.065	–0.039	1.33	0.056	14.8	2.76	70.3	0.81	1.09

Chapter 6

EQUIVALENT SINGLE DEGREE OF FREEDOM ANALYSIS

An equivalent single degree of freedom model for shear walls and diaphragms, *QUICK*, is discussed in this chapter. The *QUICK* analytical model is less complex in comparison to the finite element and *CASHEW* models discussed in Chapters 4–5. The equivalent single degree of freedom system parameters are determined in *QUICK* using two methods. In the first method, equivalent system parameters are calibrated using experimental data or using analytical data. In the second method, equivalent system parameters are estimated using the relative contribution of structural components and sheathing–to–framing connection data. The *QUICK* model is validated against measured experimental data and used in a parametric study to quantify the effects of hysteresis model parameters, including loading, unloading, pinching, and strength and stiffness degradation parameters, on dynamic response. The *QUICK* model response using estimated parameters (method 2) is also compared with the predicted monotonic response using codified deflection equations.

6.1 Simplified Analytical Models

Simplified analytical models provide a pragmatic analysis of shear walls and diaphragms. McCutcheon (1985), for example, demonstrated how energy methods can be used to determine the equivalent response of shear walls. Usually a simplified analytical model

consists of an equivalent single-degree-of-freedom system (Medearis 1970; Stewart 1987; Foliente 1995; van de Lindt and Waltz 2003) as shown in Fig. 6.1. Interestingly, an equivalent single degree of freedom analysis yields results to nearly the same accuracy as do the more complex analysis methods (Folz and Filiatrault 2001). A equivalent single-degree-of-freedom model, moreover, has the distinct advantage over more complex models because the lower computational requirement renders the equivalent model amenable to dynamic analysis routine usage.

One concern with previous equivalent single-degree-of-freedom models is the lack of models capable of analysis of diaphragms. Another concern is the lack of model integration with a dynamic time-history analysis procedure. This is especially odd since a primary advantage of equivalent models over complex models is the capability of dynamic analyses. Yet another concern with previous equivalent single-degree-of-freedom models is that the relationship between the applied force and lateral displacement at the top of a shear wall is calibrated to data from experimental testing. This method limits the equivalent model to the specific materials and configurations used during testing. In response to this concern, Folz and Filiatrault (2000; 2001) use a system identification procedure in *CASHEW* to determine an equivalent model calibrated with analytical data instead of experimental data.

An equivalent single degree of freedom model, *QUICK*, may provide a solution to these concerns by using two methods to determine the equivalent response: In the first method, an equivalent response is calibrated using experimental or analytical data. In the second method, an equivalent response is estimated based on the relative contribution of structural components using sheathing–to–framing connection data.

6.2 Solution of Equations

The equivalent single degree of freedom system response is solved in *QUICK* with a numerical time-stepping method (Chopra 1995) using an implicit direct integration procedure employing an iterative procedure for nonlinear response. The equation of motion for the equivalent system is given in Eq. 6.29.

$$p(t) = m\ddot{x} + c\dot{x} + f_s(x) \tag{6.29}$$

where

$$c = c_{cr}\,\xi \tag{6.30}$$

$$c_{cr} = 2\sqrt{km} \tag{6.31}$$

In terms of a time stepping, Eq. 6.29 may be rewritten as Eq. 6.32.

$$p_{i+1} = m\ddot{x}_{i+1} + c\dot{x}_{i+1} + (f_s)_{i+1} \tag{6.32}$$

The incremental equilibrium equation form of Eq. 6.32 is given in Eq. 6.33.

$$\Delta p = m\Delta\ddot{x}_i + c\Delta\dot{x}_i + (\Delta f_S)_i \tag{6.33}$$

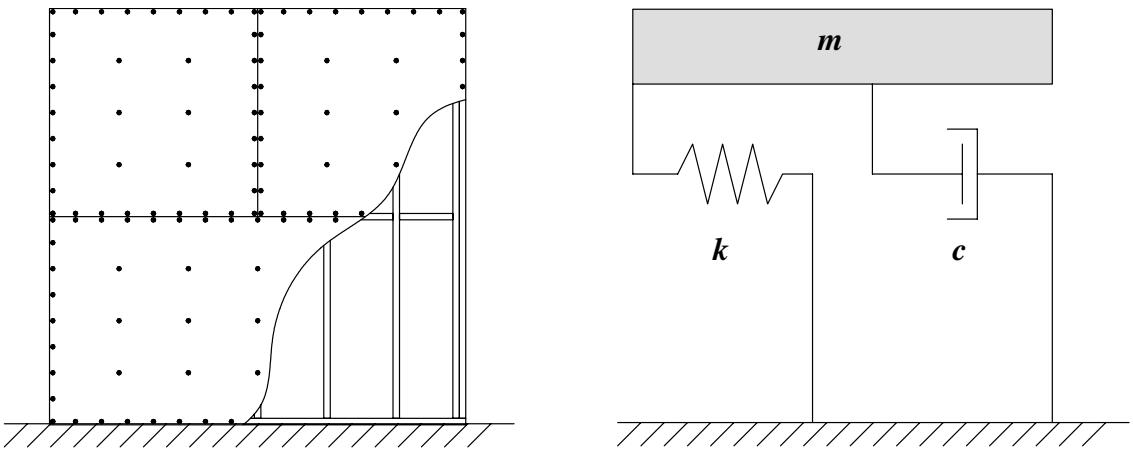

(a) Shear wall or diaphragm (b) Equivalent system

Fig. 6.1. Equivalent representation of shear walls and diaphragms

6.2.1 Integration Procedure: Newmark Average Acceleration Method

The equilibrium equation is solved using the method proposed by Newmark (1959) with the special case of average acceleration (see also Tedesco et al. 1999). The method is unconditionally stable (Bathe 1996). The corresponding intergration parameters for Newmark's method are given in Eq. 6.34 and Eq. 6.35.

$$\gamma = 0.2 \tag{6.34}$$

$$\beta = 0.25 \tag{6.35}$$

The Newmark average acceleration method uses implicit direct integration of the equation of motion. In the initial calculations, the initial acceleration is determined:

$$\ddot{x}_0 = \frac{p_0 - c\dot{x}_0 - (f_S)_0}{m} \tag{6.36}$$

The time step size Δt is selected, and a and b are also calculated:

$$a = \frac{1}{\beta \Delta t} m + \frac{\gamma}{\beta} c \tag{6.37}$$

$$b = \frac{1}{2\beta} m + \Delta t \left(\frac{\gamma}{2\beta} - 1 \right) c \tag{6.38}$$

For each time step i, the following steps are performed:

Step 1: The incremental force is determined:

$$\Delta \hat{p}_i = \Delta p_i + a\dot{x}_i + b\ddot{x}_i \tag{6.39}$$

Step 2: The tangent stiffness k_i and $\hat{k}_i$ are calculated:

$$\hat{k}_i = k_i + \frac{\gamma}{\beta \Delta t} c + \frac{1}{\beta (\Delta t)^2} m \tag{6.40}$$

Step 3: The incremental displacement Δx_i is solved from $\hat{k}_i$ and $\Delta \hat{p}_i$ using the modified Newton-Raphson iterative procedure (described on the following page).

Step 4: The incremental velocity and acceleration are calculated:

$$\Delta\dot{x}_i = \frac{\gamma}{\beta\Delta t}\Delta x_i - \frac{\gamma}{\beta}\dot{x}_i + \Delta t\left(1 - \frac{\gamma}{2\beta}\right)\ddot{x}_i \tag{6.41}$$

$$\Delta\ddot{x}_i = \frac{1}{\beta(\Delta t)^2}\Delta x_i - \frac{1}{\beta\Delta t}\dot{x}_i - \frac{1}{2\beta}\ddot{x}_i \tag{6.42}$$

Step 5: The current displacement, velocity, and acceleration are updated:

$$x_{i+1} = x_i + \Delta x_i \tag{6.43}$$

$$\dot{x}_{i+1} = \dot{x}_i + \Delta\dot{x}_i \tag{6.44}$$

$$\ddot{x}_{i+1} = \ddot{x}_i + \Delta\ddot{x}_i \tag{6.45}$$

Step 6: The previous five calculation steps are repeated for the next time step, where i is replaced by i+1.

6.2.2 Iteration Procedure: Modified Newton-Raphson Method

The Modified Newton-Raphson method is used to determine the incremental displacement Δx_i . The procedure is depicted in Fig. 6.2. At the start of the procedure, the equation values are initialized, where the superscript counter j represents the iteration number:

$$x_{i+1}^{(0)} = x_i \tag{6.46}$$

$$f_s^{(0)} = (f_s)_i \tag{6.47}$$

$$\Delta R^{(1)} = \Delta\hat{p}_i \tag{6.48}$$

$$\hat{k}_T = \hat{k}_i \tag{6.49}$$

For each iteration j, the following steps are performed:

Step 1: The incremental displacement $\Delta x^{(j)}$ is solved using Eq. 6.50.

$$\hat{k}\,\Delta u^{(j)} = \Delta R^{(j)} \tag{6.50}$$

Step 2: The incremental displacement is updated:

$$x_{i+1}^{(j)} = x_{i+1}^{(j-1)} + \Delta x^{(j)} \tag{6.51}$$

Step 3: The incremental force is updated:

$$\Delta f^{(j)} = f_S^i - f_S^{(j-1)} + (\hat{k} - k)\,\Delta x^{(j)} \tag{6.52}$$

Step 4: The residual (out-of-balance) force is updated:

$$\Delta R^{(j+1)} = \Delta R^{(j)} - \Delta f^{(j)} \tag{6.53}$$

6.2.3 Convergence Criteria

The solution of the equation of motion using the Newmark average acceleration method and the Newton-Raphson iteration method is not exact. The numerical error in the solution may be indicated by comparing the energy input into the equivalent system by an external force or input ground, with the internal energy dissipated through viscous damping and inelastic behavior (Chopra 1995; Belytschko et al. 2000). This comparison is commonly referred to as an "energy balance."

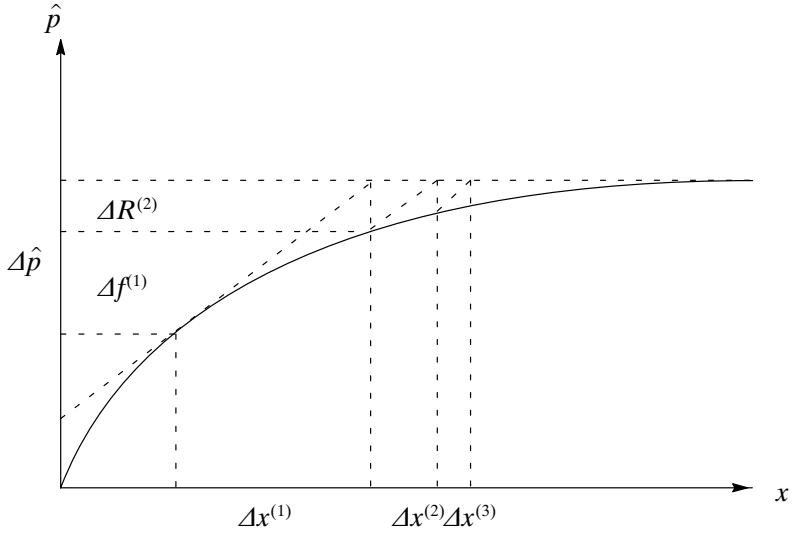

Fig. 6.2. Modified Newton-Raphson iteration procedure

Kinetic Energy. The kinetic energy due to the motion of the mass is given in Eq. 6.54. In the case of ground motion (base excitation), this kinetic energy term represents the energy of motion with respect to the ground (base). This "relative" term does not represent the kinetic energy due to the absolute motion of the mass (Chopra 1995). Using the relative energy formulation, instead of the absolute energy formulation, is insignificant for most shear walls and diaphragms with longer fundamental periods (Dolan 1989: Uang and Bertero 1988). In Eq. 6.55 the kinetic energy is calculated for each time step i.

$$E_{KENETIC} = \int_0^x m\ddot{x}(t)dx \tag{6.54}$$

$$E_{KENETIC} = (E_{KENETIC})_{i-1} + m\left[\frac{\ddot{x}_{i-1} + (\ddot{x}_{i-1} + \ddot{x}_i)}{x_i - x_{i-1}}\right] \tag{6.55}$$

Energy Dissipated through Viscous Damping. The energy dissipated by material damping and friction is given in Eq. 6.56. This term does not include the energy dissipated through the sheathing-to-framing connections. In Eq. 6.57 the damping energy dissipation is calculated for each time step i.

$$E_{DAMP} = \int_0^x c\dot{x}(t)dx \tag{6.56}$$

$$E_{DAMP} = (E_{DAMP})_{i-1} + c\left[\frac{\dot{x}_{i-1} + (\dot{x}_{i-1} + \dot{x}_i)}{x_i - x_{i-1}}\right] \tag{6.57}$$

Energy Dissipated through Inelastic Strain. The energy dissipated through inelastic strain is given in Eq. 6.58. This term includes the recoverable and yield energies dissipated through the sheathing-to-framing connections. In Eq. 6.59 the inelastic energy dissipation is calculated for each time step i.

$$E_{STRAIN} = \int_0^x f_s(x)dx \tag{6.58}$$

$$E_{STRAIN} = (E_{STRAIN})_{i-1} + \left[\frac{f_{i-1} + (f_{i-1} + f_i)}{x_i - x_{i-1}}\right] \tag{6.59}$$

Input Energy. The input energy imposed by an external force or ground motion (base excitation) is given in Eq. 6.60 and Eq. 6.61 for each time step *i*.

$$E_{INPUT} = -\int_0^x m\ddot{x}_g(t)dx \tag{6.60}$$

$$E_{INPUT} = (E_{INPUT})_{i-1} + m\left[\frac{\ddot{x_{g_{i-1}}} + \left(\ddot{x_{g_{i-1}}} + \ddot{x_{g_i}}\right)}{x_i - x_{i-1}}\right] \tag{6.61}$$

Energy Balance. The accuracy of the *QUICK* response was checked using an energy balance, where the total energy dissipated by the system E_{TOTAL} consists of the addition of (1) kinetic energy and (2) energy dissipated through damping and inelastic strain:

$$E_{TOTAL} = E_{KENETIC} + E_{DAMP} + E_{STRAIN} \tag{6.62}$$

The numerical error (%) in the solution is given by comparing the external energy input with the total internal energy dissipated, as given in Eq. 6.63.

$$ERROR = \frac{E_{TOTAL} - E_{INPUT}}{E_{TOTAL}} \times 100\% \tag{6.63}$$

6.3 Calibrated Parameters

In the first method, experimental or analytical data may be used to calibrate parameters for use in *QUICK*. In Table 6.1 *CASHEW* is used to obtain equivalent single-degree-of-freedom parameters for a 2.44×2.44 m oriented strand board shear wall.

Table 6.1. Calibrated Parameters for a 2.44 × 2.44 m Oriented Strand Board Shear Wall

	K_0 (kN/mm)	r_1	r_2	r_3	r_4	P_0 (kN)	P_1 (kN)	Δ_{ult} (mm)	α	β
Parameter value	1.44	0.081	–0.022	1.31	0.064	15.1	3.13	60.0	0.74	1.10

The equivalent model *QUICK* was then used in a nonlinear dynamic analysis with an input ground motion from the Landers 1992 Earthquake and a viscous damping ratio of 1%. The dynamic equilibrium equations were solved using implicit time integration and Newmark's average acceleration method, and convergence tolerance was monitored using an energy balance. A comparison of the measured and predicted time history responses is shown in Fig. 6.3. The predicted force-displacement response is shown in Fig. 6.4.

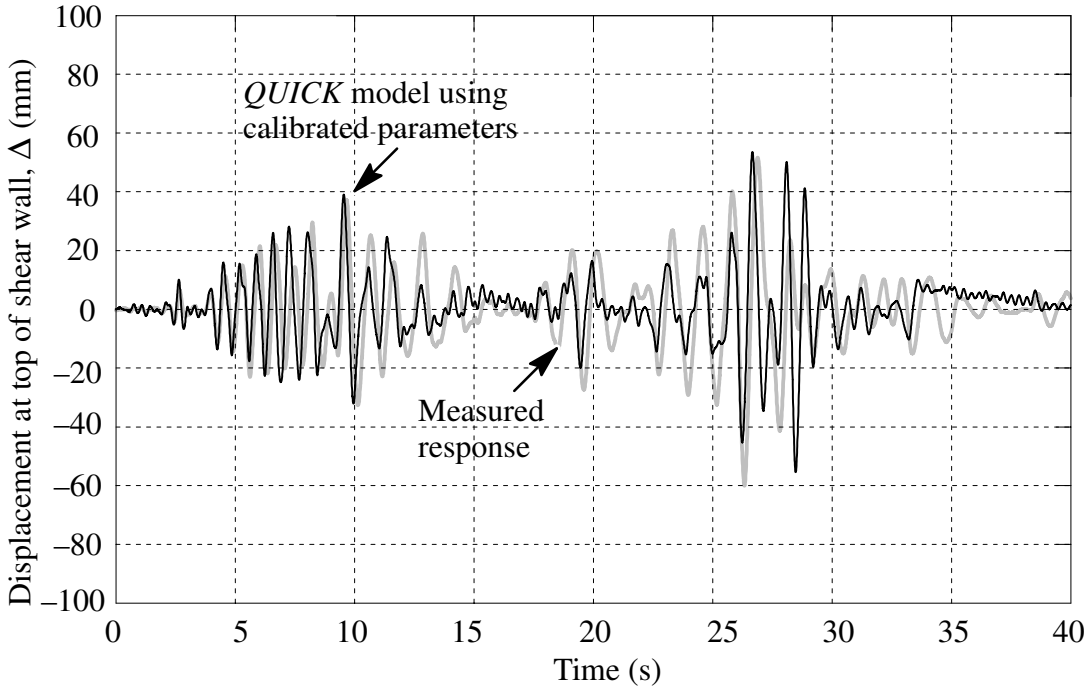

Fig. 6.3. Time-history response of 2.44 × 2.44 m oriented strand board shear wall

6.4 Parametric Analysis

A parametric analysis to quantify the effects of hysteresis model parameters (loading, unloading, pinching, and strength and stiffness degradation parameters) is accomplished using *QUICK*. For comparison, the dynamic response of the 2.44×2.44 m oriented strand board shear wall is predicted using the Clough, Q-Hyst, and modified Stewart hysteresis models.

A summary of the time-history responses is shown in Fig. 6.5. All three hysteresis models estimate the initial linear segment (0–3 seconds). During the first segment of large accelerations (3–10 seconds), yielding occurs, and the Clough and Q-Hyst models underpredict the displacement amplitude. Subsequently, during a segment of smaller accelerations (10–20 seconds), the Clough and Q-Hyst models overpredict the displacement amplitude. The Clough model underpredicts the maximum displacement by nearly 50%. The Q-Hyst

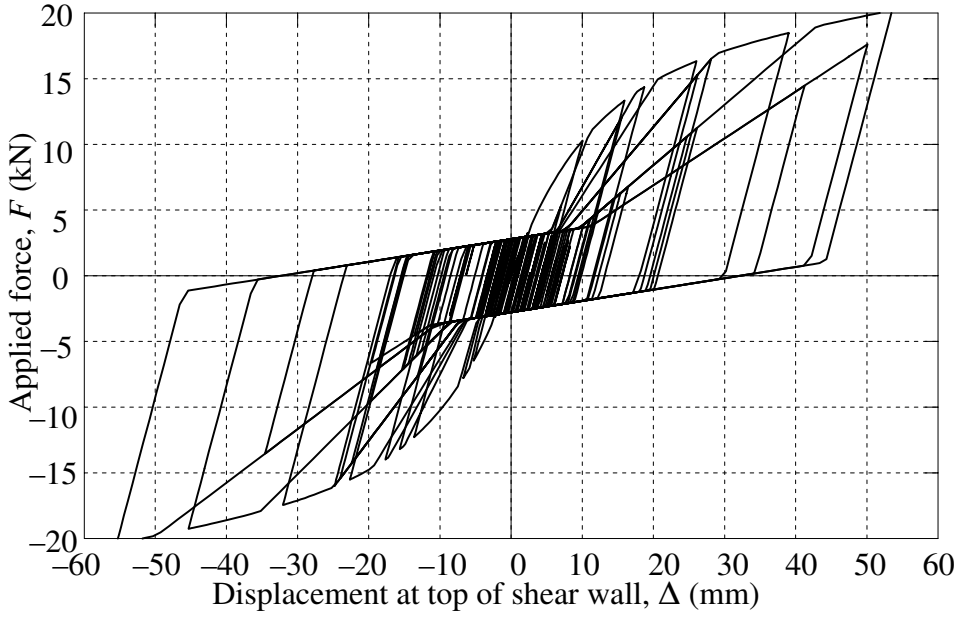

Fig. 6.4. Force-displacement response of 2.44×2.44 m oriented strand board shear wall

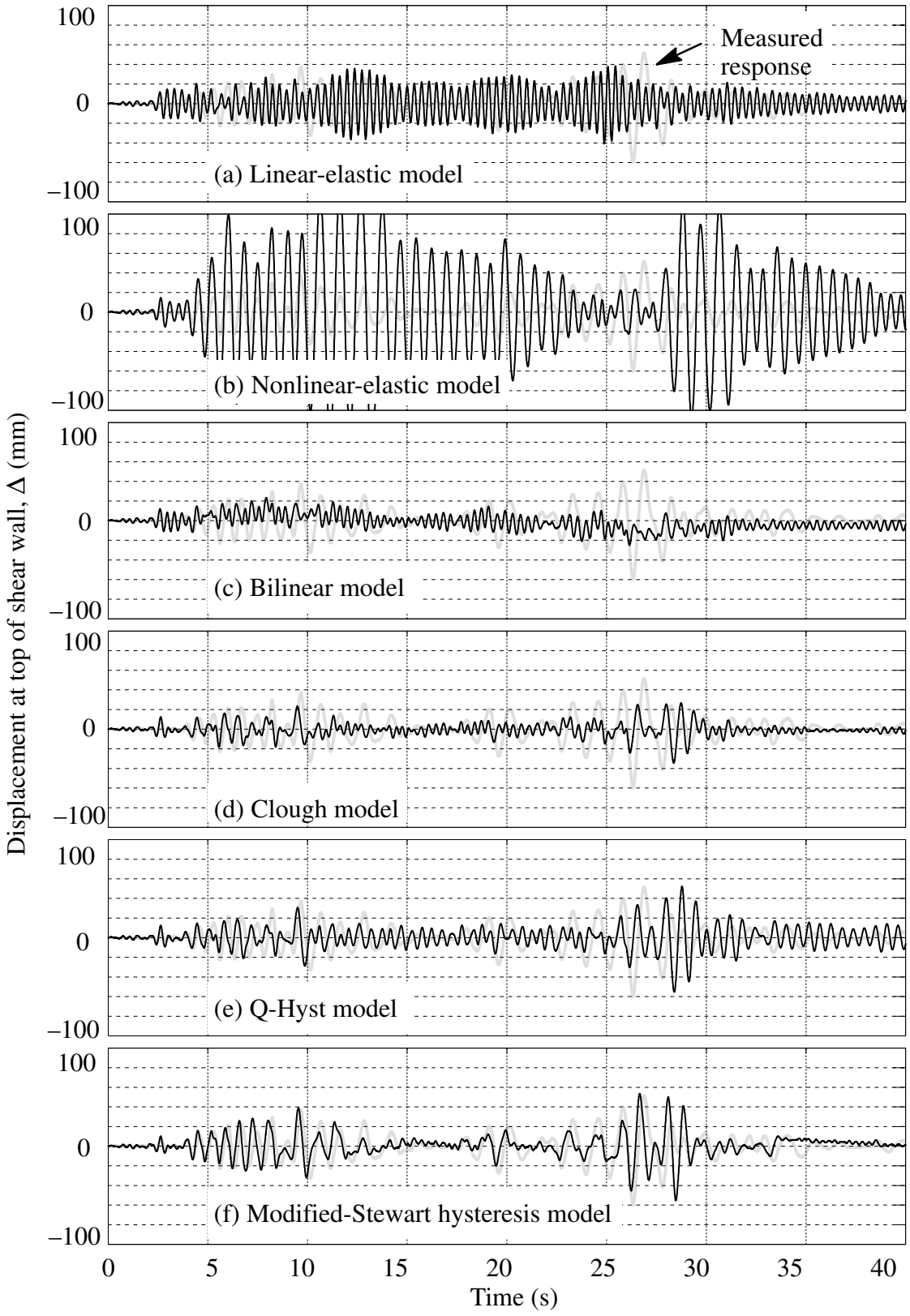

Fig. 6.5. *QUICK* model using calibrated parameters: time-history response of 2.44 $\times$2.44 m oriented strand board shear wall

model and the modified Stewart model both predict the maximum displacement within 8% of the measured value.

While the unloading degradation feature of the Clough model improved the maximum displacement prediction, the model fails to give a true prediction of the overall response. The modified Stewart model provides reasonable accuracy in terms of displacement amplitude and frequency content.

A general indication of the sensitivity of modified Stewart hysteresis model is determined by comparing an individual connector parameter value deviation with the corresponding maximum wall displacement and displacement time history response deviations. In terms of the overall dynamic response time history, changes in the pinching stiffness and pinching force values cause the greatest response deviation.

6.5 Estimated Parameters

In the second method, equivalent system parameters are estimated using the relative contribution of structural components and sheathing-to-framing connection data to the overall deflection. The deflection at the top of the shear wall (or racking deflection), for example, may be thought of as the sum of individual contributions to deflection from structural components. Such contributions to deflection include flexural (bending) and shear contributions, as well as contributions from sub-structure assembly connections; including sheathing-to-framing connections, and anchorage connections. Mathematically, this means that deflection (at the top) of a shear wall may be calculated using Eq. 6.64.

$$\begin{aligned} \Delta_{wall} &= \sum \Delta_{components} \\ &= \Delta_{bending} + \Delta_{shear} + \Delta_{nail} + \Delta_{anchorage} \end{aligned} \tag{6.64}$$

Similarly, the deflection at the midspan of a diaphragm may be thought of as the sum of individual contributions to deflection from structural components. Such contributions to deflection include flexural (bending) and shear contributions, as well as contributions from sub-structure assembly connections: including sheathing-to-framing connections and chord splice connections.

$$\begin{aligned} \Delta_{diaphragm} &= \sum \Delta_{components} \\ &= \Delta_{bending} + \Delta_{shear} + \Delta_{nail} + \Delta_{chord} \end{aligned} \tag{6.65}$$

The contributions of the deflection due to bending and shear may be derived using the virtual unit load method. If the shear wall is considered a thin cantilever beam, then for actual loading the equation for the moment and shear at some distance x from the free end are

$$\begin{aligned} M_x &= -Px \\ V_x &= -P \end{aligned}$$

where P is the applied load at the top of the wall. Similarly, the virtual moment and shear at a distance x from the free end are

$$\begin{aligned} m_x &= -x \\ v_x &= -1 \end{aligned}$$

The external work is equated to the internal work accomplished.

$$\begin{aligned} \textit{External Work} &= \textit{Internal Work} \\ 1 \cdot \Delta &= \int \frac{M_x m_x}{EI} dx + \int \frac{f_s V_x v_x}{GA} dx \end{aligned} \tag{6.66}$$

For diaphragms, the contribution to the total deflection of bending and shear may also be derived using the virtual unit load method. In the following equations, w is the ap-

plied line load, and L is the diaphragm span. If the diaphragm is considered a thin beam, the equation for the moment at some distance x from the support due to actual loading is

$$M_x = x\left(w\frac{L}{2}\right) - \frac{x}{2}(wx)$$

$$= \frac{w}{2}(Lx - x^2)$$

and the equation for the shear at some distance x due to the actual loading is

$$V_x = \frac{wL}{2} - wx$$

Likewise, the moment at a distance x due to a virtual unit load applied at the mid–span is

$$m_x = \frac{x}{2}$$

and the equation for the shear at some distance x due to the virtual loading is

$$v_x = \frac{1}{2}$$

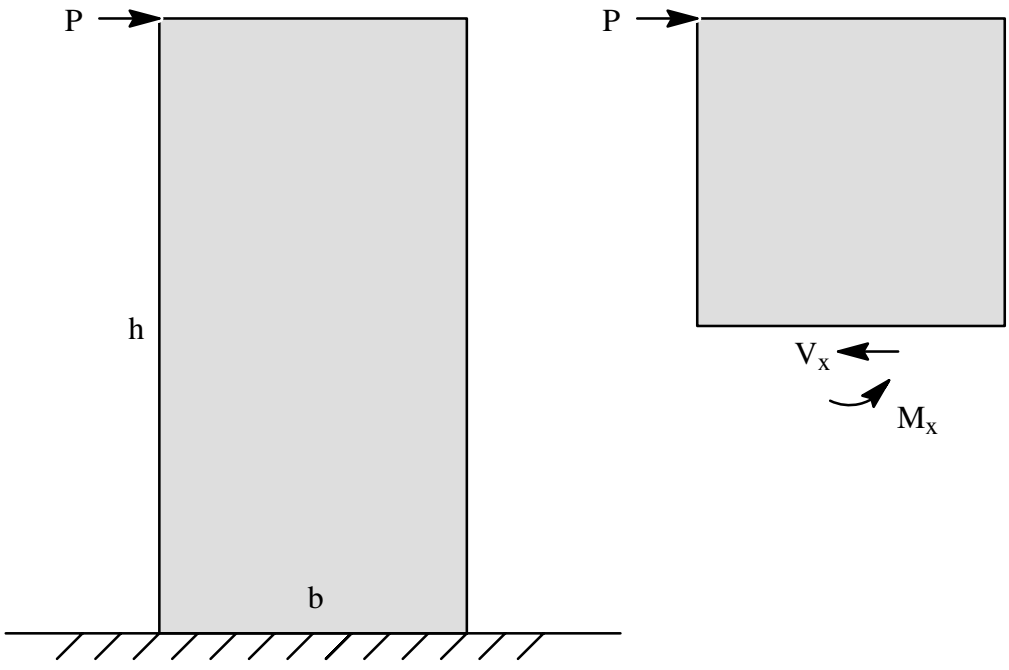

Fig. 6.6. External and internal forces for a shear wall with a concentrated load

The external work is equated to the internal work accomplished.

$$\begin{aligned} \textit{External Work} &= \textit{Internal Work} \\ 1 \cdot \Delta &= \int \frac{M_x m_x}{EI} dx + \int \frac{f_s V_x v_x}{GA} dx \end{aligned} \tag{6.67}$$

6.5.1 Flexural Contribution to Shear Wall Response

$$\begin{aligned} \Delta_{bending} &= \int \frac{M_x m_x}{EI} dx \\ &= \int_0^h (Px)(x) \frac{dx}{EI} \\ &= \frac{P}{EI} \int_0^h x^2 dx \\ &= \frac{P}{EI} \left[\frac{x^3}{3} \right]_0^h \\ &= \frac{Ph^3}{3EI} \end{aligned} \tag{6.68}$$

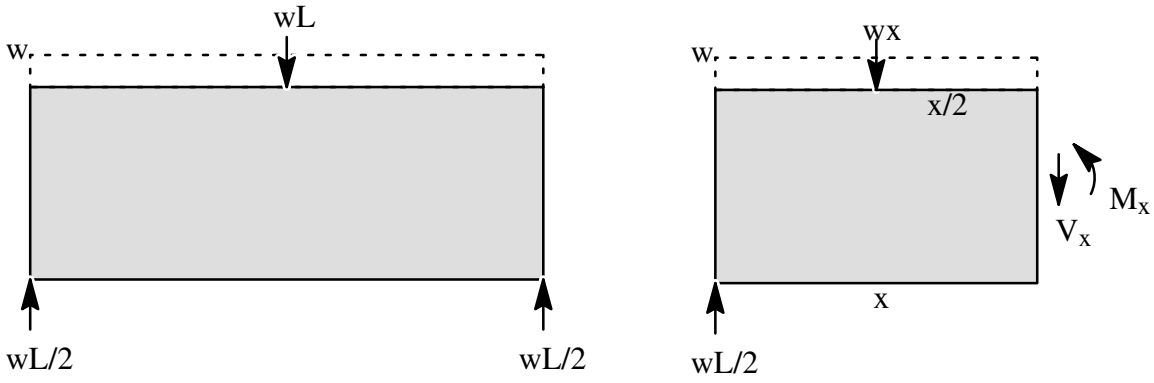

Fig. 6.7. Diaphragm reaction forces due to uniform loading along one side

where h is the wall height, and b is the wall width. Since only the vertical members at the shear wall boundary (such as chords or struts) resist bending, in this equation E is the modulus of elasticity of these boundary members (perimeter framing members). The moment of inertia, I is determined by the parallel-axis theorem.

$$I = 2\left(I_c + Ad^2\right)$$

where I_c is much smaller than I and is therefore neglected. Here, the distance from the centroid of the boundary cross–section to the beam centroid, d is $b/2$ and the cross-sectional area, A for either the top or bottom member is identical, thus $I = Ab^2/2$. Therefore Eq. 6.68 may be rewritten as

$$\Delta_{bending} = \lambda_{swb} P \tag{6.69}$$

where

$$\lambda_{swb} = \frac{2h^3}{3EAb^2} \tag{6.70}$$

6.5.2 Flexural Contribution to Diaphragm Response

$$\begin{aligned}
\Delta_{bending} &= \int \frac{M_x m_x}{EI} dx \\
&= 2\int_0^{L/2} \left[\frac{w}{2}\left(Lx - x^2\right)\right]\left[\frac{x}{2}\right]\frac{dx}{EI} \\
&= \frac{2w}{4EI}\int_0^{L/2} \left(Lx^2 - x^3\right) dx \\
&= \frac{2w}{4EI}\left[\frac{Lx^3}{3} - \frac{x^4}{4}\right]_0^{L/2} \\
&= \frac{5wL^4}{384EI}
\end{aligned} \tag{6.71}$$

Since only the chords resist bending, in this equation E is the modulus of elasticity of the chord members. As before, the moment of inertia, I is determined by the parallel–axis theorem $I = 2(I_c + Ad^2)$ where I_c is much smaller than I and is therefore neglected. Since the reaction $P = wL/2$ then the equation can be rewritten

$$\Delta_{bending} = \lambda_{db} P \tag{6.72}$$

where

$$\lambda_{db} = \frac{5L^3}{96EAb^2} \tag{6.73}$$

6.5.3 Shear Contribution to Shear Wall Response

$$\begin{aligned} \Delta_{shear} &= \int \frac{f_s V_x v_x}{GA} dx \\ &= \int_0^h f_s (1)(P) \frac{dx}{GA} \\ &= \frac{f_s Ph}{GA} \end{aligned} \tag{6.74}$$

where G is the shear modulus of the sheathing, t is the effective shear thickness of the sheathing, and f_s is the form factor for the cross-sectional area, A. Here, A is the cross–sectional area of the wall web or, namely the sheathing, so $A = bt$. For simplicity, f_s is taken as unity. Therefore Eq. 6.74 can be rewritten as

$$\Delta_{shear} = \lambda_{sws} P \tag{6.75}$$

where

$$\lambda_{sws} = \frac{h}{Gtb} \tag{6.76}$$

6.5.4 Shear Contribution to Diaphragm Response

$$\begin{aligned}
\Delta_{shear} &= \int \frac{f_s V_x v_x}{GA} dx \\
&= 2\int_0^{L/2} f_s\left[w\left(\frac{L}{2} - x\right)\right]\left[\frac{1}{2}\right]\frac{dx}{GA} \\
&= \frac{f_s w}{GA}\int_0^{L/2}\left(\frac{L}{2} - x\right)dx \\
&= \frac{f_s w}{GA}\left[\frac{Lx}{2} - \frac{x^2}{2}\right]_0^{L/2} \\
&= \frac{f_s wL^2}{8GA} \qquad (6.77)
\end{aligned}$$

As before, A is the cross–sectional area of the beam web (sheathing), $A = bt$ where b is the transverse diaphragm depth, and t is the effective shear thickness of the sheathing. Also, f_s is taken as unity. Thus, since the reaction $P = wL/2$ then Eq. 6.77 can be rewritten

$$\Delta_{shear} = \lambda_{ds} P \qquad (6.78)$$

where

$$\lambda_{ds} = \frac{L}{4Gbt} \qquad (6.79)$$

6.5.5 Sheathing-to-Framing Connection Deformation Contribution

The contribution to the total deflection due to deformation of the sheathing-to-framing connections is assumed to be analogous to the contribution due to web shear (Countryman 1952). In this approach, the perimeter nailing of a typical sheathing panel is assumed to be stressed (and strained) equally. Thus the corner sheathing-to-framing connections in the panel are deformed $e_n\sqrt{2}$ along a 45° line, where the horizontal and vertical components

of the connection deformation are equal. Here, the connection deformation, e_n is determined empirically (via coupon tests, for example). The component of this deformation along a line parallel to the sheathing panel diagonal is $e_n\sqrt{2}\cos\phi$, where $\phi = 45^\circ - \theta$ and

$$\theta = \text{atan}\left(\frac{b_{panel}}{a_{panel}}\right) \tag{6.80}$$

and b_{panel}, and a_{panel} are the dimensions of the panel parallel and perpendicular to the applied load, respectively. The total elongation of the frame, e_{frame}, with respect to the panel diagonal, is twice this value because both opposite corners (upper-left and lower-right) deform.

$$e_{frame} = 2(e_n\sqrt{2}\cos\phi) \tag{6.81}$$

Shear Walls. The elongation of the sheathing panel diagonal is a result of the horizontal shear from the loading. Therefore, the horizontal deformation, δ_h of the panel is Eq. 6.82.

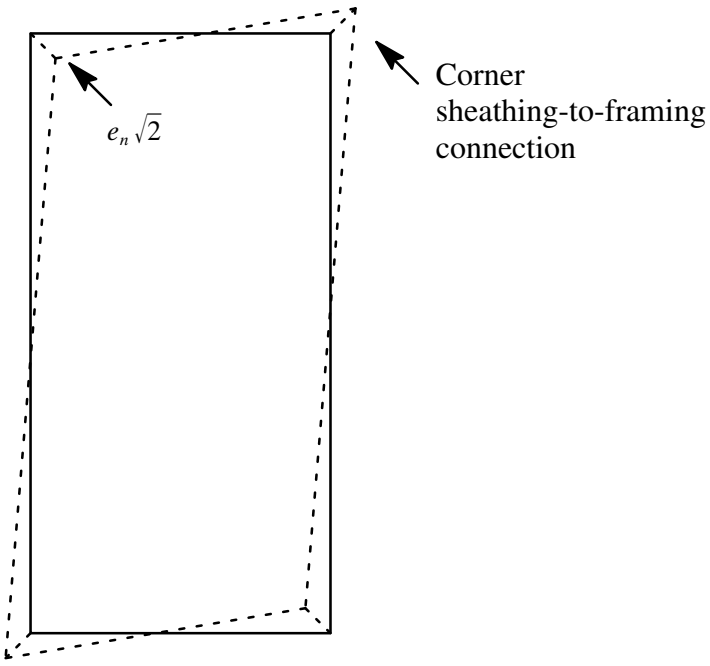

Fig. 6.8. Deflected shape of a typical frame in a shear wall or diaphragm

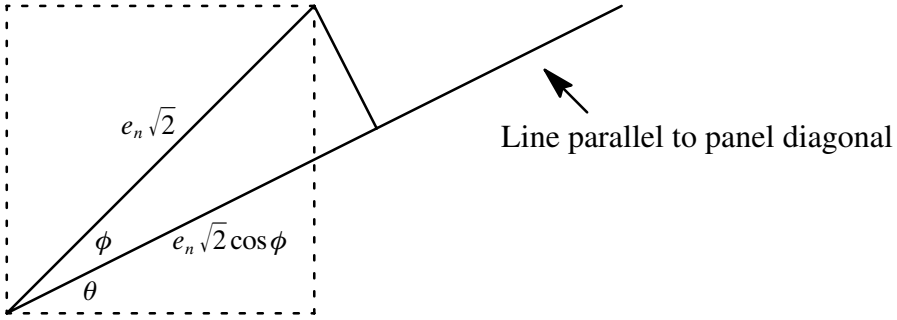

Fig. 6.9. Elongation of frame with respect to the panel diagonal

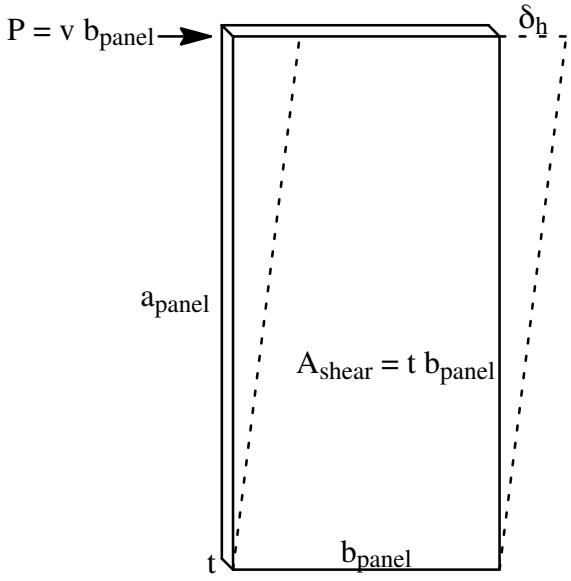

Fig. 6.10. Deformed shape of a typical sheathing panel

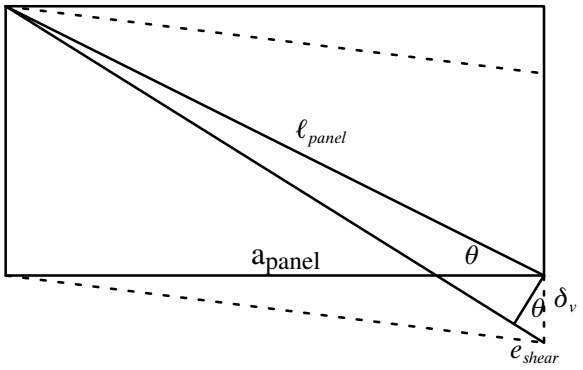

Fig. 6.11. Elongation of the sheathing panel with respect to the panel diagonal

$$\begin{aligned} \delta_h &= \frac{P a_{panel}}{A_{shear}\, G} \\ &= \frac{(v\, b_{panel})\, a_{panel}}{(t b_{panel})\, G} \\ &= \frac{v\, a_{panel}}{Gt} \end{aligned} \tag{6.82}$$

The elongation of the panel due to this vertical shear deformation (for small angles, assuming that the deformation is small compared to the dimensions of the panel) is Eq. 6.83, or, in terms of the length of the panel diagonal, ℓ_{panel}, Eq. 6.83 is becomes Eq. 6.84.

$$\begin{aligned} e_{shear} &= \delta_h \sin\theta \\ &= \left(\frac{v\, a_{panel}}{Gt}\right) \sin\theta \\ &= \frac{v\, (\ell_{panel}\, \cos\theta)\, \sin\theta}{Gt} \\ &= \frac{v\, \ell_{panel}}{2Gt} \sin 2\theta \\ &= \frac{v\, \ell_{panel}}{2Gt} \cos(90^\circ - 2\theta) \\ &= \frac{v\, \ell_{panel}}{2Gt} \cos 2\phi \end{aligned} \tag{6.83, 6.84}$$

The assertion is that the ratio of the component of deflection due to sheathing-to-framing connection deformation, Δ_{nail} and frame elongation, e_{frame} is equal to the ratio of the component of top of the wall deflection due to shear, Δ_{shear} and panel elongation due to shear, e_{shear}.

$$\begin{aligned} \frac{\Delta_{nail}}{e_{frame}} &= \frac{\Delta_{shear}}{e_{shear}} \\ \Delta_{nail} &= \Delta_{shear}\, \frac{e_{frame}}{e_{shear}} \\ &= \Delta_{shear}\, \frac{2\sqrt{2}\, e_n \cos\phi}{v\, \ell_{panel} \cos 2\phi / 2Gt} \end{aligned} \tag{6.85}$$

$$= \left(\frac{vh}{Gt}\right) \frac{2\sqrt{2}\, e_n \cos\phi}{v\, \ell_{panel} \cos 2\phi / 2Gt}$$

$$= \lambda_{swn} e_n \tag{6.86}$$

where

$$\lambda_{swn} = \frac{2\sqrt{2}\cos\phi}{\ell_{panel}\cos 2\phi} h \tag{6.87}$$

Diaphragms. The contribution to midspan diaphragm deflection due to sheathing-to-framing deformations is derived using the same logic used for shear walls: (1) the contribution to the total deflection due to deformation of the sheathing-to-framing connections is assumed to be analogous to the contribution due to web shear; and (2) the ratio of the component of mid–span deflection due to sheathing-to-framing connection deformation, Δ_{nail} and frame elongation, e_{frame} is equal to the ratio of the component of mid–span deflection due to shear, Δ_{shear} and panel elongation due to shear, e_{shear}, is asserted.

$$\frac{\Delta_{nail}}{e_{frame}} = \frac{\Delta_{shear}}{e_{shear}} \tag{6.88}$$

The difference between shear wall and diaphragm sheathing-to-framing connection contributions is that in Eq. 6.85 the deflection due to shear, Δ_{shear} is at the top of a shear wall and in Eq. 6.88 the deflection due to shear, Δ_{shear} is at the midspan of a diaphragm. Therefore,

$$\Delta_{nail} = \Delta_{shear} \frac{2\sqrt{2}\, e_n \cos\phi}{v\, \ell_{panel} \cos 2\phi / 2Gt}$$

$$= \left(\frac{vL}{4Gt}\right) \frac{2\sqrt{2}\, e_n \cos\phi}{v\, \ell_{panel} \cos 2\phi / 2Gt}$$

$$= \lambda_{dn} e_n \tag{6.89}$$

where

$$\lambda_{dn} = \frac{\sqrt{2}\cos\phi}{\ell_{panel}\cos 2\phi} L \tag{6.90}$$

6.5.6 Anchorage Connection Deformation Contribution

The contribution to shear wall deflection due to anchorage connection deformation, d_a is not well understood, even though such contribution may be significant (see *FEMA Publication 274* Commentary, FEMA 1997b). As a result, calculating the deflection contribution from anchorage details, including rotation and displacement of tie-down bolts, is determined using a wall height-to-width modifier

$$\Delta_{anchorage} = \frac{h}{b} d_a \tag{6.91}$$

6.5.7 Chord Splice Connection Deformation Contribution

The contribution to diaphragm deflection due to chord splice connection deformation is considered to be proportional to the sum of each individual splice connection deformation, Δ_c multiplied by the distance to the nearest support, X

$$\Delta_{chord} = \frac{\sum(\Delta_c X)}{2b} \tag{6.92}$$

6.5.8 Parameter Estimation

For parameter values of force, F, the equivalent force is simply the sheathing-to-framing connection force parameter multiplied by the number of resisting connections.

$$F = NP \tag{6.93}$$

For a shear wall loaded along the top edge, the "resisting" connections are the perimeter connections (on the top and bottom). Likewise, for a diaphragm loaded along the length of one chord, the "resisting" connections are primarily the transverse perimeter connections

(on each side). In the more general case where there are M types of sheathing-to-framing connections, Eq. 6.93 is rewritten as Eq. 6.94.

$$F = \sum_{i=1}^{M} N_i P_i \tag{6.94}$$

For parameter values of displacement, the equivalent displacement Δ is given in Eq. 6.95.

$$\Delta = (\lambda_b + \lambda_s) NP + \lambda_n \delta \tag{6.95}$$

where λ_b, λ_s, and λ_n were defined in the previous section as the contribution factors to bending, shear, and sheathing-to-framing connection displacement, respectively. The more general form of Eq. 6.95 for multiple connection types is Eq. 6.96.

$$\Delta = \sum_{i=1}^{M} (\lambda_b + \lambda_s) N_i P_i + \lambda_n \delta_i \tag{6.96}$$

Similarly, for parameter values of stiffness, the equivalent stiffness K is Eq. 6.97 for shear walls and diaphragms with one type of sheathing-to-framing connection, and Eq. 6.98 for multiple connection types.

$$K = \frac{1}{\lambda_b + \lambda_s + (\lambda_n / Nk)} \tag{6.97}$$

$$K = \sum_{i=1}^{M} \frac{1}{\lambda_b + \lambda_s + (\lambda_n / N_i k_i)} \tag{6.98}$$

The preceding equations do not include the contributions of anchorage and splice type connections to the response. These contributions could be incorporated in a similar fashion.

6.6 Static Analysis

A static analysis is validated using (1) the response of four 2.44 × 2.44 m plywood shear walls and three 2.44 × 2.44 m waferboard shear walls tested by Dolan (1989), and (2) one 3.66 × 7.32 m plywood diaphragm tested by Olpin (1998) described previously. The diaphragm test is considered in more detail in Chapter 7.

The *QUICK* model response is compared with the measured response in Fig 6.12 for the shear wall and Fig. 6.13 for the diaphragm. The *QUICK* model response is very close to the average measured response. The shear wall model is only slightly stiffer during initial loading. The diaphragm model provides a good estimation, despite concerns with the data from the diaphragm testing, as previously discussed in Chapter 2.

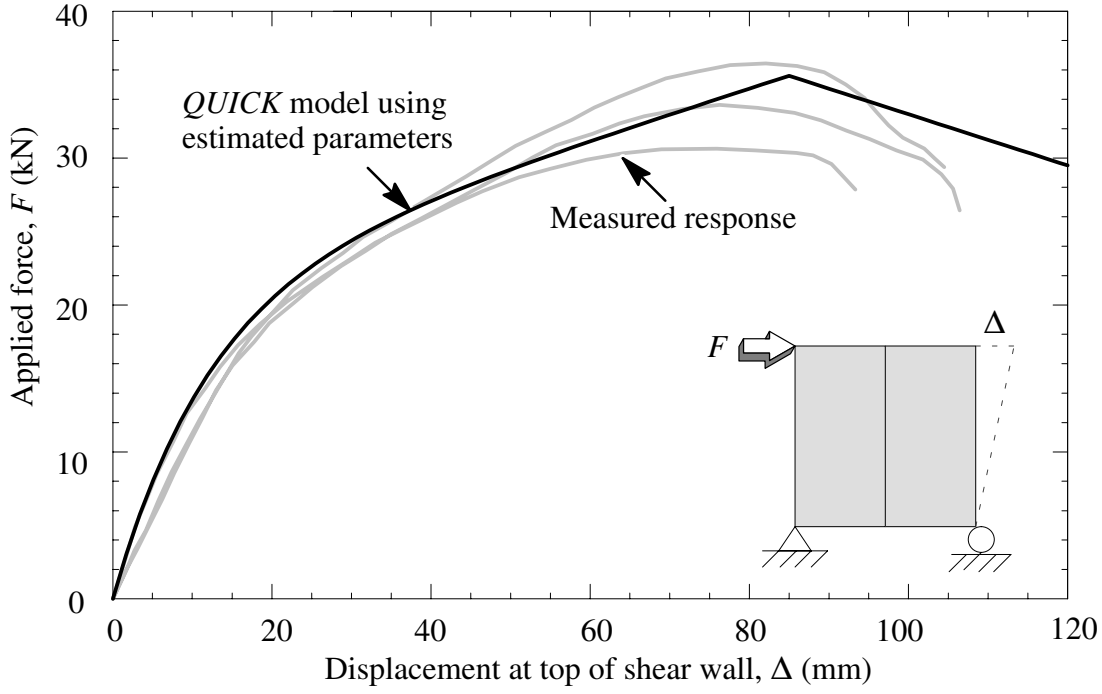

Fig. 6.12. Static analysis of 2.44 × 2.44 m plywood shear wall

6.7 Dynamic Analysis

In Table 6.2 *QUICK* is used to obtain equivalent single-degree-of-freedom parameters for the 2.44×2.44 m oriented strand board shear wall (described earlier) by using the sheathing-to-framing parameter extrapolation method (method 2). For comparison, the parameters obtained using data calibration (method 1) are given.

The *QUICK* model is also used in a nonlinear dynamic analysis of 2.44×2.44 m Oriented Strand Board Shear Wall (Durham 1998) and solved using implicit time integration and Newmark's average acceleration method. A comparison of the calibrated (method 1) and extrapolated (method 2) time history responses is shown in Fig. 6.14.

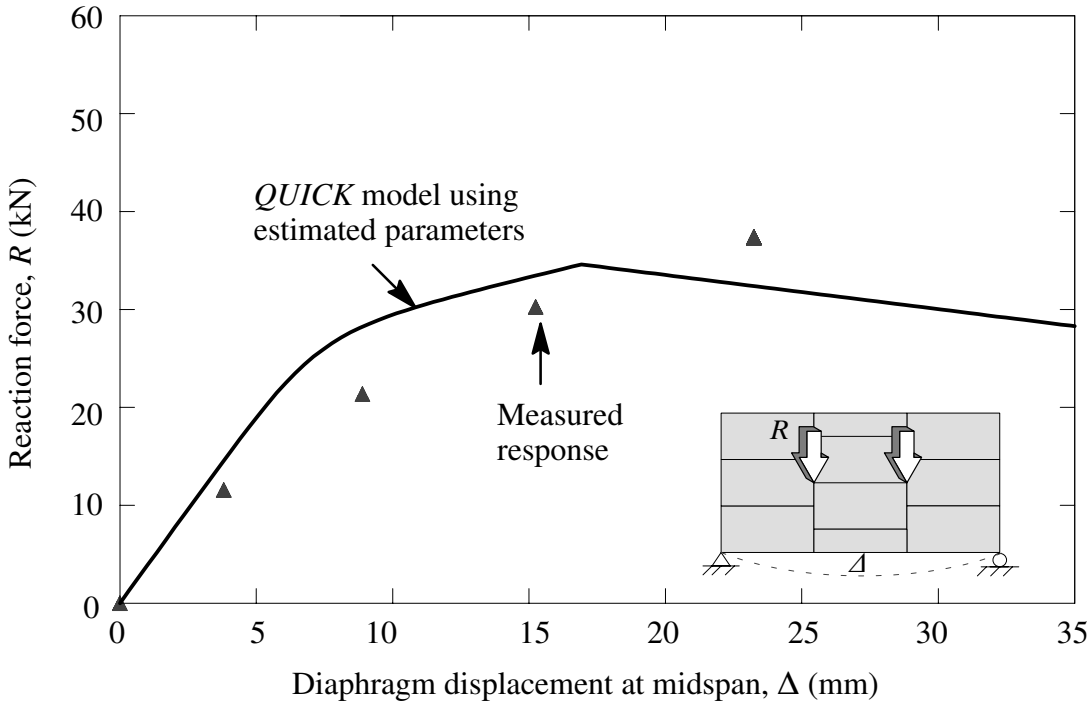

Fig. 6.13. Static analysis of plywood diaphragm

Table 6.2. Equivalent Parameters for a 2.44 × 2.44 m Oriented Strand Board Shear Wall

Method	K_0 (kN/mm)	r_1	r_2	r_3	r_4	P_0 (kN)	P_1 (kN)	Δ_{ult} (mm)	α	β
1. Calibration	1.53	0.065	–0.039	1.33	0.056	14.8	2.76	70.3	0.81	1.09
2. Estimation	1.45	0.070	–0.089	1.45	0.057	13.5	2.56	76.7	0.80	1.10

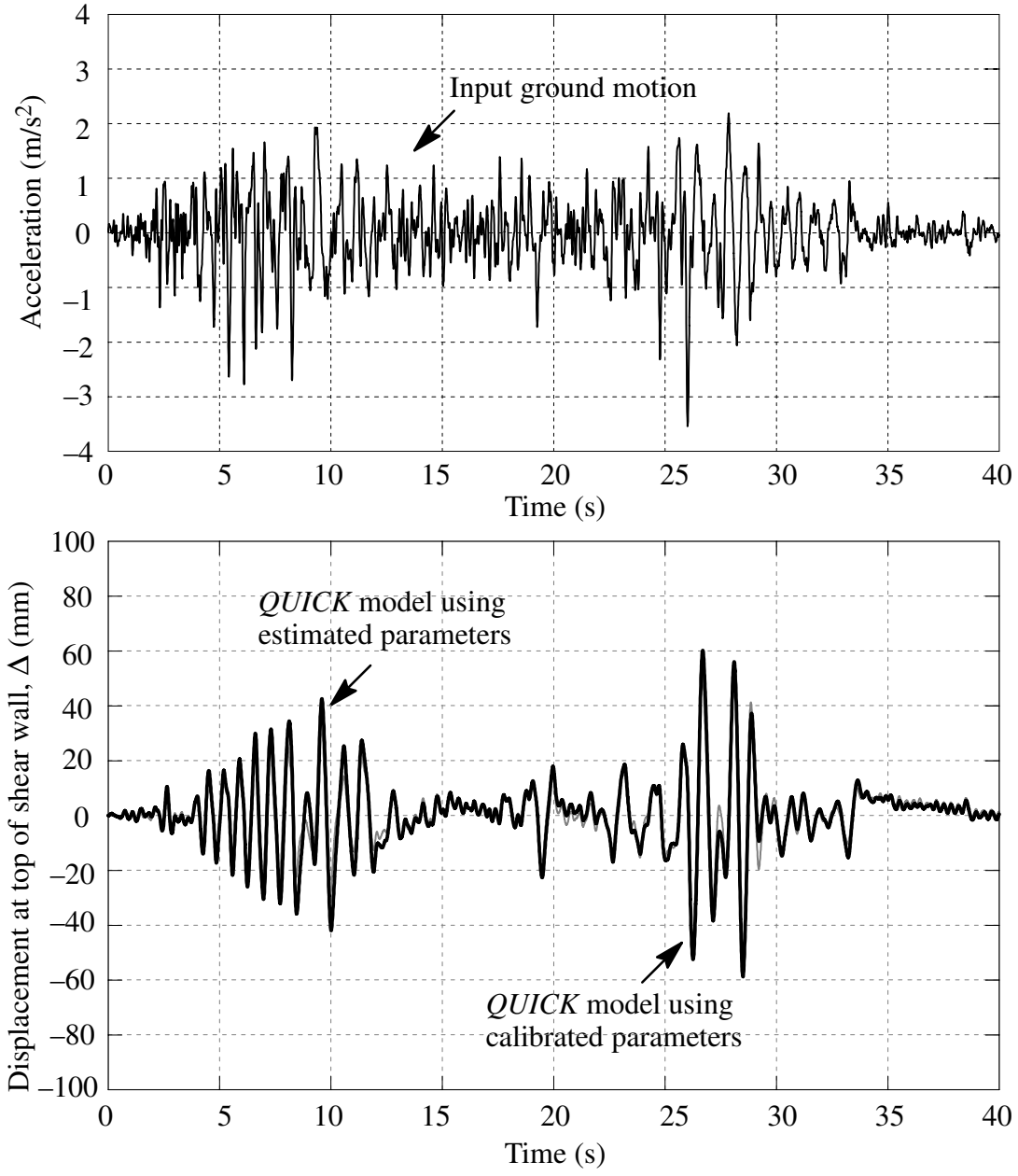

Fig. 6.14. Time-history response of 2.44 × 2.44 m oriented strand board shear wall

6.8 Comparison with Codified Deflection Equations

Equations to predict the deflection of wood-frame shear walls and diaphragms were originally developed more than 50 years ago (Countryman 1952) and subsequently incorporated into a number of building codes. Skaggs and Martin (2004) provide a comprehensive summary of codified deflection equations, methods for calculating shear wall and diaphragm deflections, equation limitations, and some comparison between predicted and measured deflections (see also Breyer et al. 2003). The *International Building Code 2003* (ICC 2003) and the *Uniform Building Code 1997* (ICBO 1997) use deflection equations, as does *FEMA publication 273* (FEMA 1997a), the Diaphragms and Shear Walls: Design/Construction Guide (APA 2004), and the NDS for Wood Construction (AF&PA 2001c). The equations were developed based on the contributions to deflection due to flexure, shear, and connection displacements (ATC 1981), described previously in this Chapter. The parameter values for the codified deflection equations, however, have not been consistently stipulated (Skaggs and Martin 2004). Simplification of the codified equations has been considered recently (Filiatrault et al. 2002).

Shear Walls. The codified shear wall deflection equations assume that the shear walls are "blocked," where each sheathing panel edge is supported, and that the shear walls use uniform spacing and type of sheathing-to-framing connections. There are no provisions for shear walls that are unblocked or have non-uniform sheathing-to-framing connections. The accuracy of the equations, moreover, for shear walls with aspect ratios greater than 2:1 has not been determined fully (APA 2004). Experimental testing by Martin and Skaggs (2002) indicates that shear wall deflection may increase 30% for aspect ratios of 2:1 and 50% for aspect ratios of 4:1. The influence of non-structural elements and finishes may also add

significant stiffness to shear walls (Cobeen et al. 2004; Filiatrault et al. 2002). As previously discussed in Chapter 4, however, these factors have not yet been quantified. In terms of the shear wall unit shear, $v = P/b$, and multiplying by 12 in./ft, the total shear wall deflection is rewritten with inborn units (length and width in feet, and thickness in inches, for example):

$$\begin{aligned} \Delta_{total} &= \sum \Delta_{components} \\ &= \Delta_{bending} + \Delta_{shear} + \Delta_{nail} + \Delta_{anchorage} \\ &= \frac{8vh^3}{EAb} + \frac{vh}{Gt} + 0.75he_n + \frac{h}{b}d_a \end{aligned} \tag{6.99}$$

Diaphragms. As was the case with shear walls, the codified diaphragm deflection equation assumes the diaphragm is blocked and uses uniform sheathing-to-framing connection spacing and type. Again, in terms of the unit shear, $v = P/b$, and multiplying by 12 in./ft, the total diaphragm deflection is rewritten with inborn units:

$$\begin{aligned} \Delta_{total} &= \sum \Delta_{components} \\ &= \Delta_{bending} + \Delta_{shear} + \Delta_{nail} + \Delta_{chord} \\ &= \frac{5vL^3}{8EAb} + \frac{vL}{4Gt} + 0.188Le_n + \frac{\sum(\Delta_c X)}{2b} \end{aligned} \tag{6.100}$$

In the case of unblocked diaphragms, two methods for determining midspan deflection have been proposed. In the first method, *FEMA publication 273* (FEMA 1997a) suggests that the unblocked diaphragm be treated as a "single straight sheathed diaphragm," using Eq. 6.101.

$$\Delta_{total} = \frac{vL^4}{G_d b^3} \tag{6.101}$$

where the unblocked diaphragm shear stiffness, G_d is 140 kN/mm (800,000 lb/in.) if chord members are used and 70 kN/mm (400,000 lb/in.) otherwise.

In the second method, the Diaphragms and Shear Walls: Design/Construction Guide (APA 2004) and Section 805.3.2 of the *Blue Book* (SEAOC 1999) suggest that Eq. 6.100 be multiplied by 2.5 if the unblocked diaphragm uses framing spacing equal to or less than 610 mm (24 in.) on center, and multiplied by 3.0 if the framing spacing is greater. The *Blue Book* suggestion is based on limited diaphragm testing (Countryman 1952; 1955; Tissell 1967).

In the case of a diaphragm with variable sheathing-to-framing connection perimeter (edge) spacing, *Report No. ATC–7* (ATC 1981) suggests that the deflection contribution due to sheathing-to-framing connection deformation, Δ_{nail} is proportional to the ratio of the average connection force with non-uniform spacing, v_n' and the average connection force had uniform spacing been used, v_n. Therefore Eq. 6.100 is rewritten as Eq. 6.102. An example using this nonuniform nailing adjustment is given by Skaggs and Martin (2004).

$$\Delta_{total} = \frac{5vL^3}{8EAb} + \frac{vL}{4Gt} + 0.188\left(\frac{v_n'}{v_n}\right)Le_n + \frac{\sum(\Delta_c X)}{2b} \tag{6.102}$$

An example using Eq. 6.102 is given in "Diaphragms and shear walls design/ construction guide" (APA 2004). In a similar way, *FEMA publication 273* (FEMA 1997a) doubles the deflection contribution due to sheathing-to-framing connection deformation, so that Eq. 6.100 is rewritten as Eq. 6.103.

$$\Delta_{total} = \frac{5vL^3}{8EAb} + \frac{vL}{4Gt} + 0.376Le_n + \frac{\sum(\Delta_c X)}{2b} \tag{6.103}$$

Chapter 7

APPLICATIONS

In this chapter applications of the previous analytical models are given. In the first example, the advantages of hybrid shear walls or diaphragms, with glass fiber reinforced polymer (GFRP) panels in conjunction with plywood panels, are discussed. In the second example, the response of shear walls with improperly driven (or overdriven) nails is determined and a method to estimate the reduction in capacity is proposed.

7.1 Hybrid Shear Walls and Diaphragms

7.1.1 Background

Conventional wood-frame shear walls and diaphragms may be limited by the capacity of the wood sheathing panels. For example, under lateral forces, the nails often tear through the sheathing panel edges, causing premature failure of the wall or diaphragm. This failure mechanism was observed during the 1994 Northridge earthquake (Hall 1996). In many cases, the wood framing remains undamaged, and some nails remain undeformed. Additionally, overdriven nails are common and difficult to avoid, because nails easily penetrate wood sheathing. These observations suggest that the diaphragm components are not being used to full advantage.

Conventional diaphragms may be overly flexible in some situations. For instance, during seismic events, lateral displacement at the midspan of these diaphragms is amplified. This may lead to incompatible deformations of anchorage devices, causing additional load to be transferred to the diaphragm sheathing-to-framing connections, thus precipitating failure. Indeed, excessive diaphragm flexibility has led to the collapse of adjacent walls.

Extensive structural and cosmetic damage related to conventional diaphragms is a concern. To illustrate, during the 1994 Northridge earthquake, property damage or loss in value to wood-frame structures was estimated at $20 billion (Kircher et al. 1997). Such dramatic loss has further generated interest in altering the life–safety emphasis in wood–frame design, with a new emphasis on limiting property damage (Diekmann 1994). To achieve this new criterion, the strength, stiffness, and energy absorption of diaphragms need to be improved.

To this end, hybrid diaphragms—diaphragms where glass fiber-reinforced polymer (GFRP) panels are used in conjunction with traditional wood panels as sheathing—may be a viable alternative to conventional diaphragms. In such diaphragms, some or all of the sheathing panels may be GFRP panels. In one approach, critical corner sheathing could employ GFRP panels, while the remaining, less critical sheathing uses wood panels.

Previous research has demonstrated the potential of using both composite materials and conventional materials (specifically wood) in a combined system (Bulleit 1992; Davalos and Barbero 1991). Hybrid diaphragms, however, have not been previously investigated, despite likely advantages.

Hybrid diaphragms can result in a stronger structural system in a number of construction applications: in existing diaphragms requiring repair or rehabilitation; in structures requiring upgrading in either use or code requirements; in new construction where superior

performance is critical; or in locations where limited space is available for shear resistance, such as garages or storefront displays (Foliente and Zacher 1994).

Diaphragm performance can be improved by using GFRP sheathing panels. Strength loss caused by overdriven nails can be eliminated (GFRP panels are not easily penetrated by a nail head), and deterioration of sheathing resulting from moisture can be retarded. Furthermore, GFRP panels are less susceptible to decay from insects (e.g., termites).

7.1.2 Objectives

Therefore, an additional objective of this study is to determine the potential of hybrid diaphragms that use both GFRP and plywood panels in a mixed sheathing arrangement. To accomplish this objective, the behavior of connections between GFRP sheathing panels and wood framing is determined. In addition, general dowel equations are used to determine the theoretical response of connections between GFRP sheathing panels and wood framing. Also, the strength and relative performance of hybrid diaphragms are compared to conventional diaphragm behavior.

The scope of this study is confined to nailed connections, although a number of methods to attach the GFRP panels to wood framing may be explored in subsequent studies. A variety of mechanical fastener types (screws, HILTI pins, etc.) may be suitable. If adhesives are used to attach GFRP panels to wood framing, it may be necessary to evaluate interface bonding (Lopez-Anido et al. 2000; Davalos et al. 2000a,b).

7.1.3 Analytical Model Validation

The finite element model is validated using measured data from two 3.66×7.32 m wood–frame diaphragm tests. The diaphragm configuration is shown in Fig. 7.1. In the first test, a diaphragm using only plywood panels was subjected to cyclic lateral loading. The primary damage observed was local failure of the corner plywood panels at connections with the wood framing. Subsequently, the diaphragm was repaired using GFRP sheathing panels in the diaphragm corners. In the second test, the strengthened diaphragm was again subjected to cyclic lateral loading. The primary damage was local failure of the remaining plywood panels. Notably, the GFRP corner panels were subjected to higher stresses. A full description of the testing configuration, diaphragm materials, and results is given in Chapter 2 and is available elsewhere (Olpin 1998; Olpin and Fonseca 1999).

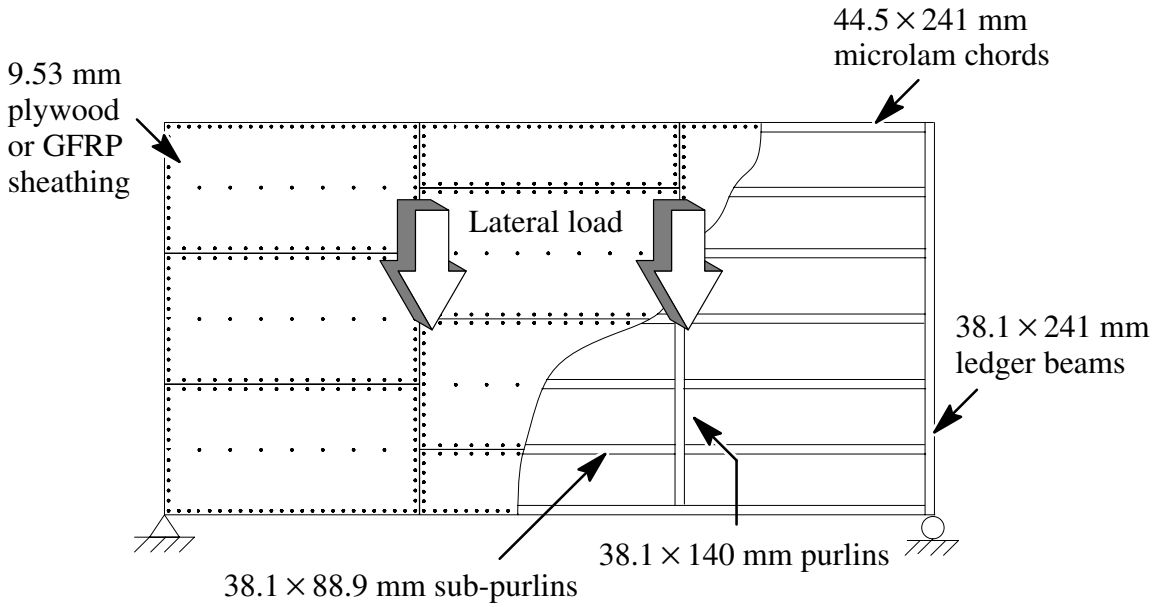

Fig. 7.1. Configuration of 3.66×7.32 m diaphragm using 3.33×63.5 mm common nails

A summary of the finite element representation is given in Table 7.1 and Table 7.2. Wood material properties used in the finite element model were estimated using standard design values available in the literature. No attempt was made to obtain the in-situ values of the material properties. Similarly, the modulus of elasticity and the shear modulus for the GFRP sheathing panels were estimated using design values provided by the manufacturer (Strongwell, Inc. 1998). Load-displacement curves and curve parameters used to define connection behavior were previously determined during connection testing.

Table 7.1. Finite Element Representation for a 3.66×7.32 m Diaphragm using 9.53 mm Plywood and 3.33 mm Common Nails

Structural Component	Finite Element Representation (*ABAQUS* element type)	Material and Section Properties
Chord	2-node linear beam element (B21)	E = 12.4 GPa (1,800,000 psi)[a]
Ledger		E = 11.0 GPa (1,600,000 psi)[a]
Purlin		E = 11.0 GPa (1,600,000 psi)[a]
Sub-Purlin		E = 11.0 GPa (1,600,000 psi)[a]
Plywood Sheathing	8-node linear reduced integration continuum element (CPS8R)	E = 12.4 GPa (1,800,000 psi)[b]
		G = 0.62 GPa (90,000 psi)[b]
		t = 7.32 mm (0.288 in.)[c]
Sheathing-to-Framing Connection	2-node nonlinear user element (U1)	9.53-PLY-3.33-COMMON-FLUSH
		Asymptotic Load-Displacement Curve Parameters[d]
		K_1 = 828 N/mm (4730 lb/in.)
		K_2 = 84.1 N/mm (480 lb/in.)
		δ_{yield} = 0.91 mm (0.036 in.)
		R = 6.15
		δ_{ult} = 2.79 mm (0.11 in.)[e]
		K_3 = 42.0 N/mm (240 lb/in.)[f]
		δ_{fail} = 27.9 mm (1.1 in.)[f]

[a] NDS for Wood Construction: Supplement (AF&PA 2001b), Table 4A.
[b] PDS (APA 1997), Table 3.
[c] PDS, Table 1 (sanded).
[d] Table 2.9, values for 2nd positive cycle; see also Dugan (1995), Table B.3.
[e] "Cyclic loading response of reinforced concrete tilt–up structures with plywood diaphragms," (Fonseca 1997).
[f] This value was assumed.

Table 7.2. Finite Element Representation for a 3.66×7.32 m Diaphragm using 6.35 mm GFRP and 9.53 mm Plywood and 3.33 mm Common Nails

Structural Component	Finite Element Representation (*ABAQUS* element type)	Material and Section Properties
Chord	2-node linear beam element (B21)	E = 12.4 GPa (1,800,000 psi)
Ledger		E = 11.0 GPa (1,600,000 psi)
Purlin		E = 11.0 GPa (1,600,000 psi)
Sub-Purlin		E = 11.0 GPa (1,600,000 psi)
GFRP Sheathing	8-node linear reduced integration continuum element (CPS8R)	E = 17.9 GPa (2,600,000 psi)[(a)] G = 2.93 GPa (425,000 psi)[(a)] t = 6.35 mm (0.25 in.)[(b)]
Plywood Sheathing		E = 12.4 GPa (1,800,000 psi) G = 0.62 GPa (90,000 psi) t = 7.32 mm (0.288 in.)
GFRP Sheathing-to-Framing Connection	2-node nonlinear user element (U1)	6.35-GFRP-3.33-COMMON-FLUSH Asymptotic Load-Displacement Curve Parameters[(c)] K_1 = 1530 N/mm (8720 lb/in.) K_2 = 20 N/mm (114 lb/in.) δ_{yield} = 0.92 mm (0.036 in.) R = 3.30 δ_{ult} = 3.08 mm (0.12 in.) K_3 = 42.0 N/mm (240 lb/in.)[(e)] δ_{fail} = 27.9 mm (1.1 in.)[(f)]
Plywood Sheathing-to-Framing Connection		9.53-PLY-3.33-COMMON-FLUSH Asymptotic Load-Displacement Curve Parameters K_1 = 828 N/mm (4730 lb/in.) K_2 = 84.1 N/mm (480 lb/in.) δ_{yield} = 0.91 mm (0.036 in.) R = 6.15 δ_{ult} = 2.79 mm (0.11 in.) K_3 = 42.0 N/mm (240 lb/in.) δ_{fail} = 27.9 mm (1.1 in.)

[(a)] Strongwell, Inc. (1998). *EXTREN Design Manual*.
[(b)] Effective shear thickness = nominal thickness
[(c)] Table 2.9, values for 2nd positive cycle.
[(e)] This value was assumed.
[(f)] This value was assumed.

Measured and finite element responses are shown in Fig. 7.2 for the plywood diaphragm, and shown in Fig. 7.3 for the strengthened diaphragm. The loading application and sheathing panel arrangements are depicted in each figure (see inset). The measured reaction forces and displacements correspond to the maximum points of each pulling excursion during cyclic loading. The opposite maximum points during each pushing excursion are not shown because of impairments reported during testing. A monotonic displacement–controlled loading history was imposed on the finite element model to provide a response envelope.

Comparison with the measured response shows that the finite element model is fairly accurate. The initial response is slightly stiffer, as generally expected during modeling. The

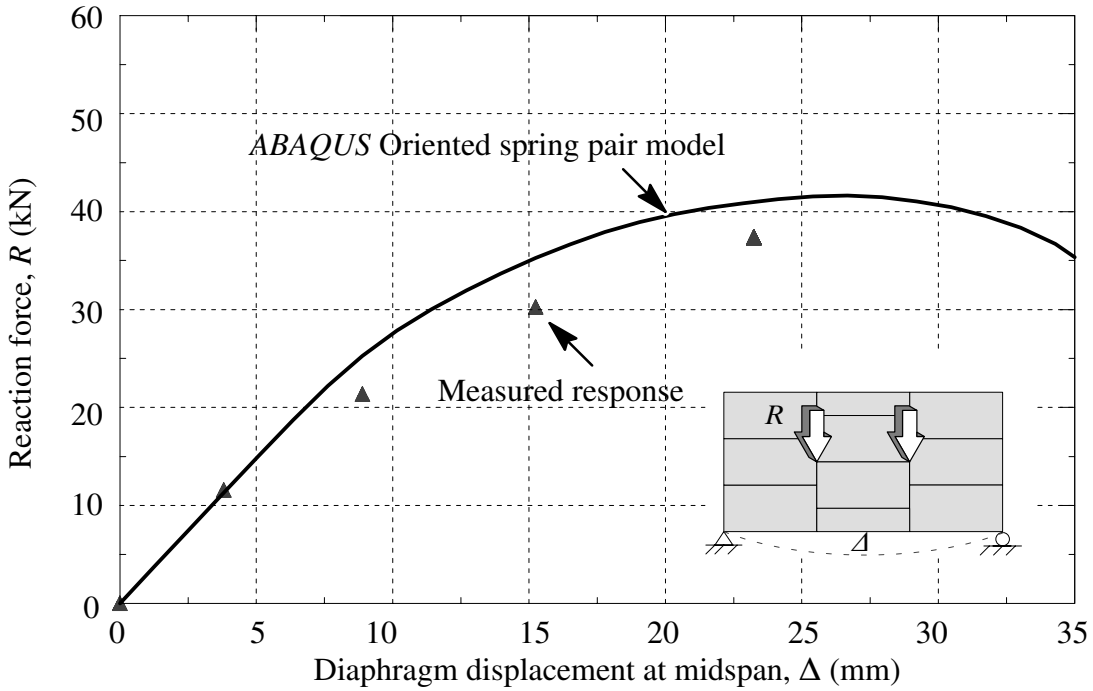

Fig. 7.2. Response of plywood diaphragm

measured maximum displacement and reaction force of the diaphragm are 23.4 mm and 37.4 kN, respectively. The finite element model overshoots these values by 12% and 14%.

For the GFRP strengthened diaphragm, the maximum displacement was 25.7 mm and 49.6 kN. Here, the model overpredicted the force and displacement values by 15%. An overarching consideration is that since material properties were estimated using design values, an exact reproduction of measured results is improbable.

7.1.4 Parametric Analysis

The finite element model is applied in a parametric analysis. The overall strength of the 3.66×7.32 m wood–frame diaphragm using different sheathing panel arrangements and different nail types is predicted. The effect of GFRP sheathing panel arrangement is

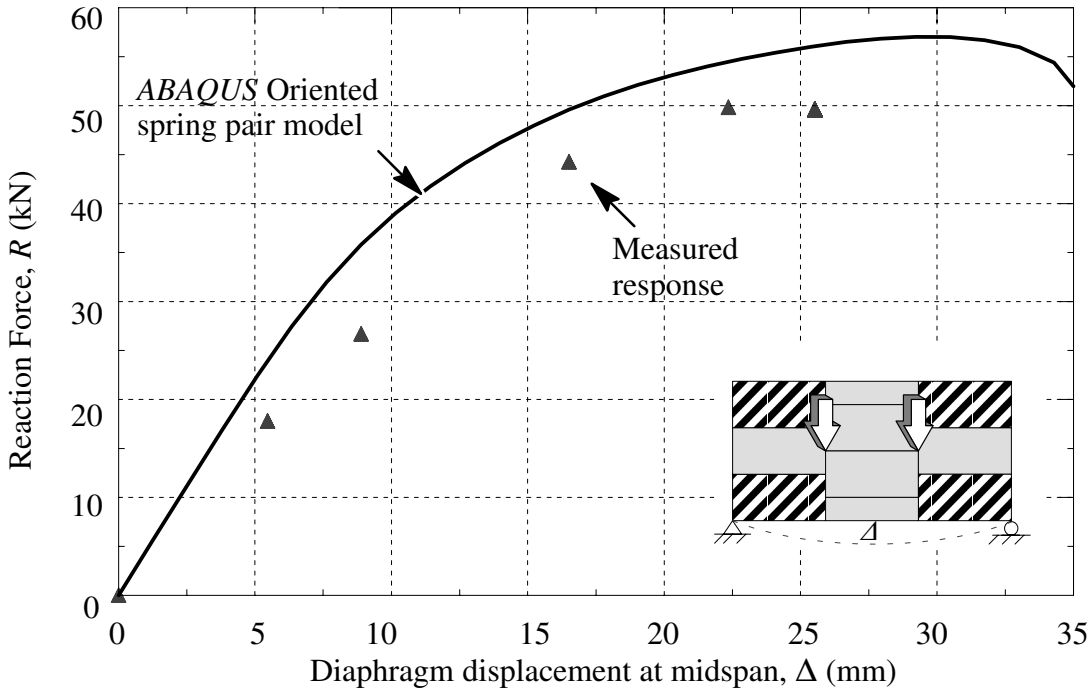

Fig. 7.3. Response of strengthened plywood diaphragm (GFRP corner sheathing panels)

shown in Fig. 7.4 (plywood diaphragm response is shown for comparison). This study indicates that strategic arrangement of GFRP panels in critical locations, such as corners, may be optimal. Employing GFRP panels in the diaphragm corners increases diaphragm strength by 37%, whereas using all GFRP sheathing panels increases strength by 66%. Diaphragms using all GFRP sheathing panels are more than twice as stiff initially than all plywood diaphragms.

In Fig. 7.5 the effect of using different nails to fasten the GFRP sheathing panels is shown for three nail types: 4.14, 3.76, and 3.33 mm common nails. For this model, the diaphragm uses only GFRP sheathing panels. This study shows that using 3.76 mm nails may be optimal. Strength increased by 144% and 133% (compared to the plywood diaphragm) using larger 4.14 mm and 3.76 mm nails, respectively. Therefore, the predicted response of the diaphragm using 4.14 mm nails is essentially the same as the diaphragm using 3.76 mm nails. Initial stiffness of the diaphragm was approximately the same for all three nail types.

The scope of these results is limited to 6.35 mm GFRP sheathing panels fastened using common nails. Notwithstanding, the purpose of this study is to explore the potential of GFRP strengthened diaphragms, rather than to stipulate the best GFRP panel type or optimal GFRP panel arrangement. Alternative GFRP panels and other design factors (e.g. cost) would be considered in a follow–up paper. Even so, the parametric study suggests that strategic arrangement of GFRP sheathing panels, coupled with stronger fastener types will yield wood–frame diaphragms with significant increases in strength.

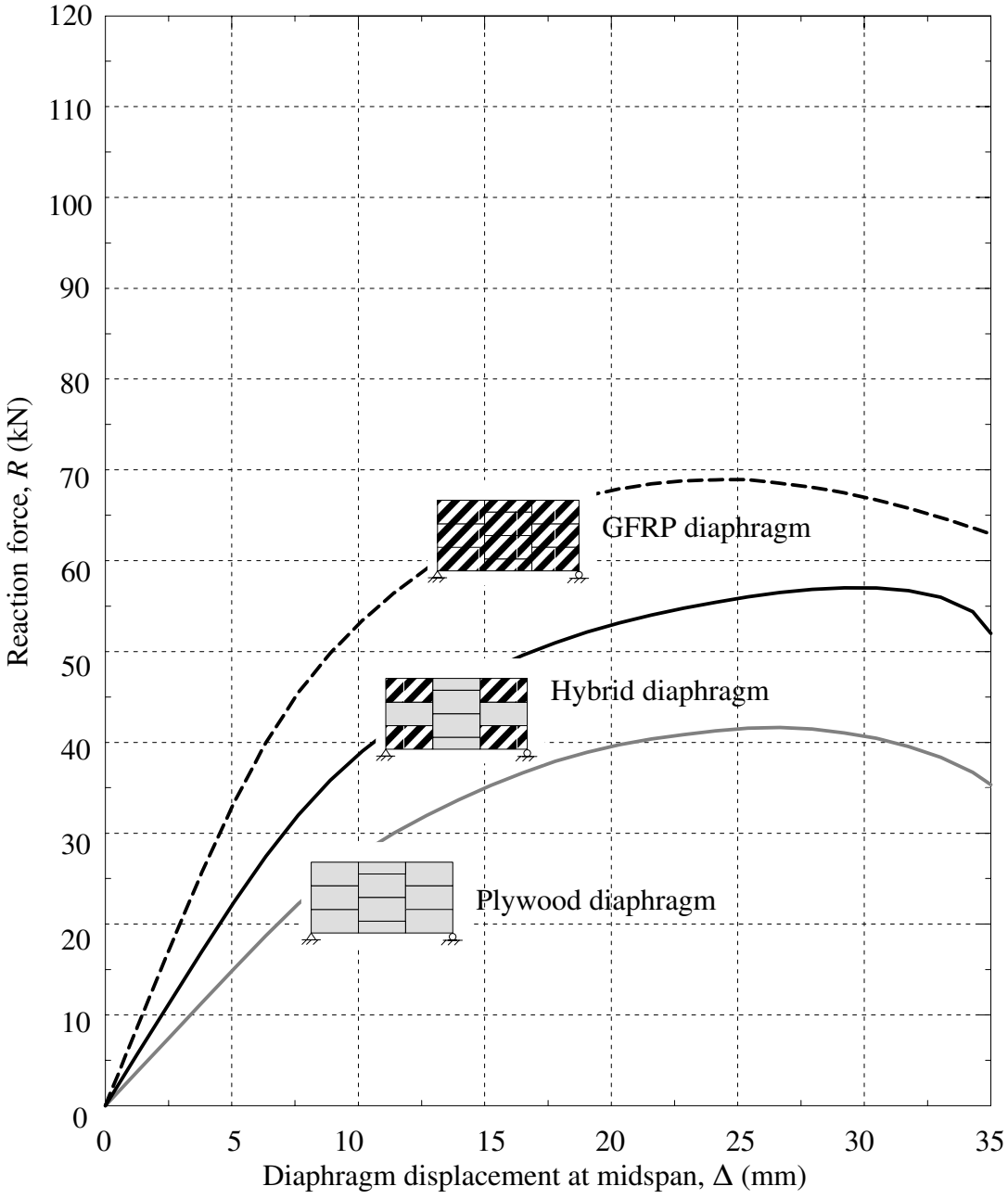

Fig. 7.4. Parametric study: strategic arrangement of GFRP sheathing panels

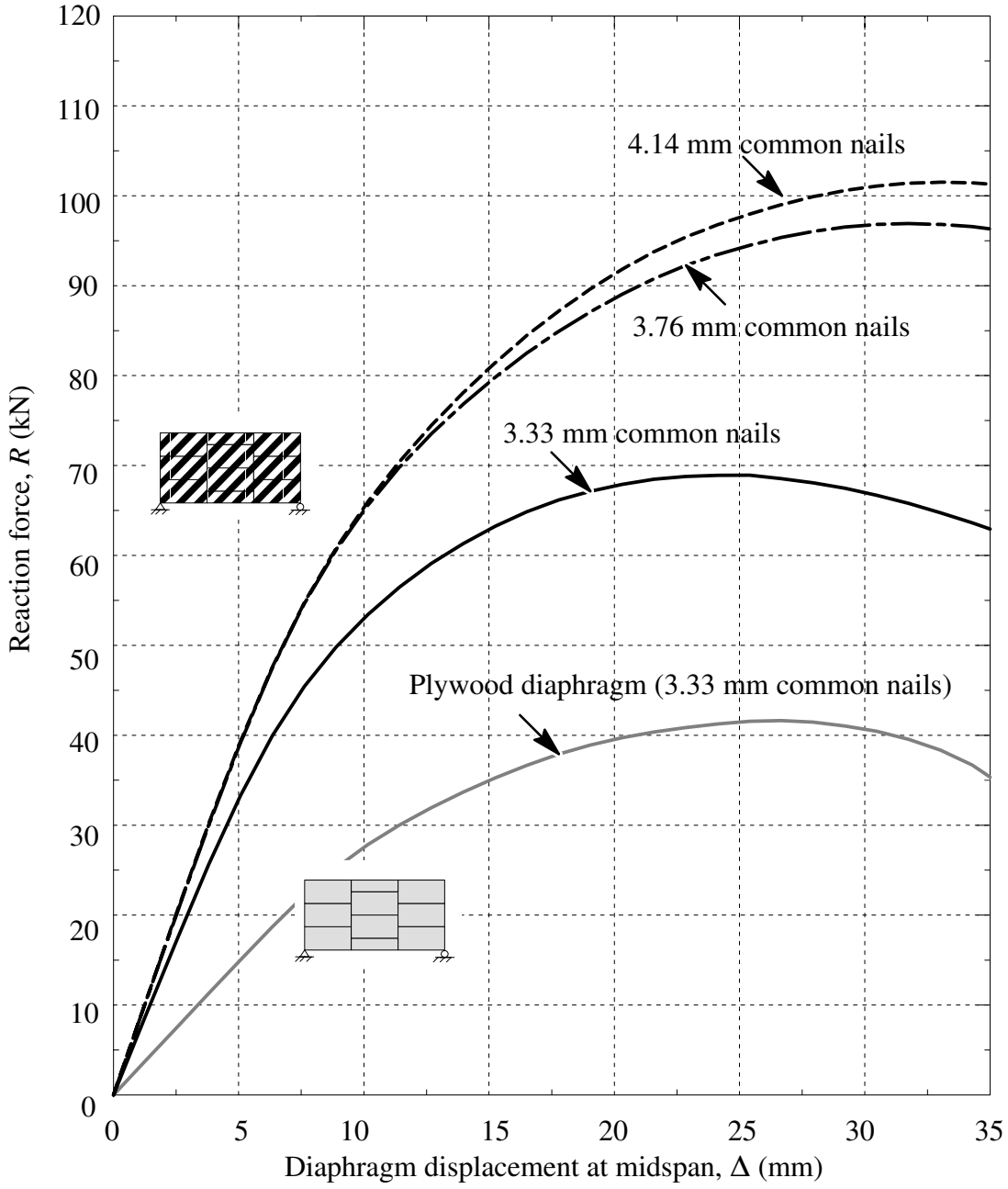

Fig. 7.5. Parametric study: sheathing-to-framing connection selection

7.1.5 Conclusions

Sheathing–to–framing connections using GFRP panels demonstrate marked improvement over traditional connections: (1) GFRP connections are 53% stronger under cyclic loading than similar connections using plywood panels, (2) GFRP connections exhibit comparatively lower strength degradation, (3) conventional plywood connections absorb from 50 to 100% less energy than GFRP connections, and (4) GFRP connections have 139% greater stiffness under monotonic loading conditions than plywood connections.

General dowel equations reasonably predict the strength of GFRP sheathing–to–framing connections. The average theoretical connection strength is 93% of the measured strength, and the theoretical controlling yield modes are in agreement with observations from coupon testing. These correlations suggest that pilot results may be extrapolated by using general dowel equations to determine the strength and behavior of connections with different sheathing materials, fastener types, and wood framing.

The mode of failure of the conventional diaphragm was tearing of the plywood panel edges by the nails. The nails remained essentially undeformed, however, indicating that the nails were within the linear elastic range, not loaded to capacity, and thus the sheathing limited the diaphragm capacity. The hybrid diaphragm did not sustain failure of the GFRP panels. The change in the mode of failure indicates that the nails may have been loaded to capacity in the hybrid diaphragm.

The hybrid diaphragm sustained 34% more load than the conventional diaphragm—notwithstanding the hybrid diaphragm had previously sustained damage. Clearly, a non–damaged diaphragm could have even greater capacity. Furthermore, the strength of a hybrid

diaphragm may be reasonably estimated using sheathing–to–framing connection strengths (determined through testing or using general dowel equations).

Existing structures requiring repair could be upgraded by replacing damaged sheathing panels with GFRP sheathing panels. For example, the strength of a diaphragm could be restored and enhanced by using this hybrid system, as opposed to discarding the entire diaphragm. Critical sheathing panels, such as corner and reentrant corner panels, could be replaced with GFRP panels while leaving less critical panels in place.

In new construction, hybrid diaphragms have promising potential. For instance, in situations where structural diaphragm or shear wall space is limited, hybrid diaphragms could provide needed strength and stiffness. In addition, excessive wood framing sizes could be eliminated, and congested nailing patterns could be reduced. Thus, hybrid diaphragms afford important advantages in both new and existing structures.

7.2 Shear Walls and Diaphragms with Overdriven Sheathing Nails

7.2.1 Background

Fig. 7.6 depicts sheathing connections with properly and improperly driven nails. A nail is underdriven when the nail head is above the sheathing panel (Fig. 7.6*a*). Nails that are driven to the proper depth are considered flush driven, since the nail head is contacting the sheathing panel surface (Fig. 7.6*b*). Nails are considered overdriven when the nail head penetrates the sheathing panel thickness (Fig. 7.6*c*).

During construction of wood-frame shear walls and diaphragms, it is common for nails to be driven improperly. In a survey of construction in the San Francisco, California area, for example, Zacher and Gray (1989) reported that approximately 80% of the nails

were overdriven 3.18 mm or more in plywood shear walls. Incidentally, overdriven nails in gypsum board covered shear walls, and roof or floor diaphragms were also observed. More recently, in a survey of construction in the Salt Lake City, Utah area, Rabe (2000) reported that more than 80% of the nails were overdriven, and that one third of these overdriven nails were driven 3.18 mm or more beyond the sheathing surface.

Overdriven nails may significantly reduce strength in shear walls. Zacher and Gray (1985, 1989) tested shear walls with plywood sheathing and overdriven nails. The test results suggested that overdriven nails caused premature failure. Andreason and Tissell (1994) observed that overdriven nail-heads reduced wall capacity. Jones and Fonseca (2002) tested shear walls with oriented strand board sheathing. For the tests, 100% of the nails were driven to specified depths. The test results indicated that overdriven nails may reduce shear wall strength from 5% to 22%, depending on the depth that the nail–heads are overdriven. Moreover, the test results suggested that shear wall strength reduction is proportional to the nail-head depth.

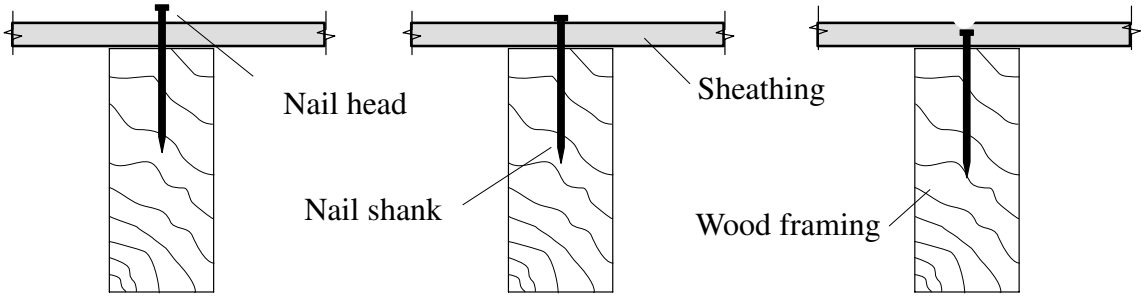

Fig. 7.6. Sheathing-to-framing connections with properly and improperly driven nails

7.2.2 Objectives

Therefore, an additional objective of this paper is to develop a method to estimate the reduction in wall strength due to various overdriven–nail–depth combinations. This objective is met by (1) developing an analytical model to predict the strength of wood shear walls with various overdriven nail depths, and (2) using the analytical model to investigate the effect of overdriven–nail–depth combinations on wall strength.

7.2.3 Analytical Model

The idealized load–displacement curves are employed in an analytical model to predict strength for shear walls with overdriven nails. The *ABAQUS* finite element program (*ABAQUS* 2003) is used to model structural elements in a standard way, where all nonlinearity is ascribed to the nailed sheathing connections.

Tables 7.3–7.6 summarize the analytical model. Wood framing is modeled using beam elements, sheathing panels are modeled using plate elements, and nailed sheathing connections are modeled using an oriented nonlinear spring pair model. The modulus of elasticity of the wood framing is approximated using design values given in the National Design Specifications (NDS) for Wood Construction: Supplement (AF&PA 2001b). The modulus of elasticity and shear modulus of the sheathing are estimated using the design values given by the PFS Research Foundation (PFS/RF 1999).

Table 7.3. Finite Element Representation for a 2.44 × 2.44 m Shear Wall using 11.1 mm OSB and 2.87 mm Cooler Nails

Structural Component	Finite Element Representation (*ABAQUS* element type)	Material and Section Properties
Double Plate Stud	2-node linear beam element (B21)	E = 9.65 GPa (1,400,000 psi)[a]
OSB Sheathing	8-node linear reduced integration continuum element (CPS8R)	E = 4.92 GPa (714,000 psi)[b] G = 1.22 GPa (177,000 psi)[c] t = 11.11 mm (0.4375 in.)[d]
Sheathing-to-Framing Connection	2-node nonlinear user element (U1)	11.11-OSB-2.87-COOLER-FLUSH Exponential Load-Displacement Curve Parameters[e] K_1 = 2,280 N/mm (13,000 lb/in.) K_2 = 35.0 N/mm (200 lb/in.) δ_{yield} = 0.43 mm (0.017 in.) R = 2.1 δ_{ult} = 3.73 mm (0.147 in.) K_3 = 135 N/mm (772 lb/in.) δ_{fail} = 5.99 mm (0.236 in.)

[a] NDS for Wood Construction: Supplement (AF&PA 2001b), Table 4A.
[b] *Technical Bulletin No. 104* (PFS/RF 2003), Table A, where EI/I = E.
[c] *Technical Bulletin No. 104*, Table A, where Gt/t = G.
[d] Effective shear thickness = nominal thickness
[e] Table 2.11; average values for the positive 2 cycle.

Table 7.4. Finite Element Representation for a 2.44 × 2.44 m Shear Wall using 11.1 mm OSB and 2.87 mm Cooler Nails 1.59 mm Overdriven

Structural Component	Finite Element Representation (*ABAQUS* element type)	Material and Section Properties
Double Plate Stud	2-node linear beam element (B21)	E = 9.65 GPa (1,400,000 psi)[a]
OSB Sheathing	8-node linear reduced integration continuum element (CPS8R)	E = 4.92 GPa (714,000 psi)[b] G = 1.22 GPa (177,000 psi)[c] t = 11.11 mm (0.4375 in.)[d]
Sheathing-to-Framing Connection	2-node nonlinear user element (U1)	11.11-OSB-2.87-COOLER-FLUSH Exponential Load-Displacement Curve Parameters[e] K_1 = 2,030 N/mm (11,600 lb/in.) K_2 = 26.3 N/mm (150 lb/in.) δ_{yield} = 0.48 mm (0.019 in.) R = 2.2 δ_{ult} = 2.64 mm (0.104 in.) K_3 = 129 N/mm (736 lb/in.) δ_{fail} = 4.95 mm (0.195 in.)

[a] NDS for Wood Construction: Supplement (AF&PA 2001b), Table 4A.
[b] *Technical Bulletin No. 104* (PFS/RF 2003), Table A, where EI/I = E.
[c] *Technical Bulletin No. 104*, Table A, where Gt/t = G.
[d] Effective shear thickness = nominal thickness
[e] Table 2.11; average values for the positive 2 cycle.

Table 7.5. Finite Element Representation for a 2.44 × 2.44 m Shear Wall using 11.1 mm OSB and 2.87 mm Cooler Nails 3.18 mm Overdriven

Structural Component	Finite Element Representation (*ABAQUS* element type)	Material and Section Properties
Double Plate Stud	2-node linear beam element (B21)	E = 9.65 GPa (1,400,000 psi)[a]
OSB Sheathing	8-node linear reduced integration continuum element (CPS8R)	E = 4.92 GPa (714,000 psi)[b] G = 1.22 GPa (177,000 psi)[c] t = 11.11 mm (0.4375 in.)[d]
Sheathing-to-Framing Connection	2-node nonlinear user element (U1)	11.11-OSB-2.87-COOLER-FLUSH Exponential Load-Displacement Curve Parameters[e] K_1 = 1,800 N/mm (10,300 lb/in.) K_2 = 43.8 N/mm (250 lb/in.) δ_{yield} = 0.48 mm (0.019 in.) R = 3.5 δ_{ult} = 2.34 mm (0.092 in.) K_3 = 217 N/mm (1,240 lb/in.) δ_{fail} = 4.11 mm (0.162 in.)

[a] NDS for Wood Construction: Supplement (AF&PA 2001b), Table 4A.
[b] *Technical Bulletin No. 104* (PFS/RF 2003), Table A, where EI/I = E.
[c] *Technical Bulletin No. 104*, Table A, where Gt/t = G.
[d] Effective shear thickness = nominal thickness
[e] Table 2.11; average values for the positive 2 cycle.

Table 7.6. Finite Element Representation for a 2.44 × 2.44 m Shear Wall using 11.1 mm OSB and 2.87 mm Cooler Nails 4.76 mm Overdriven

Structural Component	Finite Element Representation (*ABAQUS* element type)	Material and Section Properties
Double Plate Stud	2-node linear beam element (B21)	E = 9.65 GPa (1,400,000 psi)[a]
OSB Sheathing	8-node linear reduced integration continuum element (CPS8R)	E = 4.92 GPa (714,000 psi)[b] G = 1.22 GPa (177,000 psi)[c] t = 11.11 mm (0.4375 in.)[d]
Sheathing-to-Framing Connection	2-node nonlinear user element (U1)	11.11-OSB-2.87-COOLER-FLUSH Exponential Load-Displacement Curve Parameters[e] K_1 = 2,100 N/mm (12,000 lb/in.) K_2 = 0 N/mm (0 lb/in.) δ_{yield} = 0.41 mm (0.016 in.) R = 2.7 δ_{ult} = 1.91 mm (0.075 in.) K_3 = 153 N/mm (871 lb/in.) δ_{fail} = 4.19 mm (0.165 in.)

[a] NDS for Wood Construction: Supplement (AF&PA 2001b), Table 4A.
[b] *Technical Bulletin No. 104* (PFS/RF 2003), Table A, where EI/I = E.
[c] *Technical Bulletin No. 104*, Table A, where Gt/t = G.
[d] Effective shear thickness = nominal thickness
[e] Table 2.11; average values for the positive 2 cycle.

7.2.4 Analytical Model Validation

The analytical model is validated using experimental data. Eight 2.44×2.44 m shear walls were tested using a pseudo dynamic procedure by Jones and Fonseca (2002) with four nail–head depths: flush driven, 1.59 mm, 3.18 mm, and 4.76 mm overdriven. The configuration of the shear wall is shown in Fig. 7.7. Two shear walls were constructed for each overdriven depth, with all nails driven to a specified depth. Each shear wall used 38.1×88.9 mm Douglas Fir–Larch wood members and 8d cooler (2.87×60.3 mm) nails. Nails were spaced at 76.2 mm along edges and 305 mm along intermediate supports.

Table 7.7 provides a comparison between the measured and analytical shear wall strengths. The measured value is an average value from two tests. The measured response is approximately 90–95% of the analytical prediction. The overestimation in predicted

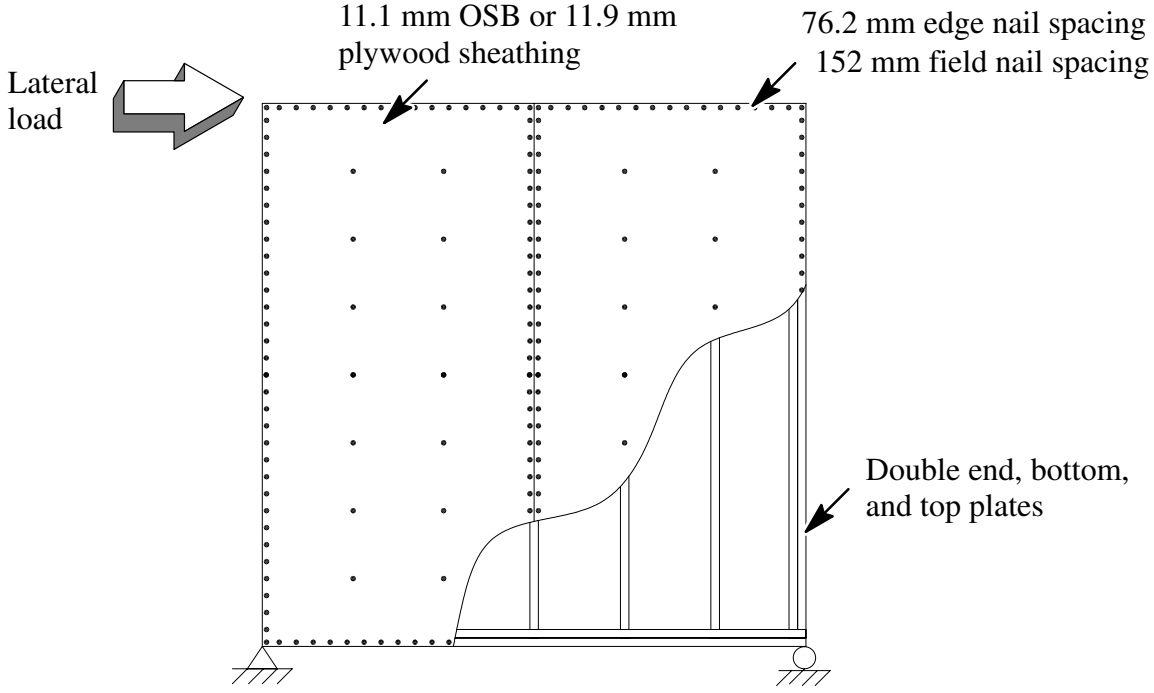

Fig. 7.7. Configuration of 2.44×2.44 m shear wall using 2.87×60.3 mm cooler nails

strength is reasonable in view of the fact that design values were used for material properties, instead of in–situ (actual) values.

Fig. 7.8 shows the relationship between strength reduction and overdriven depth. Based on the relationship, the reduction in strength for a shear wall with 100% of the nails driven to a specified depth may be estimated by assuming that shear wall strength and nail–head depth are linearly proportional (Jones and Fonseca 2002). Based on these results, the reduction in wall strength (R_{OD}) for 100% of the nails overdriven to a specified depth may be estimated using Eq. 7.1.

$$R_{OD} = F * 0.052\, d_{OD} \tag{7.1}$$

where d_{OD} = overdriven nail depth; and F = flush (properly) driven wall strength.

Table 7.7. Shear Wall Strength (kN)

Nail-head depth	Measured	Analytical Model
Flush (properly driven)	36.7	41.0
Overdriven 1.59 mm	34.7	37.5
Overdriven 3.18 mm	32.3	34.1
Overdriven 4.76 mm	28.0	30.8

7.2.5 Parametric Studies

The analytical model is used to investigate the effect of various overdriven–nail–depth combinations on wood shear wall strength. This preliminary parametric study considers six overdriven–nail–depth combinations (each combination consists of two overdriven–nail depths).

In Fig. 7.9*a* the relationship between the fraction of total nails (P_{OD}) overdriven to a specified depth and the reduction in strength is shown in terms of the overdriven nail factor (C_{OD}). The overdriven nail factor is calculated by dividing the strength reduction for a specific P_{OD} by the strength reduction for 100% of the nails overdriven to the larger depth of two specified depths. In this way, C_{OD} adjusts the reduction in wall strength due to both the percentage of nails overdriven and the overdriven depth.

The results suggest that the relationship between strength reduction and fraction of overdriven nails is nonlinear. In Fig. 7.9*b* the average overdriven nail factor for a specific P_{OD} is shown. For design purposes the average overdriven nail factor may be idealized using (7.2).

$$C_{OD} = \begin{cases} 1.61\,P_{OD}\,, & \text{if } P_{OD} \le 0.23 \\ 0.82\,P_{OD} + 0.18\,, & \text{if } P_{OD} > 0.23 \end{cases} \tag{7.2}$$

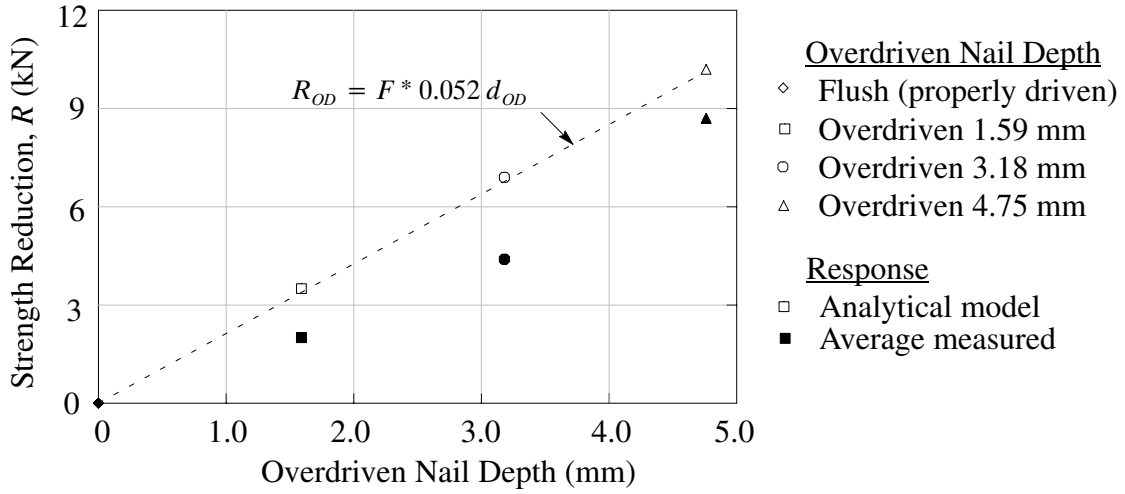

Fig. 7.8. Effect of overdriven nail depth on shear wall strength

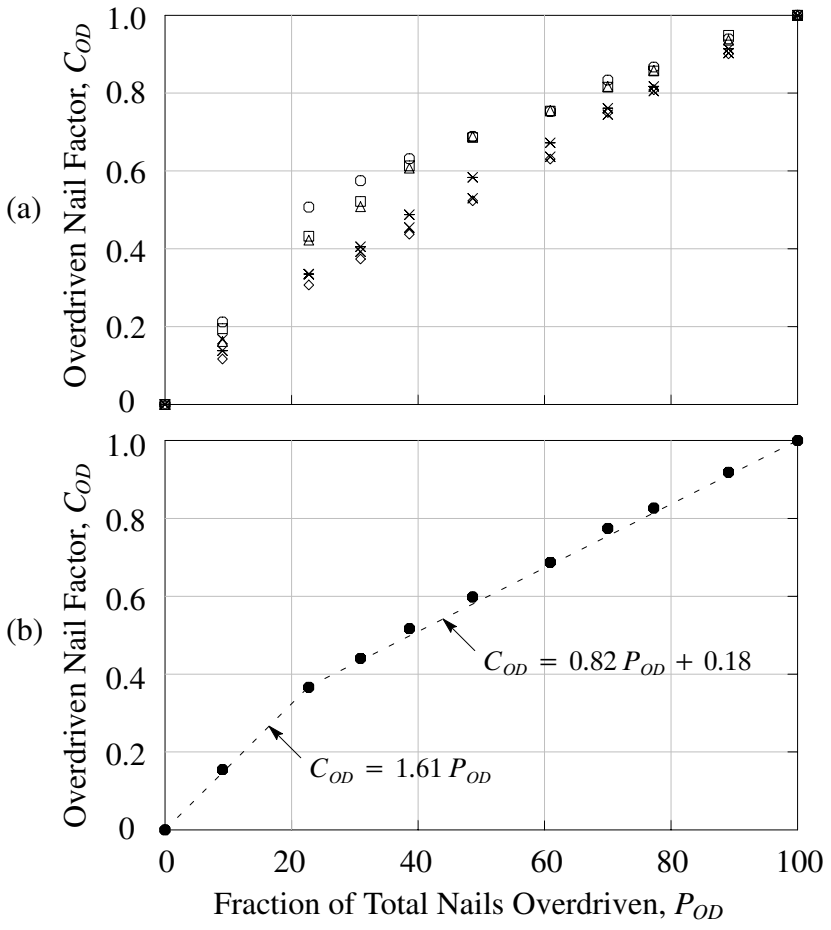

Fig. 7.9. Effect of overdriven-nail-depth combinations on shear wall strength

7.2.6 Design Example

Determine the reduction in strength of a 2.44×2.44 m shear wall with 11.1 mm oriented strand board sheathing and 8d cooler (2.87×60.3 mm) nails, with 29% of the nails overdriven 1.59 mm, 25% of the nails overdriven 3.18 mm, and 13% of the nails overdriven 4.75 mm.

Step 1. Determine the flush (properly) driven wall strength:

$$F = 41.0 \text{ kN}$$

Step 2. Calculate the wall strength reduction for each overdriven nail depth using Eq. 7.1:

$$R_{1.59} = (41.0 \text{ kN}) \times 0.052 \times (1.59) = 3.4 \text{ kN}$$

$$R_{3.18} = (41.0 \text{ kN}) \times 0.052 \times (3.18) = 6.8 \text{ kN}$$

$$R_{4.76} = (41.0 \text{ kN}) \times 0.052 \times (4.76) = 10.2 \text{ kN}$$

Step 3. Calculate the adjustment factor, C_{OD} for each overdriven nail depth using Eq. 7.2:

$$C_{1.59} = 0.82 \times (0.29) + 0.18 = 0.42$$

$$C_{3.18} = 0.82 \times (0.25) + 0.18 = 0.39$$

$$C_{4.76} = 1.61 \times (0.13) = 0.21$$

Step 4. The total reduction in wall strength is determined by adding the adjustment factor (Step 3) multiplied by the reduction in wall strength (Step 2) for each overdriven nail depth:

$$R_{TOTAL} = C_{1.59} R_{1.59} + C_{3.18} R_{3.18} + C_{4.76} R_{4.76}$$

$$= (0.42) \times 3.4 \text{ kN} + (0.39) \times 6.8 \text{ kN} + (0.21) \times 10.2 \text{ kN}$$

$$= 6.2 \text{ kN}$$

For purposes of comparison, the analytical model is used to predict the strength of the shear wall described in this design example. The average predicted strength is 36.0 kN (for three different random distributions throughout the wall of each overdriven nail depth). This corresponds to a 5.0 kN reduction in strength. As a consequence, the proposed method seems justified.

Chapter 8

SUMMARY AND CONCLUSIONS

Analytical models of wood-frame shear walls and diaphragms are presented in this thesis. The models are validated for monotonic, quasi-static (cyclic), and dynamic analyses. The effects of various of sheathing-to-framing connections parameters, hysteresis model parameters, and analytical complexity are determined.

8.1 Sheathing-to-Framing Connection Representation for Structural Analysis

Previous representations of sheathing–to–framing connections in wood shear walls and diaphragms are inadequate. Namely, the single spring model is viable for monotonic analysis but incapable of cyclic or dynamic analyses; the nonoriented spring pair model, while capable of both monotonic, cyclic, and dynamic analyses, generally overestimates the stiffness and strength of the connection. These are significant limitations.

The nonoriented spring pair model overestimates connection stiffness because the spring stiffness and force change relative to the displacement trajectory. As a consequence, connections located near sheathing panel corners have greater stiffness than connections located elsewhere, in proportion to the distance from the panel corner. The new analytical model presented in this paper represents sheathing–to–framing connections using a spring pair oriented along the initial displacement trajectory. This trajectory corresponds to experi-

mental observations of actual sheathing–to-framing connections. To validate the new analytical model, the oriented spring pair model is implemented into a general purpose finite element program, *ABAQUS* (2003) and into a specialized structural analysis program, *CASHEW* (Folz and Filiatrault 2000).

Using the oriented spring pair model in a finite element analysis of shear walls and diaphragms provides a closer fit to measured data, compared to using the nonoriented spring pair model. The model is viable for monotonic, cyclic, and dynamic analyses. The oriented spring pair model is successfully implemented into the specialized structural analysis program *CASHEW*. By implementing the oriented spring pair model, no scaling or adjustment is required in *CASHEW*.

In summary, the oriented spring pair model provides three distinct advantages:

1. The analytical model is capable of both monotonic and cyclic analysis.

2. The analytical model may be implemented in a general purpose finite element program or in a specialized structural analysis program.

3. The analytical model is rigorous; it does not need to be scaled or adjusted.

8.2 Equivalent Single Degree of Freedom Analysis

A new analysis program, *QUICK* models shear walls and diaphragms as equivalent single degree of freedom systems. The model is well suited for routine analysis or for dynamic analyses that would otherwise be too computationally costly to perform. The equivalent system parameters may be determined using either of two methods: Using method 1, equivalent parameters are calibrated using experimental or analytical data. Using method 2, equivalent parameters are determined using structural component and sheathing-to-fram-

ing connection data. In this way, *QUICK* can be used in conjunction with finite element analysis, specialized structural analysis (such as *CASHEW*), or with measured data to provide a more precise analysis, while at the same time maintaining the practicality of a single degree of freedom analysis.

8.3 Application Examples

8.3.1 Hybrid Shear Walls and Diaphragms

An accurate and versatile finite element model was developed for wood-frame shear walls and diaphragms. For the 3.66×7.32 m diaphragm considered in this thesis, the model predicted that GFRP sheathing panels increased diaphragm strength from 37% to 144% and doubled roof stiffness, depending on panel arrangement and nail type used. The parametric study suggests that a strategic arrangement of GFRP sheathing panels with 3.76 mm common nails is optimal for shear walls and diaphragms.

Wood-frame diaphragms (roofs) that are subjected to high lateral inertial and wind loads, and that are overly flexible, would be effectively strengthened using GFRP sheathing panels. Existing diaphragms could be repaired if panels are damaged, using GFRP sheathing panels, instead of replacing the entire diaphragm. Also wood-frame roofs could be retrofitted by substituting GFRP panels in critical locations, such as roof corners. Additionally, wood-frame shear walls strengthened using GFRP panels may exhibit similar improvements in stiffness and strength.

8.3.2 Shear Walls and Diaphragms with Overdriven Nails.

Reduction in shear wall strength due to overdriven nail-heads may be estimated using the overdriven nail factor, C_{OD}, which accounts for both the overdriven nail depth and the percentage of total nails overdriven. Importantly, the reduction for wood shear walls with more than two overdriven nail depths may be estimated based on the reduction in strength for each overdriven nail depth expected.

8.4 Recommendations for Future Research

Future research could expand the scope of this thesis in a number of areas. The oriented spring pair model may be refined to include off-directional stiffness using empirical data or using a discrete set of damage levels instead of using a continuous damage function. The effects of anchorage devices, non-structural finishes, support conditions, and sheathing panel interlocking need to be investigated. A comparison between analytical model response and actual (in-situ) response is needed to clarify the contribution of non-structural elements and anchorage devices to the overall structural response of shear walls and diaphragms. Future research could also expand the scope of this thesis by including other fastener types (staples and screws) and other sheathing materials.

8.5 Potential Impact of Findings

The research findings presented in this thesis are especially relevant in light of the recent developments in displacement-based design. The oriented spring pair model and the *QUICK* model provide powerful tools that may be used to develop an understanding of the

monotonic response and energy dissipation characteristics. While experimental testing may not be completely replaced, these analytical models are effective for analysis of wood-frame shear walls and diaphragms.

REFERENCES

ABAQUS. (2003). *ABAQUS/standard*, *version 6.4–1*. ABAQUS, Inc., Providence, Rhode Island.

Albert, T. J., and Johnson, J. W. (1967). "Lateral holding capacity of power–driven fasteners." *Forest Products Journal*, Forest Products Society, Vol. 17, No. 9, 59–67.

American Forest and Paper Association (AF&PA). (2001a). "National design specification (NDS) for wood construction." American Forest & Paper Association, Washington, D. C.

American Forest and Paper Association (AF&PA). (2001b). "National design specification (NDS) for wood construction supplement: Design values for wood construction." American Forest & Paper Association, Washington, D. C.

American Forest and Paper Association (AF&PA). (2001c). "National design specification (NDS) for wood construction supplement: Wood structural panel shear wall and diaphragm." American Forest & Paper Association, Washington, D. C.

American Forest and Paper Association and American Society of Civil Engineers (AF&PA/ASCE). (1996). "Standard for load and resistance factor design (LRFD) for engineered wood construction / AF&PA/ASCE." American Society of Civil Engineers, New York, New York.

American Plywood Association (APA)—The Engineered Wood Association. (1996). "Bearing strength of OSB to be used for the EYM design method." APA—The Engineered Wood Association, Tacoma, Washington.

American Plywood Association (APA)—The Engineered Wood Association. (1997). "Plywood Design Specification (PDS)." APA—The Engineered Wood Association, Tacoma, Washington.

American Plywood Association (APA)—The Engineered Wood Association. (2004). "Diaphragms and shear walls: design/construction guide." APA—The Engineered Wood Association, Tacoma, Washington.

American Society for Testing and Materials (ASTM). (2000). "Standard test methods for mechanical fasteners in wood." *ASTM D 1761-88(2000), Annual book of standards*, Vol. 1.08, American Society for Testing and Materials, Philadelphia, Pennsylvania.

American Society for Testing and Materials (ASTM). (2001a). "Standard test method for evaluating dowel-bearing strength of wood and wood-based products." *ASTM D 5764-97a, Annual book of standards*, Vol. 4.10, American Society for Testing and Materials, Philadelphia, Pennsylvania.

American Society for Testing and Materials (ASTM). (2001b). "Bearing strength of plastics." *ASTM D 953-95, Annual book of standards*, Vol. 8.01, American Society for Testing and Materials, Philadelphia, Pennsylvania.

American Society for Testing and Materials (ASTM). (2001c). "Standard test method for determining bending yield moment of nails." *ASTM F 1575-01, Annual book of standards*, Vol. 1.08, American Society for Testing and Materials, Philadelphia, Pennsylvania.

American Wood Council (AWC). (1999). "General dowel equations for calculating lateral connection values." *Technical Report No. 12.* American Forest & Paper Association, Washington, D. C.

Andreason, K. R. and Tissell, J. R. (1994). "Effects of overdriven nails in shear walls." *APA Report T94 9*, APA—The Engineered Wood Association, Technical Services Division, Tacoma, Washington.

ANSYS. (2000). *ANSYS/Structural, version 5.7*. ANSYS, Inc. Canonsburg, Pennsylvania.

Antonides, C. E., Vanderbilt, M. D., and Goodman J. R. (1979). Interlayer gap effects on nail slip modulus. *Structural Research Report No. 22*, Dept. of Civil Engineering, Colorado State University, Fort Collins, Colorado.

Applied Technology Council (ATC). (1981). "Guidelines for the design of horizontal wood diaphragms." *Report No. ATC–7*, Applied Technology Council, Berkeley, California.

Atherton, G. H., Rowe, K. E., and Bastendorff, K. M. (1980). "Damping and slip of nail joints." *Wood Science*, Forest Products Reserach Society, Vol. 12, No. 4, 218–226.

Bathe, K.–J. (1996). *Finte Element Procedures*. Pentice-Hall, Inc., Upper Saddle River, New Jersey.

Belytschko, T., Liu, W. K., and Moran, B. (2000). *Nonlinear finite elements for continua and structures*. 1st edition, John Wiley & Sons, Ltd., West Sussex, England.

Breyer, D. E., Fridley, K. J., Pollock, D. G., and Cobeen, K. E. (2003). *Design of wood structures—ASD*. 5th edition, McGraw–Hill Companies, Inc., New York, New York.

Bulleit, W. M. (1992). "Wood combined with other materials." *Procedings, Wood Products for Engineered Structures: Issues Affecting Growth and Acceptance of Engineered Wood Products*, Forest Products Society, Madison, Wisconsin, No. 47329, 44–46.

Burns, J. M. (2001). "Capacity of plywood shear walls with overdriven fasteners under fully cyclic loading." MS thesis, Brigham Young University, Provo, Utah.

Campbell, S. H. (2002). "Single fastener wood connections in fully reversed cyclic loading." MS thesis, Brigham Young University, Provo, Utah.

Ceccotti, A., and Vignoli, A. (1990). "Engineered timber structures: An evaluation of their seismic behavior." *Proceedings, 1990 International Timber Engineering Conference*, Vol. 3, 946–953.

Chopra, A. K. (1995). *Dynamics of structures: Theory and applications to earthquake engineering*. Prentice-Hall, Inc., Upper Saddle River, New Jersey.

Chui, Y. H., Ni, C., and Jiang, L. (1998). "Finite–element model for nailed wood joints under reversed cyclic load." *Journal of Structural Engineering*, American Society of Civil Engineers, Vol. 124, No. 1, 96–103.

Clough, R. W. (1966). "Effect of stiffness degradation on earthquake ductility requirements," *Technical Report No. SESM 66–16*, University of California, Berkeley, California.

Cobeen, K., Russell, J., and Dolan, J. D. (2004). "Recommendations for earthquake resistance in the design and construction of woodframe buildings." *CUREe Publication No. W–30*, Consortium of Universities for Research in Earthquake Engineering, Richmond, California.

Countryman, D. (1952). "Lateral tests on plywood sheathed diaphragms." *Laboratory Report No. 55*, APA—The Engineered Wood Association, Tacoma, Washington.

Countryman, D. (1955). "1954 Horizontal plywood diaphragm tests." *Laboratory Report No. 63*, Douglas Fir Plywood Association, Tacoma, Washington.

Cruz, H. M. P. (1993). "Nailed timber joints subjected to alternating load cycles." PhD thesis, University of Brighton, Brighton, U.K.

Davalos, J. F., and Barbero, E. J. (1991). "Modeling of glass–fiber reinforced glulam beams." *Procedings of the 1991 International Timber Engineering Conference*, Vol. 3, 3.234–3.241.

Davalos, J. F., Qiao, P. Z., and Trimble, B. S. (2000a). "Fiber–reinforced composite and wood bonded interface, part 1. Durability and shear strength." *Journal of Composites Technology and Research,* American Society for Testing and Materials, Vol 22, No. 4, 224–231.

Davalos, J. F,. Qiao, P .Z., and Trimble, B. S. (2000b). "Fiber–reinforced composite and wood bonded interface, part 2. Fracture." *Journal of Composites Technology and Research,* American Society for Testing and Materials, Vol. 22, No. 4, 232–240.

Dean, J. A. (1988). "The ductility of nailed sheathing joints in timber frame shearwalls." *Report CE 88/14*, Civil Engineering Department, University of Canterbury, Christchurch, New Zealand.

DeBonis, A. L. and Bodig, J. (1975). "Nailed wood joints under combined loading," *Wood Science and Technology*, Vol. 9, No. 2, 129–144.

Diekmann, E. F. (1990). "Design of wood diaphragms." *Wood: Engineering Design Concepts (Vol. 4).* Materials Education Council, University Park, Pennsylvania, 481–482.

Diekmann, E. F. (1994). "Design and code issues in the design of diaphragms and shearwalls." *Procedings, Research Needs Workshop on Analysis, Design and Testing of Timber Structures Under Seismic Loads*, 9 September 1994. Forest Products Laboratory, University of California, Richmond, California, 9–20.

Dinehart, D. W., and Shenton, H. W., III. (1998). "Comparison of static and dynamic response of timber shear walls." *Journal of Structural Engineering*, American Society of Civil Engineers, Vol. 124, No. 6, 686–695.

Dinehart, D. W., and Shenton, H. W., III. (2000). "Model for dynamic analysis of wood frame shear walls." *Journal of Engineering Mechanics*, American Society of Civil Engineers, Vol. 126, No. 9, 899–908.

Dolan, J. D. (1989). "The dynamic response of timber shear walls." PhD thesis, University of British Columbia, Vancouver, British Columbia, Canada.

Dolan, J. D., and Foschi, R. O. (1991). "Structural analysis model for static loads on timber shear walls." *Journal of Structural Engineering*, American Society of Civil Engineers, Vol. 117, No. 3, 851–861.

Dolan, J. D., Gutshall, S. T., and McLain, T. E. (1994). Monotonic and cyclic tests to determine short term duration of load performance of nail and bolt connections: Volume I: summary report. *Timber Engineering Report TE 1994 001*, Virginia Polytechnic Institute and State University, Blacksburg, Virginia.

Dolan, J. D., and Madsen, B. (1992). "Monotonic and cyclic nail connection tests." *Canadian Journal of Civil Engineering*, National Research Council of Canada, Vol. 19, 97–104.

Dugan, K. (1995). "Nail slip curves." *Unpublished Report*, Department of Civil Engineering, University of Illinois at Urbana–Champaign, Urbana, Illinois.

Durham, J. (1998). "Seismic response of wood shearwalls with oversized oriented strand board panels." MASc thesis, University of British Columbia, Vancouver, British Columbia, Canada.

Easley, J. T., Foomani, M., and Dodds, R. H. (1982). "Formulas for wood shear walls.' *Journal of the Structural Division*, American Society of Civil Engineers, 108(ST11), 2460–2478.

Ehlbeck, J. (1979). "Nailed joints in wood structures." *VPI&SU, Wood Research and Construction Laboratory, Bulletin No. 166*, Virginia Polytechnic Institute and State University, Blacksburg, Virginia.

Falk, R. H., and Itani, R. Y. (1989). "Finite element modeling of wood diaphragms." *Journal of Structural Engineering*, American Society of Civil Engineers, Vol. 115, No. 3, 543–559.

Federal Emergency Management Agency (FEMA). (1997a). "NEHRP Guidelines for the seismic rehabilitation of buildings." *FEMA Publication 273*, Federal Emergency Management Agency, Washington, D. C.

Federal Emergency Management Agency (FEMA). (1997b). "NEHRP Commentary on the guidelines for the seismic rehabilitation of buildings." *FEMA Publication 274*, Federal Emergency Management Agency, Washington, D. C.

Federal Emergency Management Agency (FEMA). (2000). "Prestandard and commentary for seismic rehabilitation of buildings." *Report No. FEMA 356*, Federal Emergency Management Agency, Washington, D. C.

Filiatrault, A. (1990). "Static and dynamic analysis of timber shear walls." *Canadian Journal of Civil Engineering*, National Research Council of Canada, Vol. 17, No. 4, 643–651.

Filiatrault, A., Fischer, D., Folz, B., and Uang, C.-M. (2002). "Seismic testing of two-story woodframe house: Influence of wall finish materials." *Journal of Struct. Engineering*, American Society of Civil Engineers, Vol. 128, No. 10, 1337–1345.

Filiatrault, A., and Folz, B. (2002). "Performanced-based seismic design of wood framed buildings." *Journal of Structural Engineering*, American Society of Civil Engineers (ASCE), Vol. 128, No. 1, 39–47.

Foliente, G. C. (1995). "Hystersis modeling of wood joints and structural systems." *Journal of Structural Engineering*, American Society of Civil Engineers, Vol. 121, No. 6, 1013–1022.

Foliente, G. C., and Zacher, E. G. (1994). "Performance of timber structural systems under seismic loads." *Procedings, Research Needs Workshop on Analysis, Design and Testing of Timber Structures Under Seismic Loads*, 9 September 1994. Forest Products Laboratory, University of California, Richmond, California, 21–86.

Foliente, G. C. (1997). "Modeling and analysis of timber structures under seismic loads: State-of-the-art." *Earthquake Performance and Safety of Timber Structures*, Forest Products Society, Madison, Wisconsin.

Folz, B., and Filiatrault, A. F., (2000). "CASHEW—Version 1.0, a computer program for cyclic analysis of wood shear walls." *Report No. SSRP–2000/10*, Structural Systems Research Project, Department of Structural Engineering, University of California, San Diego, La Jolla, California.

Folz, B., and Filiatrault, A. F., (2001). "Cyclic analysis of wood shear walls." *Journal of Structural Engineering*, American Society of Civil Engineers, Vol. 127, No. 4, 433–441.

Folz, B., and Filiatrault, A. F., (2002). SAWS—Version 1.0: A computer program for seismic analysis of woodframe buildings." *Report No. SSRP–2001/9*, Structural Systems Research Project, Department of Structural Engineering, University of California, San Diego, La Jolla, California.

Fonseca, F. S. (1997). "Cyclic loading response of reinforced concrete tilt–up structures with plywood diaphragms." PhD thesis, University of Illinois at Urbana–Champaign, Urbana, Illinois.

Fonseca, F. S., and Burns, J. M. (2002). "Strength of plywood joints with overdriven nails." *Unpublished Report*, Department of Civil Engineering, Brigham Young University, Provo, Utah.

Fonseca, F. S., and Judd, J. P. (2004a). "Implementation of an oriented sheathing-to-framing connector model into CASHEW." *Proceedings of the 8th World Conference on Timber Engineering*, Finnish Association of Civil Engineers RIL, Helsinki, Finland.

Fonseca, F. S., and Judd, J. P. (2004b). "Effect of overdriven-nail-depth combinations on wood shear wall strength." *Proceedings of the 8th World Conference on Timber Engineering*, Finnish Association of Civil Engineers RIL, Helsinki, Finland.

Fonseca, F. S., and Rabe, J. A. (2002). "Capacity of single nail wood joints with overdriven nails." *Unpublished Report*, Department of Civil Engineering, Brigham Young University, Provo, Utah.

Fonseca, F. S., Rose, S. K., and Campbell, S. H. (2002). "Nail, screw, and staple fastener connections." *CUREe Publication No. W-16*, Consortium of Universities for Research in Earthquake Engineering, Richmond, California.

Foschi, R. O. (1974). "Load–slip characteristics of nails." *Wood Science*, Forest Products Reserach Society, Vol. 7, No. 1, 69–74.

Foschi, R. O. (1977). "Analysis of wood diaphragms and trusses. Part I: Diaphragms." *Canadian Journal of Civil Engineering*, National Research Council of Canada, Vol. 4, No. 3, 345–352.

Foschi, R. O. (2000). "Modeling the hysteretic response of mechanical connections for structures." *Proceedings, World Conference on Timber Engineering*, Department of Civil Engineering, Department of Wood Science, and School of Architecture, University of British Columbia, Vancouver, British Columbia, Canada.

Gatto, K., and Uang, C.-M. (2003). "Effects of loading protocol on the cyclic response of woodframe shearwalls." *Journal of Structural Engineering*, American Society of Civil Engineers, Vol. 129, No. 10, 1384–1393.

Gavrilovic, P., and Gramatikov, K. (1991). "Experimental and theoretical investigations of wooden truss-frame structures under quasi-static and dynamic loads." *Proceedings, Workshop on Full-Scale Behavior of Wood-Framed Buildings in Earthquakes and High Winds*, Watford, United Kingdom.

Girhammar, U. A., and Anderson, H. (1988). "Effect of loading rate on nailed timber joint capacity." *Journal of Structural Engineering*, American Society of Civil Engineers, Vol. 114, No. 11, 2439–2456.

Gupta, A. K., and Kuo, G. P. (1987). "Wood–framed shear walls with uplifting." *Journal of Structural Engineering*, American Society of Civil Engineers, Vol. 113, No. 2, 241–259.

Gupta, A. K., and Kuo, P.-H. (1985). "Behavior of wood-framed shear walls." *Journal of Structural Engineering*, American Society of Civil Engineers, Vol. 111, No. 8, 1722–1733.

Gutkowski, R. M., and Castillo, A. L. (1988). "Single- and double-sheathed wood shear walls study." *Journal of Structural Engineering*, American Society of Civil Engineers, Vol. 114, No. 6, 1268–1284.

Gutshall, S. T., and Dolan, J. D. (1994). "Montonic and cyclic short-term performance of nailed and bolted timber connections." MS thesis, Virginia Polytechnic Institute and State University, Blacksburg, Virginia.

Hall, J. F. (editor). (1996). "Northridge earthquake of January 17, 1994 reconnaissance report: Supplement C." *Earthquake Spectra*, Earthquake Engineering Research Institute, Vol. 11, 125–196.

He, M., Lam, F., and Foschi, R. O. (2000). "Numerical analysis of statically loaded three-dimensional timber light-frame buildings." *Procedings of the World Conference on Timber Engineering*, Whistler, British Columbia, Canada.

He, M., Lam, F., and Foschi, R. O. (2001). "Modeling three-dimensional timber light-frame buildings." *Journal of Structural Engineering*, American Society of Civil Engineers, Vol. 127, No. 8, 901–913.

Heine, C. P. (2001). "Simulated response of degrading hysteretic joints with slack behavior." Ph.D. thesis, Virginia Polytechnic Institute and State University, Blacksburg, Virginia.

Heine, C. P., and Dolan, J. D. (2001). "A new model to predict the load–slip relationship of bolted connections in timber." *Wood and Fiber Science*, Society of Wood Science and Technology, Vol. 33, No. 4.

Hite, M. C., and Shenton, H. W., III. (2002) "Modeling the non-linear behavior of wood frame shear walls." *Proceedings, 15th ASCE Engineering Mechanics Division Conference*, American Society of Civil Engineers (ASCE), New York, New York.

Hunt, R. D., and Bryant, A. H. (1990). "Laterally loaded nail joints in wood." *Journal of Structural Engineering*, American Society of Civil Engineers, Vol. 116, No. 1, 111–124.

International Code Council (ICC). (2003). *International Building Code (IBC) 2003*. International Code Council, Falls Church, Virginia.

International Conference of Building Officials (ICBO). (1997). *Uniform Building Code (UBC) 1997*. International Conference of Building Officials, Whittaker, California.

International Organization for Standardization (ISO). (1983). "Timber structures—joints made with mechanical fasteners—general principles for the determination of strength and deformation characteristics." *ISO Standard 6891–1983*, International Organization for Standardization, Geneva, Switzerland.

International Organization for Standardization (ISO). (1997). "Timber structures—joints made with mechanical fasteners—quasi-static reversed-cyclic test method." WG7 Draft, ISO TC 165 Secretariat, Standards Council of Canada, Ottawa, Ontario, Canada.

Itani, R. Y., and Cheung, C. K. (1984). "Nonlinear analysis of sheathed wood diaphragms." *Journal of Structural Engineering*, American Society of Civil Engineers, Vol. 110, No. 9, 2137–2147.

Jacobsen, L. S. (1960). "Damping in composite structures." *Proceedings, Second World Conference on Earthquake Engineering*, Tokyo, Japan, Vol. 2, 1029–1044.

Jenkins, J. L., Polensek, A., and Bastendorff, K. M. (1979). Stiffness of nailed wall joints under short term and long term loads, *Wood Science*, Forest Products Reserach Society, Vol. 11, No. 3, 145–154.

Jones, S. N. (2000). "Cyclic testing of oriented strand board shear walls with overdriven nails." MS thesis, Brigham Young University, Provo, Utah.

Jones, S. N., and Fonseca, F. S. (2002). "Capacity of oriented strand board shear walls with overdriven sheathing nails." *Journal of Structural Engineering*, American Society of Civil Engineers (ASCE), Vol. 128, No. 7, 898–907.

Judd, J. P., and Fonseca, F. S. (1998). "Monotonic response of fiberglass panels fastened to wood framing," *Proceedings, 5th International Conference on Composites Engineering*, July 5–11, Las Vegas, Nevada, 441–442.

Judd, J. P., and Fonseca, F. S. (2000a). "FRP-wood nailed joint behavior," *Proceedings, 45th International SAMPE Symposium and Exhibition*, Society for the Advancement of Material and Process Engineering, May 21–25, Long Beach, California, 895–902.

Judd, J. P., and Fonseca, F. S. (2000b). "Rehabilitation of wood diaphragms with fiberglass panels." *Proceedings, 2nd Annual Conference on Durability and Disaster Mitigation in Wood–Frame Housing*, Forest Products Society, Madison, Wisconsin.

Judd, J. P., and Fonseca, F. S. (2001). "Behavior of timber-composite diaphragms under quasi-static loading." *Proceedings, 2nd International Conference on Engineering Materials*, Canadian Society for Civil Engineering and Japan Society of Civil Engineers, August 16–19, San Jose, California, Vol. 1, 391–401.

Judd, J. P., and Fonseca, F. S. (2002a). "Finite-element analysis of wood diaphragms and shear walls using ABAQUS." *Proceedings, ABAQUS Users' Conference*, ABAQUS, Inc., Providence, Rhode Island.

Judd, J. P., and Fonseca, F. S. (2002b). "Nonlinear analysis of wood shear walls and diaphragms." *Proceedings, 1st Virtual World Conference for Civil Engineering*, American Society of Civil Engineers, July 1, http://www.ceworld.org/

Judd, J. P., and Fonseca, F. S. (2002c). "Strength and behavior of hybrid diaphragms." *Journal of Composites for Construction*, American Society of Civil Engineers, Vol. 6, No. 4, 215–223.

Judd, J. P., and Fonseca, F. S. (2003a). "Analytical modeling of nailed connections in wood shear walls." *Proceedings, Forest Products Society 57th Annual Meeting*, Bellevue/ Seattle, Washington.

Judd, J. P., and Fonseca, F. S. (2003b). "FRP strengthened wood-frame roofs." *Proceedings, SAMPE 2003 Conference*, Society for the Advancement of Material and Process Engineering, May 11–15, Long Beach, California.

Judd, J. P., and Fonseca, F. S. (2004a). "Analytical modeling of nailed sheathing connections in wood shear walls." *Proceedings, 9th Brazilian Meeting in Wood and Wood Structures*, July 28–30, Cuiaba, Brazil.

Judd, J. P., and Fonseca, F. S. (2004b). "Hysteresis model parameters for nailed sheathing connections in wood shear walls." *Proceedings, 9th Brazilian Meeting in Wood and Wood Structures*, July 28–30, Cuiaba, Brazil.

Judd, J. P., and Fonseca, F. S. (2004c). "Shear wall strength reduction from overdriven nails." *Proceedings, 9th Brazilian Meeting in Wood and Wood Structures*, July 28–30, Cuiaba, Brazil.

Judd, J. P., and Fonseca, F. S. (2004d). "Hysteresis models for nailed sheathing-to-framing connections in wood shear walls and diaphragms." *Proceedings, 8th World Conference on Timber Engineering*, Finnish Association of Civil Engineers RIL, Helsinki, Finland.

Judd, J. P., and Fonseca, F. S. (2005). "Analytical model for sheathing-to-framing connections in wood shear walls and diaphragms." *Journal of Structural Engineering*, American Society of Civil Engineers, Vol. 131, No. 2, 345–352.

Kamiya, F. (1988). "Nonlinear earthquake response analysis of sheathed wood walls by a computer-actuator on-line system." *Proceedings, 1988 International Conference On Timber Engineering*, Forest Products Society, Madison, Wisconsin, Vol. 1, 838–847.

Kaneta, K. (1958). "Study of structural damping and stiffness in nailed joints." Engineering degree thesis, Stanford University, Palo Alto, California.

Kent, S., Gupta, R., and Miller, T. (1996). "Dynamic behavior of metal-plate-connected wood truss joints." *Proceedings, International Wood Engineering Conference*, Vijaya K. A. Gopu, ed., New Orleans, Louisiana, Vol. 1, 115–122.

Kircher, C. A., Reitherman, R. K., Whitman, R. V., and Arnold, C. (1997). "Estimation of earthquake losses to buildings." *Earthquake Spectra*, Earthquake Engineering Research Institute, Vol. 13, No. 4, 703–720.

Kivell, B. T., and Moss, P. J., and Carr, A. J. (1981). "Hysteretic modeling of moment resisting nailed timber joints." *Bulletin of New Zealand National Society of Earthquake Engineering*, Vol. 14, No. 4, 233–245.

Lau, P. W. C., and George, P. (1987). "Development of a load slip test apparatus for nailed joints." *Forest Products Journal*, Forest Product Society, Vol. 37, No. 11/12, 39–44.

Leach, K. E. (1964). "A survey of literature on the lateral resistance of nails. *Publication No. 1085*, Canadian Department of Forestry, Ottawa, Ontario.

Lee, S.-C. (1987). "A composite-beam finite element for seismic analysis of wood-framed buildings." PhD thesis, Oregon State University, Corvallis, Oregon.

Liu, J. Y., and Soltis, L. A. (1984). "Lateral resistance of nailed joints: A test method," *Forest Products Journal*, Forest Products Research Society, Vol. 34, No. 1, 55–60.

Lopez-Anido, R., Gardner, D. J., and Hensley, J. L. (2000). "Adhesive bonding of eastern hemlock glulam panels with E–glass/vinyl ester reinforcement." *Forest Products Journal,* Forest Products Research Society, Vol. 50, No. 11/12, 43–47.

Mack, J. J. (1960). "The strength of nailed timber joints—1. In messmate stringybark." *Technical Paper No. 9*, C*SIRO Division of Forest Products,* Commonwealth Scientific and Industrial Research Organization, Melbourne, Australia.

Mack, J. J. (1966) "The strength and stiffness of nailed joints under short duration loading." *Technical Paper No. 40,* C*SIRO Division of Forest Products*, Commonwealth Scientific and Industrial Research Organization, Melbourne, Australia.

Mack, J. J. (1977) "The load-displacement curve for nailed joints." *Journal of the Institute of Wood Science*, Institute of Wood Science, Vol. 7, No. 6, 34–36.

Martin, Z. A., and Skaggs, T. D. (2002). "Shear wall deflection and predictive equations." *APA Report T2001L65*, APA—The Engineered Wood Association, Tacoma, Washington.

McCutcheon, W. J. (1985). "Racking deformations in wood shear walls." *Journal of Structural Engineering*, American Society of Civil Engineers, Vol. 111, No. 2, 257–269.

McLain, T. E. (1975). "Curvilinear load–slip relations in laterally loaded nailed joints." PhD thesis, Colorado State University, Fort Collins, Colorado.

Medearis, K. (1970). "Structural dynamics of plywood shear walls." *Wood Science*, Forest Products Research Society, Vol. 3, No. 2, 106–110.

Menegotto, M., and Pinto, P. E. (1973). "Method of analysis for cyclically loaded reinforced concrete plane frames including changes in geometry and nonelastic behavior of ele-

ments under combined normal forces and bending." *Proceedings, IABSE Symposium on the Resistance and Ultimate Deformability of Structures Acted on by Well–Defined Loads*, International Association for Bridge and Structural Engineering, Zurich, Switzerland, 15–22.

Montrey, H. M. (1983). "Emerging structural panels for light–frame construction." *Proceedings, Wall and Floor Systems: Design and Performance of Light–Frame Structures*, Forest Products Research Society, Madison, Wisconsin, 18–24.

Newmark, N. M. (1959). "A method for computation for structural dynamics." *Journal of the Engineering Mechanics Division*, American Society of Civil Engineers, Vol. 85, 67–94.

Ni, C., and Chui, Y. H. (1994). "Response of nailed wood joints to dynamic loads." *Proceedings, Pacific Timber Engineering Conference*, Vol. 2, Timber Research and Development Council, Fortitude Valley MAC, Queensland, Australia, 9–18.

Olpin, A. H. (1998). "Behavior of diaphragms sheathed with fiber reinforced polymer panels." MS thesis, Brigham Young University, Provo, Utah.

Olpin, A. H., and Fonseca, F. S. (1999). "Behavior of diaphragms sheathed with FRP panels," *Proceedings, 8th Canadian Conference on Earthquake Engineering*, Department of Civil Engineering, University of British Columbia, Vancouver, British Columbia, Canada, 21–25.

Otani, S. (1974). "SAKE: A computer program for inelastic response of R/C frames to earthquakes." *Structural Research Series No. 413, Civil Engineering Studies*, University of Illinois at Urbana-Champaign, Urbana, Illinois.

Paevere, P. J., Foliente, G. C., and Kasal, B. (2003). "Load-sharing and redistribution in a one-story woodframe building." *Journal of Structural Engineering*, American Society of Civil Engineers, Vol. 129, No. 9, 1275–1284.

Pellicane, P. J. (1991). "Mechanical behavior of nailed joints with various side member materials." *Journal of Testing and Evaluation (JTEVA)*, American Society for Testing and Materials, Vol. 19, No. 2, 97–106.

Pellicane, P. J. (1993). "Plywood solid wood nailed joints under lateral loading." *Journal of Materials in Civil Engineering*, American Society of Civil Engineers, Vol. 5, No. 2, 226–236.

Pellicane, P. J. and Bodig, J. (1982). "Comparative study of several testing techniques to evaluate nail slip modulus." *Special Report WSL 1*, Department of Forest and Wood Sciences, Colorado State University, Fort Collins, Colorado.

Pellicane, P. J., Stone, J. L., and Vanderbuilt, M. D. (1991). "Generalized model for lateral load slip of nailed joints." *Journal of Materials in Civil Engineering*, American Society of Civil Engineers, Vol. 3, No. 1, 60–77.

PFS Research Foundation (PFS/RF). (1999). "Design values for oriented strand board." *Technical Bulletin No. 104*, PFS Research Foundation, Madison, Wisconsin.

Polensek, A., and Bastendorff, K. J. (1987). "Damping in nailed joints of light frame wood buildings, *Wood and Fiber Science*, Vol. 19, No. 2, 110–125.

Polensek, A., and Schimel, B. D. (1988). "Analysis of connection systems in wood dwellings." *Journal of Computing in Civil Engineering*, American Society of Civil Engineers, Vol. 2, No. 4, 365–379.

Rabe, J. A. (2000). "The effect of overdriven nail heads on single shear connections with oriented strand board sheathing." MS thesis, Brigham Young University, Provo, Utah.

Rabe, J. A., Judd, J. P., Fonseca, F. S. (1999). "Task 1.4.8.1 Effect of fastener head penetration on sheathing-to-wood connections: A progress report." *CUREe Unpublished Report*, Consortium of Universities for Research in Earthquake Engineering, Richmond, California.

Ramm, E. (1981). "Strategies for tracing the nonlinear response near limit points." *Nonlinear finite element analysis in structural mechanics, proceedings of the Eurpoe–U. S. Workshop*, Springer–Verlag, New York, New York, 63–89.

Richard, N., Daudeville, L., Prion, H., and Lam, F. (2002). "Timber shear walls with large openings: experimental and numerical prediction of the structural behavior." *Canadian Journal of Civil Engineering*, National Research Council of Canada, Vol. 29, 713–724.

Rosowsky, D. V. (2002). "Reliability-based seismic design of wood shear walls." *Journal of Structural Engineering*, American Society of Civil Engineers, Vol. 128, No. 11, 1439–1453.

Rosowsky, D. V., and Ellingwood, B. (2002). "Performanced-based engineering of wood frame housing." *Journal of Structural Engineering*, American Society of Civil Engineers, Vol. 128, No. 1, 32–38.

Rosowsky, D. V., and Kim, J. H. (2004). "Performance-based design of wood shearwalls considering performance of the overall structure." *Proceedings, 8th World Conference on Timber Engineering*, Finnish Association of Civil Engineers RIL, Helsinki, Finland.

Rosowsky, D. V. and Schiff, S. D. (1999). "Combined loads on sheathing to framing fasteners in wood construction." *Journal of Architectural Engineering*, American Society of Civil Engineers, Vol. 5, No. 2, 37–43.

Saiidi, M. (1982). "Hysteresis models for reinforced concrete," *Journal of the Structural Division*, American Society of Civil Engineers, Vol. 108, No. 5, 1077–1087.

Saiidi, M., and Sozen, M. A., (1979). "Simple and complex models for nonlinear seismic response of reinforced concrete structures. *Structural Research Series No. 466, Civil Engineering Studies*, University of Illinois at Urbana-Champaign, Urbana, Illinois.

Schmidt, R. J., and Moody, R. C. (1989). "Modeling laterally loaded light-frame buildings." *Journal of Structural Engineering*, American Society of Civil Engineers, Vol. 115, No. 1, 201–217.

Skaggs, T. D., and Martin, Z. A. (2004). "Estimating wood structural panel diaphragm and shear wall deflection." *Practice Periodical on Structural Design and Construction*, American Society of Civil Engineers, Vol. 9, No. 3, 136–141.

Soltis, L. A. and Mtenga, P. V. A. (1985). "Strength of nailed wood joints subjected to dynamic load, *Forest Products Journal*, Forest Products Society, Vol. 35, No. 11/12, 14–18.

Stanton, J. F,. and McNiven, H. D. (1979). "The development of a mathematical model to predict the flexural response of reinforced concrete beams to cyclic loads, using system identification." *Repert No. UCB/EERC–79/02*, Earthquake Engineering Research Center, University of California, Berkeley, California.

Stewart, W. G. (1987). "The seismic design of plywood sheathed shearwalls." PhD thesis, University of Canterbury, Christchurch, New Zealand.

Stojadinovic, B., and Thewalt, C. R. (1996). "Energy balanced hysteresis models." *Report No. UCB/EERC–96/01*, Earthquake Engineering Research Center, University of California, Berkeley, California.

Stone, J. L., Vanderbilt, M. D., Criswell, M. E., and Bodig, J. (1980). Generalized load slip curve for nailed connections. *Structural Research Report No. 30*, Department of Civil Engineering, Colorado State University, Fort Collins, Colorado.

Strongwell, Inc. (1998). *EXTREN Design Manual*. Strongwell, Inc., Bristol, Virginia.

Structural Engineers Association of California (SEAOC). (1999). *Recommended lateral force requirements and commentary (Blue Book).* 7th edition, Seismology Committee, Structural Engineers Association of California, Sacramento, California.

Symans, M. D., Cofer, W. F., Fridley, K. J., and Ying, D. (2001). "Fluid dampers for seismic energy dissipation of woodframe structures." *CUREe Task 1.4.7 Innovative Systems Draft Report*, Consortium of Universities for Research in Earthquake Engineering, Richmond, California.

Takeda, T., Sozen, M. A., and Nielsen, N. M. (1970). "Reinforced concrete response to simulated earthquakes." *Journal of the Structural Division*, American Society of Civil Engineers, Vol. 96, No. ST12, 2557–2573.

Tedesco, J. W., McDougal, W. G., and Ross, C. A. (1999). *Structural dynamics: Theory and applications*. 1st edition, Addison Wesley Longman, Inc., Meno Park, California.

Tissell, J. R. (1967). "1966 Horizontal plywood diaphragm tests." *Laboratory Report No. 106*, Douglas Fir Plywood Association, Tacoma, Washington.

Tissell, J. R. (1993). "Wood structural panel shear walls." *Research Report No. 154*, APA—The Engineered Wood Association, Tacoma, Washington.

Tissell, J. R., and Elliott, J. R. (1997). "Plywood diaphragms." *Research Report No. 138*, APA—The Engineered Wood Association, Tacoma, Washington.

Tuomi, R. L., and McCutcheon, W. J. (1978). "Racking strength of light-frame nailed walls." *Journal of Structural Engineering*, American Society of Civil Engineers, Vol. 104, No. 7, 1131–1140.

Uang, C.-M., and Bertero, V. V. (1988). "Use of energy as a design criterion in earthquake-resistant design." *Report No. UCEERC–88/18*, Earthquake Engineering Research Center, University of California, Berkeley, California.

van de Lindt, J. W. (2004). "Evolution of wood shear wall testing, modeling, and reliability analysis: Bibliography." *Practice Periodical on Structural Design and Construction*, American Society of Civil Engineers, Vol. 9, No. 1, 44–53.

van de Lindt, J. W., and Walz, M. A. (2003). "Development and application of wood shear wall reliability model." *Journal of Structural Engineering*, American Society of Civil Engineers, Vol. 129, No. 3, 405–413.

White, M. W., and Dolan, J. D. (1995). "Nonlinear shear wall analysis." *Journal of Structural Engineering*, American Society of Civil Engineers, Vol. 121, No. 11, 1629–1635.

Wilkinson, T. L. (1971). "Theoretical lateral resistance of nailed joints." *Journal of the Structural Divsion of ASCE*, American Society of Civil Engineers, Vol. 97(ST5), 1381–1398.

Wilkinson, T. L. (1972). "Analysis of nailed joints with dissimilar members." *Journal of the Structural Divsion of ASCE*, American Society of Civil Engineers, Vol. 98(ST9), 2005–2013.

Wilkinson, T. L. (1991). "Dowel bearing strength." *Research Paper FPL-RP-505*, U. S. Department of Agriculture, Forest Service, Forest Products Laboratory, Madison, Wisconsin.

Winistorfer, S. G., and Soltis, L. A. (1993). "Dynamic load effect on the lateral strength of nails for the manufactured/modular housing industry." *Wood Products for Engineered Structures: Issues Affecting Growth and Acceptance of Engineered Wood Products*, Forest Products Society, Madison, Wisconsin.

Zacher, E. G. (1994). "Past seismic performance of timber buildings." *Procedings, Research Needs Workshop on Analysis, Design and Testing of Timber Structures Under Seismic Loads*, Forest Products Laboratory, University of California, Richmond, California, 3–8.

Zacher, E. G., and Gray, R. G. (1985). "Dynamic tests of wood framed shear walls." *Proceedings, SEAOC 57th Annual Convention*, Structural Engineers Association of California, San Francisco, California, 41–61.

Zacher, E. G., and Gray, R. G. (1989). "Lessons learned from dynamic tests of shear panels." *Proceedings, Structural Congress '89: Structural design, analysis and testing*, American Society of Civil Engineers, New York, New York, 134–142.

Appendix A

SHEATHING-TO-FRAMING CONNECTION MEASURED DATA

This appendix contains data reduced from sheathing-to-framing connection tests. The connection types considered include plywood and GFRP sheathing, 3.33×63.5 mm (8d) common nails, 3.76×76.2 mm (10d) common nails, and 4.12×88.9 mm (16d) common nails. In each Table a summary of the load-displacement curve parameters (for both monotonic and cyclic loading) are given for the connection type. The curve parameters reported are the initial and secondary stiffnesses, K_1 and K_2, the apparent yield displacement $\delta_{y'}$, the transition curvature R, and the ultimate displacement and load, δ_{ult} and P_{ult}.

Table A.1. Summary of Load-Displacement Curve Parameters

Loading Protocol (cycle)	K_1 (kN/mm)	K_2 (kN/mm)	δ_y, (mm)	R	δ_{ult} (mm)	P_{ult} (kN)
(a) 9.53-PLY-3.33-COMMON-FLUSH						
Monotonic	1.643	0.094	0.514	2.000	3.736	1.139
Cyclic (Positive 1)	2.152	0.091	0.356	2.000	3.048	1.004
Cyclic (Positive 2)	0.832	0.084	0.914	6.150	2.794	0.919
Cyclic (Positive 3)	0.798	0.090	0.914	7.300	2.413	0.865
Cyclic (Negative 1)	1.024	0.063	0.838	4.250	4.445	1.085
Cyclic (Negative 2)	0.819	0.049	1.016	6.850	4.318	0.993
Cyclic (Negative 3)	0.780	0.039	1.067	5.750	3.556	0.928
(b) 6.35-FRP-3.33-COMMON-FLUSH						
Monotonic	3.922	0.020	0.413	1.500	4.466	1.673
Cyclic (Positive 1)	2.316	0.020	0.653	2.000	3.169	1.534
Cyclic (Positive 2)	1.527	0.020	0.916	3.300	3.083	1.434
Cyclic (Positive 3)	1.522	0.020	0.892	3.300	2.902	1.340
Cyclic (Negative 1)	1.522	0.070	0.895	6.000	3.235	1.526
Cyclic (Negative 2)	1.500	0.060	0.868	5.000	2.997	1.429
Cyclic (Negative 3)	1.506	0.060	0.830	5.000	2.545	1.352
(c) 6.35-FRP-3.76-COMMON-FLUSH						
Monotonic	4.663	0.040	0.454	1.350	2.488	2.056
Cyclic (Positive 1)	3.615	0.070	0.564	1.600	3.338	2.164
Cyclic (Positive 2)	2.187	0.080	0.854	2.800	3.502	2.068
Cyclic (Positive 3)	2.145	0.080	0.848	2.500	3.242	1.986
Cyclic (Negative 1)	2.305	0.060	0.824	2.600	3.135	2.017
Cyclic (Negative 2)	2.414	0.060	0.731	2.600	2.718	1.862
Cyclic (Negative 3)	2.332	0.060	0.748	2.400	2.466	1.809
(d) 6.35-FRP-4.12-COMMON-FLUSH						
Monotonic	4.738	0.050	0.597	1.000	3.420	2.555
Cyclic (Positive 1)	3.116	0.040	0.650	2.000	3.934	2.131
Cyclic (Positive 2)	2.136	0.030	0.878	3.000	3.706	1.953
Cyclic (Positive 3)	2.103	0.030	0.868	3.000	3.408	1.892
Cyclic (Negative 1)	2.286	0.140	0.839	2.500	3.444	2.262
Cyclic (Negative 2)	2.303	0.060	0.825	2.200	3.251	2.005
Cyclic (Negative 3)	2.312	0.060	0.790	2.200	3.182	1.934

Table A.2. 9.53-PLY-3.33-COMMON-FLUSH Monotonic Curve Parameters

Coupon Specimen		K_1	K_2	δ_y,		δ_{ult}	P_{ult}
No.	Side	(kN/mm)	(kN/mm)	(mm)	R	(mm)	(kN)
1	A	1.270	0.153	0.610	2.600	3.720	1.247
	B	1.144	0.113	0.813	2.800	3.584	1.237
2	A	2.139	0.153	0.356	2.200	4.288	1.363
	B	1.416	0.139	0.584	1.900	4.542	1.370
3	A	1.457	0.110	0.635	2.700	4.432	1.341
	B	1.462	0.102	0.584	2.200	5.397	1.341
4	A	1.597	0.123	0.432	2.950	2.538	0.948
	B	1.346	0.114	0.483	2.900	3.178	0.955
5	A	2.236	0.143	0.330	2.600	2.316	1.020
	B	1.329	0.115	0.559	3.550	3.013	1.025
6	A	2.009	0.106	0.432	2.000	4.469	1.293
	B	1.317	0.130	0.686	3.150	3.741	1.298
7	A	2.277	0.078	0.305	1.600	4.983	1.052
	B	1.180	0.104	0.584	2.500	4.117	1.054
8	A	4.291	0.176	0.203	1.650	2.517	1.271
	B	2.370	0.177	0.381	2.300	2.512	1.276
9	A	1.410	0.129	0.483	2.200	4.029	1.135
	B	2.820	0.109	0.254	1.600	4.035	1.125
10	A	1.152	0.105	0.660	2.350	5.020	1.215
	B	3.483	0.199	0.229	1.800	2.289	1.200
Max		4.291	0.199	0.813	3.550	5.397	1.370
Ave		1.885	0.129	0.480	2.378	3.736	1.188
Min		1.144	0.078	0.203	1.600	2.289	0.948

Table A.3. 9.53-PLY-3.33-COMMON-FLUSH Cyclic Positive 1 Curve Parameters

Coupon Specimen		K_1	K_2	δ_y,		δ_{ult}	P_{ult}
No.	Side	(kN/mm)	(kN/mm)	(mm)	R	(mm)	(kN)
11	A	4.137	0.059	0.203	1.600	2.611	0.973
	B	1.543	0.049	0.533	2.700	3.863	0.985
12	A	1.994	0.127	0.457	1.750	3.433	1.277
	B	5.254	0.152	0.178	1.350	2.492	1.267
13	A	1.585	0.079	0.483	1.650	3.988	1.029
	B	1.278	0.082	0.686	2.700	2.723	1.037
14	A	1.873	0.097	0.330	1.850	3.442	0.916
	B	2.229	0.089	0.279	1.750	3.629	0.916
15	A	2.425	0.093	0.330	1.850	2.731	1.015
	B	1.157	0.066	0.711	2.550	3.783	1.021
16	A	1.576	0.032	0.457	2.000	2.220	0.762
	B	1.596	0.033	0.457	2.400	1.872	0.767
17	A	2.855	0.059	0.254	1.650	1.609	0.785
	B	3.094	0.089	0.229	1.400	1.404	0.776
18	A	1.989	0.047	0.356	1.750	3.501	0.848
19	A	4.291	0.055	0.203	1.500	1.394	0.907
	A	3.292	0.072	0.254	1.350	1.620	0.888
20	A	1.828	0.093	0.406	2.500	3.086	0.990
21	A	1.805	0.075	0.584	3.450	2.551	1.201
	B	2.178	0.101	0.406	1.600	3.619	1.193
22	A	2.077	0.027	0.356	1.550	2.609	0.778
	B	1.915	0.022	0.381	1.700	3.636	0.793
Max		5.254	0.152	0.711	3.450	3.988	1.277
Ave		2.362	0.073	0.388	1.936	2.810	0.960
Min		1.157	0.022	0.178	1.350	1.394	0.762

Table A.4. 9.53-PLY-3.33-COMMON-FLUSH Cyclic Positive 2 Curve Parameters

Coupon Specimen		K_1	K_2	δ_y,		δ_{ult}	P_{ult}
No.	Side	(kN/mm)	(kN/mm)	(mm)	R	(mm)	(kN)
11	A	1.090	0.008	0.787	5.600	2.556	0.872
	B	0.799	0.015	1.041	5.600	3.704	0.872
12	A	1.136	0.088	0.838	2.800	3.486	1.180
	B	1.721	0.093	0.584	2.900	2.511	1.180
13	A	0.635	0.041	1.295	4.300	3.993	0.932
	B	0.754	0.031	1.168	6.050	2.894	0.934
14	A	0.603	0.061	1.143	8.700	3.457	0.830
	B	0.798	0.053	0.864	7.100	3.580	0.833
15	A	1.085	0.033	0.787	3.700	2.781	0.919
	B	0.686	0.032	1.219	4.600	3.850	0.921
16	A	0.658	0.047	1.041	6.650	2.054	0.732
	B	0.798	0.053	0.864	5.600	1.711	0.732
17	A	0.762	0.041	0.940	16.050	1.909	0.756
	B	0.709	0.046	1.016	8.450	1.767	0.755
18	A	0.788	0.022	0.914	4.350	3.564	0.779
19	A	1.056	0.000	0.813	8.500	0.806	0.788
	A	0.719	0.000	1.194	10.200	1.178	0.797
20	A	0.822	0.079	0.914	8.000	2.440	0.873
21	A	1.274	0.161	0.737	5.850	1.699	1.092
	B	0.826	0.105	1.067	4.600	3.054	1.089
22	A	0.621	0.082	1.067	11.600	1.982	0.738
	B	0.691	0.064	0.940	6.200	2.343	0.739
Max		1.721	0.161	1.295	16.050	3.993	1.180
Ave		0.865	0.053	0.965	6.700	2.605	0.879
Min		0.603	0.000	0.584	2.800	0.806	0.732

Table A.5. 9.53-PLY-3.33-COMMON-FLUSH Cyclic Positive 3 Curve Parameters

Coupon Specimen		K_1	K_2	δ_y,		δ_{ult}	P_{ult}
No.	Side	(kN/mm)	(kN/mm)	(mm)	R	(mm)	(kN)
11	A	1.006	0.048	0.787	9.900	1.801	0.840
	B	0.766	0.032	1.016	25.000	2.924	0.840
12	A	1.061	0.075	0.889	2.950	3.352	1.122
	B	1.893	0.060	0.533	2.350	2.500	1.118
13	A	0.580	0.028	1.397	5.100	3.934	0.881
	B	0.727	0.008	1.194	6.200	2.806	0.880
14	A	0.562	0.048	1.219	7.600	3.335	0.786
	B	0.766	0.040	0.889	5.950	3.542	0.788
15	A	1.022	0.080	0.762	4.900	1.935	0.870
	B	0.660	0.049	1.194	4.750	2.901	0.869
16	A	0.625	0.039	1.067	25.000	1.984	0.703
	B	0.773	0.043	0.864	7.050	1.674	0.702
17	A	0.705	0.000	1.016	25.000	1.010	0.694
	B	0.671	0.000	1.067	13.050	1.054	0.675
18	A	0.769	0.017	0.914	4.400	3.594	0.747
19	A	0.987	0.000	0.838	14.450	0.825	0.782
	A	0.679	0.000	1.219	13.650	1.208	0.783
20	A	0.772	0.082	0.940	13.250	2.429	0.847
21	A	1.203	0.149	0.762	6.950	1.711	1.057
	B	0.768	0.106	1.118	4.900	3.017	1.059
22	A	0.586	0.084	1.092	13.450	2.004	0.717
	B	0.617	0.066	1.016	25.000	2.366	0.716
Max		1.893	0.149	1.397	25.000	3.934	1.122
Ave		0.827	0.048	0.991	10.948	2.359	0.840
Min		0.562	0.000	0.533	2.350	0.825	0.675

Table A.6. 9.53-PLY-3.33-COMMON-FLUSH Cyclic Negative 1 Curve Parameters

Coupon Specimen		K_1	K_2	δ_y,		δ_{ult}	P_{ult}
No.	Side	(kN/mm)	(kN/mm)	(mm)	R	(mm)	(kN)
11	A	1.496	0.061	0.610	3.650	3.110	1.064
	B	0.961	0.054	0.940	4.000	3.878	1.062
12	A	1.035	0.231	0.864	25.000	1.709	1.089
	B	1.303	0.106	0.635	2.800	3.064	1.083
13	A	0.597	0.050	1.245	5.800	5.533	0.959
	B	0.744	0.054	1.016	2.800	4.710	0.952
14	A	0.793	0.113	0.914	4.650	4.857	1.171
	B	1.046	0.184	0.864	8.600	2.327	1.172
15	A	1.296	0.123	0.635	3.800	3.638	1.192
	B	1.015	0.087	0.864	3.300	4.502	1.191
16	A	1.295	0.096	0.711	3.450	1.863	1.023
	B	1.305	0.002	0.787	3.100	2.593	1.024
17	A	1.068	0.082	0.762	4.950	5.454	1.197
	B	0.917	0.028	0.965	5.200	11.987	1.192
18	A	1.220	0.053	0.787	2.900	4.525	1.156
19	A	1.191	0.085	0.635	9.100	6.050	1.217
	A	0.953	0.096	0.864	4.900	5.117	1.230
20	A	1.080	0.171	0.762	5.450	2.927	1.193
21	A	1.632	0.062	0.559	2.300	6.888	1.300
	B	0.971	0.119	0.889	4.500	4.551	1.298
22	A	0.823	0.087	0.838	6.950	4.875	1.040
	B	1.026	0.113	0.711	5.500	3.529	1.048
Max		1.632	0.231	1.245	25.000	11.987	1.300
Ave		1.080	0.093	0.812	5.577	4.440	1.130
Min		0.597	0.002	0.559	2.300	1.709	0.952

Table A.7. 9.53-PLY-3.33-COMMON-FLUSH Cyclic Negative 2 Curve Parameters

Coupon Specimen		K_1	K_2	δ_y,		δ_{ult}	P_{ult}
No.	Side	(kN/mm)	(kN/mm)	(mm)	R	(mm)	(kN)
11	A	1.122	0.027	0.813	4.900	3.120	0.974
	B	0.778	0.033	1.143	5.850	3.647	0.973
12	A	1.102	0.167	0.787	8.750	1.792	1.035
	B	1.123	0.078	0.737	2.700	3.395	1.030
13	A	0.506	0.061	1.372	11.550	4.135	0.861
	B	0.620	0.033	1.219	3.500	4.425	0.860
14	A	0.609	0.099	1.219	25.000	4.661	1.083
	B	0.888	0.123	1.041	11.600	2.314	1.082
15	A	1.051	0.100	0.787	5.150	2.979	1.047
	B	0.764	0.080	1.118	6.550	3.519	1.047
16	A	0.961	0.038	0.940	9.400	2.447	0.960
	B	0.981	0.147	0.889	11.650	1.512	0.963
17	A	0.762	0.050	1.092	12.400	4.979	1.026
	B	0.739	0.022	1.143	9.700	9.417	1.029
18	A	0.914	0.028	1.041	4.850	4.324	1.044
19	A	0.949	0.071	0.787	25.000	6.099	1.127
	A	0.671	0.080	1.219	16.200	5.190	1.137
20	A	0.823	0.106	1.092	6.800	2.844	1.084
21	A	1.252	0.071	0.686	3.250	5.816	1.223
	B	0.739	0.107	1.168	8.250	4.585	1.228
22	A	0.598	0.051	1.219	25.000	4.668	0.905
	B	0.773	0.031	1.041	9.250	4.266	0.905
Max		1.252	0.167	1.372	25.000	9.417	1.228
Ave		0.851	0.073	1.025	10.332	4.097	1.028
Min		0.506	0.022	0.686	2.700	1.512	0.860

Table A.8. 9.53-PLY-3.33-COMMON-FLUSH Cyclic Negative 3 Curve Parameters

Coupon Specimen		K_1	K_2	δ_y,		δ_{ult}	P_{ult}
No.	Side	(kN/mm)	(kN/mm)	(mm)	R	(mm)	(kN)
11	A	1.035	0.019	0.864	6.000	2.969	0.933
	B	0.746	0.027	1.168	8.850	3.437	0.933
12	A	1.051	0.147	0.813	9.750	1.641	0.975
	B	1.501	0.066	0.533	1.600	3.137	0.946
13	A	0.488	0.045	1.422	11.100	4.000	0.811
	B	0.595	0.039	1.219	4.200	3.422	0.808
14	A	0.573	0.090	1.295	25.000	4.617	1.040
	B	0.876	0.103	1.041	11.350	2.288	1.041
15	A	1.002	0.092	0.813	5.400	2.961	1.012
	B	0.739	0.070	1.143	6.700	3.520	1.010
16	A	0.932	0.025	0.940	25.000	2.544	0.917
	B	0.944	0.097	0.914	15.050	1.474	0.917
17	A	0.709	0.066	1.092	25.000	4.361	0.990
	B	0.697	0.023	1.168	16.450	9.050	0.993
18	A	0.876	0.033	1.016	7.800	3.918	0.986
19	A	0.907	0.057	0.838	25.000	5.823	1.045
	A	0.616	0.063	1.321	18.950	4.952	1.043
20	A	0.774	0.091	1.143	8.400	2.781	1.035
21	A	1.147	0.064	0.737	3.900	5.937	1.178
	B	0.751	0.086	1.143	6.150	4.783	1.170
22	A	0.558	0.069	1.219	25.000	3.923	0.868
	B	0.837	0.114	0.813	25.000	2.475	0.869
Max		1.501	0.147	1.422	25.000	9.050	1.178
Ave		0.834	0.068	1.030	13.257	3.819	0.978
Min		0.488	0.019	0.533	1.600	1.474	0.808

Table A.9. 6.35-FRP-3.33-COMMON-FLUSH Monotonic Curve Parameters

Coupon Specimen		K_1	K_2	δ_y,		δ_{ult}	P_{ult}
No.	Side	(kN/mm)	(kN/mm)	(mm)	R	(mm)	(kN)
1	A	4.759	0.149	0.370	1.463	2.693	2.048
	B	6.335	0.299	0.270	1.554	1.567	2.034
2	A	6.608	0.059	0.269	1.350	3.897	1.961
	B	8.048	0.098	0.211	1.207	3.227	1.940
3	A	8.696	0.204	0.204	1.187	1.718	1.970
	B	7.436	0.110	0.242	1.193	2.793	2.004
4	A	4.217	0.061	0.340	1.171	4.574	1.636
	B	6.292	0.039	0.227	1.060	6.892	1.650
5	A	1.618	0.061	0.899	1.956	3.682	1.581
	B	2.363	0.023	0.643	1.866	5.156	1.606
6	A	3.306	0.014	0.514	1.218	6.653	1.727
	B	3.337	0.028	0.506	1.371	3.961	1.716
7	A	3.560	0.026	0.454	1.037	8.157	1.743
	B	5.855	0.078	0.267	1.193	3.474	1.754
8	A	1.624	0.029	0.993	1.726	8.112	1.798
	B	4.880	0.048	0.330	1.188	4.679	1.762
9	A	3.499	0.028	0.487	1.387	5.308	1.794
	B	5.587	0.051	0.296	1.212	3.850	1.776
Max		8.696	0.299	0.993	1.956	8.157	2.048
Ave		4.890	0.078	0.418	1.352	4.466	1.806
Min		1.618	0.014	0.204	1.037	1.567	1.581

Table A.10. 6.35-FRP-3.33-COMMON-FLUSH Cyclic Positive 1 Curve Parameters

Coupon Specimen		K_1	K_2	δ_y,		δ_{ult}	P_{ult}
No.	Side	(kN/mm)	(kN/mm)	(mm)	R	(mm)	(kN)
1	A	1.566	0.092	0.890	3.846	3.608	1.643
	B	2.854	0.090	0.479	3.160	3.314	1.621
2	A	2.129	0.055	0.660	2.112	3.961	1.573
	B	3.025	0.089	0.469	2.739	2.361	1.579
3	A	1.924	0.233	0.674	5.381	1.903	1.581
	B	1.509	0.153	0.874	5.572	2.614	1.586
4	A	2.243	0.191	0.653	2.728	2.615	1.829
	B	3.493	0.102	0.448	2.445	3.009	1.820
5	A	2.873	0.089	0.427	1.972	3.709	1.511
	B	3.814	0.102	0.348	1.495	2.575	1.514
6	A	2.612	0.180	0.529	2.293	2.733	1.766
	B	1.841	0.179	0.765	2.743	2.862	1.771
7	A	1.892	0.046	0.688	2.304	4.223	1.457
	B	2.394	0.057	0.555	3.082	2.976	1.464
8	A	1.879	0.064	0.671	2.593	4.073	1.473
	B	1.909	0.116	0.659	2.747	2.525	1.463
9	A	1.775	0.079	0.667	2.216	3.715	1.413
	B	2.630	0.060	0.466	2.484	3.618	1.413
10	A	3.878	0.205	0.346	2.346	2.077	1.688
	B	4.045	0.065	0.358	1.899	4.308	1.696
Max		4.045	0.233	0.890	5.572	4.308	1.829
Ave		2.514	0.112	0.581	2.808	3.139	1.593
Min		1.509	0.046	0.346	1.495	1.903	1.413

Table A.11. 6.35-FRP-3.33-COMMON-FLUSH Cyclic Positive 2 Curve Parameters

Coupon Specimen		K_1	K_2	δ_y,		δ_{ult}	P_{ult}
No.	Side	(kN/mm)	(kN/mm)	(mm)	R	(mm)	(kN)
1	A	1.160	0.058	1.176	5.136	3.843	1.519
	B	1.831	0.060	0.736	5.929	3.390	1.508
2	A	1.262	0.033	1.088	3.796	4.197	1.472
	B	2.111	0.052	0.651	4.340	2.501	1.470
3	A	1.662	0.248	0.737	6.158	1.757	1.477
	B	1.654	0.199	0.752	5.131	2.012	1.493
4	A	1.671	0.127	0.881	4.136	2.683	1.697
	B	2.389	0.062	0.641	3.700	3.238	1.692
5	A	1.298	0.107	0.855	3.868	3.218	1.363
	B	1.542	0.207	0.717	3.421	1.974	1.358
6	A	1.805	0.098	0.794	2.919	2.971	1.637
	B	1.383	0.103	1.042	3.738	3.088	1.646
7	A	1.168	0.042	1.045	4.195	4.142	1.348
	B	1.565	0.059	0.784	5.129	3.066	1.362
8	A	1.267	0.038	0.992	3.814	4.312	1.382
	B	1.227	0.076	1.027	5.020	2.657	1.382
9	A	1.261	0.103	0.850	3.624	3.033	1.294
	B	1.674	0.070	0.674	4.259	2.850	1.280
10	A	1.884	0.165	0.710	6.107	2.149	1.574
	B	1.702	0.051	0.816	5.976	4.578	1.582
Max		2.389	0.248	1.176	6.158	4.578	1.697
Ave		1.576	0.098	0.848	4.520	3.083	1.477
Min		1.160	0.033	0.641	2.919	1.757	1.280

Table A.12. 6.35-FRP-3.33-COMMON-FLUSH Cyclic Positive 3 Curve Parameters

Coupon Specimen		K_1	K_2	δ_y,		δ_{ult}	P_{ult}
No.	Side	(kN/mm)	(kN/mm)	(mm)	R	(mm)	(kN)
1	A	1.172	0.058	1.120	5.145	3.840	1.470
	B	1.764	0.062	0.737	5.766	3.355	1.462
2	A	1.291	0.102	0.950	5.032	2.937	1.427
	B	2.014	0.143	0.617	5.651	1.856	1.421
3	A	1.629	0.189	0.764	6.172	1.777	1.435
	B	1.687	0.118	0.767	4.787	2.028	1.440
4	A	1.697	0.113	0.841	4.290	2.692	1.634
	B	2.410	0.058	0.612	4.024	3.321	1.631
5	A	1.294	0.093	0.848	3.526	3.224	1.316
	B	1.499	0.158	0.748	3.462	2.024	1.314
6	A	1.841	0.095	0.744	2.884	2.921	1.569
	B	1.355	0.093	1.021	3.856	3.140	1.577
7	A	1.226	0.051	0.959	3.680	3.033	1.277
	B	1.506	0.079	0.787	5.012	2.280	1.302
8	A	1.227	0.054	0.970	4.336	4.345	1.371
	B	1.140	0.106	1.052	5.743	2.660	1.369
9	A	1.300	0.101	0.793	3.437	2.979	1.249
	B	1.688	0.068	0.643	4.398	2.889	1.237
10	A	1.903	0.117	0.707	5.016	2.115	1.509
	B	1.722	0.033	0.804	3.742	4.629	1.512
Max		2.410	0.189	1.120	6.172	4.629	1.634
Ave		1.568	0.095	0.824	4.498	2.902	1.426
Min		1.140	0.033	0.612	2.884	1.777	1.237

Table A.13. 6.35-FRP-3.33-COMMON-FLUSH Cyclic Negative 1 Curve Parameters

Coupon Specimen		K_1	K_2	δ_y,		δ_{ult}	P_{ult}
No.	Side	(kN/mm)	(kN/mm)	(mm)	R	(mm)	(kN)
1	A	1.263	0.082	1.208	6.084	2.944	1.667
	B	2.214	0.038	0.687	3.477	4.088	1.651
2	A	1.349	0.069	1.048	3.855	4.417	1.642
	B	1.421	0.245	0.953	5.277	2.107	1.635
3	A	1.556	0.284	0.955	7.350	1.733	1.706
	B	1.670	0.118	0.904	5.908	2.586	1.708
4	A	2.363	0.114	0.705	4.763	1.865	1.796
	B	2.184	0.044	0.767	4.176	3.584	1.798
5	A	1.037	0.138	1.154	2.986	3.990	1.579
	B	1.833	0.305	0.657	3.583	1.923	1.585
6	A	1.881	0.083	0.749	3.859	2.995	1.593
	B	1.731	0.102	0.800	4.180	2.925	1.600
7	A	1.106	0.041	1.182	6.859	2.594	1.364
	B	1.221	0.029	1.064	5.033	3.357	1.364
8	A	1.408	0.085	0.870	3.894	3.623	1.458
	B	1.852	0.132	0.643	4.037	2.646	1.454
9	A	0.991	0.072	1.178	5.448	4.467	1.404
	B	0.810	0.081	1.323	2.742	5.501	1.403
10	A	2.902	0.371	0.601	6.376	1.493	2.074
	B	1.756	0.112	0.870	7.316	5.857	2.085
Max		2.902	0.371	1.323	7.350	5.857	2.085
Ave		1.627	0.127	0.916	4.860	3.235	1.628
Min		0.810	0.029	0.601	2.742	1.493	1.364

Table A.14. 6.35-FRP-3.33-COMMON-FLUSH Cyclic Negative 2 Curve Parameters

Coupon Specimen		K_1	K_2	δ_y,		δ_{ult}	P_{ult}
No.	Side	(kN/mm)	(kN/mm)	(mm)	R	(mm)	(kN)
1	A	1.268	0.051	1.157	5.575	2.845	1.552
	B	2.083	0.025	0.701	5.781	4.143	1.548
2	A	1.345	0.055	1.005	3.999	4.530	1.545
	B	1.699	0.188	0.772	4.981	2.000	1.541
3	A	2.007	0.299	0.695	5.670	1.561	1.650
	B	1.842	0.116	0.787	4.859	2.578	1.657
4	A	2.346	0.103	0.667	5.178	1.922	1.694
	B	2.411	0.041	0.651	4.044	3.771	1.696
5	A	0.934	0.087	1.286	3.357	4.135	1.443
	B	1.774	0.226	0.666	3.459	1.927	1.459
6	A	1.894	0.069	0.699	4.324	3.035	1.486
	B	1.769	0.082	0.739	4.510	2.927	1.487
7	A	1.012	0.172	1.147	7.885	1.982	1.303
	B	0.973	0.133	1.171	6.252	2.434	1.306
8	A	1.284	0.062	0.928	3.794	3.669	1.360
	B	2.079	0.105	0.555	3.362	2.574	1.364
9	A	1.029	0.076	1.127	4.947	3.366	1.328
	B	0.834	0.083	1.268	2.221	4.519	1.304
10	A	2.933	0.681	0.520	6.681	0.857	1.749
	B	1.351	0.075	1.082	6.690	5.169	1.767
Max		2.933	0.681	1.286	7.885	5.169	1.767
Ave		1.643	0.137	0.881	4.878	2.997	1.512
Min		0.834	0.025	0.520	2.221	0.857	1.303

Table A.15. 6.35-FRP-3.33-COMMON-FLUSH Cyclic Negative 3 Curve Parameters

Coupon Specimen		K_1	K_2	δ_y,		δ_{ult}	P_{ult}
No.	Side	(kN/mm)	(kN/mm)	(mm)	R	(mm)	(kN)
1	A	1.248	0.234	1.045	5.482	1.820	1.477
	B	1.957	0.103	0.667	5.744	2.344	1.478
2	A	1.349	0.047	0.982	3.756	4.538	1.491
	B	1.736	0.152	0.750	4.677	1.993	1.489
3	A	2.027	0.424	0.632	5.549	1.297	1.560
	B	1.710	0.175	0.788	5.844	2.049	1.567
4	A	2.272	0.289	0.627	5.713	1.400	1.646
	B	2.366	0.108	0.611	5.255	2.466	1.646
5	A	0.907	0.071	1.312	3.323	4.287	1.394
	B	1.773	0.194	0.662	3.332	1.899	1.405
6	A	1.794	0.107	0.701	4.507	2.131	1.409
	B	1.749	0.117	0.708	4.599	2.142	1.404
7	A	1.007	0.150	1.125	8.599	2.028	1.268
	B	0.897	0.132	1.245	6.356	2.483	1.279
8	A	1.231	0.062	0.932	4.298	3.638	1.313
	B	2.077	0.103	0.537	3.920	2.557	1.323
9	A	0.974	0.170	1.031	5.488	2.414	1.237
	B	0.790	0.155	1.053	3.400	3.687	1.237
10	A	3.089	0.627	0.482	6.398	0.808	1.687
	B	2.319	0.071	0.617	4.625	4.912	1.736
Max		3.089	0.627	1.312	8.599	4.912	1.736
Ave		1.664	0.174	0.825	5.043	2.545	1.452
Min		0.790	0.047	0.482	3.323	0.808	1.237

Table A.16. 6.35-FRP-3.76-COMMON-FLUSH Monotonic Curve Parameters

Coupon Specimen		K_1	K_2	δ_y,		δ_{ult}	P_{ult}
No.	Side	(kN/mm)	(kN/mm)	(mm)	R	(mm)	(kN)
1	A	3.381	0.509	0.480	1.658	1.428	1.984
	B	6.613	0.191	0.283	1.736	1.484	2.046
2	A	4.563	0.514	0.300	1.940	1.352	1.876
	B	6.968	0.330	0.215	1.376	1.516	1.859
3	A	3.070	0.137	0.709	2.105	2.305	2.316
	B	6.514	0.090	0.314	1.065	4.017	2.262
4	A	4.743	0.356	0.333	1.777	1.621	1.992
	B	4.182	0.437	0.405	2.562	1.256	2.035
5	A	3.297	0.407	0.328	2.175	1.275	1.445
	B	5.787	0.527	0.190	2.013	0.843	1.419
6	A	2.517	0.737	0.453	1.533	1.470	1.813
	B	6.184	0.287	0.251	1.558	1.542	1.870
7	A	4.281	0.152	0.393	1.476	2.927	2.011
	B	5.721	0.166	0.290	1.419	2.552	1.987
8	A	15.169	0.012	0.143	1.017	4.030	2.144
	B	3.392	0.010	0.640	1.489	4.673	2.141
9	A	4.212	0.041	0.513	1.391	4.186	2.236
	B	6.503	0.024	0.338	1.126	5.208	2.227
10	A	7.874	0.110	0.257	1.234	2.706	2.209
	B	3.246	0.074	0.649	1.811	3.365	2.251
Max		15.169	0.737	0.709	2.562	5.208	2.316
Ave		5.411	0.256	0.374	1.623	2.488	2.006
Min		2.517	0.010	0.143	1.017	0.843	1.419

Table A.17. 6.35-FRP-3.76-COMMON-FLUSH Cyclic Positive 1 Curve Parameters

Coupon Specimen		K_1	K_2	δ_y,		δ_{ult}	P_{ult}
No.	Side	(kN/mm)	(kN/mm)	(mm)	R	(mm)	(kN)
1	A	3.555	0.098	0.556	1.719	4.418	2.326
	B	3.000	0.117	0.668	2.140	3.703	2.337
2	A	3.213	0.050	0.700	2.027	6.231	2.515
	B	7.352	0.093	0.312	1.835	2.694	2.493
3	A	3.947	0.128	0.597	1.809	3.487	2.676
	B	3.554	0.048	0.699	1.840	5.663	2.693
4	A	3.744	0.048	0.526	2.357	4.756	2.168
	B	3.910	0.249	0.484	2.486	1.662	2.155
5	A	3.019	0.082	0.628	2.106	4.330	2.183
	B	2.286	0.191	0.810	2.497	2.646	2.169
6	A	3.122	0.098	0.522	2.501	3.596	1.925
	B	3.660	0.273	0.413	3.144	1.869	1.905
7	A	4.030	0.204	0.370	3.343	1.747	1.768
	B	3.530	0.758	0.341	4.805	1.049	1.740
8	A	8.518	0.127	0.211	1.826	2.437	2.064
	B	1.796	0.129	1.004	3.177	3.100	2.060
9	A	1.305	0.063	1.503	2.174	3.997	2.024
	B	2.239	0.038	0.862	2.356	6.021	2.116
10	A	2.034	0.349	0.618	3.174	1.709	1.625
	B	4.476	0.263	0.284	2.829	1.642	1.624
Max		8.518	0.758	1.503	4.805	6.231	2.693
Ave		3.615	0.170	0.605	2.507	3.338	2.128
Min		1.305	0.038	0.211	1.719	1.049	1.624

Table A.18. 6.35-FRP-3.76-COMMON-FLUSH Cyclic Positive 2 Curve Parameters

Coupon Specimen		K_1	K_2	δ_y,		δ_{ult}	P_{ult}
No.	Side	(kN/mm)	(kN/mm)	(mm)	R	(mm)	(kN)
1	A	2.085	0.066	0.949	2.262	4.712	2.206
	B	2.158	0.084	0.916	2.912	3.836	2.211
2	A	2.167	0.059	0.953	3.049	6.479	2.388
	B	3.635	0.104	0.582	3.602	2.910	2.355
3	A	2.526	0.085	0.903	2.835	3.673	2.501
	B	2.584	0.031	0.906	2.540	6.038	2.493
4	A	2.338	0.057	0.789	4.256	5.139	2.091
	B	2.525	0.230	0.729	4.797	1.815	2.085
5	A	2.123	0.058	0.871	2.714	4.573	2.056
	B	1.603	0.136	1.153	4.026	2.814	2.062
6	A	1.526	0.051	1.083	4.448	5.381	1.871
	B	1.984	0.126	0.821	4.366	2.543	1.844
7	A	1.795	0.241	0.767	7.252	2.006	1.675
	B	1.824	0.819	0.704	7.604	1.159	1.654
8	A	4.316	0.091	0.389	3.240	2.677	1.885
	B	1.463	0.091	1.185	4.297	3.412	1.933
9	A	1.432	0.323	0.846	3.337	3.214	1.973
	B	1.887	0.080	0.885	3.232	4.643	1.969
10	A	1.191	0.428	1.065	6.310	1.616	1.495
	B	2.578	0.273	0.454	7.561	1.411	1.432
Max		4.316	0.819	1.185	7.604	6.479	2.501
Ave		2.187	0.172	0.847	4.232	3.502	2.009
Min		1.191	0.031	0.389	2.262	1.159	1.432

Table A.19. 6.35-FRP-3.76-COMMON-FLUSH Cyclic Positive 3 Curve Parameters

Coupon Specimen		K_1	K_2	δ_y,		δ_{ult}	P_{ult}
No.	Side	(kN/mm)	(kN/mm)	(mm)	R	(mm)	(kN)
1	A	1.956	0.064	0.976	2.422	4.900	2.147
	B	2.294	0.083	0.826	2.730	3.870	2.138
2	A	2.008	0.057	0.967	3.839	6.616	2.263
	B	3.536	0.106	0.573	3.940	2.961	2.278
3	A	2.470	0.134	0.854	3.383	2.974	2.385
	B	2.579	0.057	0.843	2.908	4.534	2.378
4	A	2.268	0.088	0.762	5.139	3.718	1.990
	B	2.454	0.620	0.642	5.471	1.257	1.951
5	A	2.167	0.098	0.737	4.196	4.636	1.981
	B	1.543	0.228	1.030	5.619	2.827	1.998
6	A	1.712	0.060	0.918	4.529	3.987	1.756
	B	2.282	0.157	0.670	4.475	1.981	1.733
7	A	1.389	0.231	0.985	7.619	2.179	1.644
	B	1.748	0.791	0.746	7.071	1.147	1.617
8	A	4.542	0.107	0.346	3.347	2.691	1.821
	B	1.456	0.099	1.139	4.446	3.430	1.881
9	A	1.406	0.100	1.191	2.125	3.215	1.796
	B	1.815	0.071	0.900	3.297	4.789	1.907
10	A	1.069	0.379	1.197	6.252	1.664	1.442
	B	2.213	0.230	0.530	4.778	1.470	1.388
Max		4.542	0.791	1.197	7.619	6.616	2.385
Ave		2.145	0.188	0.842	4.379	3.242	1.925
Min		1.069	0.057	0.346	2.125	1.147	1.388

Table A.20. 6.35-FRP-3.76-COMMON-FLUSH Cyclic Negative 1 Curve Parameters

Coupon Specimen		K_1	K_2	δ_y,		δ_{ult}	P_{ult}
No.	Side	(kN/mm)	(kN/mm)	(mm)	R	(mm)	(kN)
1	A	0.851	0.169	1.346	4.610	3.471	1.502
	B	2.309	0.318	0.521	5.747	1.311	1.454
2	A	2.285	0.027	0.926	2.264	9.656	2.344
	B	3.899	0.073	0.548	2.811	3.158	2.320
3	A	3.316	0.194	0.628	4.158	2.423	2.428
	B	2.826	0.118	0.774	4.129	3.554	2.513
4	A	2.103	0.023	0.787	3.480	4.752	1.745
	B	2.646	0.095	0.616	4.119	1.858	1.744
5	A	1.746	0.095	0.870	3.279	3.932	1.806
	B	1.836	0.689	0.624	5.669	1.549	1.782
6	A	2.311	0.073	0.776	2.517	5.888	2.161
	B	2.293	0.222	0.767	2.923	2.569	2.145
7	A	1.717	0.202	0.854	5.709	2.344	1.767
	B	3.241	0.720	0.454	6.791	0.838	1.746
8	A	2.270	0.247	0.747	3.472	2.163	2.036
	B	2.543	0.074	0.716	2.820	3.513	2.021
9	A	1.914	0.333	1.150	5.076	1.811	2.387
	B	1.660	0.103	1.332	5.390	3.915	2.477
10	A	1.590	0.753	0.795	7.466	1.456	1.761
	B	2.736	0.114	0.568	2.632	2.530	1.766
Max		3.899	0.753	1.346	7.466	9.656	2.513
Ave		2.305	0.232	0.790	4.253	3.135	1.995
Min		0.851	0.023	0.454	2.264	0.838	1.454

Table A.21. 6.35-FRP-3.76-COMMON-FLUSH Cyclic Negative 2 Curve Parameters

Coupon Specimen		K_1	K_2	δ_y,		δ_{ult}	P_{ult}
No.	Side	(kN/mm)	(kN/mm)	(mm)	R	(mm)	(kN)
1	A	1.046	0.179	1.002	4.648	2.936	1.392
	B	2.433	0.380	0.450	5.329	1.134	1.354
2	A	2.533	0.058	0.715	2.920	6.027	2.117
	B	4.174	0.215	0.430	3.649	1.847	2.097
3	A	3.294	0.158	0.612	3.788	2.392	2.292
	B	3.011	0.083	0.685	3.597	3.723	2.314
4	A	2.237	0.070	0.649	4.840	3.267	1.636
	B	2.723	0.419	0.474	4.356	1.329	1.645
5	A	1.961	0.062	0.746	2.784	3.931	1.654
	B	2.067	0.310	0.680	3.006	1.523	1.633
6	A	2.413	0.067	0.695	2.354	5.843	2.018
	B	2.483	0.204	0.664	2.932	2.501	2.014
7	A	1.726	0.214	0.781	4.583	2.262	1.663
	B	3.252	0.742	0.416	6.194	0.803	1.637
8	A	1.959	0.147	0.864	3.840	2.562	1.936
	B	2.592	0.047	0.670	2.673	4.903	1.932
9	A	1.838	0.409	1.109	5.108	1.620	2.206
	B	1.883	0.178	1.050	4.044	2.631	2.248
10	A	1.597	0.657	0.782	6.558	1.358	1.624
	B	3.053	0.265	0.418	4.616	1.762	1.631
Max		4.174	0.742	1.109	6.558	6.027	2.314
Ave		2.414	0.243	0.695	4.091	2.718	1.852
Min		1.046	0.047	0.416	2.354	0.803	1.354

Table A.22. 6.35-FRP-3.76-COMMON-FLUSH Cyclic Negative 3 Curve Parameters

Coupon Specimen		K_1	K_2	δ_y,		δ_{ult}	P_{ult}
No.	Side	(kN/mm)	(kN/mm)	(mm)	R	(mm)	(kN)
1	A	1.021	0.191	0.952	4.615	2.870	1.338
	B	2.279	0.362	0.465	4.929	1.151	1.307
2	A	2.563	0.052	0.695	2.732	6.097	2.057
	B	4.201	0.191	0.423	3.329	1.856	2.047
3	A	3.287	0.190	0.578	4.376	1.953	2.160
	B	2.890	0.131	0.665	4.649	2.544	2.167
4	A	2.164	0.075	0.644	4.593	3.292	1.593
	B	2.558	0.399	0.492	4.202	1.326	1.586
5	A	1.916	0.051	0.745	2.723	3.913	1.584
	B	2.016	0.169	0.716	3.113	1.542	1.546
6	A	2.218	0.084	0.708	2.577	4.562	1.887
	B	2.331	0.264	0.654	3.489	2.054	1.888
7	A	1.632	0.226	0.790	4.341	2.230	1.613
	B	3.164	0.761	0.407	6.276	0.804	1.587
8	A	1.822	0.222	0.864	4.350	2.049	1.830
	B	2.488	0.070	0.652	2.852	3.686	1.832
9	A	1.848	0.526	1.026	5.078	1.610	2.177
	B	1.889	0.211	0.980	3.938	2.666	2.198
10	A	1.570	0.709	0.794	5.302	1.286	1.586
	B	2.787	0.244	0.450	4.420	1.824	1.589
Max		4.201	0.761	1.026	6.276	6.097	2.198
Ave		2.332	0.256	0.685	4.094	2.466	1.779
Min		1.021	0.051	0.407	2.577	0.804	1.307

Table A.23. 6.35-FRP-4.12-COMMON-FLUSH Monotonic Curve Parameters

Coupon Specimen		K_1	K_2	δ_y,		δ_{ult}	P_{ult}
No.	Side	(kN/mm)	(kN/mm)	(mm)	R	(mm)	(kN)
1	A	1.935	0.279	0.640	2.282	2.116	1.620
	B	4.337	0.250	0.276	1.614	1.929	1.581
2	A	8.348	0.025	0.356	1.005	12.094	3.184
	B	9.814	0.033	0.306	1.040	8.326	3.176
3	A	8.348	0.063	0.318	1.116	4.804	2.833
	B	9.814	0.093	0.273	1.183	3.083	2.820
4	A	3.762	0.395	0.544	1.761	2.045	2.546
	B	5.875	0.480	0.346	1.536	1.597	2.526
5	A	1.554	0.215	0.617	1.794	2.093	1.229
	B	3.614	0.798	0.219	1.900	0.792	1.223
6	A	3.878	0.628	0.252	1.914	1.087	1.476
	B	3.727	0.618	0.267	2.370	1.078	1.485
7	A	2.138	0.548	0.392	1.491	1.705	1.514
	B	4.800	0.708	0.218	1.963	0.985	1.565
8	A	4.080	0.047	0.576	1.050	4.680	2.324
	B	6.205	0.041	0.384	1.052	4.235	2.377
9	A	4.080	0.047	0.576	1.050	4.680	2.324
	B	6.205	0.041	0.384	1.052	4.235	2.377
Max		9.814	0.798	0.640	2.370	12.094	3.184
Ave		5.140	0.295	0.386	1.510	3.420	2.121
Min		1.554	0.025	0.218	1.005	0.792	1.223

Table A.24. 6.35-FRP-4.12-COMMON-FLUSH Cyclic Positive 1 Curve Parameters

Coupon Specimen		K_1	K_2	δ_y,		δ_{ult}	P_{ult}
No.	Side	(kN/mm)	(kN/mm)	(mm)	R	(mm)	(kN)
1	A	2.525	0.035	0.680	2.043	5.832	1.889
	B	2.478	0.026	0.699	1.918	7.006	1.885
2	A	2.348	0.162	0.684	3.057	2.131	1.826
	B	2.257	0.068	0.698	2.049	4.612	1.826
3	A	3.947	0.128	0.597	1.809	3.487	2.676
	B	3.554	0.048	0.699	1.840	5.663	2.693
4	A	3.037	0.081	0.646	2.276	4.393	2.256
	B	4.706	0.112	0.398	2.516	3.340	2.199
5	A	2.860	0.034	0.808	1.617	5.847	2.429
	B	3.628	0.047	0.638	1.497	4.213	2.398
6	A	4.702	0.298	0.480	2.867	2.209	2.764
	B	5.421	0.342	0.407	2.483	1.967	2.721
7	A	4.563	0.158	0.435	1.741	3.277	2.405
	B	3.572	0.286	0.553	2.315	2.180	2.408
8	A	1.558	0.100	1.188	1.938	4.821	2.159
	B	2.330	0.132	0.778	2.444	3.736	2.188
9	A	1.538	0.259	0.912	3.395	2.724	1.865
	B	3.245	0.891	0.464	4.789	0.885	1.872
10	A	2.136	0.045	0.986	1.882	5.622	2.275
	B	1.916	0.056	1.103	2.575	4.733	2.297
Max		5.421	0.891	1.188	4.789	7.006	2.764
Ave		3.116	0.166	0.693	2.352	3.934	2.251
Min		1.538	0.026	0.398	1.497	0.885	1.826

Table A.25. 6.35-FRP-4.12-COMMON-FLUSH Cyclic Positive 2 Curve Parameters

Coupon Specimen		K_1	K_2	δ_y,		δ_{ult}	P_{ult}
No.	Side	(kN/mm)	(kN/mm)	(mm)	R	(mm)	(kN)
1	A	2.108	0.034	0.730	2.625	5.799	1.709
	B	1.825	0.025	0.850	2.685	7.222	1.712
2	A	1.770	0.226	0.852	5.076	1.776	1.710
	B	1.707	0.093	0.851	2.791	3.589	1.699
3	A	2.526	0.085	0.903	2.835	3.673	2.501
	B	2.584	0.031	0.906	2.540	6.038	2.493
4	A	2.195	0.124	0.792	3.730	3.349	2.052
	B	2.974	0.135	0.579	4.206	2.827	2.027
5	A	2.051	0.100	0.934	2.574	4.600	2.270
	B	1.995	0.195	0.915	3.524	3.396	2.303
6	A	3.121	0.355	0.670	4.991	1.786	2.485
	B	3.139	0.437	0.656	5.321	1.609	2.473
7	A	2.148	0.197	0.863	4.108	2.890	2.251
	B	2.311	0.338	0.809	5.430	1.921	2.242
8	A	1.155	0.082	1.522	3.299	5.010	2.033
	B	1.792	0.125	0.947	2.916	3.934	2.060
9	A	1.255	0.164	1.124	5.487	3.142	1.741
	B	2.597	0.867	0.570	5.620	0.856	1.710
10	A	1.566	0.063	1.174	3.243	5.844	2.129
	B	1.897	0.074	0.966	3.137	4.855	2.118
Max		3.139	0.867	1.522	5.620	7.222	2.501
Ave		2.136	0.188	0.881	3.807	3.706	2.086
Min		1.155	0.025	0.570	2.540	0.856	1.699

Table A.26. 6.35-FRP-4.12-COMMON-FLUSH Cyclic Positive 3 Curve Parameters

Coupon Specimen		K_1	K_2	δ_y,		δ_{ult}	P_{ult}
No.	Side	(kN/mm)	(kN/mm)	(mm)	R	(mm)	(kN)
1	A	2.061	0.031	0.720	2.613	5.783	1.638
	B	1.678	0.023	0.891	2.805	7.328	1.643
2	A	1.805	0.188	0.815	5.735	1.742	1.643
	B	1.653	0.073	0.868	2.887	3.696	1.635
3	A	2.470	0.134	0.854	3.383	2.974	2.385
	B	2.579	0.057	0.843	2.908	4.534	2.378
4	A	2.177	0.115	0.778	3.568	3.350	1.987
	B	2.979	0.127	0.561	3.859	2.870	1.963
5	A	1.999	0.081	0.942	2.632	4.653	2.172
	B	1.961	0.151	0.930	2.754	3.498	2.196
6	A	3.099	0.323	0.663	5.011	1.800	2.418
	B	2.999	0.397	0.677	5.285	1.655	2.415
7	A	2.128	0.186	0.849	4.176	2.908	2.187
	B	2.327	0.331	0.777	5.446	1.904	2.178
8	A	1.208	0.116	1.323	3.630	3.801	1.876
	B	1.733	0.151	0.912	3.345	3.146	1.912
9	A	1.165	0.106	1.248	4.950	3.234	1.663
	B	2.634	0.678	0.554	5.587	0.853	1.645
10	A	1.651	0.092	1.043	3.196	4.564	2.041
	B	1.751	0.111	0.985	3.623	3.857	2.041
Max		3.099	0.678	1.323	5.735	7.328	2.418
Ave		2.103	0.174	0.862	3.870	3.408	2.001
Min		1.165	0.023	0.554	2.613	0.853	1.635

Table A.27. 6.35-FRP-4.12-COMMON-FLUSH Cyclic Negative 1 Curve Parameters

Coupon Specimen		K_1	K_2	δ_y,		δ_{ult}	P_{ult}
No.	Side	(kN/mm)	(kN/mm)	(mm)	R	(mm)	(kN)
1	A	2.132	0.102	0.643	4.468	2.067	1.515
	B	1.223	0.065	1.116	4.386	3.708	1.532
2	A	1.744	0.057	0.923	2.206	4.104	1.767
	B	2.601	–0.067	0.730	1.810	2.823	1.670
3	A	3.316	0.194	0.628	4.158	2.423	2.428
	B	2.826	0.118	0.774	4.129	3.554	2.513
4	A	2.261	0.071	0.821	2.384	4.662	2.117
	B	2.707	0.184	0.677	3.223	2.258	2.113
5	A	1.592	0.149	1.350	3.293	3.856	2.504
	B	2.115	0.190	1.006	2.647	2.911	2.446
6	A	3.172	0.197	0.678	2.619	2.879	2.566
	B	3.554	0.121	0.616	2.422	3.610	2.540
7	A	2.456	0.077	0.919	2.430	6.027	2.638
	B	2.467	0.052	0.988	2.742	4.819	2.624
8	A	1.469	0.210	1.097	4.504	3.844	2.188
	B	1.512	0.241	1.163	4.786	2.912	2.176
9	A	1.182	0.465	1.136	6.174	2.230	1.850
	B	3.080	0.778	0.473	6.440	0.873	1.764
10	A	2.484	0.056	0.861	1.964	5.572	2.376
	B	1.830	0.133	1.140	3.076	3.744	2.417
Max		3.554	0.778	1.350	6.440	6.027	2.638
Ave		2.286	0.170	0.887	3.493	3.444	2.187
Min		1.182	–0.067	0.473	1.810	0.873	1.515

Table A.28. 6.35-FRP-4.12-COMMON-FLUSH Cyclic Negative 2 Curve Parameters

Coupon Specimen		K_1	K_2	δ_y,		δ_{ult}	P_{ult}
No.	Side	(kN/mm)	(kN/mm)	(mm)	R	(mm)	(kN)
1	A	1.729	0.097	0.732	6.388	2.170	1.404
	B	1.059	0.063	1.189	6.796	3.835	1.425
2	A	1.836	0.043	0.818	2.135	4.014	1.615
	B	2.702	0.045	0.552	1.986	2.721	1.558
3	A	3.294	0.158	0.612	3.788	2.392	2.292
	B	3.011	0.083	0.685	3.597	3.723	2.314
4	A	2.104	0.112	0.774	2.890	3.494	1.927
	B	2.880	0.253	0.560	3.430	1.827	1.925
5	A	1.588	0.158	1.210	3.885	3.952	2.351
	B	2.274	0.221	0.814	2.858	2.859	2.288
6	A	3.281	0.189	0.610	2.650	2.579	2.359
	B	3.696	0.107	0.564	2.377	3.188	2.351
7	A	2.304	0.094	0.864	3.046	5.387	2.412
	B	2.590	0.085	0.840	2.908	3.446	2.387
8	A	1.489	0.160	1.046	3.933	3.828	2.000
	B	1.642	0.165	1.012	4.724	2.914	1.973
9	A	1.185	0.449	1.086	5.881	2.185	1.778
	B	3.233	0.673	0.442	5.894	0.862	1.707
10	A	2.288	0.038	0.890	1.948	5.866	2.203
	B	1.881	0.082	1.070	2.880	3.777	2.217
Max		3.696	0.673	1.210	6.796	5.866	2.412
Ave		2.303	0.164	0.819	3.700	3.251	2.024
Min		1.059	0.038	0.442	1.948	0.862	1.404

Table A.29. 6.35-FRP-4.12-COMMON-FLUSH Cyclic Negative 3 Curve Parameters

Coupon Specimen		K_1	K_2	δ_y,		δ_{ult}	P_{ult}
No.	Side	(kN/mm)	(kN/mm)	(mm)	R	(mm)	(kN)
1	A	2.271	0.099	0.529	4.794	2.049	1.353
	B	1.315	0.062	0.913	5.254	3.689	1.371
2	A	1.889	0.073	0.712	2.221	3.938	1.567
	B	2.571	0.134	0.479	2.836	2.808	1.541
3	A	3.287	0.190	0.578	4.376	1.953	2.160
	B	2.890	0.131	0.665	4.649	2.544	2.167
4	A	2.057	0.084	0.790	2.937	3.532	1.849
	B	2.937	0.190	0.548	3.289	1.817	1.841
5	A	1.584	0.138	1.161	3.685	4.017	2.228
	B	2.275	0.192	0.787	2.753	2.851	2.169
6	A	3.326	0.121	0.611	2.456	2.712	2.266
	B	3.718	0.083	0.554	2.362	3.240	2.268
7	A	2.219	0.074	0.893	2.930	5.406	2.310
	B	2.558	0.065	0.828	3.076	3.587	2.290
8	A	1.441	0.122	1.106	3.475	3.836	1.921
	B	1.589	0.128	1.045	4.620	2.956	1.901
9	A	1.161	0.427	1.110	5.139	2.162	1.733
	B	3.347	0.807	0.388	5.623	0.855	1.675
10	A	2.183	0.031	0.906	2.055	5.942	2.114
	B	1.805	0.069	1.082	3.078	3.750	2.123
Max		3.718	0.807	1.161	5.623	5.942	2.310
Ave		2.321	0.161	0.784	3.580	3.182	1.942
Min		1.161	0.031	0.388	2.055	0.855	1.353

Appendix B

DOWEL-BENDING STRESS TEST DATA

This appendix contains data extracted from dowel-bending tests performed by Rabe (2000). Rabe reported only the 5% offset values. For this research the proportional limit, 5% offset, and ultimate dowel-bending stress values are required. The original data and extracted values (maximum, average, and minimum values) are shown in Table B.1 and Table B.2, respectively, for 3.33×63.5 mm (8d) common nails, and 2.87×60.3 mm (8d) cooler nails.

Table B.1. 3.33×63.5 mm Common Nails: Dowel-Bending Stress (MPa)

Nail test number	$f_{b,pl}$	$f_{b,5\%}$	$f_{b,ult}$
1	607	752	904
2	593	752	883
3	614	794	925
4	759	814	918
5	628	821	987
6	662	759	904
7	649	745	856
8	642	807	966
9	731	835	973
10	593	766	918
11	552	725	897
12	621	821	1007
13	545	759	925
14	683	835	994
15	725	849	1001
Max	759	849	1007
Ave	640	789	937
Min	545	725	856

Table B.2. 2.87×60.3 mm Cooler Nails: Dowel-Bending Stress (MPa)

Nail test number	$f_{b,pl}$	$f_{b,5\%}$	$f_{b,ult}$
1	624	753	1032
2	602	742	1043
3	581	731	1043
4	516	677	1011
5	452	731	1021
6	473	763	1043
7	527	731	1011
8	634	774	1064
9	548	763	1054
10	613	774	1064
11	505	742	1054
12	591	710	1032
13	495	720	1032
14	624	753	1054
15	602	742	1043
Max	634	774	1064
Ave	559	740	1040
Min	452	677	1011

Appendix C

MODIFIED *CASHEW* SUBROUTINES

This appendix contains the primary modified *CASHEW* (Folz and Filiatrault 2000; 2001) subroutines used in this thesis. The following modifications were made to the FORTRAN code to incorporate the oriented spring pair element: (1) elimination of the `TIMER` portions of the code in the `MAIN` routine; (2) addition of author/modification information into title blocks; (3) elimination of adjustment of connector spacing in subroutine `STATIC1`; (4) redefinition of the local displacements in subroutine `PSTIF2` and `UPDATE`, and redefinition of the element (panel) stiffness in subroutine `PSTIF2`; (5) addition of a loop to extract the initial orientation (displacements) from each sheathing-to-framing connection in subroutine `STATIC1`; and (6) expansion of the size of the `CSTOR1` and `CSTOR2` arrays in all routines.

C.1 `static1` Subroutine to Perform Static Analysis

```
*-----------------------------------------------------------------------
*     SUBROUTINE STATIC1 PERFORMS STATIC ANALYSIS OF THE WALL
*-----------------------------------------------------------------------
*
      SUBROUTINE STATIC1
      IMPLICIT DOUBLE PRECISION (A - H, O - Z)
      PARAMETER    (MDOF = 41, MP = 10, ML = 10, MC = 50, MDAT = 20000)
      COMMON /B01/ HTWALL, IANALY, IMODE, NPANEL, NDOF
      COMMON /B02/ HORZP(MP), VERTP(MP), XGLOB(MP), YGLOB(MP),
     .             GMOD(MP), THICKP(MP), NHLINE(MP), NVLINE(MP),
     .             NHCON(MP,ML), NVCON(MP,ML)
      COMMON /B03/ XLOCAL(MP,ML), SPACEH(MP,ML),
     .             XSTART(MP,ML), XEND(MP,ML),
     .             YLOCAL(MP,ML), SPACEV(MP,ML),
     .             YSTART(MP,ML), YEND(MP,ML)
      COMMON /B09/ CSTOR1(12,MP,ML,MC,2,2), CSTOR2(12,MP,ML,MC,2,2)
      COMMON /B10/ GKS(MDOF,MDOF), GKT(MDOF,MDOF), PKS(5,5), PKT(5,5),
     .             GD(MDOF), GD0(MDOF), GDD(MDOF), GF(MDOF), GF0(MDOF),
     .             GF2(MDOF), GRF(MDOF)
      COMMON /B12/ GD1(MDAT), GDP(MDAT), NDISP
      COMMON /B13/ GDST(MDAT), GFST(MDAT), GDCY(MDAT), GFCY(MDAT),
     .             GKWALL, GFULT, GDULT, GDELTA, IDMAX, IFIT
      DIMENSION    SPHOLD(MP,ML), SPVOLD(MP,ML)
      DIMENSION    NHCOLD(MP,ML), NVCOLD(MP,ML)
      DIMENSION    GDS1(200), GFS1(200)
*
      WRITE (*,10)
  10  FORMAT (2X, 'Performing initial static analysis ...', /)
*
*     Initialize variables.
*
      NDOF = (4 * NPANEL) + 1
      NITER = 50
      NLD = 200
      TOL = 1.0D-04
      IMODE = 0
      JMODE = 0
      IFLAG1 = 1
      DO I = 1, NDOF
        GD(I) = 0.0D0
        GD0(I) = 0.0D0
        GF(I) = 0.0D0
      END DO
      GF(1) = 1.0D0
*
*     Perform linear static analysis.
*
*     Loop over all the panels to build global stiffness matrix.
*
      DO IP = 1, NPANEL
*
*       Call subroutine PSTIF1 to obtain stiffness contribution from
*       each panel.
*
        CALL PSTIF1 (IP)
*
*       Call subroutine GSTIF to add the panel stiffness contribution
*       to the global secant stiffness matrix.
*
        CALL GSTIF (IP)
      END DO
*
*     Solve for unknown displacements.
*
      CALL GAUSS (GKS, GD, GF, DET, NDOF, MDOF, IERROR)
```

```
*
*     Obtain initial stiffness of the shear wall.
*
      GKWALL = GF(1) / GD(1)
*
*     ALTERED 6 FEB 2003 Added the following DO Loop
*     Obtain the initial orientations
*
*     Loop over the panels
*
      DO IP = 1, NPANEL
        II = (4 * IP) - 2
        UF = GD(1)
        USI = GD(II)
        UI  = GD(II+1)
        VI  = GD(II+2)
        THETAI = GD(II+3)
        YBAR  = YGLOB (IP)
        BP  = HORZP(IP)
        HP  = VERTP(IP)
        HW = HTWALL
*
*       Start looping over horizontal connector lines in the panel.
*
*        WRITE (3,*) 'Horizontal connections'
        DO IL = 1, NHLINE(IP)
          YC  = YLOCAL(IP,IL)
          SPACE = SPACEH(IP,IL)
          DO IC = 1, NHCON(IP,IL)
            XC = (SPACE*(IC-1)) + XSTART(IP,IL)
            UPI = UI + (2*YC*USI/HP) - (THETAI*YC)
            UFI = (YC + YBAR)*UF/HW
            USLIP = UPI - UFI
            VSLIP = VI + (THETAI*XC)
*
*           Calculate slip in r direction
*
            RSLIP = DSQRT(USLIP*USLIP + VSLIP*VSLIP)
*
*           Define local u axis unit vector
*
            UNIT_UX = USLIP/RSLIP
            UNIT_UY = VSLIP/RSLIP
*            WRITE (3,15) UNIT_UX, UNIT_UY, IP, IL, IC
*   15       FORMAT (E18.6,E18.6,1X,I3,1X,I3,1X,I3)
            CSTOR1(11,IP,IL,IC,1,1) = UNIT_UX
            CSTOR1(12,IP,IL,IC,1,1) = UNIT_UY
          END DO
        END DO
*
*       Start looping over vertical connector lines in the panel.
*
*        WRITE (3,*) 'Vertical connections'
        DO IL = 1, NVLINE(IP)
          XC  = XLOCAL(IP,IL)
          SPACE = SPACEV(IP,IL)
          DO IC = 1, NVCON(IP,IL)
            YC = (SPACE*(IC-1)) + YSTART(IP,IL)
            UPI = UI + (2*YC*USI/HP) - (THETAI*YC)
            UFI = (YC + YBAR)*UF/HW
            USLIP = UPI - UFI
            VSLIP = VI + (THETAI*XC)
*
*           Calculate slip in r direction
*
            RSLIP = DSQRT(USLIP*USLIP + VSLIP*VSLIP)
*
*           Define local u axis unit vector
*
```

```
            UNIT_UX = USLIP/RSLIP
            UNIT_UY = VSLIP/RSLIP
*            WRITE (3,15) UNIT_UX, UNIT_UY, IP, IL, IC
*   17       FORMAT (E18.6,E18.6,1X,I3,1X,I3,1X,I3)
            CSTOR1(11,IP,IL,IC,2,1) = UNIT_UX
            CSTOR1(12,IP,IL,IC,2,1) = UNIT_UY
          END DO
        END DO
      END DO
*
      IF (IERROR .EQ. 1) THEN
        WRITE (*,20)
  20    FORMAT (/, 2X, 'Program stopped: ',
     .                'System matrix not positive definite!', //)
        STOP
      END IF
*
      IMODE = 1
*
*     Re-initialize variables.
*
  30  DO I = 1, NDOF
        GD(I) = 0.0D0
        GD0(I) = 0.0D0
        GF(I) = 0.0D0
      END DO
*
*     Estimate maximum load based on 1% drift of wall under
*     linear response. If necessary reduce drift level.
*
      IF (IFLAG1 .EQ. 1) THEN
        FACD = 0.01D0
        GFMAX = (FACD * HTWALL) * GKWALL
      ELSE
        FACD = 0.75D0 * FACD
        GFMAX = (FACD * HTWALL) * GKWALL
      END IF
*
*     Start looping over the load increments to generate the
*     envelope curve for the wall.
*
      GFINC = GFMAX / NLD
      DO ILD = 1, NLD
        GF(1) = GFINC * ILD
*
*       Start iterating at the given load level.
*
        ITER = 1
   40   CONTINUE
        DO I = 1, NDOF
          DO J = 1, NDOF
            GKS(I,J) = 0.0D0
          END DO
        END DO
*
*       Loop over all the panels to build the global stiffness matrix.
*
*
        DO IP = 1, NPANEL
*
*         Call subroutine PSTIF1 to obtain stiffness contribution from
*         each panel.
*
          CALL PSTIF1 (IP)
*
*         Call subroutine GSTIF to add the panel stiffness contribution
*         to the global secant stiffness matrix.
*
          CALL GSTIF (IP)
```

```
        END DO
*
*       Solve for unknown displacements for the current iteration.
*
        CALL GAUSS (GKS, GD, GF, DET, NDOF, MDOF, IERROR)
*
        IF (IERROR .NE. 1) THEN
*
*         Check solution convergence, assuming the stiffness matrix
*         is non-singular.
*
          FAC1 = 0.0D0
          FAC2 = 0.0D0
          DO I = 1, NDOF
            FAC1 = FAC1  + (GD(I)**2)
            FAC2 = FAC2 + ((GD(I)-GD0(I))**2)
          END DO
          EPSILN = DSQRT(FAC2/FAC1)
          IF (EPSILN .LE. TOL) THEN
*
*           Solution converged ...
*
*           write (2,50) gd(1), gf(1)  ! Write statement for debugging.
* 50        format (2E15.4)
            DO I = 1, NDOF
              GD0(I) = GD(I)
            END DO
            GDMAX1 = GD(1)
            GDS1(ILD) = GD(1)
            GFS1(ILD) = GF(1)
*
          ELSE IF (EPSILN .GT. TOL) THEN
*
*           Convergence not achieved ...
*
            ITER = ITER + 1
            IF(ITER .EQ. NITER) THEN
              IFLAG1 = IFLAG1 + 1
              IF (IFLAG1 .LT. 10) GO TO 30
                WRITE (*,60) NITER
  60            FORMAT (/, 2X, 'Program stopped: ',
     .                           'No convergence in ', I2,
     .                           ' iterations!', //)
              STOP
            END IF
            DO I = 1, NDOF
              GD0(I) = GD(I)
            END DO
            GO TO 40
          END IF
        ELSE IF (IERROR .EQ. 1) THEN
          IFLAG1 = IFLAG1 + 1
          IF (IFLAG1 .LT. 10) GO TO 30
*
*         Global stiffness matrix is singular ....
*
          WRITE (*,70)
  70      FORMAT (/, 2X, '  Global stiffness matrix is singular!', //)
          EXIT
        END IF
      END DO
*
*     Evaluate hysteretic energy of wall up to (0.9 * GDMAX1).
*
      GDMAX1 = 0.9D0 * GDMAX1
      EHYST1 = (GFS1(1) / 2.0D0) * GDS1(1)
      DO ILD = 2, NLD
        IF(GDS1(ILD) .LT. GDMAX1) THEN
          FAC1 = (GFS1(ILD) + GFS1(ILD-1)) /2.0D0
```

```
          FAC2 = GDS1(ILD) - GDS1(ILD-1)
          EHYST1 = EHYST1 + (FAC1 * FAC2)
        ELSE
          EXIT
        END IF
      END DO
*
*     Evaluate wall response using two springs per connector.
*
  80  CONTINUE
*
*     Initialize variables.
*
      ICON = 0
      TOL = 1.0D-04
      NLD = 200
      IMODE = 2
      EHYST2 = 0.0D0
      GDOLD = 0.0D0
      DO I = 1, NDOF
        GD(I) = 0.0D0
        GD0(I) = 0.0D0
      END DO
      GFINC = (1.20D0 * GFMAX) / NLD
*
*     Start Newton-Raphson solution procedure.
*     Increment the loads on the structure.
*
      DO ILD = 1, NLD
        ITER = 0
  90   CONTINUE
*
*       Initialize global secant and tangent stiffness matrices.
*
        DO I = 1, NDOF
          DO J = I, NDOF
            GKS(I,J) = 0.0D0
            GKT(I,J) = 0.0D0
          END DO
        END DO
*
*       Loop over all the panels to build global stiffness matrices.
*
        DO IP = 1, NPANEL
*
*         Call subroutine PSTIF to obtain stiffness contribution from
*         each panel.
*
          CALL PSTIF2 (IP, JFLAG)
*
*         Call subroutine GSTIF to add the panel stiffness contribution
*         to the global secant and tangent stiffness matrices.
*
          CALL GSTIF (IP)
        END DO
*
*       Assemble the global residual force vector.
*
        CALL RESID (GFINC, FACLD, ILD)
*
*       Solve for unknown displacements.
*
        CALL GAUSS (GKT, GDD, GRF, DET, NDOF, MDOF, IERROR)
*
*       ALTERED  We added the next lines for debugging 5 FEB 2003
        WRITE (3,95) GD(1), GF(1), ILD, ITER
   95   FORMAT (E18.6,E18.6,1X,I3,1X,I2)
*
        IF (IERROR .EQ. 1) EXIT
```

```
*
        DO I = 1, NDOF
          GD(I) = GD0(I) + GDD(I)
        END DO
*
*       Check convergence of the solution vector.
*
        CALL CONVRG (ILD, IDP, ITER, TOL, ICON)
        ITER = ITER + 1
        IF(ITER .EQ. NITER) THEN
          WRITE (*,100) NITER
 100      FORMAT (/, 2X, 'No convergence in ', I2, ' iterations!', //)
          RETURN
        END IF
*
*       Update previous solution vector.
*       If no convergence iterate again.
*
        DO I = 1, NDOF
          GD0(I) = GD(I)
        END DO
        IF(ICON .EQ. 0) GO TO 90
*
*       If solution converged write results to screen.
*
*       write (2,110) gd(1), gf(1)    ! Write statement for debugging.
* 110   format (2E15.4)
        IF(GD(1) .LT. GDMAX1) THEN
          FAC1 = GF(1) - (GFINC/2.0D0)
          FAC2 = GD(1) - GDOLD
          EHYST2 = EHYST2 + (FAC1 * FAC2)
          GDOLD = GD(1)
        ELSE
          EXIT
        END IF
      END DO
*     ALTERED:  We commented out the next section 5 FEB 2003
*      EDIFF = EHYST2 - EHYST1
*      IF (EDIFF .GT. 0.0D0) EPLUS = EDIFF
*      IF ((JMODE .EQ. 1) .AND. (EDIFF .LE. 0.0D0)) THEN
*        IF (DABS(EDIFF) .LE. EPLUS) THEN
*          RETURN
*        ELSE
*          DO IP = 1, NPANEL
*            DO IL = 1, NHLINE(IP)
*              NHCON(IP,IL) = NHCOLD(IP,IL)
*              SPACEH(IP,IL) = SPHOLD(IP,IL)
*            END DO
*            DO IL = 1, NVLINE(IP)
*              NVCON(IP,IL) = NVCOLD(IP,IL)
*              SPACEV(IP,IL) = SPVOLD(IP,IL)
*            END DO
*          END DO
*          RETURN
*        END IF
*      END IF
*
*     Adjust connector spacing
*
*     ALTERED:  We commented out the next section 4 FEB 2003
*      DO IP = 1, NPANEL
*        DO IL = 1, NHLINE(IP)
*          NHCOLD(IP,IL) = NHCON(IP,IL)
*          SPHOLD(IP,IL) = SPACEH(IP,IL)
*          IF (NHCON(IP,IL) .GT. 3) THEN
*            XLEN = DABS(XEND(IP,IL)-XSTART(IP,IL))
*            NHCON(IP,IL) = NHCON(IP,IL) - 1
*            SPACEH(IP,IL) = XLEN / (NHCON(IP,IL)-1)
*          END IF
```

```
*         END DO
*         DO IL = 1, NVLINE(IP)
*           NVCOLD(IP,IL) = NVCON(IP,IL)
*           SPVOLD(IP,IL) = SPACEV(IP,IL)
*           IF (NVCON(IP,IL) .GT. 3) THEN
*             YLEN = DABS(YEND(IP,IL)-YSTART(IP,IL))
*             NVCON(IP,IL) = NVCON(IP,IL) - 1
*             SPACEV(IP,IL) = YLEN / (NVCON(IP,IL)-1)
*           END IF
*         END DO
*       END DO
*       JMODE = 1
*       GO TO 80
      END
```

C.2 `pstif2` Subroutine to Calculate Stiffness Using Nonoriented Spring Pair Model

```
*-----------------------------------------------------------------------
*     SUBROUTINE PSTIF2 RETURNS THE PANEL STIFFNESS MATRIX, INCLUDING THE
*     CONTRIBUTION FROM THE FRAMING-TO-PANEL CONNECTORS.
*     EACH CONNECTOR IS MODELED USING TWO ORTHOGONAL NON-LINEAR SPRINGS.
*-----------------------------------------------------------------------
*
      SUBROUTINE PSTIF2 (IP, JFLAG)
      IMPLICIT DOUBLE PRECISION (A - H, O - Z)
      PARAMETER    (MDOF = 41, MP = 10, ML = 10, MC = 50, MDAT = 20000)
      COMMON /B01/ HTWALL, IANALY, IMODE, NPANEL, NDOF
      COMMON /B02/ HORZP(MP), VERTP(MP), XGLOB(MP), YGLOB(MP),
     .             GMOD(MP), THICKP(MP), NHLINE(MP), NVLINE(MP),
     .             NHCON(MP,ML), NVCON(MP,ML)
      COMMON /B03/ XLOCAL(MP,ML), SPACEH(MP,ML),
     .             XSTART(MP,ML), XEND(MP,ML),
     .             YLOCAL(MP,ML), SPACEV(MP,ML),
     .             YSTART(MP,ML), YEND(MP,ML)
      COMMON /B04/ F0, FI, DU, S0, R1, R2, R3, R4, ALPHA, BETA
      COMMON /B05/ F0H(MP,ML), FIH(MP,ML), DUH(MP,ML), S0H(MP,ML),
     .             R1H(MP,ML), R2H(MP,ML), R3H(MP,ML), R4H(MP,ML),
     .             ALPHAH(MP,ML), BETAH(MP,ML),
     .             F0V(MP,ML), FIV(MP,ML), DUV(MP,ML), S0V(MP,ML),
     .             R1V(MP,ML), R2V(MP,ML), R3V(MP,ML), R4V(MP,ML),
     .             ALPHAV(MP,ML), BETAV(MP,ML)
      COMMON /B06/ LPATH, IYPLUS, IYMINS, LPPREV, NUBC, NCYC
      COMMON /B07/ ICSTR1(4,MP,ML,MC,2,2), ICSTR2(4,MP,ML,MC,2,2)
      COMMON /B08/ DOLD, DUNP, FUNP, DUNM, FUNM, DMAXP, FMAXP, DMAXM,
     .             FMAXM, SP
      COMMON /B09/ CSTOR1(12,MP,ML,MC,2,2), CSTOR2(12,MP,ML,MC,2,2)
      COMMON /B10/ GKS(MDOF,MDOF), GKT(MDOF,MDOF), PKS(5,5), PKT(5,5),
     .             GD(MDOF), GD0(MDOF), GDD(MDOF), GF(MDOF), GF0(MDOF),
     .             GF2(MDOF), GRF(MDOF)
*
*    Initialize variables.
*
*      WRITE (3,*) 'We are in subroutine PSTIF2'
      DO I = 1, 5
        DO J = 1, 5
          PKS(I,J) = 0.0D0
          PKT(I,J) = 0.0D0
        END DO
      END DO
      II = (4 * IP) - 2
      UF = GD(1)
      USI = GD(II)
      UI  = GD(II+1)
      VI  = GD(II+2)
      THETAI = GD(II+3)
      YBAR  = YGLOB (IP)
      BP  = HORZP(IP)
      HP  = VERTP(IP)
      HW = HTWALL
*
*     Obtain panel shear stiffness contribution.
*
      PKS(2,2) = 4.0D0 * GMOD(IP) * THICKP(IP) * (BP / HP)
      PKT(2,2) = 4.0D0 * GMOD(IP) * THICKP(IP) * (BP / HP)
*
*     Start looping over horizontal connector lines in the panel.
*
      DO IL = 1, NHLINE(IP)
        YC  = YLOCAL(IP,IL)
```

```
          SPACE = SPACEH(IP,IL)
          F0 = F0H(IP,IL)
          FI = FIH(IP,IL)
          DU = DUH(IP,IL)
          S0 = S0H(IP,IL)
          R1 = R1H(IP,IL)
          R2 = R2H(IP,IL)
          R3 = R3H(IP,IL)
          R4 = R4H(IP,IL)
          ALPHA = ALPHAH(IP,IL)
          BETA  = BETAH(IP,IL)
          DO IC = 1, NHCON(IP,IL)
            XC = (SPACE*(IC-1)) + XSTART(IP,IL)
            UPI = UI + (2*YC*USI/HP) - (THETAI*YC)
            UFI = (YC + YBAR)*UF/HW
            USLIP = UPI - UFI
            VSLIP = VI + (THETAI*XC)
*
*           Define slip in global directions
*
            XSLIP = USLIP
            YSLIP = VSLIP
*           ALTERED  We added the next lines for debugging 5 FEB 2003
*            WRITE (3,10) USLIP, VSLIP, IP, IL, IC
*            IF ((IP .EQ. 1) .AND. (IL .EQ. 1) .AND. (IC .EQ. 1)) THEN
*               WRITE (3,10) USLIP, VSLIP, IP, IL, IC
*  10           FORMAT (E18.6,E18.6,1X,I3,1X,I3,1X,I3)
*            ENDIF
*
*           Define local axis
*
*           Define using a direction vector
*            DIRU = 1.0D0
*            DIRV = 0.5D0
*            DIRR = DSQRT(DIRU*DIRU + DIRV*DIRV)
*            UNIT_UX = DIRU/DIRR
*            UNIT_UY = DIRV/DIRR
*
*           Define using an initial orientation vector
            UNIT_UX = CSTOR1(11,IP,IL,IC,1,1)
            UNIT_UY = CSTOR1(12,IP,IL,IC,1,1)
            UNIT_VX = -UNIT_UY
            UNIT_VY = UNIT_UX
*
*           Define slip in local directions
*
            USLIP = XSLIP*UNIT_UX + YSLIP*UNIT_UY
            VSLIP = XSLIP*UNIT_VX + YSLIP*UNIT_VY
*
            IF (IMODE .EQ. 2) THEN
              DO I = 1, 2
                IF (I .EQ. 1) THEN
                  DISPL = USLIP
                ELSE IF (I .EQ. 2) THEN
                  DISPL = VSLIP
                END IF
                IF (DABS(DISPL) .LE. DU) THEN
                  FAC1 = F0 + (R1 * S0 * DABS(DISPL))
                  FAC2 = 1.0D0 - DEXP(-S0*DABS(DISPL)/F0)
                  FAC3 = 1 - FAC2
                  FORCE = FAC1 * FAC2
                  IF (DISPL .LT. 0.0D0) FORCE = -FAC1 * FAC2
                  SKT = (FAC1 * (S0/F0) * FAC3) + (R1 * S0 * FAC2)
                ELSE IF (DABS(DISPL) .GT. DU) THEN
                  FAC1 = F0 + (R1 * S0 * DU)
                  FAC2 = 1.0D0 - DEXP(-S0*DU/F0)
                  FU = FAC1 * FAC2
                  FORCE = FU + (R2*S0*(DISPL - DU))
                  SKT = R2 * S0
```

```
            END IF
            IF (I .EQ. 1) THEN
              SKTU = SKT
              IF ((FORCE .EQ. 0.0D0) .AND. (DISPL .EQ. 0.0D0)) THEN
                SKSU = S0
              ELSE
                SKSU = FORCE / DISPL
              END IF
            ELSE IF (I .EQ. 2) THEN
              SKTV = SKT
              IF ((FORCE .EQ. 0.0D0) .AND. (DISPL .EQ. 0.0D0)) THEN
                SKSV = S0
              ELSE
                SKSV = FORCE / DISPL
              END IF
            END IF
          END DO
        ELSE IF (IMODE .EQ. 3) THEN
          DO I = 1, 2
            LPATH  = ICSTR1(1,IP,IL,IC,1,I)
            IYPLUS = ICSTR1(2,IP,IL,IC,1,I)
            IYMINS = ICSTR1(3,IP,IL,IC,1,I)
            LPPREV = ICSTR1(4,IP,IL,IC,1,I)
            DOLD   = CSTOR1(1,IP,IL,IC,1,I)
            DUNP   = CSTOR1(2,IP,IL,IC,1,I)
            FUNP   = CSTOR1(3,IP,IL,IC,1,I)
            DUNM   = CSTOR1(4,IP,IL,IC,1,I)
            FUNM   = CSTOR1(5,IP,IL,IC,1,I)
            DMAXP  = CSTOR1(6,IP,IL,IC,1,I)
            FMAXP  = CSTOR1(7,IP,IL,IC,1,I)
            DMAXM  = CSTOR1(8,IP,IL,IC,1,I)
            FMAXM  = CSTOR1(9,IP,IL,IC,1,I)
            SP     = CSTOR1(10,IP,IL,IC,1,I)
*
*           Call subroutine HYSTER to determine connector force and
*           stiffness corresponding to deformation DELTA.
*
            IF (I .EQ. 1) THEN
              CALL HYSTR (USLIP, UFORCE, SKTU, JFLAG)
              IF (JFLAG .EQ. 1) RETURN
              IF ((UFORCE .EQ. 0.0D0) .AND. (USLIP .EQ. 0.0D0)) THEN
                SKSU = S0
              ELSE
                SKSU = UFORCE / USLIP
              END IF
            ELSE IF (I .EQ. 2) THEN
              CALL HYSTR (VSLIP, VFORCE, SKTV, JFLAG)
              IF (JFLAG .EQ. 1) RETURN
              IF ((VFORCE .EQ. 0.0D0) .AND. (VSLIP .EQ. 0.0D0)) THEN
                SKSV = S0
              ELSE
                SKSV = VFORCE / VSLIP
              END IF
            END IF
          END DO
        END IF
*
*       Define stiffness in global directions
*
*       Secant stiffness
        SKS11 = SKSU*UNIT_UX*UNIT_UX + SKSV*UNIT_UY*UNIT_UY
        SKS22 = SKSU*UNIT_UY*UNIT_UY + SKSV*UNIT_UX*UNIT_UX
        SKS12 = SKSU*UNIT_UX*UNIT_UY - SKSV*UNIT_UX*UNIT_UY
*
*       Tangent stiffness
        SKT11 = SKTU*UNIT_UX*UNIT_UX + SKTV*UNIT_UY*UNIT_UY
        SKT22 = SKTU*UNIT_UY*UNIT_UY + SKTV*UNIT_UX*UNIT_UX
        SKT12 = SKTU*UNIT_UX*UNIT_UY - SKTV*UNIT_UX*UNIT_UY
*
```

```
*      WRITE (3,10) SKS11, SKS22, SKS12
*   10 FORMAT (E18.6,E18.6,E18.6)
*
*         Add in the stiffness contribution from the horizontal
*         connector line.
*
*         Secant stiffness
          PKS(1,1) = PKS(1,1) + (((YC + YBAR)**2)*SKS11/(HW*HW))
          PKS(1,2) = PKS(1,2) - (2.0D0*YC*(YC + YBAR)*SKS11/(HP*HW))
          PKS(1,3) = PKS(1,3) - ((YC + YBAR)*SKS11/HW)
          PKS(1,4) = PKS(1,4) - ((YC + YBAR)*SKS12/HW)
          PKS(1,5) = PKS(1,5) + ((YC*(YC + YBAR))*SKS11/HW)
     +               - (SKS12*XC*(YC + YBAR)/HW)
          PKS(2,2) = PKS(2,2) + (4.0D0*SKS11*YC*YC/(HP*HP))
          PKS(2,3) = PKS(2,3) + (2.0D0*SKS11*YC/HP)
          PKS(2,4) = PKS(2,4) + (2.0D0*SKS12*YC/HP)
          PKS(2,5) = PKS(2,5) - (2.0D0*SKS11*YC*YC/HP)
     +                + (2.0D0*SKS12*YC*XC/HP)
          PKS(3,3) = PKS(3,3) + SKS11
          PKS(3,4) = PKS(3,4) + SKS12
          PKS(3,5) = PKS(3,5) - (YC*SKS11) + (XC*SKS12)
          PKS(4,4) = PKS(4,4) + SKS22
          PKS(4,5) = PKS(4,5) + (XC*SKS22) - (YC*SKS12)
          PKS(5,5) = PKS(5,5) + ((SKS22*(XC**2)) + (SKS11*(YC**2))
     +               - (2.0D0*XC*YC*SKS12))
*
*         Tangent stiffness
          PKT(1,1) = PKT(1,1) + (((YC + YBAR)**2)*SKT11/(HW*HW))
          PKT(1,2) = PKT(1,2) - (2.0D0*YC*(YC + YBAR)*SKT11/(HP*HW))
          PKT(1,3) = PKT(1,3) - ((YC + YBAR)*SKT11/HW)
          PKT(1,4) = PKT(1,4) - ((YC + YBAR)*SKT12/HW)
          PKT(1,5) = PKT(1,5) + ((YC*(YC + YBAR))*SKT11/HW)
     +                - (SKT12*XC*(YC + YBAR)/HW)
          PKT(2,2) = PKT(2,2) + (4.0D0*SKT11*YC*YC/(HP*HP))
          PKT(2,3) = PKT(2,3) + (2.0D0*SKT11*YC/HP)
          PKT(2,4) = PKT(2,4) + (2.0D0*SKT12*YC/HP)
          PKT(2,5) = PKT(2,5) - (2.0D0*SKT11*YC*YC/HP)
     +                + (2.0D0*SKT12*YC*XC/HP)
          PKT(3,3) = PKT(3,3) + SKT11
          PKT(3,4) = PKT(3,4) + SKT12
          PKT(3,5) = PKT(3,5) - (YC*SKT11) + (XC*SKT12)
          PKT(4,4) = PKT(4,4) + SKT22
          PKT(4,5) = PKT(4,5) + (XC*SKT22) - (YC*SKT12)
          PKT(5,5) = PKT(5,5) + ((SKT22*(XC**2)) + (SKT11*(YC**2))
     +                - (2.0D0*XC*YC*SKT12))
*
        END DO
       END DO
*
*      Start looping over vertical connector lines in the panel.
*
       DO IL = 1, NVLINE(IP)
         XC  = XLOCAL(IP,IL)
         SPACE = SPACEV(IP,IL)
         F0 = F0V(IP,IL)
         FI = FIV(IP,IL)
         DU = DUV(IP,IL)
         S0 = S0V(IP,IL)
         R1 = R1V(IP,IL)
         R2 = R2V(IP,IL)
         R3 = R3V(IP,IL)
         R4 = R4V(IP,IL)
         ALPHA = ALPHAV(IP,IL)
         BETA  = BETAV(IP,IL)
         DO IC = 1, NVCON(IP,IL)
           YC = (SPACE*(IC-1)) + YSTART(IP,IL)
           UPI = UI + (2*YC*USI/HP) - (THETAI*YC)
           UFI = (YC + YBAR)*UF/HW
           USLIP = UPI - UFI
```

```
          VSLIP = VI + (THETAI*XC)
*
*         Define slip in global directions
*
          XSLIP = USLIP
          YSLIP = VSLIP
*
*         Define local axis
*
*         Define using a direction vector
*          DIRU = 1.0D0
*          DIRV = 0.5D0
*          DIRR = DSQRT(DIRU*DIRU + DIRV*DIRV)
*          UNIT_UX = DIRU/DIRR
*          UNIT_UY = DIRV/DIRR
*
*         Define using an initial orientation vector
          UNIT_UX = CSTOR1(11,IP,IL,IC,2,1)
          UNIT_UY = CSTOR1(12,IP,IL,IC,2,1)
          UNIT_VX = -UNIT_UY
          UNIT_VY = UNIT_UX
*         Define slip in local directions
*
          USLIP = XSLIP*UNIT_UX + YSLIP*UNIT_UY
          VSLIP = XSLIP*UNIT_VX + YSLIP*UNIT_VY
*
          IF (IMODE .EQ. 2) THEN
            DO I = 1, 2
              IF (I .EQ. 1) THEN
                DISPL = USLIP
              ELSE IF (I .EQ. 2) THEN
                DISPL = VSLIP
              END IF
              IF (DABS(DISPL) .LE. DU) THEN
                FAC1 = F0 + (R1 * S0 * DABS(DISPL))
                FAC2 = 1.0D0 - DEXP(-S0*DABS(DISPL)/F0)
                FAC3 = 1 - FAC2
                FORCE = FAC1 * FAC2
                IF (DISPL .LT. 0.0D0) FORCE = -FAC1 * FAC2
                SKT = (FAC1 * (S0/F0) * FAC3) + (R1 * S0 * FAC2)
              ELSE IF (DABS(DISPL) .GT. DU) THEN
                FAC1 = F0 + (R1 * S0 * DU)
                FAC2 = 1.0D0 - DEXP(-S0*DU/F0)
                FU = FAC1 * FAC2
                FORCE = FU + (R2*S0*(DISPL - DU))
                SKT = R2 * S0
              END IF
              IF (I .EQ. 1) THEN
                SKTU = SKT
                IF ((FORCE .EQ. 0.0D0) .AND. (DISPL .EQ. 0.0D0)) THEN
                  SKSU = S0
                ELSE
                  SKSU = FORCE / DISPL
                END IF
              ELSE IF (I .EQ. 2) THEN
                SKTV = SKT
                IF ((FORCE .EQ. 0.0D0) .AND. (DISPL .EQ. 0.0D0)) THEN
                  SKSV = S0
                ELSE
                  SKSV = FORCE / DISPL
                END IF
              END IF
            END DO
          ELSE IF (IMODE .EQ. 3) THEN
            DO I = 1, 2
              LPATH  = ICSTR1(1,IP,IL,IC,2,I)
              IYPLUS = ICSTR1(2,IP,IL,IC,2,I)
              IYMINS = ICSTR1(3,IP,IL,IC,2,I)
              LPPREV = ICSTR1(4,IP,IL,IC,2,I)
```

```
              DOLD   = CSTOR1(1,IP,IL,IC,2,I)
              DUNP   = CSTOR1(2,IP,IL,IC,2,I)
              FUNP   = CSTOR1(3,IP,IL,IC,2,I)
              DUNM   = CSTOR1(4,IP,IL,IC,2,I)
              FUNM   = CSTOR1(5,IP,IL,IC,2,I)
              DMAXP  = CSTOR1(6,IP,IL,IC,2,I)
              FMAXP  = CSTOR1(7,IP,IL,IC,2,I)
              DMAXM  = CSTOR1(8,IP,IL,IC,2,I)
              FMAXM  = CSTOR1(9,IP,IL,IC,2,I)
              SP     = CSTOR1(10,IP,IL,IC,2,I)
*
*             Call subroutine HYSTER to determine connector force and
*             stiffness corresponding to deformation DELTA.
*
              IF (I .EQ. 1) THEN
                CALL HYSTR (USLIP, UFORCE, SKTU, JFLAG)
                IF (JFLAG .EQ. 1) RETURN
                IF ((UFORCE .EQ. 0.0D0) .AND. (USLIP .EQ. 0.0D0)) THEN
                  SKSU = S0
                ELSE
                  SKSU = UFORCE / USLIP
                END IF
              ELSE IF (I .EQ. 2) THEN
                CALL HYSTR (VSLIP, VFORCE, SKTV, JFLAG)
                IF (JFLAG .EQ. 1) RETURN
                IF ((VFORCE .EQ. 0.0D0) .AND. (VSLIP .EQ. 0.0D0)) THEN
                  SKSV = S0
                ELSE
                  SKSV = VFORCE / VSLIP
                END IF
              END IF
            END DO
          END IF
*
*         Define stiffness in global directions
*
*         Secant stiffness
          SKS11 = SKSU*UNIT_UX*UNIT_UX + SKSV*UNIT_UY*UNIT_UY
          SKS22 = SKSU*UNIT_UY*UNIT_UY + SKSV*UNIT_UX*UNIT_UX
          SKS12 = SKSU*UNIT_UX*UNIT_UY - SKSV*UNIT_UX*UNIT_UY
*
*         Tangent stiffness
          SKT11 = SKTU*UNIT_UX*UNIT_UX + SKTV*UNIT_UY*UNIT_UY
          SKT22 = SKTU*UNIT_UY*UNIT_UY + SKTV*UNIT_UX*UNIT_UX
          SKT12 = SKTU*UNIT_UX*UNIT_UY - SKTV*UNIT_UX*UNIT_UY
*
*         Add in the stiffness contribution from the horizontal
*         connector line.
*
*         Secant stiffness
          PKS(1,1) = PKS(1,1) + (((YC + YBAR)**2)*SKS11/(HW*HW))
          PKS(1,2) = PKS(1,2) - (2.0D0*YC*(YC + YBAR)*SKS11/(HP*HW))
          PKS(1,3) = PKS(1,3) - ((YC + YBAR)*SKS11/HW)
          PKS(1,4) = PKS(1,4) - ((YC + YBAR)*SKS12/HW)
          PKS(1,5) = PKS(1,5) + ((YC*(YC + YBAR))*SKS11/HW)
     +                         - (SKS12*XC*(YC + YBAR)/HW)
          PKS(2,2) = PKS(2,2) + (4.0D0*SKS11*YC*YC/(HP*HP))
          PKS(2,3) = PKS(2,3) + (2.0D0*SKS11*YC/HP)
          PKS(2,4) = PKS(2,4) + (2.0D0*SKS12*YC/HP)
          PKS(2,5) = PKS(2,5) - (2.0D0*SKS11*YC*YC/HP)
     +                 + (2.0D0*SKS12*YC*XC/HP)
          PKS(3,3) = PKS(3,3) + SKS11
          PKS(3,4) = PKS(3,4) + SKS12
          PKS(3,5) = PKS(3,5) - (YC*SKS11) + (XC*SKS12)
          PKS(4,4) = PKS(4,4) + SKS22
          PKS(4,5) = PKS(4,5) + (XC*SKS22) - (YC*SKS12)
          PKS(5,5) = PKS(5,5) + ((SKS22*(XC**2)) + (SKS11*(YC**2))
     +                         - (2.0D0*XC*YC*SKS12))
*
```

```
*          Tangent stiffness
           PKT(1,1) = PKT(1,1) + (((YC + YBAR)**2)*SKT11/(HW*HW))
           PKT(1,2) = PKT(1,2) - (2.0D0*YC*(YC + YBAR)*SKT11/(HP*HW))
           PKT(1,3) = PKT(1,3) - ((YC + YBAR)*SKT11/HW)
           PKT(1,4) = PKT(1,4) - ((YC + YBAR)*SKT12/HW)
           PKT(1,5) = PKT(1,5) + ((YC*(YC + YBAR))*SKT11/HW)
     +                 - (SKT12*XC*(YC + YBAR)/HW)
           PKT(2,2) = PKT(2,2) + (4.0D0*SKT11*YC*YC/(HP*HP))
           PKT(2,3) = PKT(2,3) + (2.0D0*SKT11*YC/HP)
           PKT(2,4) = PKT(2,4) + (2.0D0*SKT12*YC/HP)
           PKT(2,5) = PKT(2,5) - (2.0D0*SKT11*YC*YC/HP)
     +                 + (2.0D0*SKT12*YC*XC/HP)
           PKT(3,3) = PKT(3,3) + SKT11
           PKT(3,4) = PKT(3,4) + SKT12
           PKT(3,5) = PKT(3,5) - (YC*SKT11) + (XC*SKT12)
           PKT(4,4) = PKT(4,4) + SKT22
           PKT(4,5) = PKT(4,5) + (XC*SKT22) - (YC*SKT12)
           PKT(5,5) = PKT(5,5) + ((SKT22*(XC**2)) + (SKT11*(YC**2))
     +                 - (2.0D0*XC*YC*SKT12))
*
         END DO
       END DO
*
*      Fill out panel stiffness matrix by symmetry.
*
       DO I = 1, 5
         DO J = I, 5
           PKS(J,I) = PKS(I,J)
           PKT(J,I) = PKT(I,J)
         END DO
       END DO
*
       RETURN
       END
```

C.3 `update` Subroutine to Update Connector Properties

```
*-----------------------------------------------------------------------
*     SUBROUTINE UPDATE DETERMINES THE CONNECTOR PARAMETERS FOR THE NEW
*     EQUILIBRIUM POSTION OF THE WALL (CALLED BY SUBROUTINE CYCLIC)
*-----------------------------------------------------------------------
*
*
      SUBROUTINE UPDATE (ICSTOR)
      IMPLICIT DOUBLE PRECISION (A - H, O - Z)
      PARAMETER    (MDOF = 41, MP = 10, ML = 10, MC = 50, MDAT = 20000)
      COMMON /B01/ HTWALL, IANALY, IMODE, NPANEL, NDOF
      COMMON /B02/ HORZP(MP), VERTP(MP), XGLOB(MP), YGLOB(MP),
     .             GMOD(MP), THICKP(MP), NHLINE(MP), NVLINE(MP),
     .             NHCON(MP,ML), NVCON(MP,ML)
      COMMON /B03/ XLOCAL(MP,ML), SPACEH(MP,ML),
     .             XSTART(MP,ML), XEND(MP,ML),
     .             YLOCAL(MP,ML), SPACEV(MP,ML),
     .             YSTART(MP,ML), YEND(MP,ML)
      COMMON /B04/ F0, FI, DU, S0, R1, R2, R3, R4, ALPHA, BETA
      COMMON /B05/ F0H(MP,ML), FIH(MP,ML), DUH(MP,ML), S0H(MP,ML),
     .             R1H(MP,ML), R2H(MP,ML), R3H(MP,ML), R4H(MP,ML),
     .             ALPHAH(MP,ML), BETAH(MP,ML),
     .             F0V(MP,ML), FIV(MP,ML), DUV(MP,ML), S0V(MP,ML),
     .             R1V(MP,ML), R2V(MP,ML), R3V(MP,ML), R4V(MP,ML),
     .             ALPHAV(MP,ML), BETAV(MP,ML)
      COMMON /B06/ LPATH, IYPLUS, IYMINS, LPPREV, NUBC, NCYC
      COMMON /B07/ ICSTR1(4,MP,ML,MC,2,2), ICSTR2(4,MP,ML,MC,2,2)
      COMMON /B08/ DOLD, DUNP, FUNP, DUNM, FUNM, DMAXP, FMAXP, DMAXM,
     .             FMAXM, SP
      COMMON /B09/ CSTOR1(12,MP,ML,MC,2,2), CSTOR2(12,MP,ML,MC,2,2)
      COMMON /B10/ GKS(MDOF,MDOF), GKT(MDOF,MDOF), PKS(5,5), PKT(5,5),
     .             GD(MDOF), GD0(MDOF), GDD(MDOF), GF(MDOF), GF0(MDOF),
     .             GF2(MDOF), GRF(MDOF)
*
*     Initialize connector parameters for start of analysis.
*
*      WRITE (*,*) 'We are in subroutine UPDATE'
      IF (ICSTOR .EQ. 1) THEN
        DO IP = 1, NPANEL
          DO IL = 1, NHLINE(IP)
            DO IC = 1, NHCON(IP,IL)
              ICSTR1(1,IP,IL,IC,1,1) = 1
              ICSTR1(2,IP,IL,IC,1,1) = 0
              ICSTR1(3,IP,IL,IC,1,1) = 0
              ICSTR1(4,IP,IL,IC,1,1) = 1
              DO I = 1, 4
                ICSTR1(I,IP,IL,IC,1,2) = ICSTR1(I,IP,IL,IC,1,1)
                ICSTR2(I,IP,IL,IC,1,1) = ICSTR1(I,IP,IL,IC,1,1)
                ICSTR2(I,IP,IL,IC,1,2) = ICSTR1(1,IP,IL,IC,1,1)
              END DO
              DO I = 1,5
                CSTOR1(I,IP,IL,IC,1,1) = 0.0D0
                CSTOR1(I,IP,IL,IC,1,2) = 0.0D0
                CSTOR2(I,IP,IL,IC,1,1) = 0.0D0
                CSTOR2(I,IP,IL,IC,1,2) = 0.0D0
              END DO
              CSTOR1(6,IP,IL,IC,1,1) = FIH(IP,IL) / S0H(IP,IL)
              CSTOR1(7,IP,IL,IC,1,1) = FIH(IP,IL)
              CSTOR1(8,IP,IL,IC,1,1) = -FIH(IP,IL) / S0H(IP,IL)
              CSTOR1(9,IP,IL,IC,1,1) = -FIH(IP,IL)
              CSTOR1(10,IP,IL,IC,1,1) = S0H(IP,IL)
              DO I = 6, 10
                CSTOR1(I,IP,IL,IC,1,2) = CSTOR1(I,IP,IL,IC,1,1)
                CSTOR2(I,IP,IL,IC,1,1) = CSTOR1(I,IP,IL,IC,1,1)
                CSTOR2(I,IP,IL,IC,1,2) = CSTOR1(I,IP,IL,IC,1,1)
              END DO
```

```
            END DO
          END DO
          DO IL = 1, NVLINE(IP)
            DO IC = 1, NVCON(IP,IL)
              ICSTR1(1,IP,IL,IC,2,1) = 1
              ICSTR1(2,IP,IL,IC,2,1) = 0
              ICSTR1(3,IP,IL,IC,2,1) = 0
              ICSTR1(4,IP,IL,IC,2,1) = 1
              DO I = 1, 4
                ICSTR1(I,IP,IL,IC,2,2) = ICSTR1(I,IP,IL,IC,2,1)
                ICSTR2(I,IP,IL,IC,2,1) = ICSTR1(I,IP,IL,IC,2,1)
                ICSTR2(I,IP,IL,IC,2,2) = ICSTR1(1,IP,IL,IC,2,1)
              END DO
              DO I = 1,5
                CSTOR1(I,IP,IL,IC,2,1) = 0.0D0
                CSTOR1(I,IP,IL,IC,2,2) = 0.0D0
                CSTOR2(I,IP,IL,IC,2,1) = 0.0D0
                CSTOR2(I,IP,IL,IC,2,2) = 0.0D0
              END DO
              CSTOR1(6,IP,IL,IC,2,1) = FIV(IP,IL) / S0V(IP,IL)
              CSTOR1(7,IP,IL,IC,2,1) = FIV(IP,IL)
              CSTOR1(8,IP,IL,IC,2,1) = -FIV(IP,IL) / S0V(IP,IL)
              CSTOR1(9,IP,IL,IC,2,1) = -FIV(IP,IL)
              CSTOR1(10,IP,IL,IC,2,1) = S0V(IP,IL)
              DO I = 6, 10
                CSTOR1(I,IP,IL,IC,2,2) = CSTOR1(I,IP,IL,IC,2,1)
                CSTOR2(I,IP,IL,IC,2,1) = CSTOR1(I,IP,IL,IC,2,1)
                CSTOR2(I,IP,IL,IC,2,2) = CSTOR1(I,IP,IL,IC,2,1)
              END DO
            END DO
          END DO
        END DO
*
*     Up-date connector parameters for new equilibrium postion.
*
      ELSE IF (ICSTOR .EQ. 2) THEN
*
*       Loop over all panels in the wall.
*
        HW = HTWALL
        DO IP = 1, NPANEL
*
*         Initialize variables.
*
          II = (4 * IP) - 2
          UF = GD(1)
          USI = GD(II)
          UI  = GD(II+1)
          VI  = GD(II+2)
          THETAI = GD(II+3)
          YBAR  = YGLOB (IP)
          HP  = VERTP(IP)
*
*         Start looping over horizontal connector lines in the panel.
*
          DO IL = 1, NHLINE(IP)
            YC  = YLOCAL(IP,IL)
            SPACE = SPACEH(IP,IL)
            F0 = F0H(IP,IL)
            FI = FIH(IP,IL)
            DU = DUH(IP,IL)
            S0 = S0H(IP,IL)
            R1 = R1H(IP,IL)
            R2 = R2H(IP,IL)
            R3 = R3H(IP,IL)
            R4 = R4H(IP,IL)
            ALPHA = ALPHAH(IP,IL)
            BETA  = BETAH(IP,IL)
            DO IC = 1, NHCON(IP,IL)
```

```
              XC = (SPACE*(IC-1)) + XSTART(IP,IL)
              UPI = UI + (2*YC*USI/HP) - (THETAI*YC)
              UFI = (YC + YBAR)*UF/HW
              USLIP = UPI - UFI
              VSLIP = VI + (THETAI*XC)
*
*             Define slip in global directions
*
              XSLIP = USLIP
              YSLIP = VSLIP
*
*             Define local axis
*
*             Define using a direction vector
*              DIRU = 1.0D0
*              DIRV = 0.5D0
*              DIRR = DSQRT(DIRU*DIRU + DIRV*DIRV)
*              UNIT_UX = DIRU/DIRR
*              UNIT_UY = DIRV/DIRR
*
*             Define using an initial orientation vector
              UNIT_UX = CSTOR1(11,IP,IL,IC,1,1)
              UNIT_UY = CSTOR1(12,IP,IL,IC,1,1)
              UNIT_VX = -UNIT_UY
              UNIT_VY = UNIT_UX
*
*             Define slip in local directions
*
              USLIP = XSLIP*UNIT_UX + YSLIP*UNIT_UY
              VSLIP = XSLIP*UNIT_VX + YSLIP*UNIT_VY
*
              DO I = 1, 2
                LPATH  = ICSTR2(1,IP,IL,IC,1,I)
                IYPLUS = ICSTR2(2,IP,IL,IC,1,I)
                IYMINS = ICSTR2(3,IP,IL,IC,1,I)
                LPPREV = ICSTR2(4,IP,IL,IC,1,I)
                DOLD   = CSTOR2(1,IP,IL,IC,1,I)
                DUNP   = CSTOR2(2,IP,IL,IC,1,I)
                FUNP   = CSTOR2(3,IP,IL,IC,1,I)
                DUNM   = CSTOR2(4,IP,IL,IC,1,I)
                FUNM   = CSTOR2(5,IP,IL,IC,1,I)
                DMAXP  = CSTOR2(6,IP,IL,IC,1,I)
                FMAXP  = CSTOR2(7,IP,IL,IC,1,I)
                DMAXM  = CSTOR2(8,IP,IL,IC,1,I)
                FMAXM  = CSTOR2(9,IP,IL,IC,1,I)
                SP     = CSTOR2(10,IP,IL,IC,1,I)
*
*               Call subroutine HYSTER to update the connector load and
*               stiffness parameters associated with the new equilibrium
*               position.
*
                IF (I .EQ. 1) THEN
                  CALL HYSTR (USLIP, UFORCE, SKTU, JFLAG)
                  IF (JFLAG .EQ. 1) RETURN
*
*                 Debug statement to track the load-displacement
*                 response of particular connectors along a
*                 horizontal connector line.
*
*                 if ((ip .eq. 1) .and. (il .eq. 1) .and.
*    .                 (ic.eq. 1)) then
*                   write (2,1000) uslip, uforce, lpath
*1000               format (2e18.10, i8)
*                 end if
                ELSE IF (I .EQ. 2) THEN
                  CALL HYSTR (VSLIP, VFORCE, SKTV, JFLAG)
                  IF (JFLAG .EQ. 1) RETURN
*
*                 Debug statement to track the load-displacement
```

```
*                 response of particular connectors along a
*                 vertical connector line.
*
*                 if ((ip .eq. 1) .and. (il .eq. 1) .and.
*    .                 (ic.eq. 8)) then
*                   write (2,2000) vslip, vforce, lpath
*2000               format (2e18.4, i8)
*                 end if
                  END IF
*
                  ICSTR2(1,IP,IL,IC,1,I) = LPATH
                  ICSTR2(2,IP,IL,IC,1,I) = IYPLUS
                  ICSTR2(3,IP,IL,IC,1,I) = IYMINS
                  ICSTR2(4,IP,IL,IC,1,I) = LPPREV
                  DO J = 1, 4
                    ICSTR1(J,IP,IL,IC,1,I) = ICSTR2(J,IP,IL,IC,1,I)
                  END DO
                  CSTOR2(1,IP,IL,IC,1,I) = DOLD
                  CSTOR2(2,IP,IL,IC,1,I) = DUNP
                  CSTOR2(3,IP,IL,IC,1,I) = FUNP
                  CSTOR2(4,IP,IL,IC,1,I) = DUNM
                  CSTOR2(5,IP,IL,IC,1,I) = FUNM
                  CSTOR2(6,IP,IL,IC,1,I) = DMAXP
                  CSTOR2(7,IP,IL,IC,1,I) = FMAXP
                  CSTOR2(8,IP,IL,IC,1,I) =  DMAXM
                  CSTOR2(9,IP,IL,IC,1,I) = FMAXM
                  CSTOR2(10,IP,IL,IC,1,I) = SP
                  DO J = 1, 10
                    CSTOR1(J,IP,IL,IC,1,I) = CSTOR2(J,IP,IL,IC,1,I)
                  END DO
                END DO
              END DO
            END DO
*
*           Start looping over vertical connector lines in the panel.
*
            DO IL = 1, NVLINE(IP)
              XC  = XLOCAL(IP,IL)
              SPACE = SPACEV(IP,IL)
              F0 = F0V(IP,IL)
              FI = FIV(IP,IL)
              DU = DUV(IP,IL)
              S0 = S0V(IP,IL)
              R1 = R1V(IP,IL)
              R2 = R2V(IP,IL)
              R3 = R3V(IP,IL)
              R4 = R4V(IP,IL)
              ALPHA = ALPHAV(IP,IL)
              BETA  = BETAV(IP,IL)
              DO IC = 1, NVCON(IP,IL)
                YC = (SPACE*(IC-1)) + YSTART(IP,IL)
                UPI = UI + (2*YC*USI/HP) - (THETAI*YC)
                UFI = (YC + YBAR)*UF/HW
                USLIP = UPI - UFI
                VSLIP = VI + (THETAI*XC)
*
*               Define slip in global directions
*
                XSLIP = USLIP
                YSLIP = VSLIP
*
*               Define local axis
*
*               Define using a direction vector
*                DIRU = 1.0D0
*                DIRV = 0.5D0
*                DIRR = DSQRT(DIRU*DIRU + DIRV*DIRV)
*                UNIT_UX = DIRU/DIRR
*                UNIT_UY = DIRV/DIRR
```

```
*
*             Define using an initial orientation vector
              UNIT_UX = CSTOR1(11,IP,IL,IC,2,1)
              UNIT_UY = CSTOR1(12,IP,IL,IC,2,1)
              UNIT_VX = -UNIT_UY
              UNIT_VY = UNIT_UX
*
*             Define slip in local directions
*
              USLIP = XSLIP*UNIT_UX + YSLIP*UNIT_UY
              VSLIP = XSLIP*UNIT_VX + YSLIP*UNIT_VY
*
              DO I = 1, 2
                LPATH  = ICSTR2(1,IP,IL,IC,2,I)
                IYPLUS = ICSTR2(2,IP,IL,IC,2,I)
                IYMINS = ICSTR2(3,IP,IL,IC,2,I)
                LPPREV = ICSTR2(4,IP,IL,IC,2,I)
                DOLD   = CSTOR2(1,IP,IL,IC,2,I)
                DUNP   = CSTOR2(2,IP,IL,IC,2,I)
                FUNP   = CSTOR2(3,IP,IL,IC,2,I)
                DUNM   = CSTOR2(4,IP,IL,IC,2,I)
                FUNM   = CSTOR2(5,IP,IL,IC,2,I)
                DMAXP  = CSTOR2(6,IP,IL,IC,2,I)
                FMAXP  = CSTOR2(7,IP,IL,IC,2,I)
                DMAXM  = CSTOR2(8,IP,IL,IC,2,I)
                FMAXM  = CSTOR2(9,IP,IL,IC,2,I)
                SP     = CSTOR2(10,IP,IL,IC,2,I)
*
*               Call subroutine HYSTER to update the connector load and
*               stiffness parameters associated with the new equilibrium
*               position.
*
                IF (I .EQ. 1) THEN
                  CALL HYSTR (USLIP, UFORCE, SKTU, JFLAG)
                  IF (JFLAG .EQ. 1) RETURN
                ELSE IF (I .EQ. 2) THEN
                  CALL HYSTR (VSLIP, VFORCE, SKTV, JFLAG)
                  IF (JFLAG .EQ. 1) RETURN
                END IF
                ICSTR2(1,IP,IL,IC,2,I) = LPATH
                ICSTR2(2,IP,IL,IC,2,I) = IYPLUS
                ICSTR2(3,IP,IL,IC,2,I) = IYMINS
                ICSTR2(4,IP,IL,IC,2,I) = LPPREV
                DO J = 1, 4
                  ICSTR1(J,IP,IL,IC,2,I) = ICSTR2(J,IP,IL,IC,2,I)
                END DO
                CSTOR2(1,IP,IL,IC,2,I) = DOLD
                CSTOR2(2,IP,IL,IC,2,I) = DUNP
                CSTOR2(3,IP,IL,IC,2,I) = FUNP
                CSTOR2(4,IP,IL,IC,2,I) = DUNM
                CSTOR2(5,IP,IL,IC,2,I) = FUNM
                CSTOR2(6,IP,IL,IC,2,I) = DMAXP
                CSTOR2(7,IP,IL,IC,2,I) = FMAXP
                CSTOR2(8,IP,IL,IC,2,I) =  DMAXM
                CSTOR2(9,IP,IL,IC,2,I) = FMAXM
                CSTOR2(10,IP,IL,IC,2,I) = SP
                DO J = 1, 10
                  CSTOR1(J,IP,IL,IC,2,I) = CSTOR2(J,IP,IL,IC,2,I)
                END DO
              END DO
            END DO
          END DO
        END DO
      END IF
      RETURN
      END
```